

**NEW DISCOTIC LIQUID CRYSTALS BASED ON
LARGE POLYCYCLIC AROMATIC HYDROCARBONS
AS MATERIALS FOR MOLECULAR ELECTRONICS**

Dissertation

zur Erlangung des Grades
"Doktor der Naturwissenschaften"

dem Fachbereich Chemie und Pharmazie der
Johannes Gutenberg-Universität Mainz
vorgelegt von

Željko Tomović

geboren in Kragujevac, Serbien

Mainz 2004

Tag der mündlichen Prüfung: 02.03.2005

Dedicated to my wife, brother and parents

Contents

1. Introduction	1
1.1 Polycyclic Aromatic Hydrocarbons.....	1
1.2 "All-Benzenoid" PAHs and the Clar rule of the aromatic sextet.....	2
1.3 Synthesis of PAHs.....	5
1.3.1 Synthesis of PAHs via intramolecular Diels-Alder reaction.....	7
1.3.2 Synthesis of PAHs via cyclotrimerization of diphenylacetylenes.....	9
1.3.3 Synthesis of PAHs via intermolecular Diels-Alder reaction.....	10
1.4 "Superbenzene" chemistry	14
1.5 Discotic liquid crystals.....	16
1.5.1 Mesophase characterization.....	23
1.5.2 Charge carrier mobility.....	25
1.6 Discotic liquid crystals as semiconductors in electronic and optoelectronic devices.....	27
1.6.1 Field effect transistors (FETs).....	27
1.6.2 Photovoltaic devices.....	28
1.6.3 Light emitting diodes (LEDs).....	29
1.7 Motivation and objectives.....	30
1.8 Literature.....	34
2. Superphenalene-Based Columnar Liquid Crystals	39
2.1 Synthesis of hexa-substituted "Superphenalenes".....	39
2.2 Supramolecular characterization.....	52
2.3 Charge carrier mobility.....	61
2.4 Uniaxial alignment of C ₉₆ -C ₁₂ by solution processing.....	66

2.5 Self-assembly and electrical properties of supramolecular architectures of C ₉₆ -C ₁₂ studied by Scanning Force Microscopy (SFM) and Kelvin Probe Force Microscopy (KPFM).....	72
2.5.1 C ₉₆ -C ₁₂ at the interface with Au electrodes.....	75
2.5.2 Electrical properties.....	78
2.6 Superphenalene derivatives with lower symmetry.....	86
2.6.1 Synthesis.....	88
2.6.2 Phase characterization.....	92
2.6.3 Charge carrier mobility.....	93
2.7 Study of the oxidative cyclodehydrogenation reaction.....	95
2.8 Literature.....	101
3. Control of the Homeotropic Order of Discotic Columnar Systems.....	106
3.1 Introduction.....	106
3.2 Synthesis of hexa-alkylether substituted HBC and C ₉₆ discs.....	108
3.3 Phase characterization of hexa-alkylether substituted HBCs.....	114
3.3.1 Thermal phase characterization.....	114
3.3.2 Structure investigation by X-ray scattering.....	117
3.3.3 Homeotropic arrangement.....	120
3.4 Literature.....	125
4. Synthesis and Properties of Dendronized Superphenalenes.....	128
4.1 Introduction.....	128
4.2 Synthesis and structural characterization.....	131
4.2.1 Synthesis of hexa(4-iodophenyl)-C ₉₆	131
4.2.2 Functionalization of hexa(4-iodophenyl)-C ₉₆ by Hagihara-Sonogashira coupling reaction towards dendronized superphenalenes.....	133

4.3 UV/Vis absorption and fluorescence measurements.....	138
4.4 Literature.....	144
5. Graphitic Molecules with Partial "Zig-Zag" Periphery.....	147
5.1 Introduction.....	147
5.2 Synthesis	149
5.3 UV/Vis and fluorescence characterization.....	154
5.4 Synthesis and characterization of soluble "zig-zag" superphenalene.....	156
5.5 Literature.....	163
6. Summary.....	166
7. Experimental Section.....	173
7.1 General methods.....	173
7.2 Materials.	174
7.3 Syntheses.....	175
Acknowledgements.....	234
List of publications.....	236
Curriculum Vitae.....	238

CHAPTER 1

Introduction

1.1 Polycyclic Aromatic Hydrocarbons

Polycyclic aromatic hydrocarbons (PAHs), which can be formally regarded as two-dimensional graphite subunits, represent one of the most intensively investigated class of compounds.^[1-4] PAHs were first discovered in coal tar in the middle of the 19th century and helped to initiate the rapid development of industrial organic chemistry, especially in the field of dyes. PAHs are generally formed during incomplete combustion or pyrolysis of organic matter containing carbon and hydrogen. Hence, a variety of PAHs can be found in nature in fossil fuels, in the residues of domestic and natural combustion of coal, wood and other organic materials, in the emissions from forest fires and volcanoes, and in interstellar media.^[5-8] They usually occur as a mixture of two or more PAHs and other chemicals. However, for a systematic study of PAHs or their application as materials, selective synthetic methods had to be established. Fundamental contributions to the directed synthesis and characterization of polycyclic aromatics were made by the pioneering work of R. Scholl,^[9-12] E. Clar,^[13-16] and M. Zander,^[17-19] who achieved the synthesis of numerous aromatic compounds under drastic conditions at high temperatures in strongly oxidizing reaction melts. Until recently, the number of PAHs isolated and/or synthesized was relatively small and limited to small sizes. Very recently, a synthetic breakthrough has been achieved as a result of progress of analytical techniques and has made the selective synthesis of various PAHs, with a broad range of sizes and shapes and under mild conditions, possible.^[20]

PAHs have attracted the interest of the scientific community for different reasons. One of the intrinsic properties of the PAHs is their aromaticity, which has attracted the interest of theoreticians for a long time.^[21-25] Large PAHs are

well defined model systems for graphite, and different theoretical methods have been applied to estimate the electronic properties of graphite based on PAHs with increasing size and varying topologies.^[26] PAHs are also of special interest because of their electronic and opto-electronic properties.^[21,26] Besides synthetic challenges, correlations between the chemical structure of PAHs and their properties, as well as their packing behavior in the solid state are key concerns.^[27] The intrinsic electronic properties of PAHs promoted their use as active components in molecular electronics such as organic field effect transistors, light-emitting diodes and photovoltaic devices.^[28] The physiological effect of extended aromatics is also of interest in the light of the increasing level of discussion about environmental pollutants.^[29] The presence of large graphite segments in interstellar space is important regarding the formation of the universe. Lastly, ultra-large polycyclic aromatics, as preferentially planar structures with defined topology, possess considerable importance for a deeper understanding of the materials science of soot, graphite, the spherical fullerenes, and nanotubes.^[30-33]

1.2 "All-Benzenoid" PAHs and the Clar rule of the aromatic sextet

All-benzenoid aromatics belong to the large class of alternating aromatic hydrocarbons which contain only fused six membered benzenoid rings.^[23] They are differentiated from other alternating aromatics by their benzene-like character, first described in Clar's model of the aromatic sextet.^[21] The smallest example of all-benzenoid PAH is the triphenylene (**1**), one of the five *cata*-condensed isomers with four benzene rings (Figure 1). Concerning its properties, triphenylene differs distinctly from the other isomers and occupies a special position: in contrast to [4]helicene (**2**), chrysene (**3**), benz[*a*]anthracene (**4**), and tetracene (**5**), triphenylene shows lower chemical reactivity and higher thermodynamic stability, and within a molecular orbital description triphenylene has the largest resonance energy,^[34] the highest first ionization energy,^[35] and the largest HOMO-LUMO gap.^[35] Triphenylene is more benzene-like in its

chemical and physical properties, while the other isomers are more olefin like. This "benzene-like behavior" can be adequately described in terms of Clar's model of the aromatic sextet.^[21]

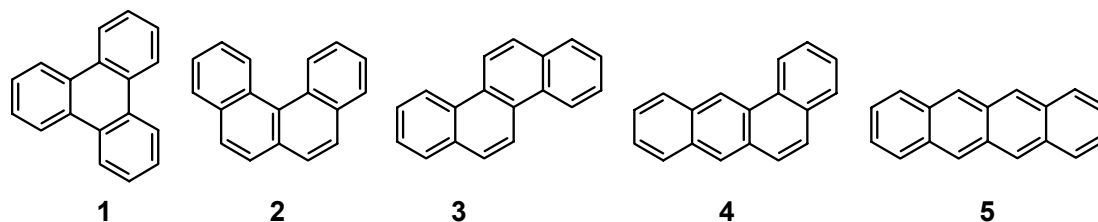


Figure 1. Triphenylene (**1**) and its *cata*-condensed isomers.

In the 1970s Clar proposed that the chemical reactivities and other properties of PAHs could be best understood in terms of localization of the aromatic sextets present in the molecule. He proposed to assign the π -electrons that can participate in aromatic sextets to particular rings in such a way as to obtain the maximum number of π -electron sextets. A Clar model may be viewed as a distribution of the π -electrons of the respective benzenoid molecule. Hexagons in which an aromatic sextet is located are populated by six π -electrons. Hexagons without an aromatic sextet contain the π -electrons in the double bonds (if any), belonging to this hexagon; if a double bond is shared by two hexagons, then one π -electron is attributed to each hexagon. Thus, in all-benzenoid aromatic hydrocarbons, the number of carbon atoms necessary is an integral multiple of six. In contrast to tetracene (**5a-d**), only one Clar formula can be drawn for triphenylene (**1**), as shown in Figure 2. Such compounds, with unique Clar formula, belong to the group of all-benzenoid aromatic hydrocarbons. According to this model, with the same number of carbons, all-benzenoid PAHs are clearly less reactive and thermodynamically more stable than the corresponding non all-benzenoid PAHs. The Clar structure enables the differentiation between bonds which are more olefinic or more aromatic. Robinson's circle^[36] serves as an illustration of the benzene likeness of the electronic sextet (Figure 2).

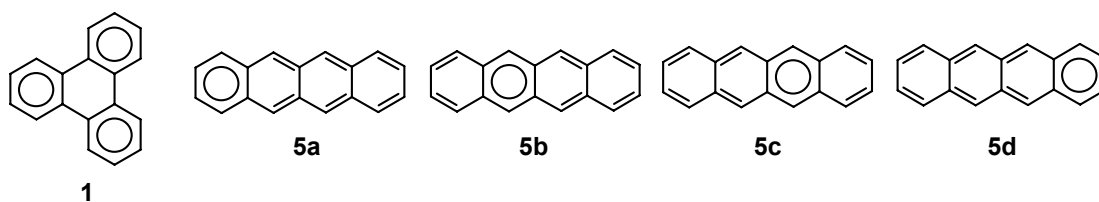


Figure 2. Clar aromatic sextet formulas of triphenylene (**1**) and tetracene (**5a-d**).

Within the class of polycyclic aromatics the all-benzenoid PAHs represent only a small group. Thus, from the total of roughly 20600 possible alternating hydrocarbons with 4 to 10 fused benzene rings, only 17 are all-benzenoid. However, they play an very important role in the development of the theory of polycyclic aromatics.^[23]

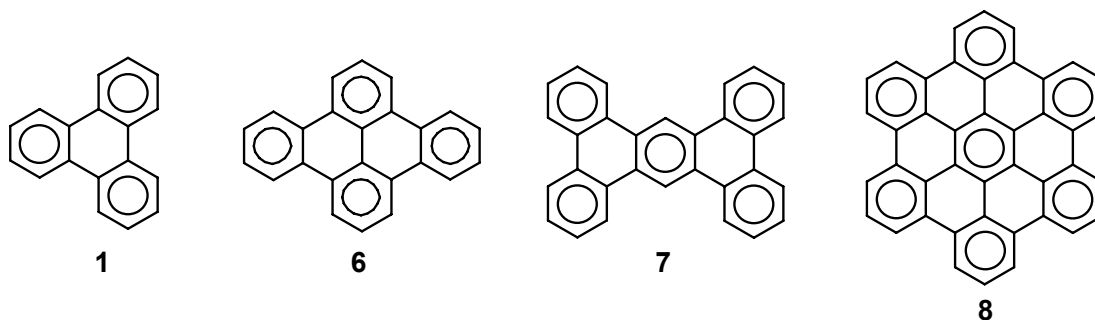


Figure 3. "All-benzenoid" PAHs: triphenylene (**1**), dibenzo[*fg,op*]naphthacene (**6**), tetrabenzo[*a,c,h,j*]anthracene (**7**), and hexa-*peri*-hexabenzocoronene (**8**).

Although the Clar theory of benzenoid hydrocarbons is based more on chemical intuition than on some well founded physical principles (such as the quantum theory), it is very encouraging to see that after a long time finally rigorous *ab initio* quantum chemical calculations appear to support an intuitive picture of Clar of benzenoid hydrocarbons.^[37-39] Chemical and physical evidence suggest that Clar's model, with its emphasis on π -electron sextet, provides a reasonably accurate representation of physical reality.

1.3 Synthesis of PAHs

Small PAHs like naphthalene, anthracene or phenanthrene can be isolated by the separation of complex mixtures, either from coal tar or side products of the catalytic hydrocracking of petroleum.^[40,41] A far more specific preparation of PAHs is possible by the means of synthetic organic chemistry, as shown by the pioneering work of R. Scholl,^[9-12] E. Clar^[13-16] and M. Zander.^[17-19] Two different methods can be used for the synthesis of PAHs: one is the non-selective method, in which a mixture of numerous PAHs is formed simultaneously under often drastic conditions such as high temperature and strong oxidative reagents, followed by separation and characterization of the products. An example of non-selective synthesis of PAHs is shown in Figure 4. The transformation of a mixture of ketones **9** and **10** in a zinc dust/zinc chloride/sodium chloride melt at 330-350 °C, gave a mixture of the PAHs **11**, **12**, **13**, and **14**, in quantities that could be preparatively isolated.^[42] Non-selective reactions can be of advantage if the starting material is accessible in large scale and the resulting mixture is separable.

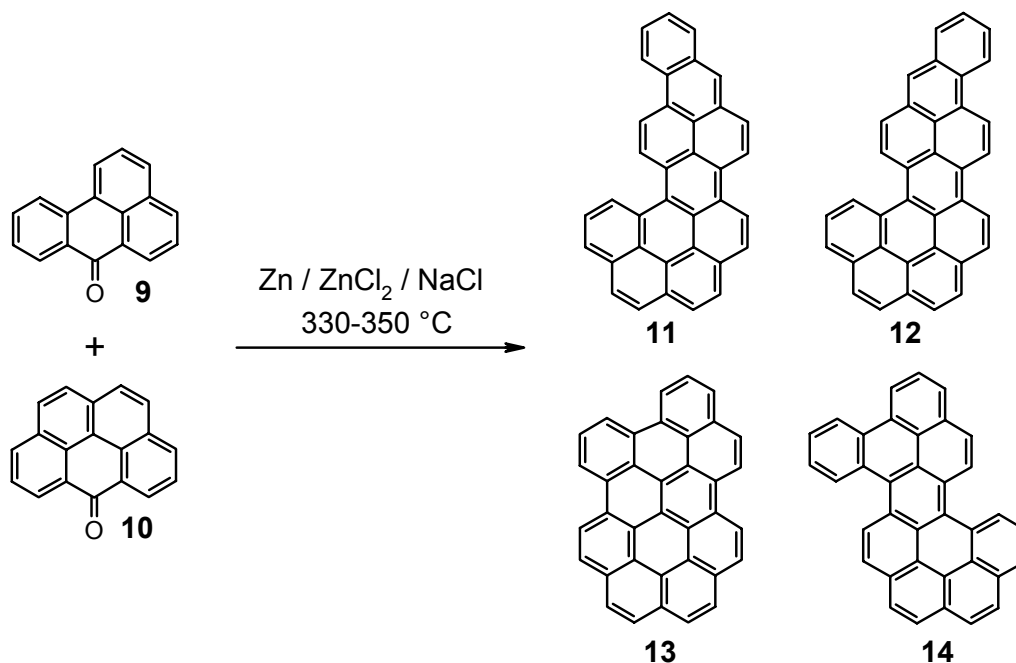


Figure 4. An example of non-selective synthesis of PAHs.

The other method is the selective synthesis of PAHs, which involves a specific, multistep sequence, leading to a single desired product. Hence, this requires a high synthetic effort. Some classical routes for the selective preparation of PAHs are shown in Figure 5; comprehensive summaries of synthetic routes to PAHs can be found in references [1], [3] and [4].

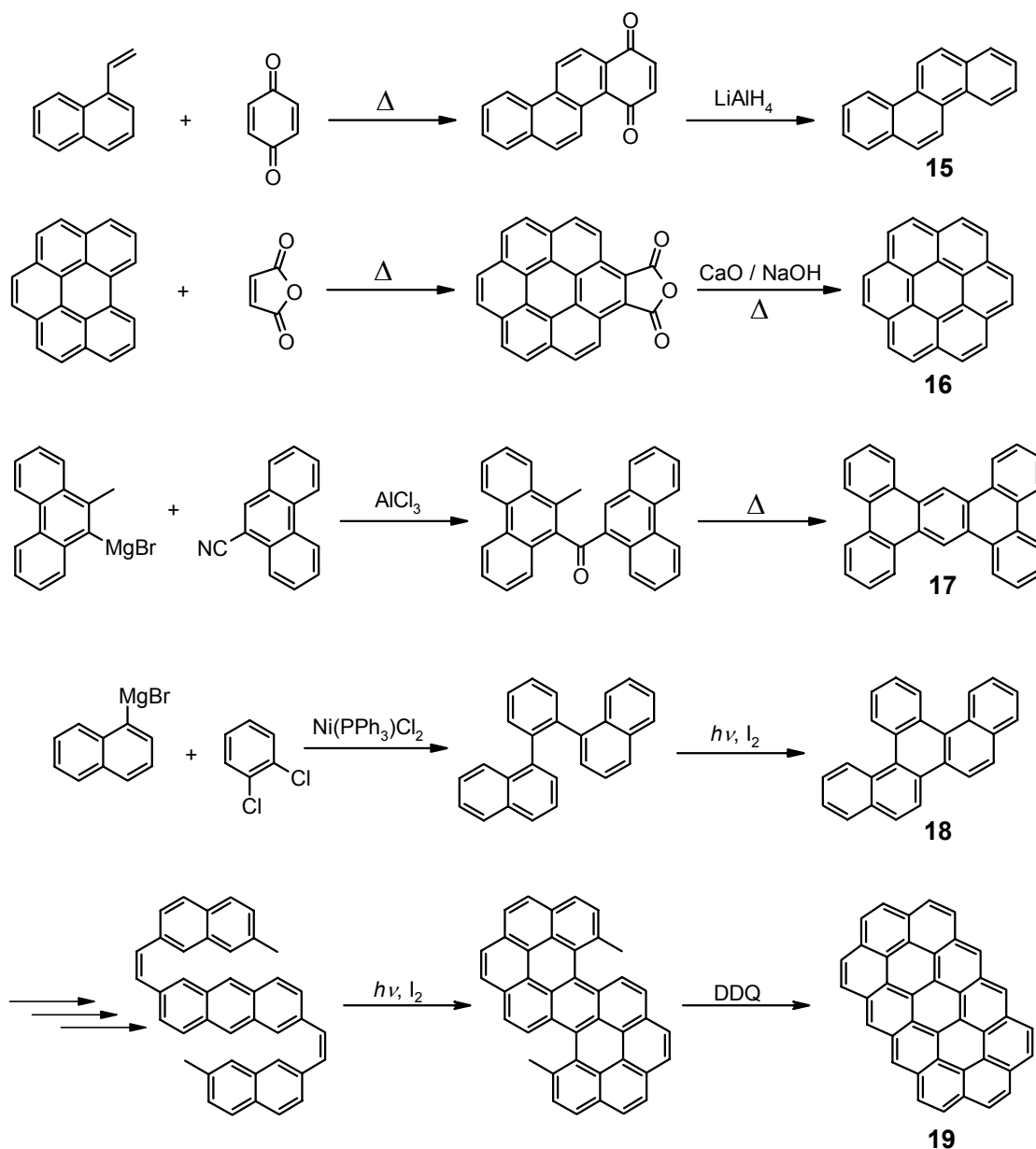


Figure 5. Selective syntheses of chrysene (15), coronene (16), tetrabenz[*a,c,h,j*]anthracene (17), benzo[*s*]picene (18) and circumanthracene (19).

One of the difficulties dealing with larger PAHs is the fact that with increasing size of the molecule, the solubility decreases dramatically, which prevents purification, complete spectroscopic characterization, investigation of their physical properties, and limits their application. A widely applied concept for increasing solubility of PAHs is the introduction of flexible alkyl side chains to the periphery, usually done at an early stage of the synthesis.^[43,44] Hereby, it becomes possible to create alkylated, high molecular weight PAHs, possessing considerably better solubility in organic solvents than their parent core structures. This is of great advantage for the analysis of spectroscopic and physical properties, and for the processing of the molecule. Further, introduction of these substituents modifies the materials properties dramatically, yielding a novel class of liquid crystalline compounds, where the all-benzenoid PAH cores serve as the rigid element.

In the group of Prof. Müllen, a synthetic approach was developed in recent years for the preparation of all-benzenoid PAHs in a size which was previously not thought possible. This synthetic concept is based on two steps: first, construction of a soluble, non-planar oligophenylene precursor of well-defined structure with a close spatial arrangement of the phenyl rings, which is similar to the framework of the target molecule, and second, planarization of this precursor to the target molecule by intramolecular oxidative cyclodehydrogenation. The synthesis of the necessary oligophenylene precursors can be achieved via three different routes: the intramolecular Diels-Alder reaction, the cyclotrimerization of diphenylacetylene derivatives and the intermolecular Diels-Alder reaction.

1.3.1 Synthesis of PAHs via intramolecular Diels-Alder reaction

An elegant entry to oligophenylene structures can be achieved by intramolecular [4+2] cycloaddition of suitable phenylene-vinylene derivatives, followed by aromatization of the newly formed cyclohexene structures. An example for such strategy is the synthesis of rhombic tribenzo [*hi,o,uv*]triphenylene[2,1,12,11-*bcdef*]ovalene (**23**), shown in Figure 6.^[45] The

para-terphenyl derivative (**20**) is subjected to a nearly quantitative intramolecular [4+2] cycloaddition at 135 °C to form the cyclohexene derivative **21**. Aromatization of **21** with 2,3-dichloro-5,6-dicyanoquinone (DDQ) yields corresponding tetraphenyl substituted tetrabenzo[*a,c,h,j*]anthracene (**22**), which is finally dehydrogenated oxidatively by copper dichloride/aluminium trichloride in carbon disulfide at room temperature, to the desired rhombic tribenzo[*hi,o,uv*]triphenylene[2,1,12,11-*bcdef*]ovalene (**23**).

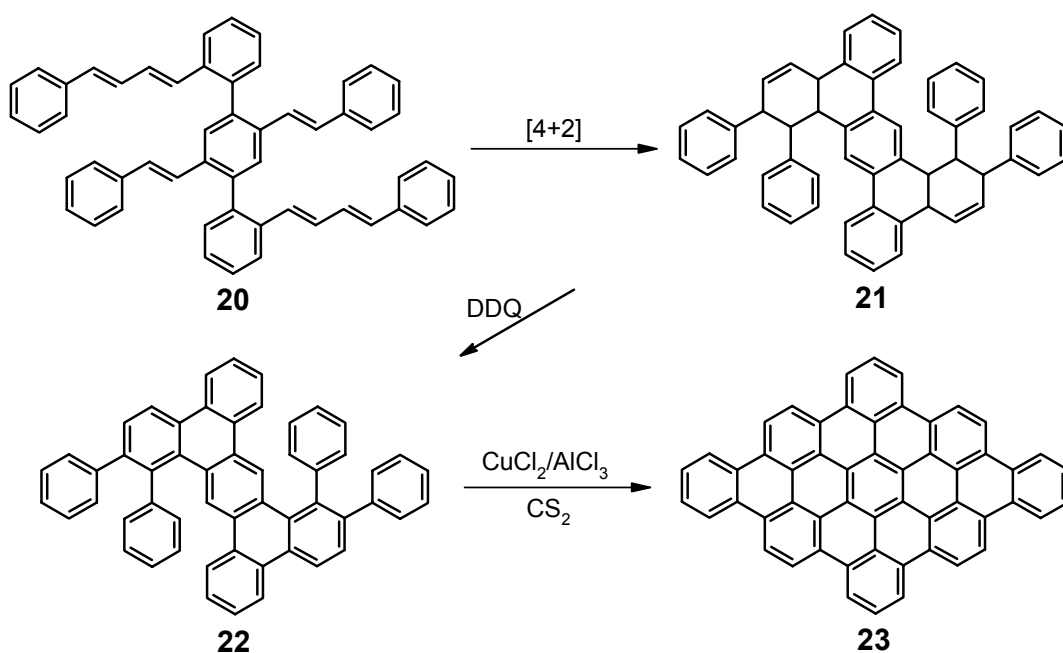


Figure 6. Synthesis of the tribenzo[*hi,o,uv*]triphenylene[2,1,12,11-*bcdef*]ovalene (**23**).

Simple variations in the phenylene-vinylene type starting material, following the synthetic concept introduced herein, permit entry to a series of other oligophenylenes with defined topology. However, access to the required Diels-Alder active phenylene-vinylene precursors is, in some cases, preparatively demanding. In addition, only certain topologies are accessible. Hence, this synthetic route is not applicable as a general concept for a wide variety of different PAH topologies and substitution patterns.

1.3.2 Synthesis of PAHs via cyclotrimerization of diphenylacetylenes

From a supramolecular aspect, the synthesis of all-benzenoid hydrocarbons with the hexagonal symmetry of benzene is of particular interest. The first homologue of this series of hexagonal aromatics is the hexa-*peri*-hexabenzocoronene (HBC) (**26**, Figure 7), which can be prepared by intramolecular cyclodehydrogenation of hexaphenylbenzene (**25**).^[46,47] The dicobalt octacarbonyl catalyzed cyclotrimerization of diphenylacetylene (also known as tolane) (**24**) is a well-established method for the synthesis of hexaphenylbenzene (**25**).^[48]

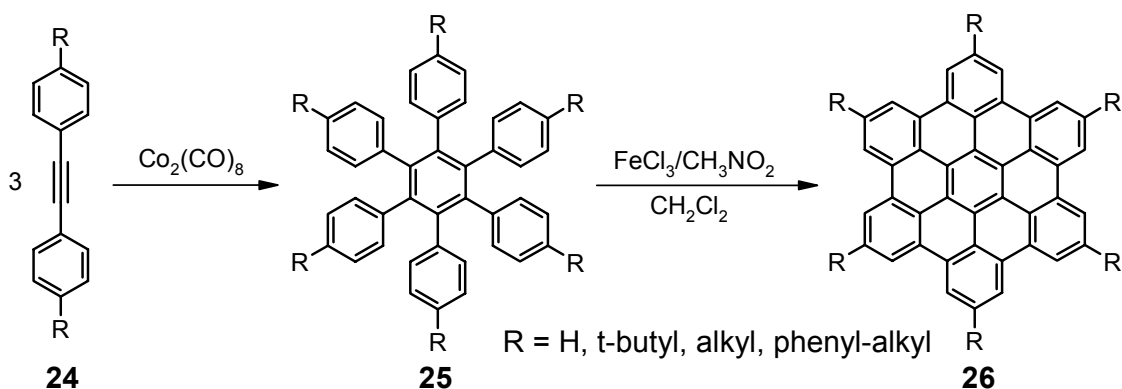


Figure 7. Synthesis of an HBC via cyclotrimerization of diphenylacetylene and subsequent oxidative cyclodehydrogenation.

The diphenylacetylene derivatives (**24**) are easily accessible by palladium-catalyzed ethynyl-aryl coupling, according to the methods of Heck,^[49] Cassar,^[50] or Hagihara and Sonogashira.^[51] However, it should be noticed that only symmetrical diphenylacetylenes lead to isomerically pure hexaphenylbenzenes. As the reaction conditions required for the trimerization of tolane tolerate a variety of functional groups such as alkyl or halogen, the cyclotrimerization offers a preparatively convenient route to all-benzenoid hydrocarbons with hexagonal symmetry, and the possibility of introducing solubilizing substituents, and further derivatization. The final, key step in the synthesis of HBC is the oxidative cyclodehydrogenation of the appropriate hexaphenylbenzene. Different oxidative

agents can be used for the cyclodehydrogenation reaction. In earlier work aluminium(III) chloride was widely used, however antimony(V) chloride and molybdenum(V) chloride were also examined. The cyclodehydrogenation using the above oxidative agents suffers from partial cyclization, chlorination of the aromatic core, phenyl ring migration and alkyl chain cleavage, which preclude the realization of clean alkylated HBC. To date the highest yields and widest tolerance towards functionalities other than simple alkyl chains has been achieved with iron(III) chloride dissolved in nitromethane, as a Lewis-acid and oxidant.^[52] These cyclodehydrogenation conditions were adopted and modified from the work of Kovacic, who discovered that benzene could be polymerized to poly-*para*-phenylenes by a Lewis-acid and an oxidant.^[53-55] A detailed history and description of the development of the dehydrogenation methods is discussed in reference [56].

1.3.3 Synthesis of PAHs via intermolecular Diels-Alder reaction

The cyclotrimerization of diphenylacetylene derivatives allows only the uniform functionalization of all six phenyl substituents in hexaphenylbenzene (**25**, Figure 7), or formation of non-uniform product mixtures. However, if one subjects diphenylacetylene derivatives (**24**) to an intermolecular [4+2] cycloaddition with a suitably substituted tetraphenylcyclopentadienone (**27**) (also known as tetracyclones), intermediate Diels-Alder adducts are formed that spontaneously extrude carbon monoxide at 200-250 °C to give the corresponding hexaphenylbenzene (**28**) (Figure 8).^[57-59] High boiling solvents such as diphenylether, are required for the intermolecular Diels-Alder reaction with diphenylacetylenes. The final step, oxidative cyclodehydrogenation of the hexaphenylbenzene, using iron(III) chloride dissolved in nitromethane, results in the desired HBC compound (**29**).

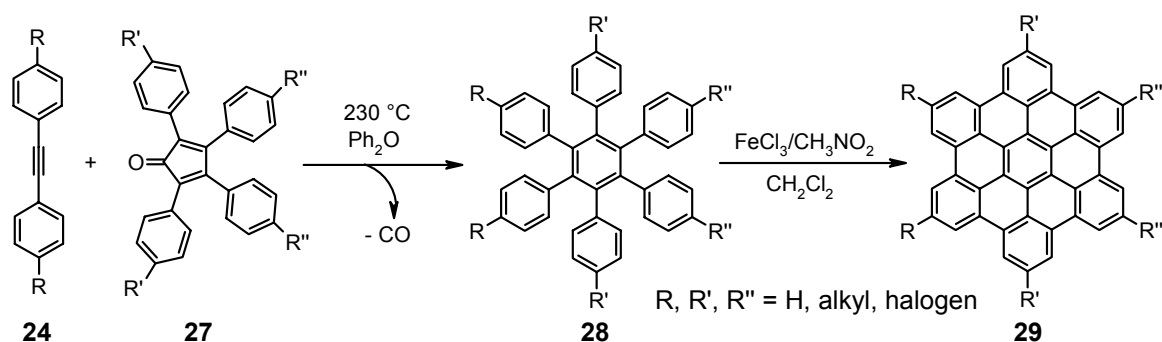


Figure 8. Synthesis of an HBC via intermolecular Diels-Alder reaction of diphenylacetylene and tetraphenylcyclopentadienone, and subsequent oxidative cyclodehydrogenation.

With the choice of appropriate substituents on the diphenylacetylene or tetraphenylcyclopentadienone, the intermolecular Diels-Alder reaction followed by a cyclodehydrogenation, opens the way to a broad spectrum of hexa-*peri*-hexabenzocoronenes, as shown in Figure 9. The nomenclature of "ortho" and "para" substitution is given in analogy to benzene, considering the hexagonal structure of HBC as "superbenzene". Further, the functions X can include for instance halogen atoms, which enable a further functionalization of the HBC using palladium-catalyzed coupling reactions. In this way, a multitude of HBC derivatives, with electron-withdrawing (ester, cyano) and -donating (alkoxy, amino) groups, which influence the electronic properties of the core, have been prepared.^[52]

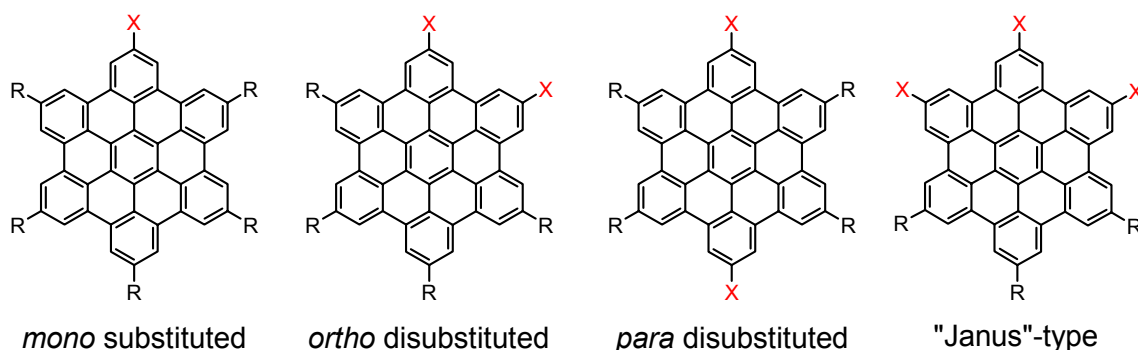


Figure 9. Different substitution patterns of HBC-derivatives.

Extended, structurally defined oligophenylene derivatives as precursors for large, all-benzenoid hydrocarbons with various topologies can be prepared by intermolecular [4+2] cycloaddition of other phenylethyne derivatives with tetraphenylcyclopentadienones.^[60-62] Suitable phenylethylenes are accessible by palladium-catalyzed Hagihara-Sonogashira coupling of bromine or iodine functionalized aromatics with acetylenes. As an example, synthesis of the polybenzenoid C₇₈H₂₆ hydrocarbon (**33**) via a double Diels-Alder reaction of 1,4-di(phenylethynyl)benzene (**30**) and tetraphenylcyclopentadienone (**31**), and subsequent cyclodehydrogenation of obtained oligophenylene (**32**) is shown in Figure 10.^[61]

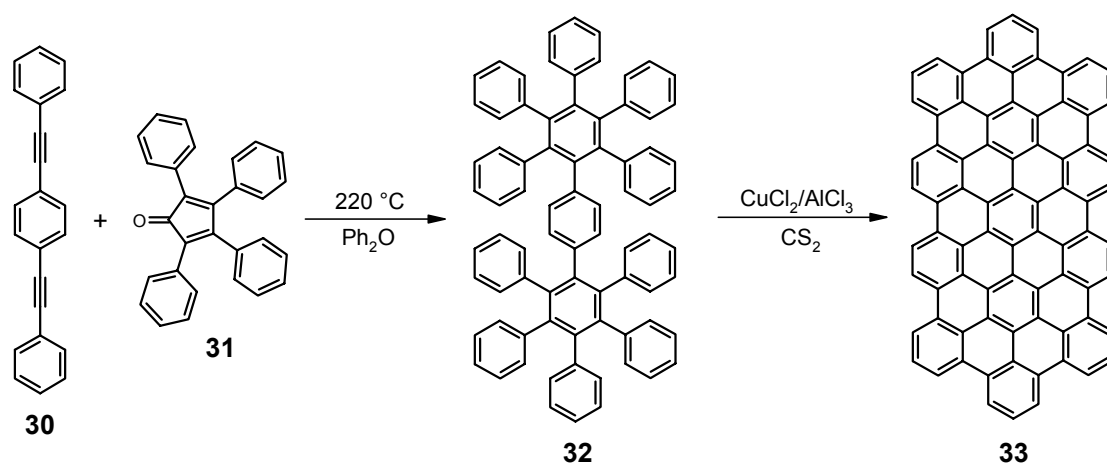


Figure 10. Route to a large C₇₈H₂₆ PAH (**33**) via double intermolecular Diels-Alder reaction and subsequent cyclodehydrogenation.

Terminal ethynyl groups are less sterically hindered and more reactive than the phenylethynyl derivatives described above. Thus, they may also be employed in a cycloaddition with tetraphenylcyclopentadienone, so that the wealth of easily accessible oligophenylene derivatives can be further extended.^[63,64] As an example, synthesis of the large polybenzenoid C₁₃₂H₃₄ hydrocarbon (**36**) via Diels-Alder reaction of 3,5,3',5'-tetraethynyl-biphenyl (**34**), containing four terminal ethynyl groups, with tetraphenylcyclopentadienone (**31**), and subsequent cyclodehydrogenation of obtained oligophenylene (**35**) is shown in Figure 11. In the case of terminal ethynyl groups, Diels-Alder reaction can be completed in refluxing *o*-xylene, at a lower temperature (145 °C). A combination of

aluminium(III) chloride and copper(II) trifluoromethanesulfonate or copper(II) chloride in carbon disulfide, as well as iron(III) chloride in nitromethane have in many cases proven to be the best reagents for the planarization of these unsubstituted oligophenylenes.

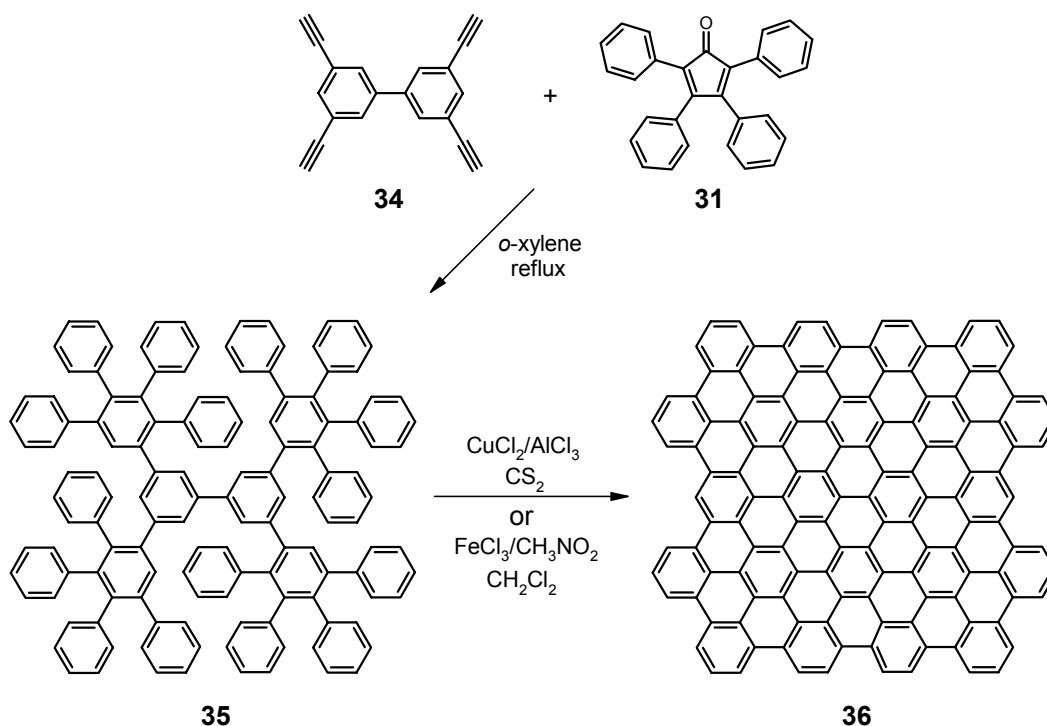


Figure 11. Route to larger $\text{C}_{132}\text{H}_{34}$ PAH (**36**) via intermolecular Diels-Alder reaction and subsequent cyclodehydrogenation.

The poor solubility of large non-substituted PAHs such as **33** and **36** limits their conventional spectroscopic characterization in solution. Alternatively, solid-state analytical methods such as matrix-assisted laser desorption/ionization time-of-flight (MALDI-TOF) mass spectrometry, solid-state UV/Vis and Raman spectroscopy are standard tools for the characterization of insoluble PAHs.^[65-68] Furthermore, they could be deposited onto substrate surfaces such as highly ordered pyrolytic graphite, molybdenum sulphide, copper and gold as ordered monolayers with characteristic lattice parameters, determined by low-energy electron diffraction (LEED) or by scanning tunneling microscopy (STM).^[45,69-72]

1.4 "Superbenzene" chemistry

One of the major goals of PAH chemistry is the synthesis of ever improved, molecularly defined graphite model compounds. By employing the previously described synthetic concept of planarization of suitable oligophenylenes, PAHs containing up to 222 carbon atoms have become accessible (Figure 12).^[73]

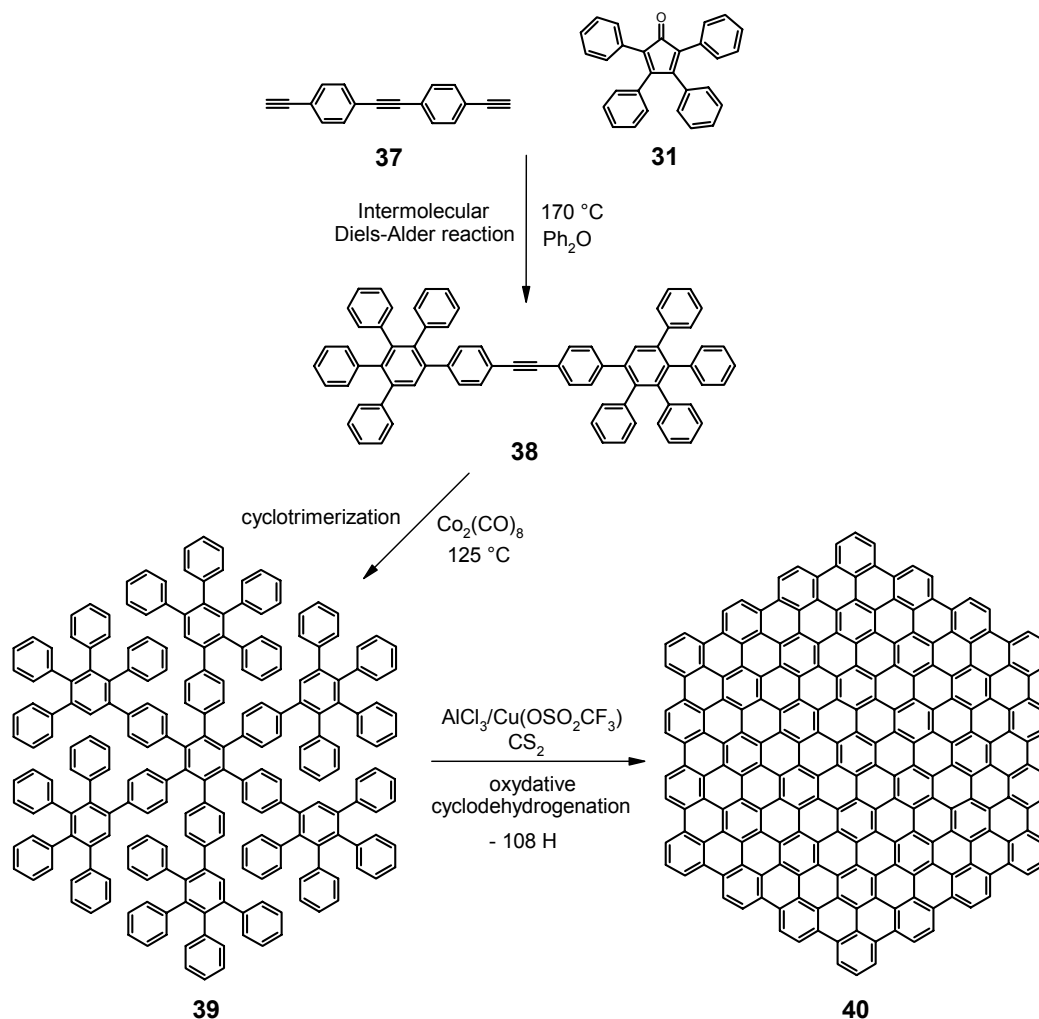


Figure 12. Synthesis of C₂₂₂H₄₂ PAH (**40**).

Thus, the synthesis of the oligophenylene derivate **39**, which is composed of 37 phenyl rings, involves a double intermolecular Diels-Alder reaction of tetraphenylcyclopentadienone (**31**) with the terminal ethynyl groups of tolane **37**,

followed by the cyclotrimerization of the newly formed, phenyl-substituted tolane **38**. MALDI-TOF mass spectrometry proves that, indeed, 108 hydrogens are removed upon transition from **39** to **40**, and the resulting organic material is 99% pure. $C_{222}H_{42}$ (**40**) is the largest PAH that has been synthesized so far.

As already mentioned, HBC with its hexagonal symmetry can be considered as a "superbenzene" where each peripheral benzene ring is equal to one sp^2 -carbon of benzene. In this fashion, one includes the well-known nomenclature for substitution patterns for benzene such as *ortho*, *meta*, and *para*.^[52] Furthermore, higher homologous PAHs which have been synthesized, can be regarded as "supernaphthalene" (**41**),^[60] "superbiphenyl" (**42**),^[74] "superphenalene" (**43**),^[60] and "supertriphenylene" (**44**),^[60] in which two, three and four "superbenzenes" are fused, respectively (Figure 13).

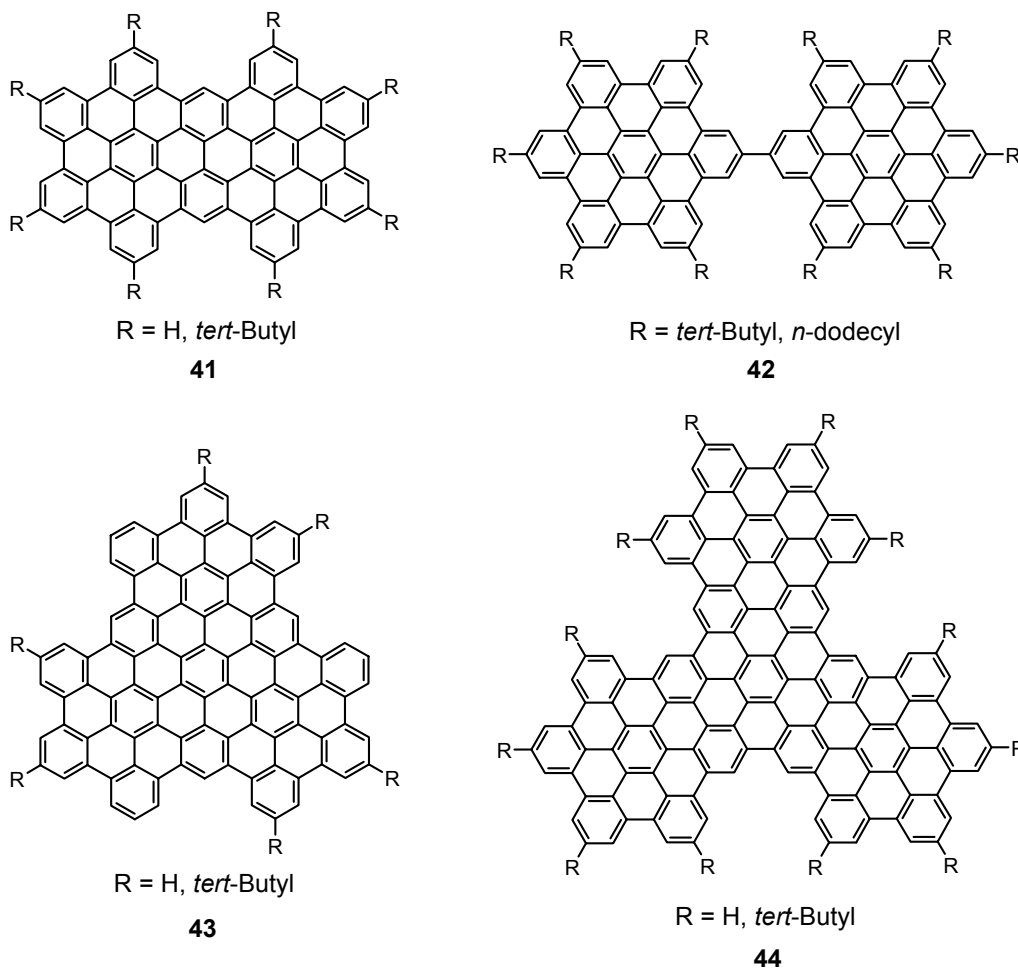


Figure 13. Structures of "supernaphthalene" (**41**), "superbiphenyl" (**42**), "superphenalene" (**43**), and "supertriphenylene" (**44**).

1.5 Discotic liquid crystals

The liquid crystal (LC) phase (mesophase) is a well-known state of matter, which lies between the solid and isotropic liquid phases. In the crystal phase the molecules have a high degree of order, occupying fixed positions in the lattice. Conversely, in the isotropic liquid phase only a short-range order dominates, the molecules are mobile and have no orientation with respect to each other. The LC phase (mesophase) shares properties of both the crystal and liquid phases, possessing an intermediate molecular order between the perfect three-dimensional long range positional and orientational order found in crystals, and the absence of long-range order found in the isotropic liquids. The LC state is characterized by having a long-range orientational order and possible partial positional order (Figure 14).

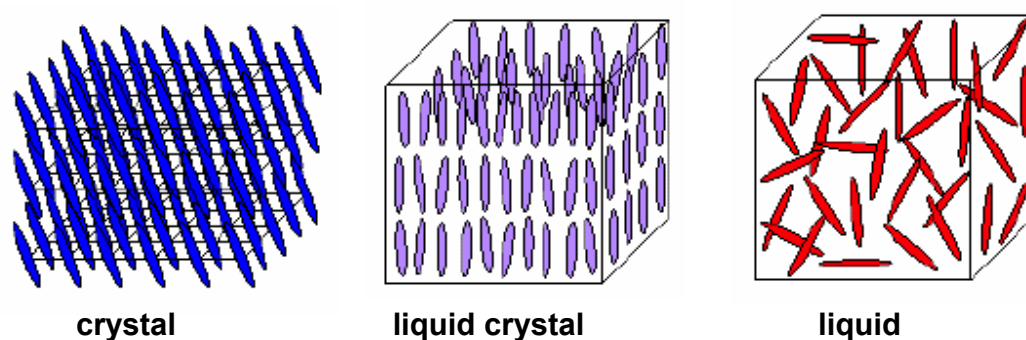


Figure 14. Schematic representation of crystal-, liquid crystal- and liquid-phase.

The discovery of liquid crystals in 1888 is commonly attributed to the Austrian botanist F. Reinitzer, who observed that a material known as cholesteryl benzoate had two distinct melting points.^[75] The crystals of this material melted at 145.5 °C into a hazy liquid, which upon further heating to 178.5 °C became clear. Since then, immense efforts in research and development have pushed this field to where it now stands.

According to classic concept, LCs are divided into two main classes: thermotropic LCs, whose mesophase formation is temperature dependent, and lyotropic LCs, whose mesophase formation is concentration and solvent

dependent. The essential requirement for a molecule to be a thermotropic is a structure consisting of a central rigid core (often aromatic) and a flexible peripheral moiety (generally aliphatic groups). The shape of the molecules is an important criterion for determining the LC behavior. This structural requirement leads to two general classes of LCs: calamitic LCs, characterized by the rod-like shape of molecules, and discotic LCs, characterized by the disc-like core of the molecule.

The first discotic LC was discovered by S. Chandrasekhar in 1977, in the hexa-alkanoyloxy-benzenes (**45**, Figure 17).^[76] With a few exceptions, discotic LCs consist of planar central rigid core surrounded by flexible aliphatic chains at its periphery. Discotic LCs can show three types of mesophase, with varying degrees of organization: columnar (col), nematic-discotic (N_d) and lamellar-discotic, where the structure of the latter has not yet been completely elucidated (Figure 15).^[77]

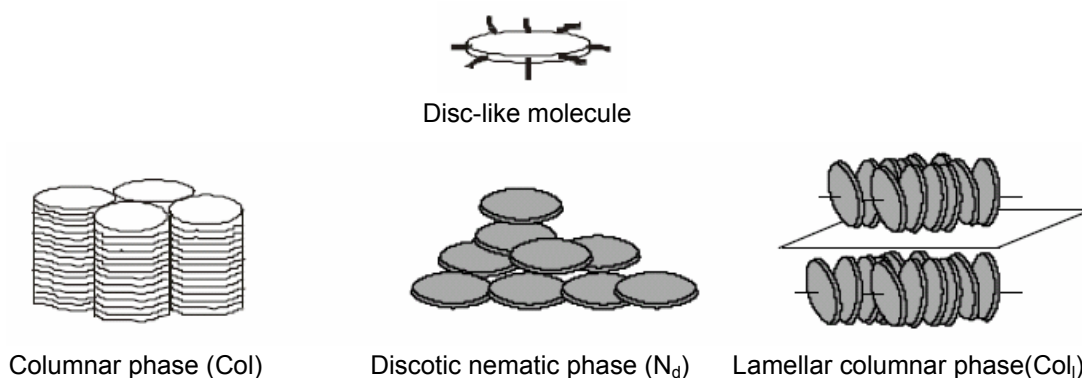


Figure 15. Schematic representation of different mesophases of discotic LCs.

Nematic discotic (N_d) is the least ordered mesophase in which the positional order is lost, molecules have only orientational order, and the short axes of the molecules preferably align parallel. The most common mesophases formed by discotic molecules are columnar mesophases, in which the molecules stack one on the top of another forming columns, which can further arrange into different lattices corresponding to hexagonal, rectangular and oblique columnar phases

(Figure 16). Additionally, the degree of established organisation within the columns can be denoted with ordered (o), disordered (d) and tilted (t), as depicted in Figure 16, bottom.

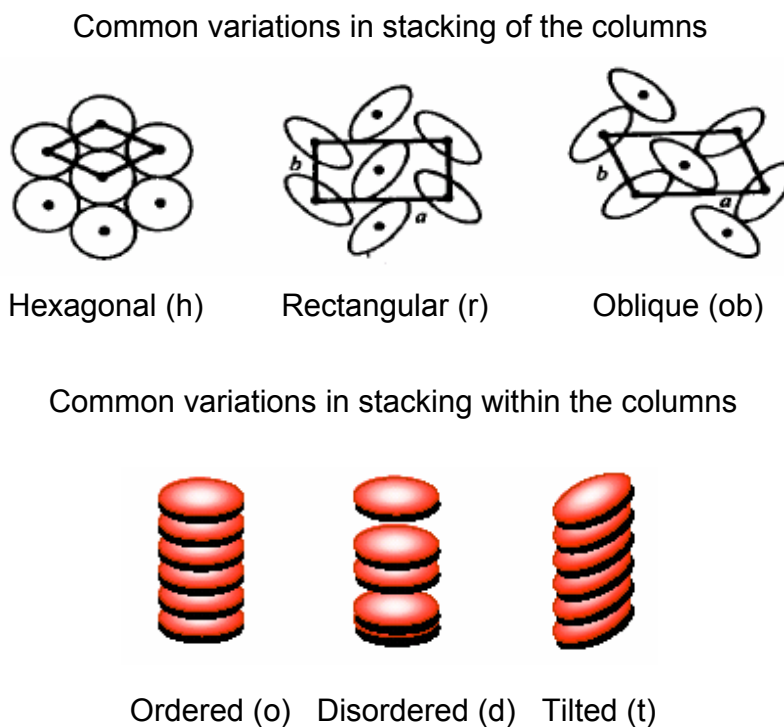


Figure 16. Schematic representation of structures of columnar mesophases.

The discovery of discotic liquid crystals opened up a whole new field of liquid crystal research. The number of known discotic LCs is growing continuously; currently more than 1500 different discotics are known.^[78] Their columnar arrangement is an especially promising structure for anisotropic transport of charge carriers along the columns. Discotic LC are being recognized for their potential applications in photovoltaic devices, field effect transistors (FETs), light emitting diodes (LEDs) and other molecular electronics.^[79] In Figure 17 some of the most prominent discotic LC are displayed. These range from the first reported discotic LC namely hexa-alkanoyloxy-benzenes (**45**), to porphyrins (**46**),^[80] phthalocyanines (**47**),^[80] hexaazatriphenylenes (**48**),^[81] perylenes (**49**),^[82] triphenylenes (**50**),^[80] dibenzopyrenes (**51**),^[83] and hexabenzocoronenes (HBC)

(**52**)^[46,47,52,84-86] which possess the most extended aromatic core. The latter four belong to the class of polycyclic aromatic hydrocarbons (PAHs).

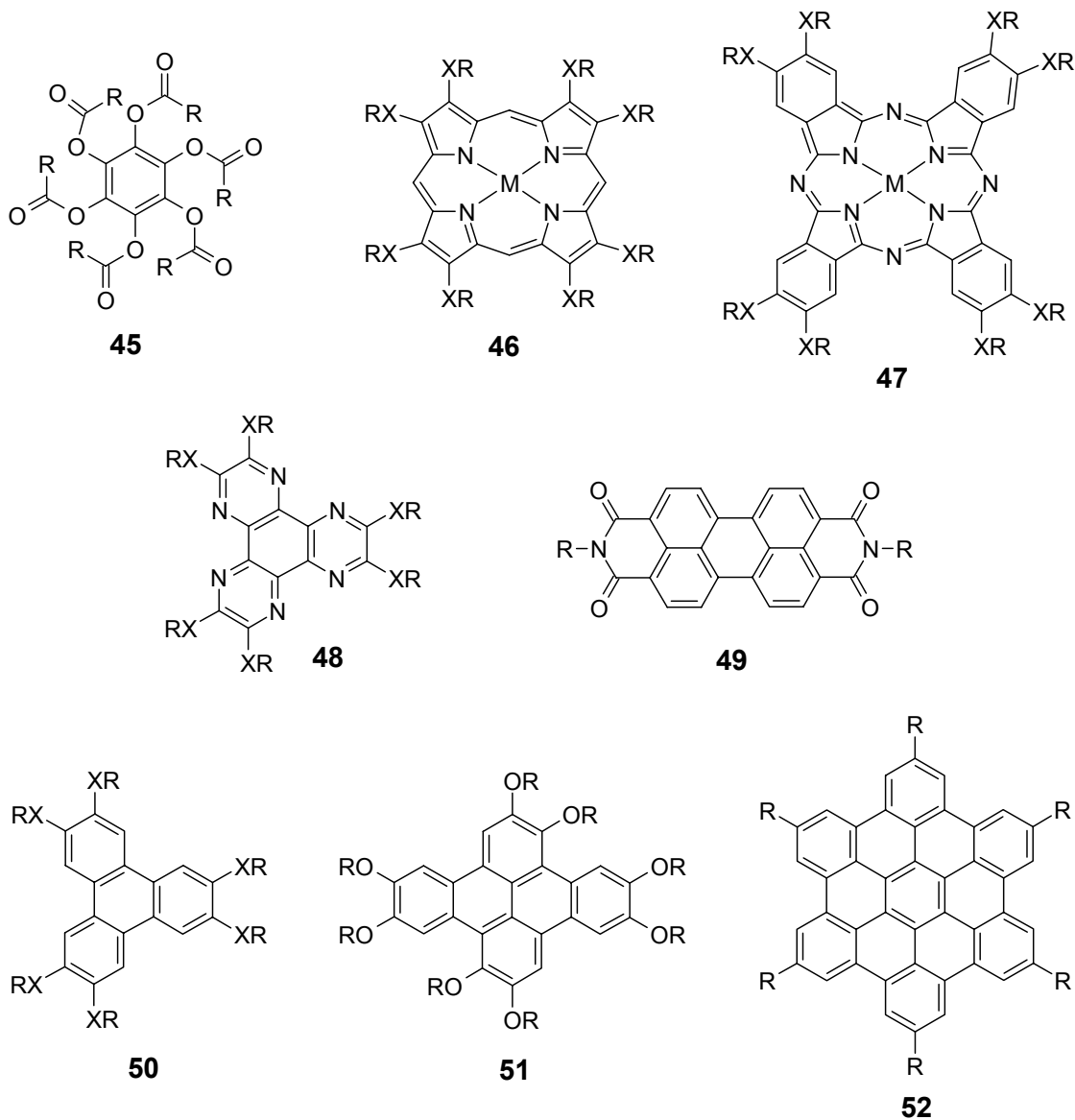


Figure 17. Selection of discotic liquid crystals.

Among the above mentioned liquid crystalline PAHs, triphenylenes (**50**) are the ones that have been studied most extensively in view of their mechanism of charge transport,^[87] one-dimensional energy transport,^[88] photoconductivity,^[89] ordering of multilayers (investigated by using Langmuir-Blodgett techniques),^[90] orientation of two-dimensional crystals (investigated using scanning tunneling

microscopy (STM))^[91] and their alignment under the influence of a magnetic field^[92] or infrared irradiation.^[93] The synthesis of triphenylene derivatives is relatively easy and straightforward,^[94] and generally they possess good solubility, long range order in the mesophase and a high charge carrier mobility along the columns, as well as thermal and chemical stability. However, symmetrically substituted triphenylenes suffer from having only a very narrow temperature range for liquid crystallinity. The greatest range of liquid crystallinity which has been observed is 53 °C for 2,3,6,7,10,11-hexapentyloxytriphenylene.^[95] Elongation of the alkyl tails leads to a lowering of the crystal-liquid crystal transition temperature, but also the isotropization temperature; making the alkyl chains shorter precludes the mesophase formation, but increases the mobilities by an order of magnitude. Adam and co-workers discovered that 2,3,6,7,10,11-hexahexylthiotriphenylene exhibits a helical columnar phase, which leads to an increase of charge carrier mobility to an order of magnitude comparable with organic single crystals.^[89] Ringsdorf and co-workers have shown that the introduction of a single electron-withdrawing group directly onto the polyaromatic core produces a broader range of liquid crystallinity relative to the fully symmetrical compounds.^[96] It has been also shown by Wendorff that introduction of bulky substituents destabilizes the mesophase; the isotropization temperature is lowered and the melting point of the crystalline phase, as well as the tendency to crystallize from the mesophase, is increased.^[97] Unsymmetrically substituted triphenylene derivatives were also prepared and they can also form ordered columnar phases when appropriate substituents were introduced.^[98] From the examples given above, it can be seen that by varying the substituents on the perimeter of the triphenylene disc, the properties change dramatically.

Increasing the size of the core results in enhanced π - π overlap, thus giving rise to larger phase widths and more stable mesophases. Alkyl or phenyl-alkyl substituted hexabenzocoronenes (HBCs) and their functionalized derivatives are discotic LC materials with one of the largest PAH cores (approximately three times the size of triphenylene). Since the first alkyl substituted HBC was synthesized in 1995 by P. Herwig,^[46] both the methods for synthesis and understanding of the structure-property relationships have been subjects of

intense investigation in the group of Prof. Müllen. Two different synthetic routes for the preparation of HBCs have already been described in Section 1.3. Some of the alkyl and phenyl-alkyl hexa-substituted HBCs are shown in Figure 18.

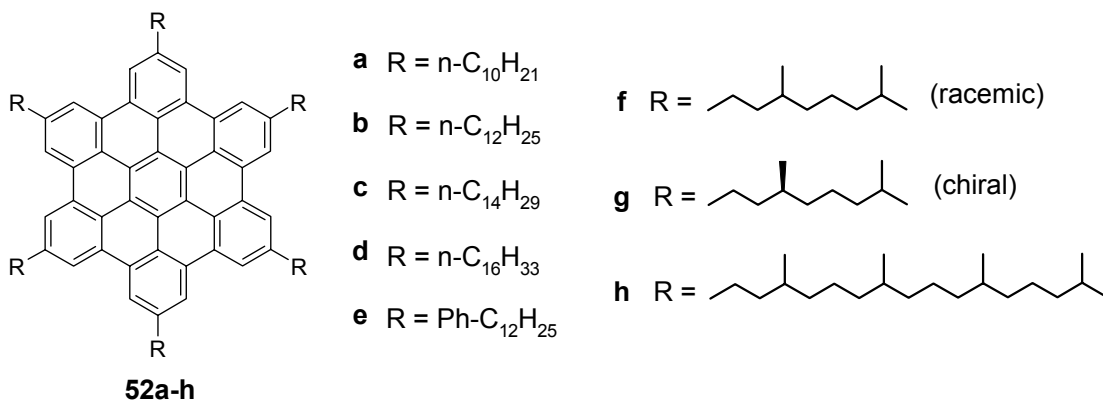


Figure 18. Selection of hexa-substituted HBCs.

The HBC based LC materials normally have a low temperature phase, which is traditionally called a "crystalline" phase, followed by at least one or more columnar LC phases. The "crystalline" phase is characterized by a higher degree of order than the high temperature phase, loss of mobility of aromatic core and tilting of the discs relative to the columnar axis (Figure 19).

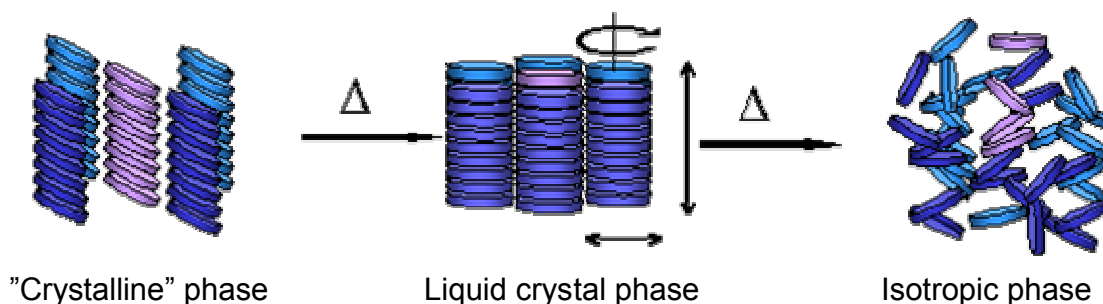


Figure 19. Schematic representation of "crystal"-liquid crystal and liquid crystal-isotropic transitions for HBC.

At elevated temperatures, depending upon the substituents, a transition from "crystalline" to LC phase can be observed. In the LC phase, the aliphatic chains are molten and the aromatic cores, which have also some translational and

rotational mobility, are stacked orthogonally to the columnar axis, and the columns arranged in a two-dimensional, usually hexagonal, lattice. Transition to the isotropic state or breaking the columnar aggregates, requires a high energy and occurs at higher temperatures ($> 400\text{ }^{\circ}\text{C}$) which is in most cases higher than the on-set of decomposition (decomposition starts at $300\text{ }^{\circ}\text{C}$ by cleavage of alkyl chains). For example, hexakis(*n*-dodecyl)-*peri*-hexabenzocoronene (**52b**, HBC-C₁₂) shows a crystalline phase below $107\text{ }^{\circ}\text{C}$, and above a hexagonally ordered LC phase until isotropization at $417\text{ }^{\circ}\text{C}$, where the compound enters the liquid state (Table 1).

Compound	T _m [$^{\circ}\text{C}$]	T _i [$^{\circ}\text{C}$]	Phase width [$^{\circ}\text{C}$]
52 b	107	417	310
52 e	15	420	405
52 f	96	430	334
52 g	81	420	339
52 h	-36	231	267

Table 1. Phase transition temperatures of hexa-substituted HBCs.

The phase transition temperatures can be tailored by choosing the type of alkyl chain periphery. By introducing bulky or branched alkyl substituents, the transition temperatures can be lowered and the solubility increased. Thus, introduction of six chiral or racemic 3,7-dimethyloctanyl chains at the periphery of the HBC (**52f**, **52g**, HBC-C_{8,2}) increased solubility and processability of compounds, while the thermal crystalline-LC transitions are shifted to lower temperatures, relative to analogous HBC carrying *n*-alkyl chains.^[85] The isotropization temperature can be further lowered by six long branched alkyl chains such as 3,7,11,15-tetramethylhexadecanyl (**52h**, HBC-C_{16,4}).^[86] By introducing phenyl-alkyl substituents, a room temperature liquid crystalline HBC (**52e**, HBC-PhC₁₂) was obtained.^[84] The *mono*- and *di*-bromo-functionalized HBC derivatives (Figure 9) were subjected to palladium-catalyzed coupling reactions to give donor (alkoxy, amino) as well as acceptor (ester, cyano) substituted

derivatives.^[52] Their mesoscopic behavior as well as their packing in two and three dimensions was studied. It was shown that the different substituents in HBC derivatives induce only small differences in the mesophase structure and stability. This is in contrast to observations made for triphenylenes where the mesophase stability is very sensitive towards different substituents or substitution patterns. An explanation for the different properties of substituted HBCs compared with triphenylenes is the stronger π - π interactions and the larger size of the aromatic core in case of HBC, which dramatically stabilizes the mesophase and allows the incorporation of different substituents without losing mesomorphic properties. The direct visualization of two-dimensional crystals and liquid crystals of HBC derivatives on surfaces such as highly oriented pyrolytic graphite (HOPG) and molybdenum disulfide was achieved by STM techniques.^[46,52,99] The *mono*-bromo-substituted HBC was also used as a starting material for synthesis of new amphiphilic HBC derivatives, carrying five branched alkyl side chains and one polar group. The polar group is either a carboxylic acid moiety or an electron acceptor moiety (anthraquinone).^[100] It was shown that well-defined thin films of these amphiphilic HBC derivatives may be obtained by Langmuir-Blodgett techniques.^[101] Recently, hexakis-(4-iodophenyl)-*peri*-hexabenzocoronene, a novel functionalizable mesogenic building block was prepared by a rational multistep synthesis^[102]. Although insoluble in common solvents, it can be obtained in pure form and then further functionalized via six-fold palladium-catalyzed Hagihara-Sonogashira coupling to give HBC derivatives with an extended rigid core, which exhibit highly ordered columnar superstructures (helical columnar mesophases).

1.5.1 Mesophase characterization

For potential applications of discotic LC materials in electronic devices, a deeper understanding of the order in the bulk material is a key to optimization. Differential scanning calorimetry (DSC), polarized optical microscopy (POM), thermogravimetric analysis (TGA) and X-ray diffractometry are necessary tools

for structural characterization of LC materials. The temperature of phase transitions of the materials are determined by DSC. TGA gives information about thermal stability of the material (under nitrogen). The transition to the mesophase is often accompanied by birefringence and the formation of characteristic textures. These textures, which can be observed by polarized optical microscopy, provide an indication of the type of mesophase. The macroscopic arrangement of the molecules within different phases is best determined by X-ray scattering methods. A lot of information regarding the nature of the phases can be obtained by powder X-ray diffraction, however, it is not possible to distinguish between reflections arising from intercolumnar and intracolumnar order. Therefore, temperature dependent X-ray measurements are performed on oriented samples. Good macroscopic orientation of the columnar structures along the axes of filaments can be accomplished by extrusion of samples through a circular orifice. Wide angle X-ray scattering (WAXS) measurements recorded with vertical orientation of filaments, perpendicular with respect to the incident X-ray beam provide 2D diffractograms with information about the ordering within the columns and the arrangement of these columns, partitioned along the vertical and horizontal axis, respectively (Figure 20). If some 3D correlation exists, then reflexes appear along the diagonals.

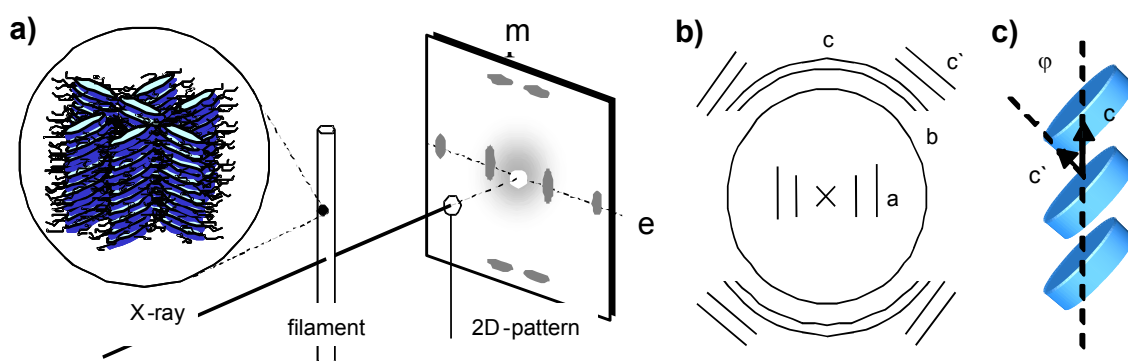


Figure 20. (a) Experimental setup for the X-ray analysis of extruded filaments; (b) schematic representation of the X-ray diffractogram; (c) intracolumnar spacing in the tilted columns.

The recorded diffractograms can be analyzed equatorially (e), meridionally (m) or integrated over the azimuthal angle. A schematic representation of a

diffraction pattern is shown in Figure 20b where common Bragg reflections from the columnar packing are in the fiber plane and lie on the equator (a). The diffuse scattering of aliphatic side chains, which are not oriented appear as a ring (b). The discs belonging to the same column are parallel to the fiber axis and give rise to reflections that lie on the meridian (c). If discs are tilted within the column, then additional reflexes appear along the diagonal (c').

Solid-state NMR spectroscopy is also a very powerful tool to understand the packing mode and dynamics on a molecular level, and can be used in combination with X-ray scattering.^[103]

1.5.2 Charge carrier mobility

Overlapping π -orbitals in the stacked aromatic cores provide coaxially-insulated conductive pathways which offer a unique possibility for the one-dimensional transport of charge. This makes discotic compounds serious candidates for application as organic charge transport layers in a variety of devices such as field effect transistors (FETs), photovoltaic cells and electroluminescent displays. The mobilities of the charge carriers can be estimated in a number of ways including time of flight (TOF) photoconductivity, pulse radiolysis time-resolved microwave conductivity (PR-TRMC), and in standard device (e.g. FET) configurations.^[104] PR-TRMC utilizes a rapidly oscillating electric field to probe charge carrier motion without the need for electrodes, which are required in the case of TOF measurement. The mobility values for the LC phases of HBCs, recorded by PR-TRMC are the highest ever found for discotic materials, and are well in excess of the value of $0.1 \text{ cm}^2\text{V}^{-1}\text{s}^{-1}$ found by both PR-TRMC and TOF techniques for the helical columnar phase of 2,3,6,7,10,11-hexahexylthiotriphenylene.^[105] The values are in fact comparable with the room-temperatures mobilities determined for single crystals of aromatic compounds. The highest values ($1.13 \text{ cm}^2\text{V}^{-1}\text{s}^{-1}$) are observed in some of the "crystalline" phases, while transition to the mesophases coincides with a distinct decrease in mobilities ($0.17\text{-}0.46 \text{ cm}^2\text{V}^{-1}\text{s}^{-1}$).^[106] As an example, temperature

dependence of one-dimensional charge carrier mobility for HBC-C₁₂ (**52b**) is depicted in Figure 21.

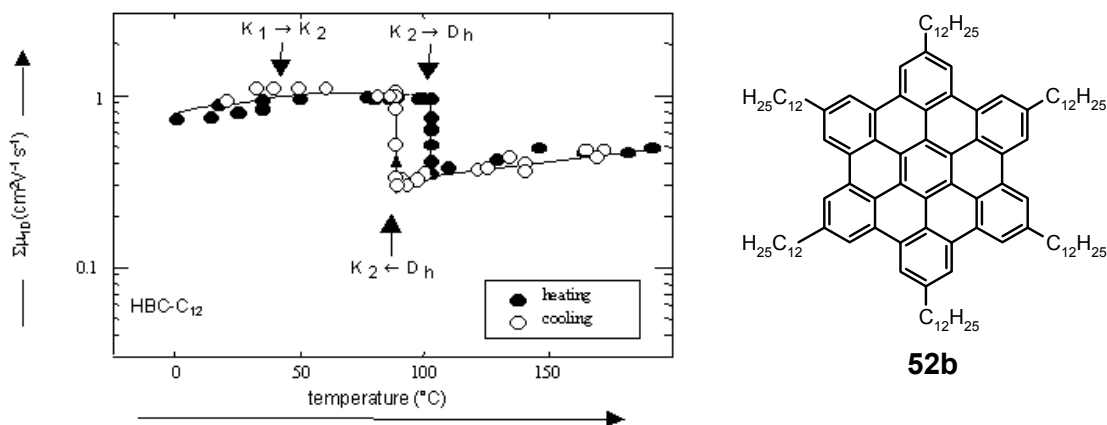


Figure 21. The temperature dependence of one-dimensional charge carrier mobility of HBC-C₁₂ (**52b**)

In case of HBC-C₁₂ (**52b**), upon heating mobility remains almost constant at 0.96 cm²V⁻¹s⁻¹ up to approximately 105 °C, where an abrupt decrease in charge carrier mobility down to 0.38 cm²V⁻¹s⁻¹ occurs within a few degrees Celsius. After this, no further change in mobility is observed up to the maximum temperature of 200 °C attainable in the PR-TRMC measurements. Upon cooling, the same behavior is detected with a slight hysteresis (Figure 21). The drop in charge carrier mobility occurs at the temperature at which the HBC-C₁₂ transforms from the crystalline phase into the columnar hexagonal mesophase, and is most probably due to the onset of uniaxial rotation of the molecules. A similar temperature dependant behavior has been reported for the charge carrier mobility of triphenylenes and phthalocyanines.^[107] On the other hand, for HBC-PhC₁₂ (**52e**) which is LC at room temperature, no evidence is found for an abrupt change in charge carrier mobility at any temperature within the range studied, and the absolute value of the mobilities at elevated temperatures were very close to those for the mesophases of alkyl substituted HBCs.^[106]

1.6 Discotic liquid crystals as semiconductors in electronic and optoelectronic devices

Considerable scientific and technological efforts have recently been devoted to discotic liquid crystals as functional materials for applications as active components of field-effect transistors (FETs), photovoltaic cells, and light-emitting diodes (LED).^[79,108-110] This interest can be explained by the increased charge carrier mobility in discotics as compared to conventional conjugated polymers. Generally, the high charge carrier mobility results from the ability of the discotics to self-organize into columns thereby maximizing the overlap of frontier orbitals. Furthermore, their liquid crystalline properties offer the possibility of obtaining extensive, well-organized layers in which the columnar orientation can be controlled and self-healing of structural defects can occur. They also have the advantage that they can be processed extremely cheaply over large areas at low temperatures by processing directly from solution.

1.6.1 Field effect transistors (FETs)

Phthalocyanines were probably the first reported organic semiconductors, and the ones that have been studied the most. They are thermally stable up to 400 °C and are easy to evaporate under vacuum. The field effect was reported in phthalocyanines as early as 1970 and FETs were made in 1988.^[111] Their field-effect mobility ranges between 10^{-4} and 10^{-2} $\text{cm}^2\text{V}^{-1}\text{s}^{-1}$.^[111-113] The key problem with phthalocyanines remains their extreme sensitivity to oxygen.

Recently, it was shown that substituted HBCs (HBC-PhC₁₂, HBC-C_{8,2}) can be processed from solution, to form films with supramolecularly ordered columnar stacks which lie parallel to the substrate and can be oriented uniaxially onto poly(tetrafluoroethylene) (PTFE) alignment layers.^[114] This high interfacial order achieved by solution processing under ambient conditions is a required for FETs. By implementation of these aligned semiconducting films, high FET mobility up to 10^{-3} $\text{cm}^2\text{V}^{-1}\text{s}^{-1}$ and a high on/off ratio of 10^4 was achieved. A typical FET

configuration with discotic molecules as the electronically active component is shown in Figure 22.

The control of the order and orientation of discotic liquid crystalline materials is a crucial point for the successful device application. An "edge-on" arrangement of the columnar mesophase is required for devices such as organic FETs, while photovoltaic cells and LEDs dictate "face-on" arrangement (homeotropic alignment) as shown in Figure 22. Phenomenologically, "edge-on" alignment is the preferred orientation of discotic molecules and can be achieved by different processing techniques.^[114-120] Homeotropic alignment in thick films can be achieved thermally by cooling columnar materials from the melt, or annealing just below the isotropization temperature of materials.^[121-123]

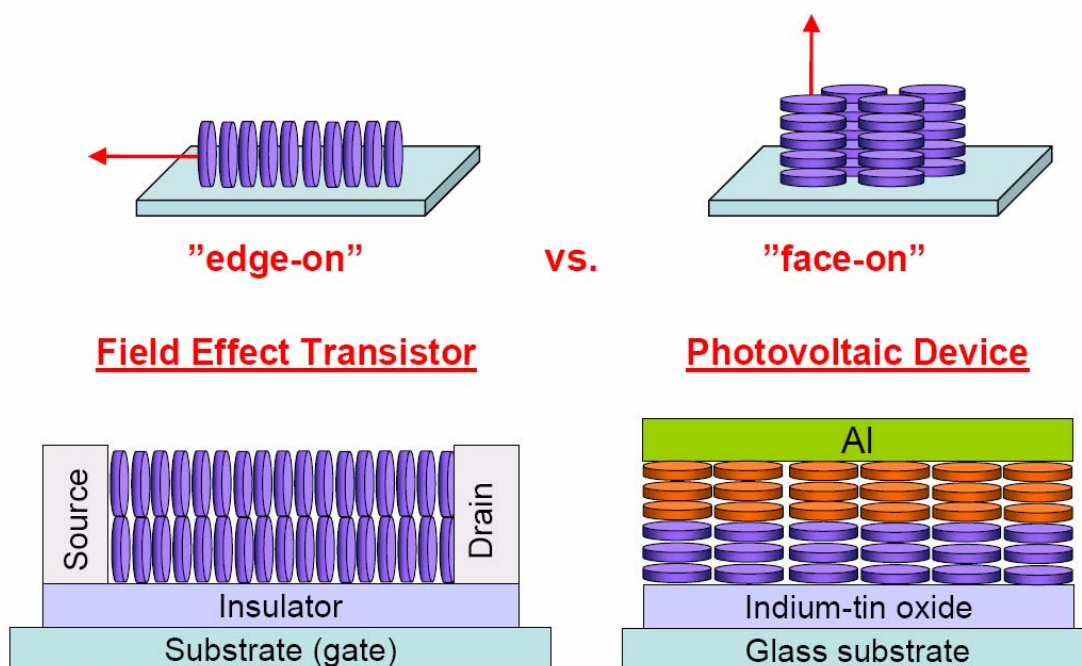


Figure 22. Schematic representation of two different electronic device types and their desired arrangement of discotic molecules as electronically active components: "edge on" for FETs *versus* "face-on" for photovoltaic devices.

1.6.2 Photovoltaic devices

Solar cells with high efficiency are usually fabricated from inorganic semiconductors.^[124] Flat-plate photovoltaic technology of today is based mainly

on single or polycrystalline silicon solar cells. However, the technology is too expensive for many applications to be viable. Organic thin-film solar cells are very attractive for flat-plate terrestrial applications because they can be fabricated using potentially low-cost methods, which can process a large area substrate in an economic way. The basic structure of a solar cell consists of two layers of semiconductors that form a p-n junction that are sandwiched between two electrodes, one of which being transparent (Figure 22).

Early attempts to produce photovoltaic cells with phthalocyanine LC resulted in devices with low efficiency, probably due to poor alignment of the LC.^[125] Recently, Schmidt-Mende and co-workers constructed a p-n type photovoltaic solar cell using discotic liquid crystal HBC-PhC₁₂ as the hole transporting layer and crystalline perylene diimide (PDI) dye as electron transporting layer.^[126] A mixture of HBC-PhC₁₂ and PDI in solution were spin-coated onto indium tin oxide (ITO). Photodiodes were prepared by the evaporation of aluminum onto HBC:perylene blend films. External quantum efficiencies of up to 34% (at 490 nm) and power efficiencies of 2% were obtained. These efficiencies are comparable with the best ones reported for organic photovoltaic devices.

1.6.3 Light emitting diodes (LEDs)

π -Stacked organic materials are also capable of electroluminescence and over recent years they have been of interest to investigate their potential for applications in the area of organic light emitting diodes (OLEDs). Initially triphenylene based discotic LCs were employed as hole transport materials.^[127,128] More recently, with the development of new columnar LCs pyrene and perylene derivatives, OLEDs have been constructed using discotic LCs as both the electron and hole transporters.^[129] Some groups have explored the electroluminescence and charge transport properties of photo-crosslinked and conjugated-bridged triphenylene derivatives in OLED applications.^[130]

1.7 Motivation and objectives

As was pointed out in previous sections, discotic liquid crystals, especially those based on triphenylene and hexa-*peri*-hexabenzocoronene, show excellent electronic and optoelectronic properties, low-cost solution processing with good film-formation, alignment by standard techniques and the capability of self-healing. However, despite these recent advancements, there are still further possibilities for improvement of the properties of these materials via modifications of molecular structures.

Larger disc cores should lead to liquid crystals with increased columnar stability and order, and as believed, to materials with higher charge-carrier mobilities. At some critical size, new types of mesophases should be obtained in which the tendency of smaller discs to tilt against the columnar axes will be replaced by a simple lateral offset (graphite-like stacking adopted to optimize orbital interactions). It may at first appear challenging to synthesize larger soluble graphitic subunits with discrete sizes, symmetry, and substitution patterns, all of which may critically affect future device performance.

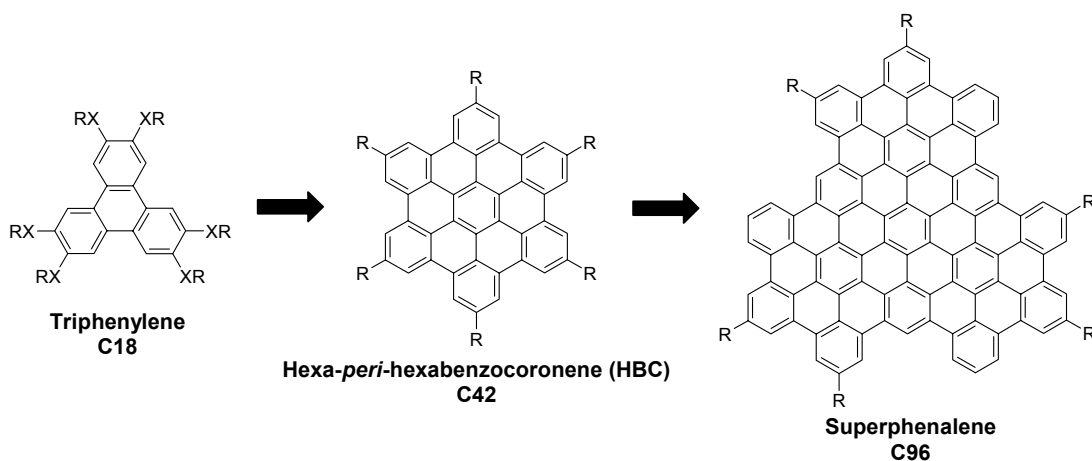


Figure 23. Molecular structures of selected PAHs with increasing core size.

Here the attention is focused on "superphenalene" (Figure 23) in which the all-benzenoid PAH core is about six times larger than that of triphenylene and 2.5-3 times larger than HBC. In addition, its symmetry (D_{3h}) and straightforward

regiospecific (C_3 -symmetric) functionalization on the periphery could lead to helical bulk phases and chiral expression during 2D surface patterning. Highly efficient face-to-face stacking in the bulk should be realized from such a truncated near-triangular shape, unperturbed by tethered side chains located near its apexes. Improved solubility will allow purification of new materials (very important for applications in devices) but also influence the processability in terms of spincoating from solution or the use of printing techniques to produce homogeneous thin films that might find application in devices. It was shown by M. Wehmeier that the introduction of six *tert*-butyl groups around the superphenalene core is not enough to solubilize this large PAH.^[60] For this purpose, suitable solubilizing groups, such as long alkyl chains, have to be selected, which can sufficiently compensate for the strong π - π stacking tendency of the large aromatic cores to make the molecules soluble enough for solution analysis and processing, but still preserve the π - π stacking as a favorable driving force for supramolecular ordering.

For successful, highly efficient devices, the order and orientation of the material are crucial points. To achieve control over these two parameters, an understanding of the structure-property relations is required and is currently far from complete, at least in the field of discotic liquid crystals. While edge-on alignment is the preferred orientation of discotics, homeotropic or face-on alignment has so far only been achieved by cooling columnar materials from the melt. Since the isotropization temperature (T_i) for most HBC derivatives is much higher than the on-set of decomposition, lowering of the isotropization temperature is essential. It was shown in the work of A. Fechtenkötter that the introduction of six long branched alkyl chains, such as 3,7,11,15-tetramethylhexadecanyl, around the HBC core, led to an effective lowering of T_i .^[86] The affinity of the discs toward face on arrangement can be also increased by the introduction of heteroatoms, such as oxygen, into the side chains. The merging of these two ideas should lead to materials with improved thermal properties and a proclivity for face-on alignment on surfaces.

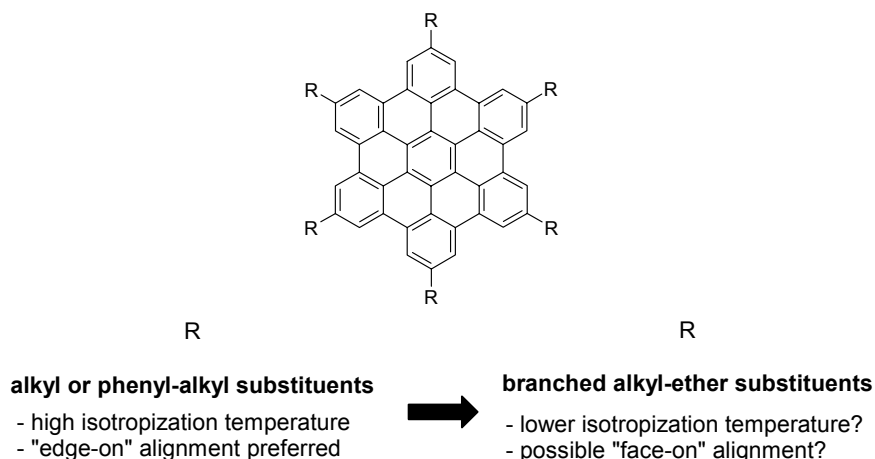


Figure 24. Improvement of material properties through side-group variation.

Self-assembly for materials applications can be controlled by appropriate structural modification at the core periphery. Attachment of rigid polyphenylene dendrimers to the core should induce steric hindrance which is expected to affect the efficient π - π stacking of the cores. Hence, the investigation of self-assembly behavior and photophysical properties of derivatives bearing such bulky groups can reveal the basic relationship between the structure and properties.

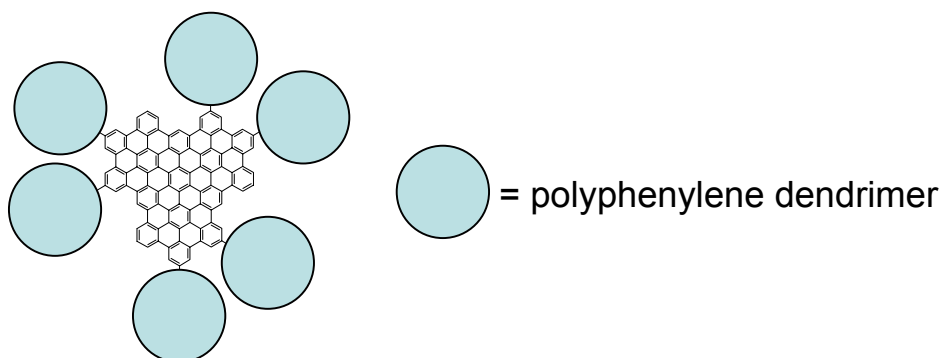


Figure 25. Superphenalene core with the bulky groups at the periphery.

Substitution of HBC in a benzene-analogous way with electron-donating and withdrawing groups has been found to have little effect on the electronic properties of the core.^[52] A far more significant change of these properties can be achieved by changing the size and symmetry of the core, as has been demonstrated in the work of C. Simpson, for a series of all-benzenoid PAHs.

However, to date few large PAHs with "zig-zag" periphery have been selectively synthesized, and the effect of this geometric variation on their properties evaluated. The integration of "zig-zag" edges to the parent PAH disc, such as HBC or superphenalene, should influence, not only its electronic properties but also its two- and three-dimensional self-assembly behavior.

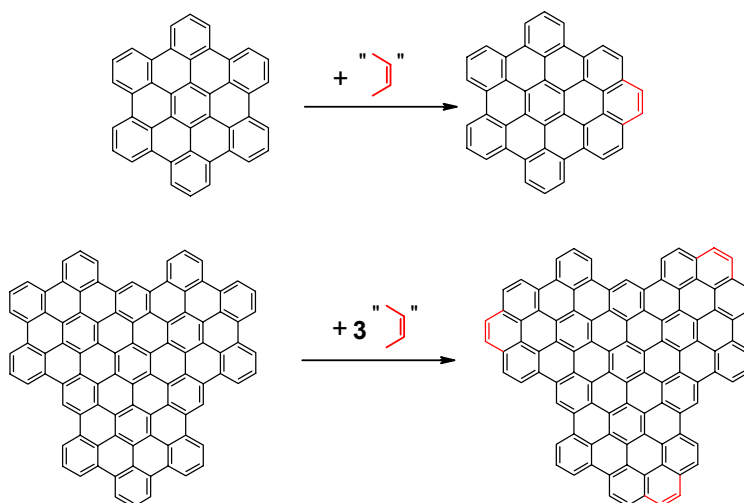


Figure 26. Conceptual incorporation of "zig-zag" edges to parent all-benzenoid PAHs (HBC and superphenalene).

The main objectives of this study can be summarized by the following points:

- to efficiently synthesize superphenalene discs with appropriate solubilizing side chains that enable purification, characterization (solution and bulk) and processing;
- the synthesis of HBC derivatives with branched alkyl-ether substituents on the periphery, and the assessment of the thermal and supramolecular properties of the columnar mesophases that they form;
- the synthesis of dendronized superphenalenes and the investigation of the self-assembly behavior in solution;
- to develop a synthetic route to a new family of graphitic molecules (HBC and superphenalene related) with partial "zig-zag" periphery, and to evaluate their properties (in particular electronic properties).

1.8 Literature

- [1] E. Clar, *Polycyclic Hydrocarbons*, Academic Press, New York, **1964**.
- [2] J. R. Dias, *Handbook of Polycyclic Hydrocarbons, Part A: Benzenoid Hydrocarbons*, Elsevier, Amsterdam, **1987**.
- [3] M. Zander, *Polycyclische Aromaten: Kohlenwasserstoffe und Fullerene*, B. G. Teubner, Stuttgart, **1995**.
- [4] R. G. Harvey, *Polycyclic Aromatic Hydrocarbons*, Wiley-VCH, New York, **1997**.
- [5] A. M. Mastral, M. S. Callén, R. Murillo, T. García, *Polyc. Arom. Comp.* **2000**, *18*, 1-11.
- [6] Y. A. Levendis, A. Atal, J. Carlson, Y. Dunayevskiy, P. Vouros, *Environ. Sci. Technol.* **1996**, *30*, 2742-2754.
- [7] L. J. Allamandola, *Top. Curr. Chem.* **1990**, *153*, 1-25.
- [8] D. J. Cook, S. Schlemmer, N. Balucani, D. R. Wagner, B. Steiner, R. J. Saykally, *Nature* **1996**, *380*, 227-229.
- [9] R. Scholl, C. Seer, R. Weitzenböck, *Chem. Ber.* **1910**, *43*, 2202-2209.
- [10] R. Scholl, C. Seer, *Liebigs Ann. Chem.* **1912**, *394*, 111-123.
- [11] R. Scholl, H. Neumann, *Chem. Ber.* **1922**, *55*, 118-126.
- [12] R. Scholl, C. Seer, *Chem. Ber.* **1922**, *55*, 330-341.
- [13] E. Clar, *Nature* **1948**, *161*, 238-239.
- [14] E. Clar, *Chem. Ber.-Recl.* **1948**, *81*, 52-63.
- [15] E. Clar, *Chem. Ber.-Recl.* **1949**, *82*, 495-514.
- [16] E. Clar, D. G. Stewart, *J. Am. Chem. Soc.* **1953**, *75*, 2667-2672.
- [17] M. Zander, W. Franke, *Chem. Ber.-Recl.* **1958**, *91*, 2794-2797.
- [18] M. Zander, *Chem. Ber.-recl.* **1959**, *92*, 2744-2749.
- [19] M. Zander, *Angew. Chem. Int. Ed. Engl.* **1960**, *72*, 513-520.
- [20] S. Hagen, H. Hopf, *Top. Curr. Chem.* **1998**, *196*, 44-89.
- [21] E. Clar, *The Aromatic Sextet*, 1st ed., John Wiley and Sons, London, **1972**.
- [22] M. Randić, *Chem. Rev.* **2003**, *103*, 3449-3605.
- [23] I. Gutman, S. Cyvin, *Introduction to the theory of benzenoid hydrocarbons*, Springer, Berlin, **1989**.
- [24] I. Gutman, S. J. Cyvin (eds.) *Advances in the Theory of Benzenoid Hydrocarbons*, *Top. Curr. Chem.* **1990**, *153*, 57-292.
- [25] I. Gutman, (ed.) *Advances in the Theory of Benzenoid Hydrocarbons II*, *Top. Curr. Chem.* **1992**, *162*, whole issue.
- [26] S. E. Stein, R. L. Brown, *J. Am. Chem. Soc.* **1987**, *109*, 3721-3729.
- [27] N. Tyutyulkov, N. Ivanov, K. Müllen, A. Staykov, F. Dietz, *J. Phys. Chem. B* **2004**, *108*, 4275-4282.
- [28] C. D. Simpson, J. Wu, M. D. Watson, K. Müllen, *J. Mater. Chem.* **2004**, *14*, 494-504.

- [29] T. Vo-Dinh, J. Fetzer, A. D. Campiglia, *Talanta* **1998**, *47*, 943-969.
- [30] T. Ishiguro, Y. Takatori, K. Akihama, *Combust. Flame* **1997**, *108*, 231-234.
- [31] R. H. Hurt, Y. Hu, *Carbon* **1999**, *37*, 281-292.
- [32] H. W. Kroto; A. W. Allaf, S. P. Balm, *Chem. Rev.* **1991**, *91*, 1213-1235.
- [33] P. M. Ajayan, *Chem. Rev.* **1999**, *99*, 1787-1799.
- [34] B. A. Hess, L. S. Schaad, *J. Am. Chem. Soc.* **1971**, *93*, 305-310.
- [35] D. Biermann, W. Schmidt, *J. Am. Chem. Soc.* **1980**, *102*, 3163-3173.
- [36] J. W. Armit, R. Robinson, *J. Chem. Soc.* **1925**, 1604-1618.
- [37] P. v. R. Schleyer, C. Maerker, A. Dransfeld, H. Jiao, N. J. R. van Eikema Hommes, *J. Am. Chem. Soc.* **1996**, *118*, 6317-6318.
- [38] D. Moran, F. Stahl, H. F. Bettinger, H. F. Schaefer III, P. v. R. Schleyer, *J. Am. Chem. Soc.* **2003**, *125*, 6746-6752.
- [39] J. L. Ormsby, B. T. King, *J. Org. Chem.* **2004**, *69*, 4287-4291.
- [40] I. F. Paterson, B. Z. Chowdhry, S. A. Leharne, *Chemosphere* **1999**, *38*, 3095-3107.
- [41] R. F. Sullivan, M. M. Boduszynski, J. C. Fetzer, *Energy and Fuels* **1989**, *3*, 603-612.
- [42] J. C. Fetzer, W. R. Biggs, *Org. Prep. Proced. Int.* **1988**, *20*, 223-230.
- [43] M. Rehahn, A. D. Schlüter, G. Wegner, W. J. Feast, *Polymer* **1989**, *30*, 1054-1059.
- [44] K. H. Koch, K. Müllen, *Chem. Ber.* **1991**, *124*, 2091-2100.
- [45] M. Müller, J. Petersen, R. Strohmaier, C. Günther, N. Karl, K. Müllen, *Angew. Chem. Int. Ed. Engl.* **1996**, *35*, 886-888.
- [46] A. Stabel, P. Herwig, K. Mullen, J. P. Rabe, *Angew. Chem. Int. Ed. Engl.* **1995**, *34*, 1609-1611.
- [47] P. Herwig, C. W. Kayser, K. Müllen, H. W. Spiess, *Adv. Mater.* **1996**, *8*, 510-513.
- [48] K. P. C. Vollhardt, *Acc. Chem. Res.* **1977**, *10*, 1-8.
- [49] H. A. Dieck, F. R. Heck, *J. Organomet. Chem.* **1975**, *93*, 259-263.
- [50] L. Cassar, *J. Organomet. Chem.* **1975**, *93*, 253-257.
- [51] S. Takahashi, Y. Koroyama, K. Sonogashira, N. Hagihara, *Synthesis* **1980**, *8*, 627-630.
- [52] S. Ito, M. Wehmeier, J. D. Brand, C. Kübel, R. Epsch, J. P. Rabe, K. Müllen, *Chem. Eur. J.* **2000**, *6*, 4327-4342.
- [53] P. Kovacic, A. Kyriakis, *Tetrahedron Lett.* **1962**, *11*, 467-469.
- [54] P. Kovacic, F. W. Koch, *J. Org. Chem.* **1963**, *28*, 1864-1867.
- [55] P. Kovacic, M. B. Jones, *Chem. Rev.* **1987**, *87*, 357-379.
- [56] F. Dötz, *Dissertation*, Johannes Gutenberg Universität, Mainz, **2000**.
- [57] W. Diltthey, W. Schommer, O. Trösken, *Chem. Ber.* **1933**, *66*, 1627-1628.
- [58] W. Diltthey, G. Hurtig, *Chem. Ber.* **1934**, *67*, 2004-2007.
- [59] L. F. Fieser, *Organic experiments*, D. C. Heath, Boston, **1964**, 307-308.
- [60] V. S. Iyer, M. Wehmeier, J. D. Brand, M. A. Keegstra, K. Müllen, *Angew. Chem. Int. Ed. Engl.* **1997**, *36*, 1604-1607.

- [61] M. Müller, V. S. Iyer, C. Kübel, V. Enkelmann, K. Müllen, *Angew. Chem. Int. Ed. Engl.* **1997**, *36*, 1607-1610.
- [62] F. Dötz, J. D. Brand, S. Ito, L. Gherghel, K. Müllen, *J. Am. Chem. Soc.* **2000**, *122*, 7707-7717.
- [63] F. Morgenroth, C. Kübel, M. Müller, U. M. Wiesler, A. J. Beresheim, M. Wagner, K. Müllen, *Carbon* **1998**, *36*, 833-837.
- [64] F. Morgenroth, E. Reuther, K. Müllen, *Angew. Chem. Int. Ed. Engl.* **1997**, *36*, 631-634.
- [65] L. Przybilla, J. D. Brand, K. Yoshimura, H. J. Räder, K. Müllen, *Anal. Chem.* **2000**, *72*, 4591-4597.
- [66] K. Yoshimura, L. Przybilla, S. Ito, J. D. Brand, M. Wehmeir, H. J. Räder, K. Müllen, *Macromol. Chem. Phys.* **2001**, *202*, 215-222.
- [67] M. D. Watson, A. Fechtenkötter, K. Müllen, *Chem. Rev.* **2001**, *101*, 1267-1300.
- [68] E. Di Donato, M. Tommasini, G. Fustella, L. Brambilla, C. Castiglioni, G. Zerbi, C. D. Simpson, K. Müllen, F. Negri, *Chem. Phys.* **2004**, *301*, 81-93.
- [69] U. Zimmermann, N. Karl, *Surf. Sci.* **1992**, *268*, 296-306.
- [70] F. Sellam, T. Schmitz-Hübsch, M. Toerker, S. Mannsfeld, H. Proehl, T. Fritz, K. Leo, C. Simpson, K. Müllen, *Surf. Sci.* **2001**, *478*, 113-121.
- [71] P. Ruffieux, O. Gröning, M. Biemann, C. Simpson, K. Müllen, L. Schlapbach, P. Gröning, *Phys. Rev. B* **2002**, *66*, 073409.
- [72] P. Samori, N. Severin, C. D. Simpson, K. Müllen, J. P. Rabe, *J. Am. Chem. Soc.* **2002**, *124*, 9454-9457.
- [73] C. D. Simpson, J. D. Brand, A. J. Beresheim, L. Przybilla, H. J. Räder, K. Müllen, *Chem. Eur. J.* **2002**, *8*, 1424-1429.
- [74] S. Ito, P. T. Herwig, T. Böhme, J. P. Rabe, W. Rettig, K. Müllen, *J. Am. Chem. Soc.* **2000**, *122*, 7698-7706.
- [75] F. Reinitzer, *Monatsh. Chem.* **1888**, *9*, 421.
- [76] S. Chandrasekhar, B. K. Sadashiva, K. A. Suresh, *Pramana* **1977**, *7*, 471-480.
- [77] S. Chandrasekhar, S. K. Prasad, *Contemp. Phys.* **1999**, *40*, 237-245.
- [78] R. J. Bushby, O. R. Lozman, *Curr. Opin. Coll. Interf. Sci.* **2002**, *7*, 343-354.
- [79] M. O'Neill, S. M. Kelly, *Adv. Mater.* **2003**, *15*, 1135-1146.
- [80] H. Eichorn, *J. Porphyrins Phthalocyanines* **2000**, *4*, 88-102.
- [81] O. Roussel, G. Kestemont, J. Tant, V. de Halleux, R. G. Aspe, J. Levin, A. Remacle, I. R. Gearba, D. Ivanov, M. Lehmann, Y. Geerts, *Mol. Cryst. Liq. Cryst.* **2003**, *396*, 35-39.
- [82] G. R. J. Müller, C. Meiners, V. Enkelmann, Y. Geerts, K. Müllen, *J. Mater. Chem.* **1998**, *8*, 61-64.
- [83] S. Kumar, J. J. Naidu, D. S. S. Rao, *J. Mater. Chem.* **2002**, *12*, 1335-1341.
- [84] A. Fechtenkötter, K. Saalwächter, M. A. Harbison, K. Müllen, H. W. Spiess, *Angew. Chem. Int. Ed. Engl.* **1999**, *38*, 3039-3042.

- [85] A. Fechtenkötter, N. Tchebotareva, M. Watson, K. Müllen, *Tetrahedron* **2001**, *57*, 3769-3783.
- [86] C. Y. Liu, A. Fechtenkötter, M. D. Watson, K. Müllen, A. J. Bard, *Chem. Mater.* **2003**, *15*, 124-130.
- [87] A. M. van de Craats, L. D. A. Siebbeles, I. Bleyl, D. Haarer, Y. A. Berlin, A. A. Zharikov, J. M. Warman, *J. Phys. Chem. B* **1998**, *102*, 9625-9634.
- [88] D. Markovitsi, A. Germain, P. Millie, P. Lecuyer, L. K. Gallos, P. Argyrakis, H. Bengs, H. Ringsdorf, *J. Phys. Chem.* **1995**, *99*, 1005-1017.
- [89] D. Adam, P. Schuhmacher, J. Simmerer, L. Häussling, K. Siemensmeyer, K. H. Eitzbach, H. Ringsdorf, D. Haarer, *Nature* **1994**, *371*, 141-143.
- [90] A. Vaes, M. van der Auweraer, F. C. De Schryver, B. Laguitton, A. Jonas, P. Henderson, H. Ringsdorf, *Langmuir* **1998**, *14*, 5250-5254.
- [91] F. Charra, J. Cousty, *Phys. Rev. Lett.* **1998**, *80*, 1682-1685.
- [92] S. Ikeda, Y. Takanishi, K. Ishikawa, H. Takezoe, *Mol. Cryst. Liq. Cryst.* **1999**, *329*, 589-595.
- [93] H. Monobe, K. Kiyohara, N. Terasawa, M. Heya, K. Awazu, Y. Shimizu, *Adv. Funct. Mater.* **2003**, *13*, 919-924.
- [94] N. Boden, R. J. Bushby, A. N. Cammidge, *J. Chem. Soc. Chem. Commun.* **1994**, *4*, 465-466.
- [95] A. N. Cammidge, R. J. Bushby, *Handbook of Liquid Crystals*, Wiley-VCH, Weinheim, **1998**, 693-748.
- [96] J. A. Rego, S. Kumar, H. Ringsdorf, *Chem. Mater.* **1996**, *8*, 1402-1409.
- [97] A. Kettner, J. H. Wendorff, *Liq. Cryst.* **1999**, *26*, 483-487.
- [98] S. J. Cross, J. W. Goodby, A. W. Hall, M. Hird, S. M. Kelly, K. J. Toyne, C. Wu, *Liq. Cryst.* **1998**, *25*, 1-11.
- [99] P. Samori, A. Fechtenkötter, F. Jäckel, T. Böhme, K. Müllen, J. P. Rabe, *J. Am. Chem. Soc.* **2001**, *123*, 11462-11467.
- [100] P. Samori, X. Yin, N. Tchebotareva, Z. Wang, T. Pakula, F. Jäckel, M. D. Watson, A. Venturini, K. Müllen, J. P. Rabe, *J. Am. Chem. Soc.* **2004**, *126*, 3567-3575.
- [101] B. W. Laursen, K. Nørgaard, N. Reitzel, J. B. Simonsen, C. B. Nielsen, J. Als-Nielsen, T. Bjørnholm, T. I. Sølling, M. M. Nielsen, O. Bunk, K. Kjaer, N. Tchebotareva, M. D. Watson, K. Müllen, J. Piris, *Langmuir* **2004**, *20*, 4139-4146.
- [102] J. Wu, M. D. Watson, L. Zhang, Z. Wang, K. Müllen, *J. Am. Chem. Soc.* **2004**, *126*, 177-186.
- [103] I. Fischbach, T. Pakula, P. Minkin, A. Fechtenkötter, K. Müllen, H. W. Spiess, *J. Phys. Chem. B* **2002**, *106*, 6408-6418.
- [104] K. Ohta, K. Hatsuaka, M. Sugibayashi, M. Ariyoshi, K. Ban, F. Maeda, R. Naito, K. Nishizawa, A. M. van de Craats, J. M. Warman, *Mol. Cryst. Liq. Cryst.* **2003**, *396*, 325-345.

- [105] A. M. van de Craats, J. M. Warman, *Adv. Mater.* **2001**, *13*, 130-133.
- [106] A. M. van de Craats, J. M. Warman, A. Fechtenkötter, J. D. Brand, M. A. Harbison, K. Müllen, *Adv. Mater.* **1999**, *11*, 1469-1472.
- [107] A. M. van de Craats, J. M. Warman, *Mol. Cryst. Liq. Cryst.* **2003**, *396*, 41-72.
- [108] R. J. Bushby, O. R. Lozman, *Curr. Opin. Solid State Mater. Sci.* **2002**, *6*, 569-578.
- [109] C. D. Dimitrakopoulos, P. R. L. Malenfant, *Adv. Mater.* **2002**, *14*, 99-117.
- [110] G. Horowitz, *Adv. Mater.* **1998**, *10*, 365-377.
- [111] R. Madru, G. Guillaud, M. Al Sadoun, M. Maitrot, J. J. André, J. Simon, R. Even, *Chem. Phys. Lett.* **1988**, *145*, 343-346.
- [112] C. Clairisse, M. T. Riou, *J. Appl. Phys.* **1991**, *69*, 3324-3327.
- [113] Z. Bao, A. J. Lovinger, A. Dodabalapur, *Appl. Phys. Lett.* **1996**, *69*, 3066-3068.
- [114] A. M. van de Craats, N. Schutzmann, O. Bunk, M. M. Nielsen, M. Watson, K. Müllen, H. D. Chanzy, H. Sirringhaus, R. H. Friend, *Adv. Mater.* **2003**, *15*, 495-499.
- [115] O. Karthaus, H. Ringsdorf, V. V. Tsukruk, J. H. Wendorff, *Langmuir* **1992**, *8*, 2279-2283.
- [116] N. Reitzel, T. Hassenkam, K. Balashev, T. R. Jensen, P. B. Howes, K. Kjaer, A. Fechtenkötter, N. Tchebotareva, S. Ito, K. Müllen, T. Bjørnholm, *Chem. Eur. J.* **2001**, *7*, 4894-4901.
- [117] A. Tracz, J. K. Jeszka, M. D. Watson, W. Pisula, K. Müllen, T. Pakula, *J. Am. Chem. Soc.* **2003**, *125*, 1682-1683.
- [118] C. Y. Liu, A. J. Bard, *Chem. Mater.* **2000**, *12*, 2353-2362.
- [119] O. Bunk, M. M. Nielsen, T. I. Solling, A. M. van de Craats, N. Stutzmann, *J. Am. Chem. Soc.* **2003**, *125*, 2252-2258.
- [120] S. Zimmermann, J. H. Wendorff, C. Weder, *Chem. Mater.* **2002**, *14*, 2218-2223.
- [121] N. Terasawa, H. Monobe, K. Kiyohara, Y. Shimizu, *Chem. Commun.* **2003**, 1678-1679.
- [122] A. N. Cammidge, H. Gopee, *J. Mater. Chem.* **2001**, *11*, 2773-2783.
- [123] K. Hatsusaka, K. Ohta, I. Yamamoto, H. Shirai, *J. Mater. Chem.* **2001**, *11*, 423-433.
- [124] S. Kumar, *Curr. Sci.* **2002**, *82*, 256-257.
- [125] K. Petritsch, R. H. Friend, A. Lux, G. Rozenberg, S. C. Moratti, A. B. Holmes, *Synth. Met.* **1999**, *102*, 1776-1777.
- [126] L. Schmidt-Mende, A. Fechtenkötter, K. Müllen, E. Moons, R. H. Friend, J. D. MacKenzie, *Science* **2001**, *293*, 1119-1122.
- [127] S. Tanaka, C. Adachi, T. Koyama, Y. Taniguchi, *Chem. Lett.* **1998**, *27*, 975-976.
- [128] T. Christ, B. Glösen, A. Greiner, A. Kettner, R. Sander, V. Stümpflen, V. Tsukruk, J. H. Wendorff, *Adv. Mater.* **1997**, *9*, 48-51.
- [129] A. M. van de Craats, J. M. Warman, P. Schlichting, U. Rohr, Y. Geerts, K. Müllen, *Synth. Met.* **1999**, *102*, 1550-1551.
- [130] A. Bacher, C. H. Erdelen, W. Paulus, H. Ringsdorf, H. W. Schmidt, P. Schuhmacher, *Macromolecules* **1999**, *32*, 4551-4557.

CHAPTER
2

Superphenalene-Based Columnar Liquid Crystals

2.1 Synthesis of hexa-substituted "Superphenalenes"

The synthesis of the hexa-substituted "superphenalene" (henceforth referred to as C96) discs **53a-g** (Figure 27), based on our general route to large PAHs, can be completed in two steps from readily available starting materials.^[1-6] The first step is construction of a well-defined polyphenylene scaffold with a close spatial arrangement of the phenyl rings which is similar to the framework of the target molecule, and second, planarization of this precursor to the target molecule by oxidative cyclodehydrogenation. The general synthetic route to the hexa-substituted "superphenalenes" (**53a-g**) is outlined in Figure 27. Diels-Alder reaction of commercially available 1,3,5-triethynylbenzene (**54**) with excess (3.6 equiv) disubstituted tetraphenylcyclopentadienones **55a-g**, in *o*-xylene at 170 °C gave the corresponding polyphenylene compounds **56a-g**. The workup of these first generation dendrimers was by evaporation of the solvent, followed by column chromatography to afford colorless solids (**56a,b,e-g**) or highly viscous oils (**56c,d**), in nearly quantitative yields. All were readily soluble in organic solvents and their structures and purities were unequivocally confirmed by ¹H and ¹³C NMR spectroscopy, FD or MALDI-TOF mass spectrometry, and elemental analysis.

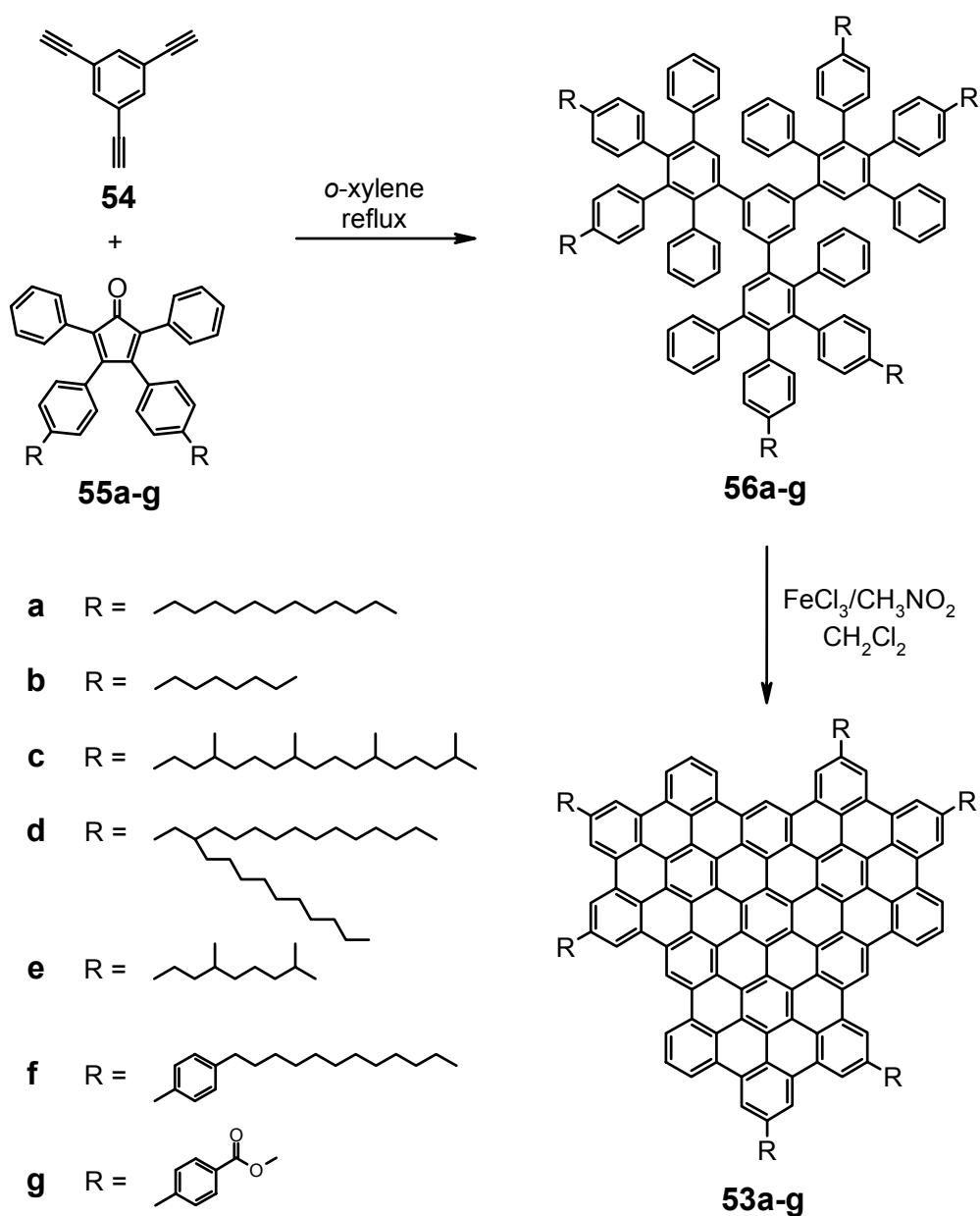


Figure 27. Synthesis of hexa-substituted "superphenalene" (**53a-g**).

The required disubstituted tetraphenylcyclopentadienones **55a-g** were prepared via three different synthetic routes. The synthesis of 3,4-bis(4-dodecylphenyl)-2,5-diphenylcyclopentadienone (**55a**) and 3,4-bis(4-heptylphenyl)-2,5-diphenylcyclopentadienone (**55b**) is shown in Figure 28.

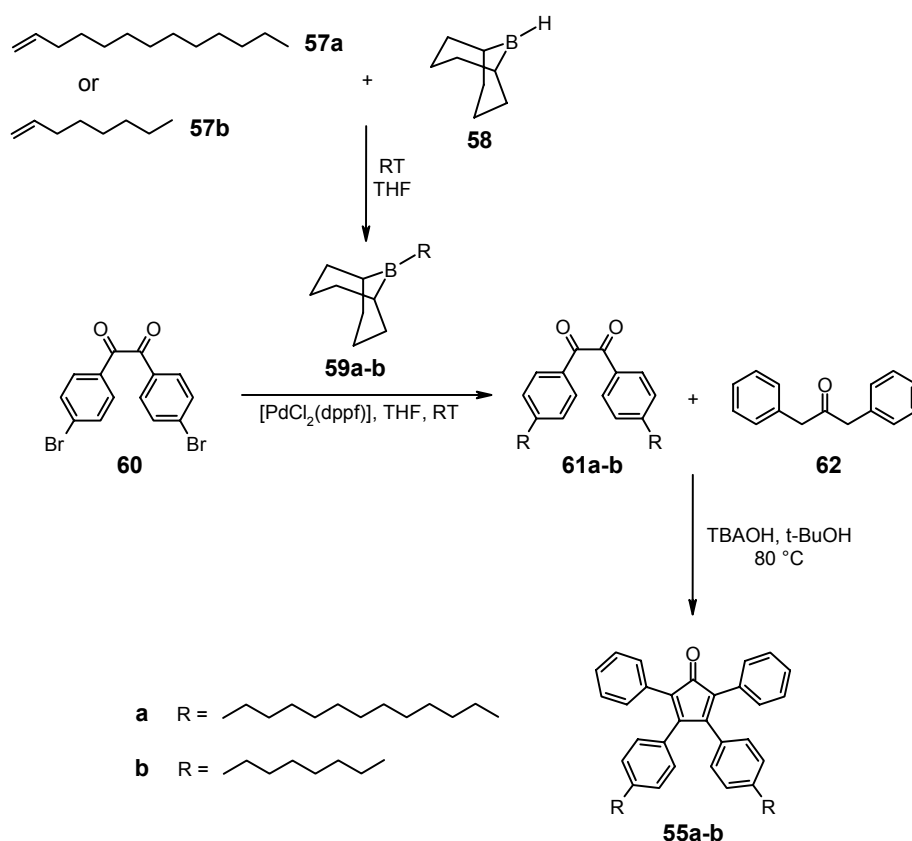


Figure 28. Synthesis of disubstituted tetraphenylcyclopentadienones (**55a-b**) from 4,4'-dibromobenzil (**60**).

4,4'-Didodecylbenzil (**61a**) and 4,4'-diheptylbenzil (**61b**) were easily synthesized in a one-pot reaction from commercially available 4,4'-dibromobenzil (**60**). First, hydroboration^[7-9] of 1-dodecene (**57a**) or 1-heptene (**57b**) with 9-borabicyclo[3.3.1]nonane (**58**) in THF at room temperature, overnight, gave the corresponding intermediate organoboranes **59a-b**, which were then directly used in the subsequent Suzuki coupling^[10-12] with 4,4'-dibromobenzil (**60**) in the presence of catalytic PdCl₂(dppf). Reactions were complete after 5 hours at room temperature, and 4,4'-didodecylbenzil (**61a**) and 4,4'-diheptylbenzil (**61b**) were isolated in 72-73% yield, after column chromatographic purification. The route previously used in our group for the synthesis of 4,4'-didodecylbenzil (**61a**) involved the four-step synthesis of 4,4'-didodecyldiphenylacetylene, followed by its oxidation with iodine in DMSO.^[13] The new, general route for the synthesis of *n*-alkyl substituted benzils presented here is synthetically less demanding and

overall higher yielding. 4,4'-Didodecylbenzil (**61a**) and 4,4'-diheptylbenzil (**61b**) were reacted in the next step in a double Knoevenagel condensation with commercially available 1,3-diphenyl-2-propanone (**62**) to afford the tetraphenylcyclopentadienones **55a-b**,^[14] as dark purple, viscous oils in 73 and 89% yield, respectively, after purification by column chromatography.

The synthetic pathway to 3,4-bis[4-(3,7,11,15-tetramethylhexadecyl)phenyl]-2,5-diphenylcyclopentadienone (**55c**), 3,4-bis[4-(2-decyltetradecyl)phenyl]-2,5-diphenylcyclopentadienone (**55d**), 3,4-bis[4-(3,7-dimethyloctyl)phenyl]-2,5-diphenylcyclopentadienone (**55e**) and 3,4-bis[4'-(4''-dodecylphenyl)phenyl]-2,5-diphenylcyclopentadienone (**55f**) is outlined in Figure 29. These disubstituted tetraphenylcyclopentadienones were accessible by coupling of the alkyl chains to 4,4'-dibromodiphenylacetylene (**63**), oxidation of the triple bond to a diketone (**66c-f**) and reaction of this in a double Knoevenagel condensation with 1,3-diphenyl-2-propanone (**62**).

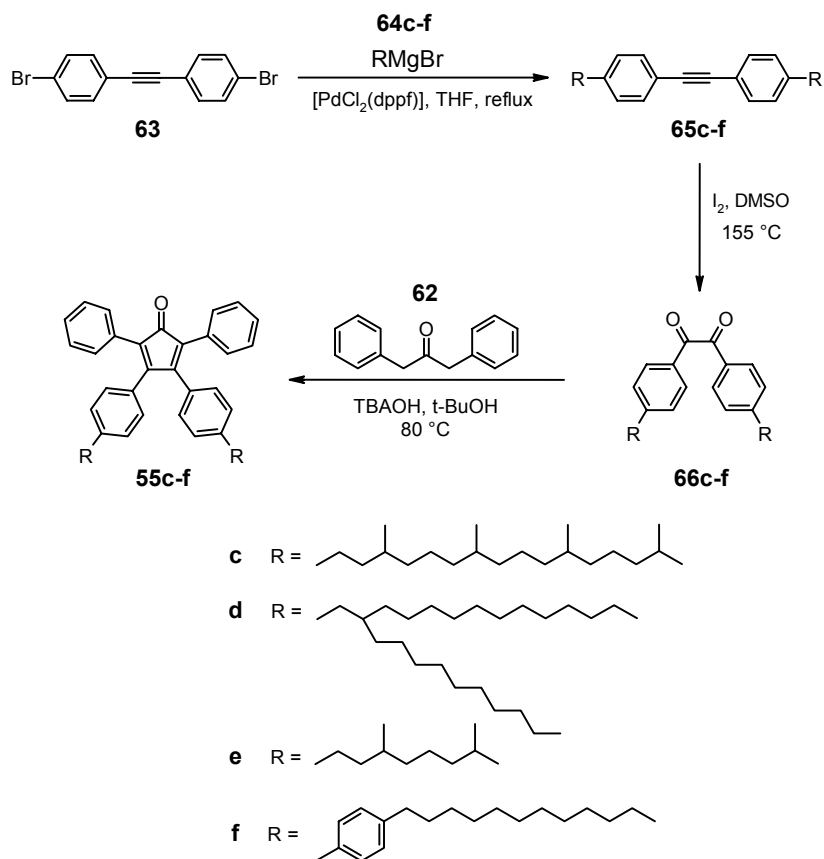


Figure 29. Synthesis of disubstituted tetraphenylcyclopentadienones (**55c-f**) from 4,4'-dibromodiphenylacetylene (**63**).

The synthesis of disubstituted diphenylacetylenes, 4,4'-bis(3,7,11,15-tetramethyl hexadecyl)diphenylacetylene (**65c**), 4,4'-bis(2-decyltetradecyl)diphenylacetylene (**65d**), 4,4'-bis(3,7-dimethyloctyl)diphenylacetylene (**65e**), and 4,4'-bis(4-dodecylphenyl)diphenylacetylene (**65f**), was carried out according to procedures used before by our group:^[15-20] under Kumada coupling conditions using PdCl₂(dppf) as the catalyst in THF, Grignard reagents **64c-f** were coupled with 4,4'-dibromodiphenylacetylene (**63**), which can be prepared in a two step synthesis, according to literature procedures, on several hundred gram scale.^[21,22] Oxidation of the above synthesized disubstituted diphenylacetylenes **65c-f** with iodine in DMSO at 155 °C resulted in the corresponding 4,4'-disubstituted diketones **66c-f**. Two-fold Knoevenagel condensation of **66c-f** with 1,3-diphenyl-2-propanone (**62**), using tetrabutylammonium hydroxide as base, gave disubstituted tetraphenylcyclopentadienones **55c-f** in good yield (64-77%).

The third synthetic route used for the preparation of disubstituted tetraphenylcyclopentadienone building blocks is depicted in Figure 30.

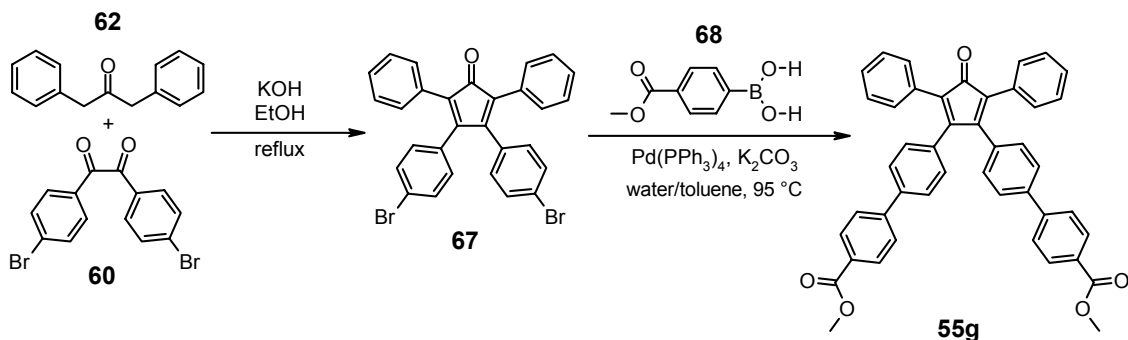


Figure 30. Synthesis of disubstituted tetraphenylcyclopentadienone (**55g**) from dibromo-substituted tetraphenylcyclopentadienone (**67**).

Namely, 3,4-bis[4'-(4''-methoxycarbonylphenyl)phenyl]-2,5-diphenylcyclopentadienone (**55g**) could be synthesized directly from 3,4-bis(4-bromophenyl)-2,5-diphenylcyclopentadienone (**67**) via coupling with commercially available (4-methoxycarbonylphenyl)boronic acid (**68**) under Suzuki conditions with palladium catalysis in a two phase system of toluene and water.^[12] This synthesis is a modification of the general procedure described in the PhD thesis of T. Weil.^[23]

The starting material (**67**) can be easily prepared by double Knoevenagel condensation of 4,4'-dibromobenzil (**60**) and 1,3-diphenyl-2-propanone (**62**) on a multigram scale. The Suzuki coupling between **67** and **68** was accompanied by a small degree of dehalogenation of **67**, leading to a small percentage of monosubstituted tetraphenylcyclopentadienone in the product. Such a side reaction is not a problem as the desired product **55g** could be separated and purified by column chromatography due to the difference in polarity, and was isolated in 67% yield.

The final, key step of the synthesis of hexa-substituted superphenalenes (**53a-g**) is the oxidative cyclodehydrogenation of polyphenylene precursors (**56a-g**) under Lewis acid conditions (Figure 31).^[22,24] The cyclodehydrogenation to the superphenalene disc required the removal of 36 hydrogens and the formation of 18 carbon-carbon bonds in a single reaction step; this is three times the number required for HBC. Hence, longer reaction times and greater oxidant excess were required to obtain the near-quantitative conversions typically realized during HBC synthesis. It has been found that 2.5 equivalents of iron(III) chloride per hydrogen to be removed and 15-18 hours reaction time resulted in the best results, leading to the formation of **53a-g** (in case of hexa(4-methoxycarbonylphenyl)-C96 (**53g**), 140 equivalents of iron(III) chloride and 48 hours were required, see experimental section). For example, polyphenylene precursor **56a** was dissolved in dichloromethane and planarization was effected with iron(III) chloride (90 equiv, i.e. 2.5 equiv per hydrogen to be removed) slowly added as a nitromethane solution. Throughout the duration of the reaction, a constant stream of argon was bubbled through the mixture to remove HCl gas formed *in situ*. Fresh dichloromethane was added intermittently to replace that which had evaporated. After 18 hours, a deep red-brown solid was precipitated from the reaction mixture with methanol, dried, and purified by column chromatography to afford the desired product, hexadodecyl-C96 (**53a**) as a chestnut red-brown waxy solid. The low solubilities of hexa(3,7-dimethyloctyl)-C96 (**53e**) and hexa(4-dodecylphenyl)-C96 (**53f**), have so far precluded preparative chromatography.

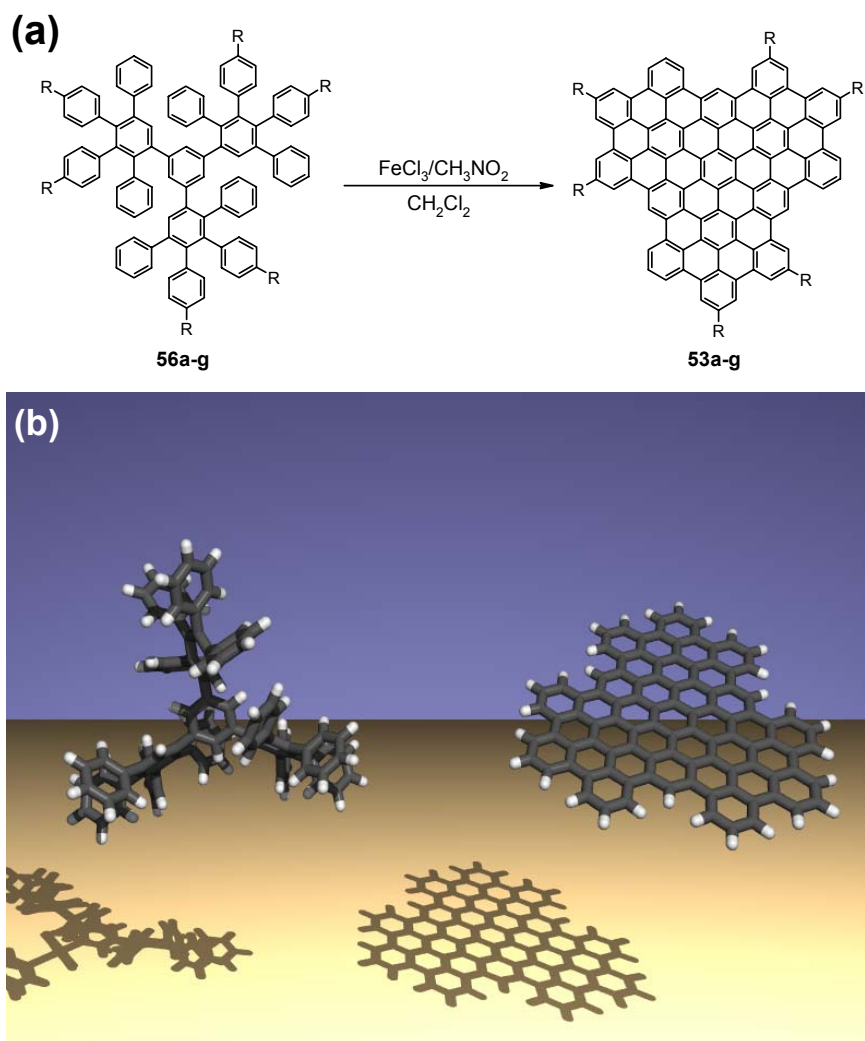
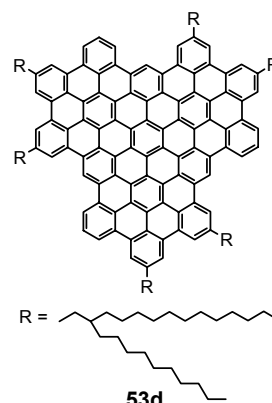
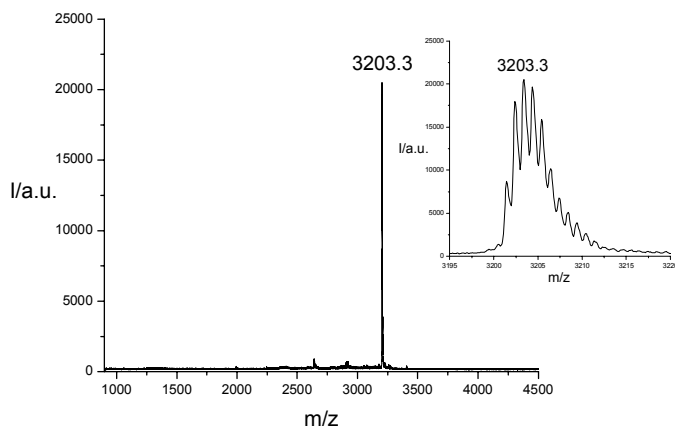


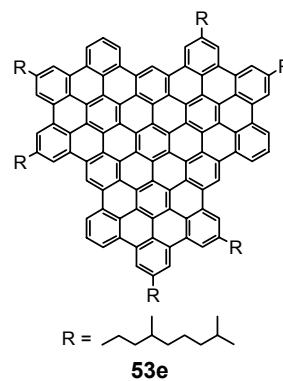
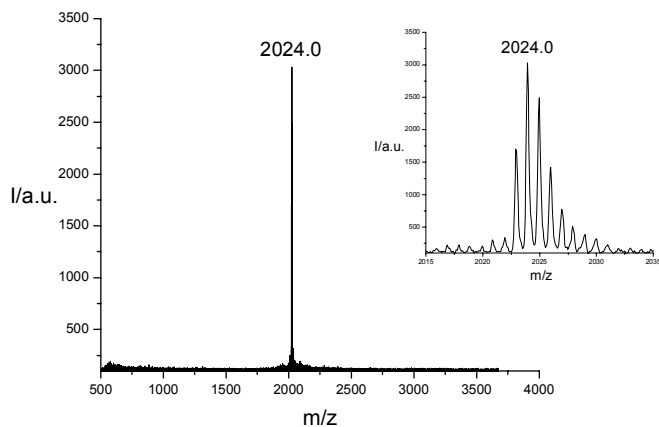
Figure 31. (a) Cyclodehydrogenation of polyphenylene precursors **56a-g** to the corresponding superphenalene (C₉₆) derivatives (**53a-g**) and (b) their computer-generated three-dimensional structures^[25] (alkyl chains omitted for clarity).

Compounds **53a-g** were identified by MALDI-TOF mass spectrometry,^[26,27] proving the loss of exactly 36 hydrogen atoms during the formation of 18 new carbon-carbon bonds. The MALDI-TOF mass spectra, measured with 7,7,8,8-tetracyanoquinodimethane (TCNQ) as matrix, revealed a single species with isotopic distribution, which is in strong agreement with simulated spectra. The isotopically resolved MALDI-TOF mass spectra of **53a-g** are shown in Figure 32.

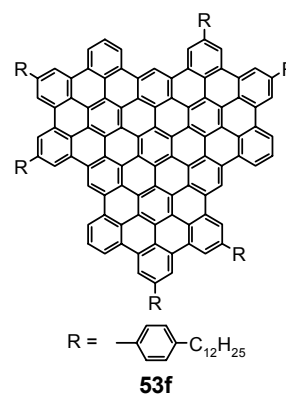
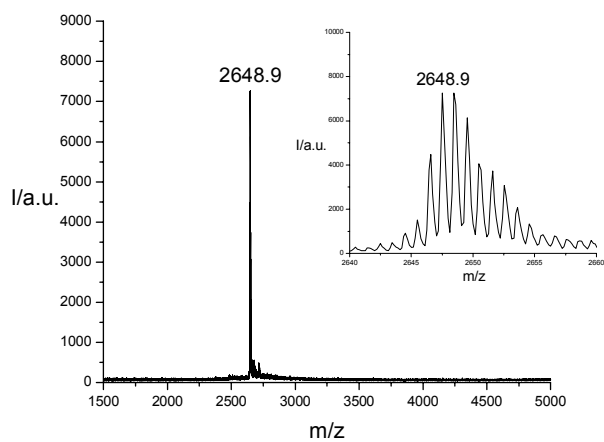
Superphenalene-Based Columnar Liquid Crystals



Calculated average mass: 3203.2
Calculated mass of most intense peak: 3202.5



Calculated average mass: 2024.9
Calculated mass of most intense peak: 2024.2



Calculated average mass: 2649.8
Calculated mass of most intense: 2649.6

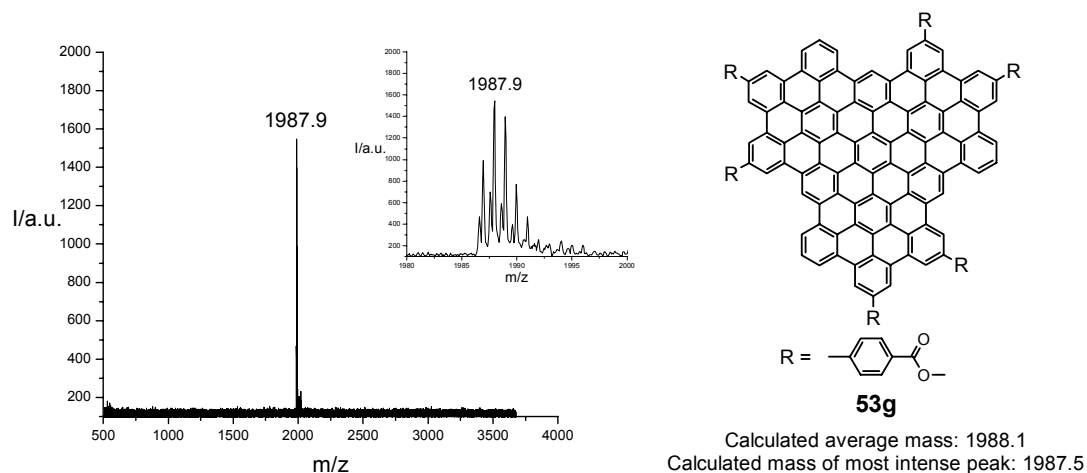


Figure 32. MALDI-TOF mass spectra of **53a-g**; inset shows isotopic distribution.

In all ^1H NMR spectra of compounds **53a-d**, regardless of solvent and temperature (up to 170°C), resonances arising from the mobile alkyl side chains could be resolved, but not those of the aromatic-core protons due to low mobility and the multitude of local environments associated with dynamic aggregation.^[1,28] Hexadodecyl-C96 (C96-C₁₂, **53a**) aggregates so strongly in solution that analysis by gel permeation chromatography gives a bimodal molecular weight distribution (THF, polystyrene standards) extending to 2×10^5 Dalton. Dilution by an order of magnitude and heating just prior to measurement resulted in a monomodal eluogram with a maximum of $\sim 2 \times 10^3$ Dalton, clearly indicating dynamic aggregation.

The one-dimensional ^1H and ^{13}C solid-state NMR spectra of C96-C₁₂ (**53a**) at different temperatures, look rather similar with very few resolved peaks, as shown in Figure 33.^[29] The alkyl proton peak narrows upon increasing the temperature due to increasing mobility of the side chains.

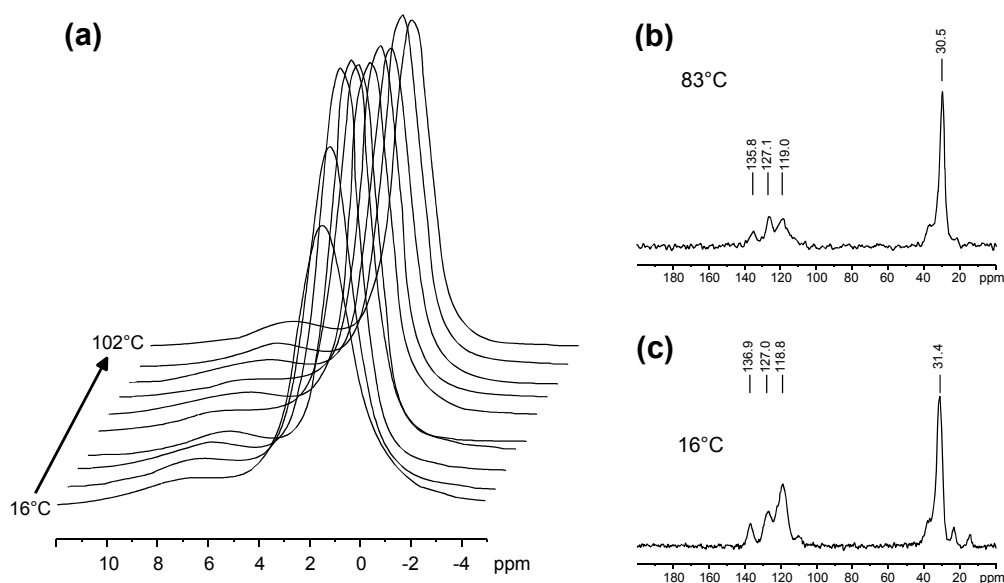


Figure 33. (a) ^1H and (b,c) ^{13}C solid-state NMR spectra of C96-C₁₂ (**53a**) at varied temperatures.

The solution UV/Vis absorption spectra of **53a-g** show a broad, featureless profile ($\lambda_{\text{max}} \approx 460\text{-}475$ nm) with a low-energy tail extending to ~ 700 nm, again a consequence of aggregation. UV/Vis absorption and fluorescence spectra of C96-C₁₂ (**53a**) measured under varying concentration or temperature are shown in Figure 34. The maximum of absorption (λ_{max}) is located at 462 nm. UV/Vis measurements showed no dependence on concentration over the range 10^{-4} – 10^{-8} M. The variable temperature UV/Vis measurements in 10^{-5} M toluene solution did not show any temperature dependence, over the range 20 °C – 85 °C (85 °C was the experimental maximum; small variations in the absorbance are within the limit of experimental error). C96-C₁₂ (**53a**) in THF gives a broad unstructured emission centered at ≈ 570 nm, significantly red-shifted compared to alkyl substituted HBCs (≈ 480 nm);^[30] a shoulder at ≈ 640 nm (10^{-5} M) increases in relative intensity with decreasing concentration as shown in Figure 34c. The reason why relative intensity of the peak at 640 nm changes with concentration while the peak at 570 nm remains unchanged is currently not known. In contrast, variation of temperature over the range 300 – 400K has no influence on the fluorescence spectrum of **53a** in 1,2-dichlorobenzene (Figure 34d). The absorption maxima of hexa(4-dodecylphenyl)-C96 (**53f**) and hexa(2-

decyltetradecyl)-C96 (**53d**) are located at 474 nm, each red-shifted 12 nm compared to **53a** ($\lambda_{\max} = 462$ nm). This can be explained, in the case of **53f** by the extension of the conjugated π -system, while for **53d**, by the introduction of long dove-tailed alkyl substituents. These dove-tailed groups with branching at close proximity to the aromatic core, dramatically influence the self-organization behavior, leading to less aggregate formation.

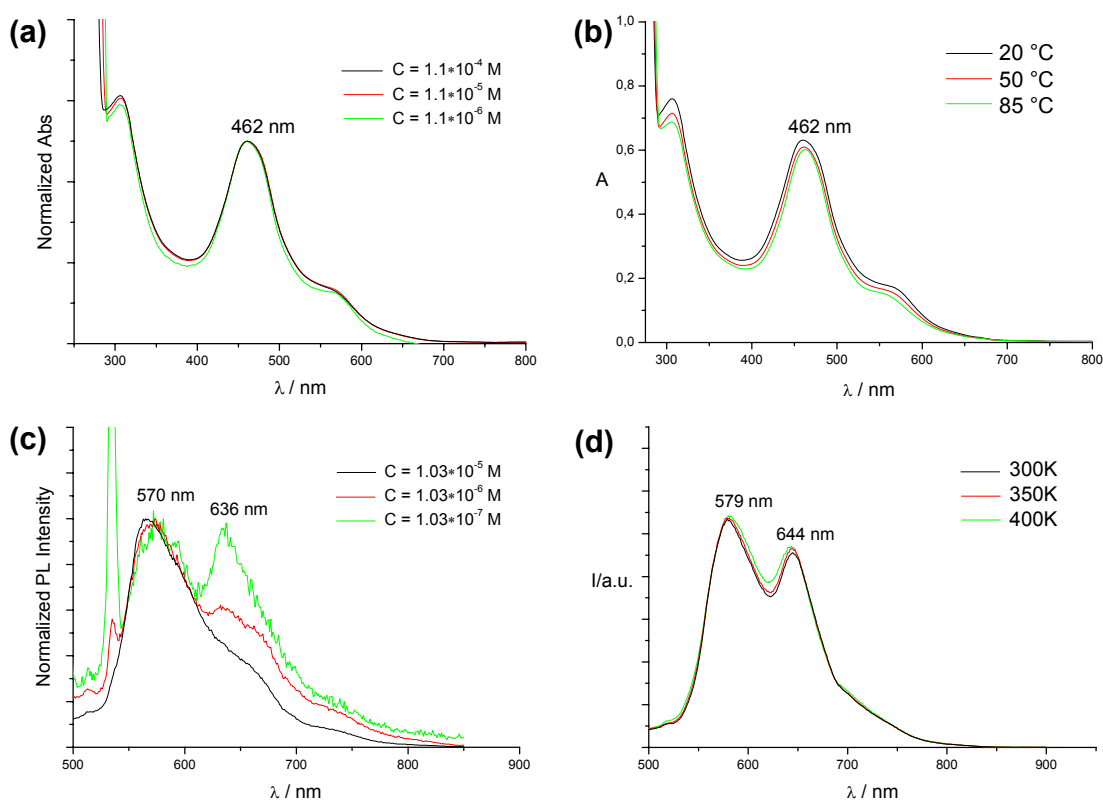


Figure 34. (a) Concentration dependence of UV/Vis absorption spectra of **53a** in toluene and (b) temperature dependence in a 1.1×10^{-5} M toluene solution; (c) concentration dependence of fluorescence spectra of **53a** in THF (excited at 462 nm), and (d) temperature dependence in a 10^{-5} M 1,2-dichlorobenzene solution (excited at 462 nm).

A good correlation between the size of all-benzenoid PAHs and their absorption λ_{\max} has been put forth,^[1,31] and the values for C96 compounds fit nicely onto this curve. The maximum absorption of hexa-substituted C96 derivatives is shifted, relative to HBC ($\lambda_{\max} \approx 360$ nm), to a position within the visible solar spectrum that could provide more effective photovoltaic performance.

The solubility behaviors of compounds **53a-g** have so far been completely unpredictable. Despite their large aromatic core, derivatives **53a-d** readily dissolve at room temperature (**53b** upon gentle heating), in common organic solvents such as dichloromethane, chloroform, THF, and toluene, and do not precipitate upon concentration to lyotropic phases. This is in marked contrast to the significantly smaller HBC-C₁₂ (**52**, R = *n*-C₁₂H₂₅), which virtually completely precipitates from heated organic solvents upon cooling to room temperature, even at concentrations lower than micromolar. Under suitable conditions, **53a** slowly precipitates to - or can be solvent cast to - soft films, unlike the analogous HBC-C₁₂, which rapidly self-assembles to micro and nanofibers, gelling the mother liquor.^[32] Moreover, hexa(2-decyltetradecyl)-C96 (**53d**) is the first substituted large PAH known to be soluble in nonpolar solvents such as pentane or hexane. In contrast, hexa(3,7-dimethyloctyl)-C96 (**53e**) and hexa(4-dodecylphenyl)-C96 (**53f**), bearing side chains that induce high solubility in HBC's, display very low solubility regardless of solvent and temperature. Counterintuitively, the short 4-methoxycarbonyl-phenylene side chains of hexa(4-methoxycarbonylphenyl)-C96 (**53g**) induce very high solubility in opposition to the very poor solubility imparted by long flexible 4-*n*-C₁₂H₂₅-phenylene side chains (**53f**). Solubility is clearly a function of side-chain space-filling/packing, (strong solution aggregation indicates that dissolution occurs by solvent penetration inter-rather than intracolumnarly), though no clear correlation can be derived as yet.

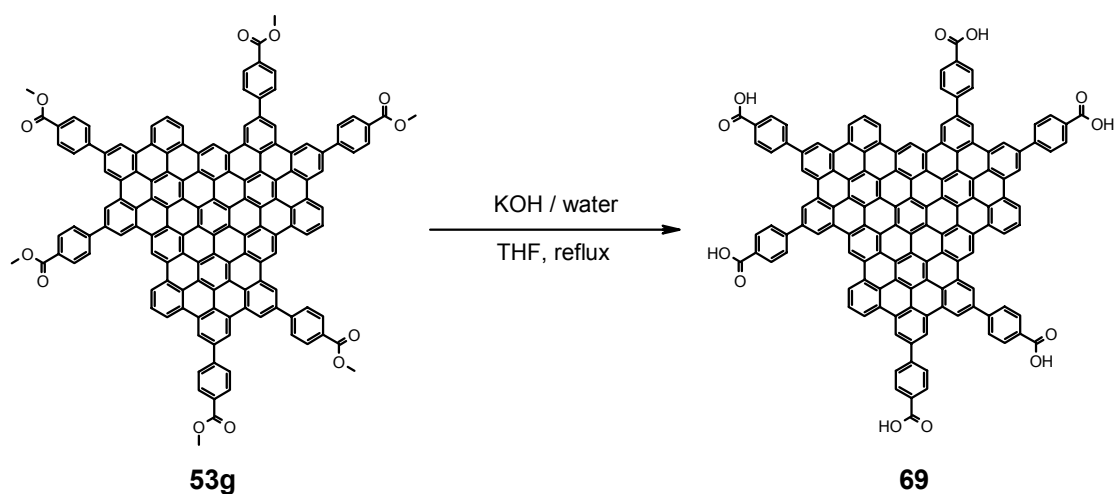


Figure 35. Hydrolysis of the ester groups of **53g** to carboxylic acids of **69**.

Although a hexaphenylbenzene carrying the same functionality as in **56g** resists cyclodehydrogenation to the analogous HBC, hexa(4-methoxycarbonylphenyl)-C96 (**53g**) was obtained under standard conditions. Soluble hexa(4-methoxycarbonylphenyl)-C96 (**53g**) is a novel functionalizable mesogenic building block, offering new possibilities for post-synthesis chemical modification of the ester groups, e.g. (non)covalent attachment of additional electronic components for columnar "double cables",^[33] polymer arms, etc. Hydrolysis of the ester groups of **53g** to carboxylic acids (Figure 35) imparts high solubility in alkaline water, most likely in the form columnar micelles.

2.2 Supramolecular characterization

Solid samples of **53a-g** were characterized by thermogravimetric analysis (TGA), differential scanning calorimetry (DSC), polarized optical microscopy (POM), and wide-angle X-ray scattering (WAXS). A prerequisite for the supramolecular behavior and phase characterization of the molecules studied is their thermal stability, which was investigated by thermogravimetric analysis (TGA) using nitrogen as inert gas. A typical example is shown in Figure 36.

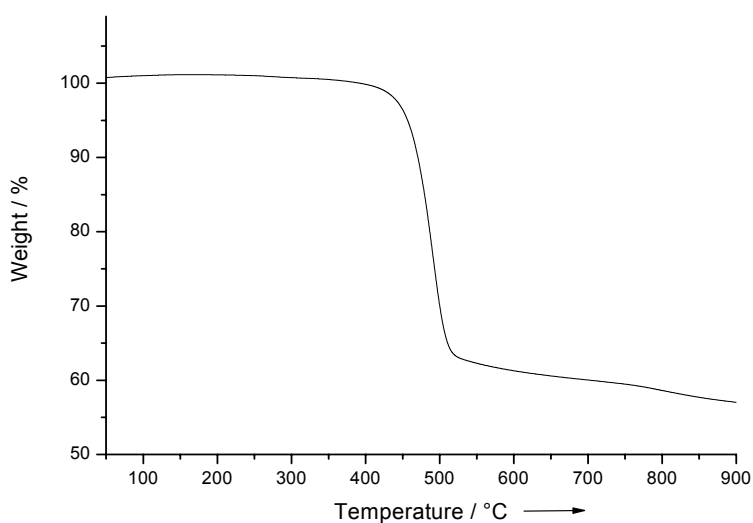


Figure 36. TGA analysis of C96-C₁₂ (**53a**)

Up to temperatures of about 300 °C the alkyl substituted C96 discs are stable, shortly thereafter a steady mass loss sets in up to about 500 °C which can be attributed to the decomposition of the alkyl chains.^[34] Above 500 °C thermal degradation of the aromatic core occurs, which remains incomplete up to a temperature of 900 °C, where still about 50% of the total mass remains. Therefore, when treating the studied compounds thermally, the temperature was kept well below the decomposition temperature.

Differential scanning calorimetry (DSC) was used to determine the temperatures at which structural transitions occur in the sample. The first heating curve often is dependent on the thermal and the treatment history of the sample, e.g. the conditions of precipitation. In order to evaluate reproducible results, the values from the second heating curve were taken into account. While **53b-g** show no thermal transitions (DSC) in the interval from -100 °C to 250 °C, **53a** gives a single, reversible first-order endotherm at 34 °C on heating (Figure 37). The endothermic enthalpy change that corresponds for this transition is 31.4 kJ/mol.

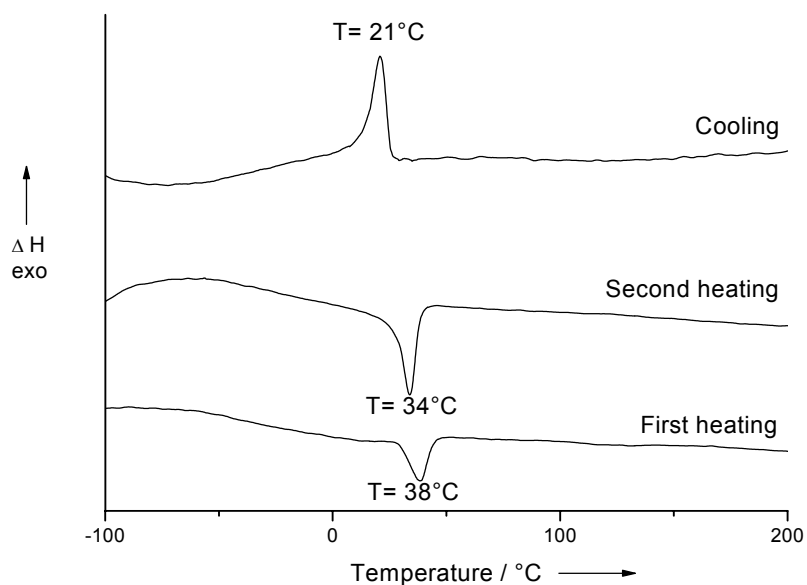


Figure 37: Differential scanning calorimetry scans of **53a** (10 K/min).

The liquid-crystalline character of **53a-d** was confirmed by the observation of birefringent, shearable thin films between crossed-polars, but no sharp changes with temperature were seen (Figure 38). Instead, we noted a steady increase in birefringence and the development of some as yet unassignable textures while annealing at 150 °C. This birefringence persists, i.e. the sample does not become isotropic, up to the experimentally accessible maximum, 550 °C (compare to HBC-C₁₂: $T_{\text{isotropization}} \approx 410\text{-}420$ °C). However, a characteristic fan-like texture typical for mesophases could not be observed, because the samples could not be first melted due to the high isotropisation temperatures of **53a-d**.

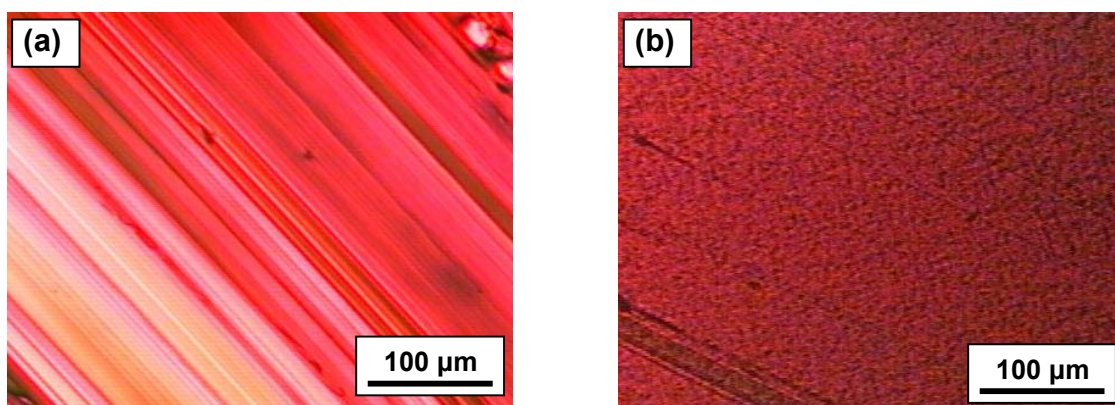


Figure 38. Polarized optical microscopy images of sheared film of (a) **53a** and (b) **53d**, at room temperature.

Surprisingly, **53a** is a soft waxy material at room temperature, in contrast to HBC-C₁₂ (**52**, R = *n*-C₁₂H₂₅)^[35] which is a microcrystalline powder, due to crystallization (tilting) of the discs within their columns and partial crystallization of the side chains. The C96 derivatives **53b-d** also possess the same waxy and soft consistency of **53a** at room temperature. To understand the structure of the materials in the bulk, temperature dependent X-ray scattering was measured for oriented fibers (as described in the Introduction). Fibers with coincident columnar and fiber axes were produced from **53a-d** by extrusion through a 0.7-mm orifice.^[35] Compounds **53e-g** could not be forced through the extruder, even

when heated as high as 200 °C. 2D-WAXD diffractograms of **53a-c** reveal hexagonally packed columnar mesophases with disc planes perpendicular to the columnar axes, derived from the three main features: *I.* equatorial reflections with relative reciprocal spacings $1, \sqrt{3}, \sqrt{4}, \dots$, indicating a hexagonal packing, *II.* a diffuse halo arising from liquid-like side chains, and *III.* intense symmetric arcs on the meridian at $d = 0.34$ nm, typical for π - π stacking (Figure 39 and 40). The broadness and low relative intensity of the higher order equatorial reflections may reflect the electron density profile (large disc cross-section with "thin" alkyl mantle), or may indicate short-range order lateral to the columns, again pointing to the high solubility in spite of very strong stacking.

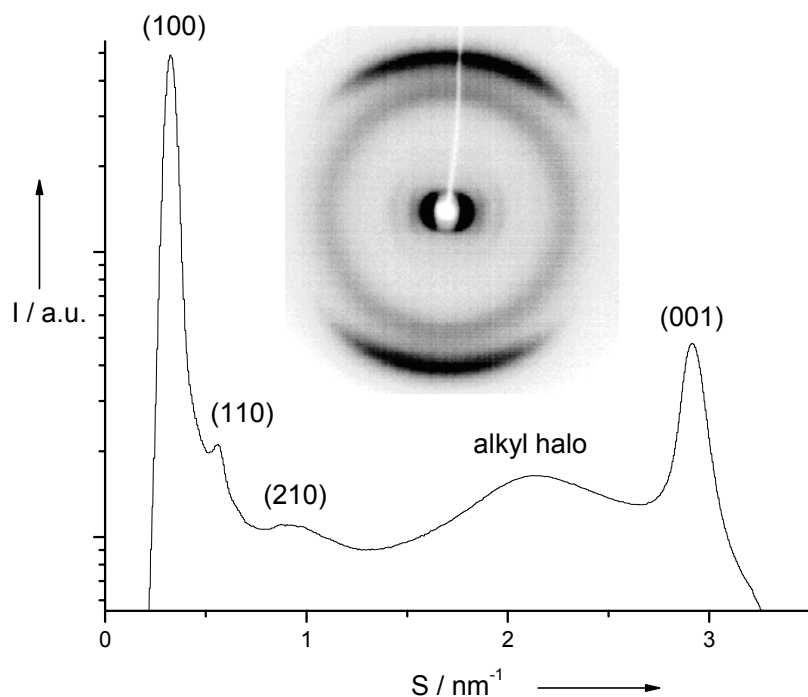


Figure 39. 2D X-ray diffraction pattern of an extruded fiber of **53a** and its integrated intensity distribution (room temperature after annealing at 150 °C for 12h).

At 30 °C, the unit cell parameter of the lattice in the hexagonal columnar arrangement of C96-C₁₂ (**53a**) and C96-C_{16,4} (**53c**) is expanded to $a = 3.19$ nm and $a = 3.83$ nm, respectively, relative to $a = 2.80$ nm for C96-C₇ (**53b**). This is

attributed to increasing the length of the alkyl substituents on the periphery of the core. Increasing the temperature to 150 °C results in slightly higher values of unit cell parameter, due to the thermal expansion of the system (for example, in case of C96-C₇ (**53b**) at 30 °C, $a = 2.80$ nm, while at 150 °C, $a = 2.88$ nm). The angle in a hexagonal cell is $\alpha = 120^\circ$.

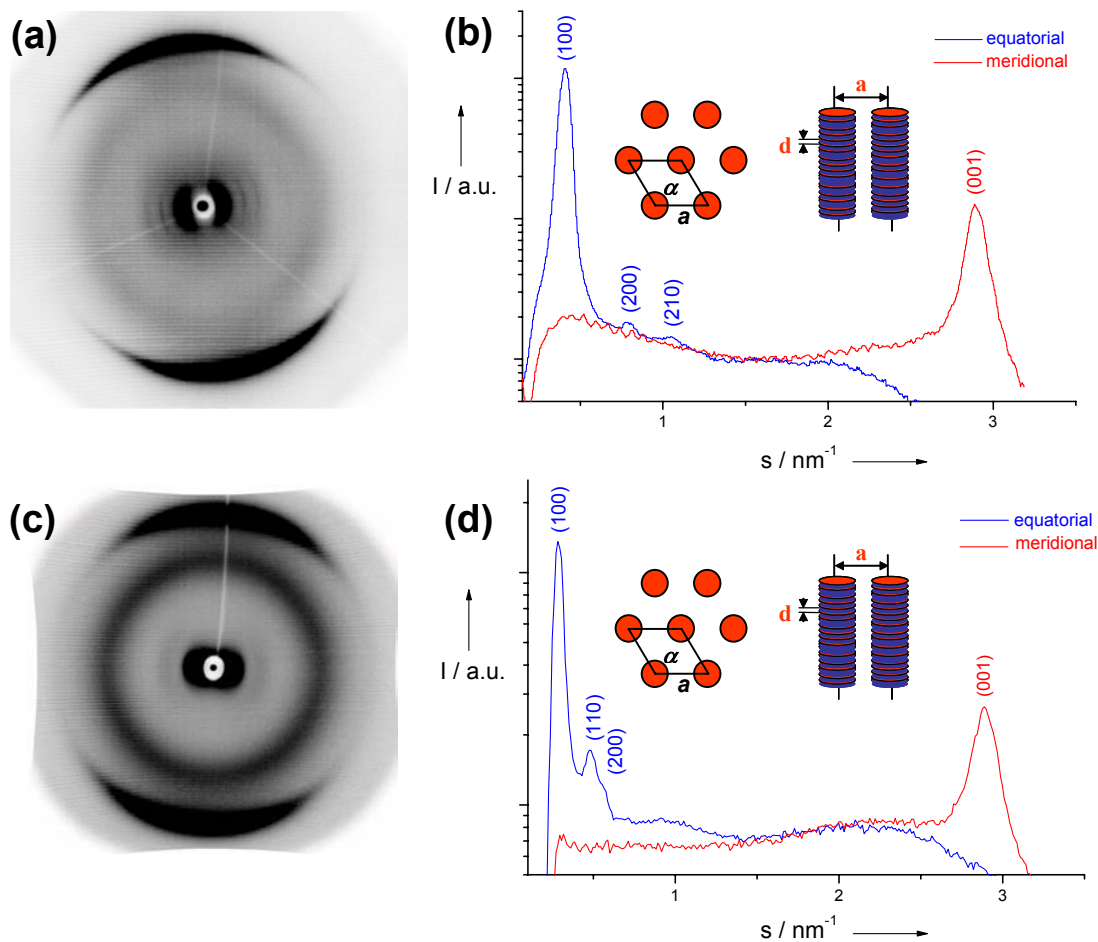


Figure 40. 2D-WAXS diffractogram of (a) C96-C₇ (**53b**) and (c) C96-C_{16,4} (**53c**) at 30 °C (after heating up to 150 °C and cooling back to room temperature); (b), (d) : intensity distribution along the equator and meridian.

The meridional reflexes ($d = 0.34$ nm, labeled 001) are relatively intense suggesting long-range intracolumnar order. "Crystallization" (tilting) of the cores, often observed in columnar discotics and planar π -systems in general,^[36,37] is completely suppressed at room temperature in the case of **53a-c**. In concord with

POM observations, there was no abrupt change in the diffraction pattern with temperature, but instead all peaks became sharper and more intense after annealing at 150 °C for 12 hours.

Cooling **53a** well below its endothermic transition and then measuring at room temperature reveals reversible reorganization to a superstructure superimposed on the hexagonal columnar arrangement. Additional weak smaller-angle meridional/equatorial reflexes and off-meridional reflexes flanking the original ~ 0.34 nm reflex appear while selected equatorial arcs split with minima at the equator, as shown in Figure 41. Measurement with a film camera and overexposure visualize weak diffraction results in additional meridional reflections at intermediate angle (Figure 41c). These suggest a superstructure which may arise from helical stacking.

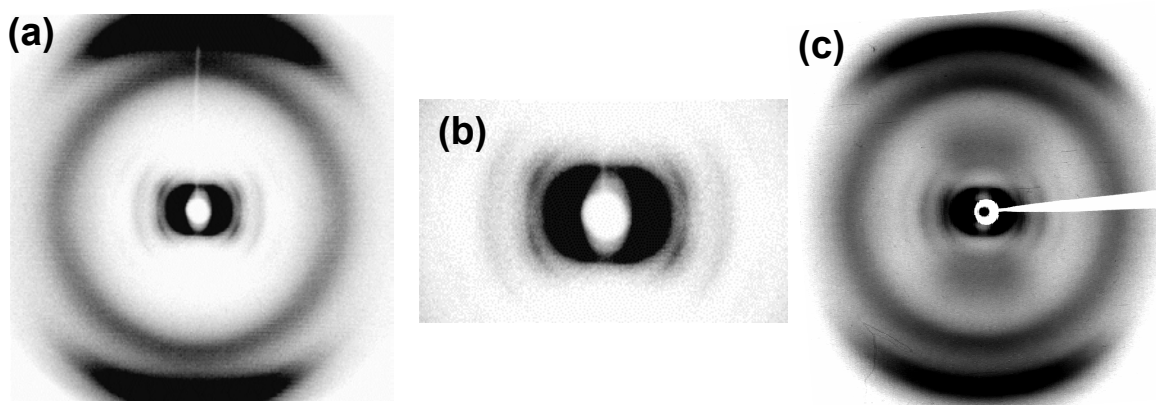


Figure 41. (a) 2D-WAXS pattern from extruded fiber of **53a** at room temperature after annealing at -30 °C overnight and (b) magnification of central region showing split equatorial reflections; (c) measurement with a film camera .

Preliminary studies also indicate that such a phase is present in HBC-PhC₁₂ in the low temperature phase, where thermal energy is sufficiently reduced and disc rotation ceases. The solid-state NMR and rheological measurements for C96-C₁₂ (**53a**) indicate cessation of disc mobility and a more rigid phase below the endothermic transition (Figure 42). These effects are ascribed to the predicted

helical stacking and/or formation of a "plastic"^[38] or "glassy"^[39] mesophase promoted by the "pinwheel" substitution pattern and the extended all-benzenoid PAH core. Smaller discotic π -systems become immobile and tilt to optimize intermolecular orbital interactions,^[37] a thermodynamic contribution which is overwhelmed at higher temperature. In the absence of tilting, favorable orbital interactions might be achieved instead by a lateral disc offset (graphite-like stacking).

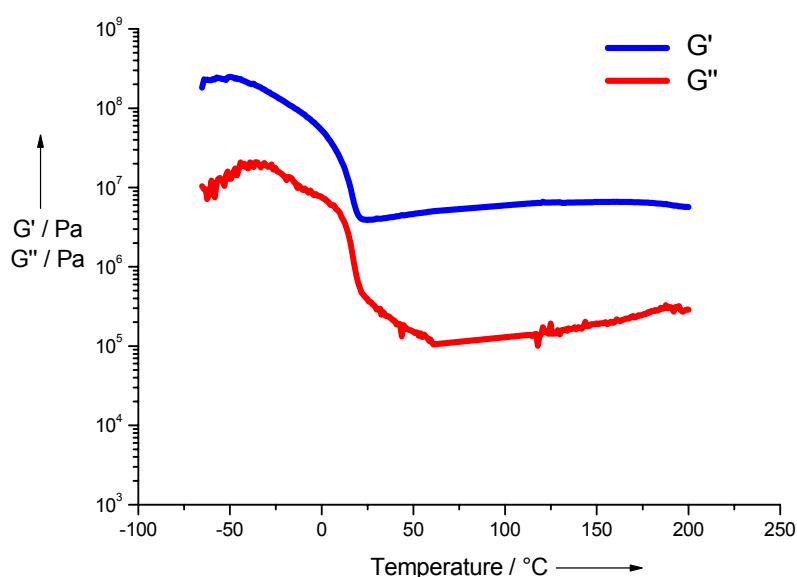


Figure 42. Storage (blue line) and loss (red line) moduli of **53a** recorded as a function of temperature during cooling (cooling rate is 2 °C/min.) The dynamic mechanical experiments revealed a change in shear storage modulus from more than 10⁸ Pa to 10⁷ Pa.

The 2D-WAXS patterns of hexa(2-decyltetradecyl)-C96 (C96-C_{14,10}, **53d**), measured at 30 °C and 150 °C are shown in Figure 43, and at both temperatures reveal that the molecules stack in columns which are arranged in a hexagonal lattice. This follows from the characteristic peaks for hexagonal ordering observed at scattering angle positions $1, \sqrt{3}, \sqrt{4}, \dots$. These peaks correspond to

the 10, 11, and 20 reflections in a two dimensional hexagonal lattice. The unit cell parameter is $a = 3.48$ nm, and this value remains the same from 30 °C to 150 °C.

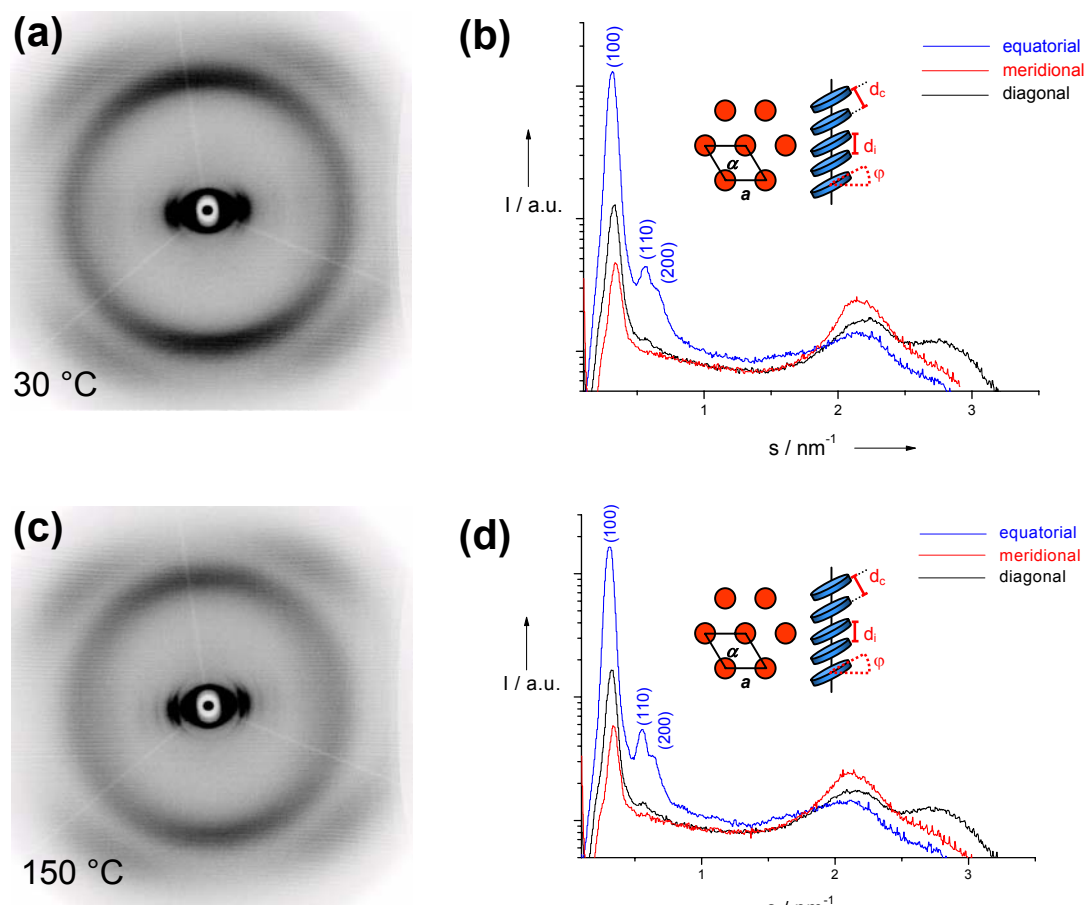


Figure 43. 2D-WAXS patterns of **53d** at 30 °C **(a)** and 150 °C **(c)**. **(b)**, **(d)**: intensity distributions along the equator, the meridian and the diagonal.

Reflexes seen on the meridian at 0.47 nm indicated that discs are tilted by an angle of $\varphi = 38^\circ$ relative to the columnar axis. The tilt angle is calculated using the equation $\varphi = \arccos(d_c/d_i)$ (see Figure 43). The repeat distance along the column d_i corresponds to the first peak in the meridional distribution (for **53d** the value of d_i is 0.46 nm). The cofacial distance d_c corresponds to the π - π stacking distance and is generally about 0.34 nm for flat π -systems. Introduction of the

long "dove-tail" alkyl chains around the core does not have an influence on the thermal behavior of **53d** (no phase transition in DSC). However, it shows a strong influence on the discs arrangement, and causes tilting of the discs within the columns with the respect to the columnar axis. This can be attributed to the branching at the β -position combined with the rotational freedom around the C96-C α bond, which induce a large steric demand and decrease the strong interaction of the aromatic cores.

All attempts to extrude fibers of **53e-g** failed. These compounds could not be forced through the extruder, even when heated to as high as 200 °C. Non-extruded samples of **53e-g** were measured at room temperature in a Θ - Θ -X-ray diffractometer, then heated to 150 °C and measured, cooled down and measured again. Typical powder X-ray diffractograms of **53e-g** are shown in Figure 44.

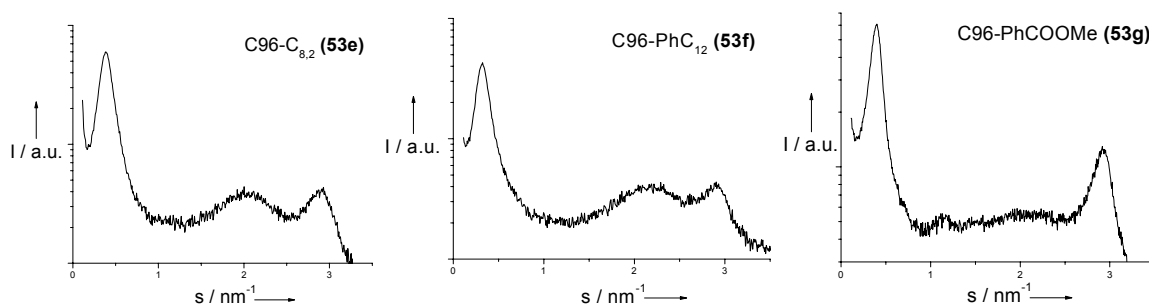


Figure 44. Powder X-ray diffraction patterns of **53e-g** at room temperature.

Independent of temperature, three main features can be observed: *I.* intense reflexes at $d = 2.56, 3.03$ and 2.56 nm for C96-C_{8,2} (**53e**), C96-PhC₁₂ (**53f**), and C96-PhCOOMe (**53g**), respectively, which are attributed to the lateral column-column spacing *II.* broad alkyl halo with a maximum at $d = 0.45$ nm, caused by the amorphous side chains (absent in the case of C96-PhCOOMe), and *III.* a broad reflex at $d = 0.34$ nm, which indicates the presence of the columns. Upon heating up to 150 °C and then cooling back to room temperature, no changes in the structure were detected. Compounds **53e-g** did not display a well-defined

correlation between columns. The only peak observed in the small angle region is consistent with a lateral column-column distance. The shape of this peak is rather broad and together with the absence of higher order reflexes (even at 150 °C) indicates that there is no long-range positional correlation between units.

2.3 Charge carrier mobility

The results presented in this section are the direct outcome of a strong collaboration with Dr. Michael G. Debije and Jorge Piris in the group of Prof. John M. Warman, TU Delft, The Netherlands.

The coaxially-insulated, conductive pathways provided by the columnarly stacked macrocyclic cores in mesomorphic discotic materials offer a unique possibility for one-dimensional charge transport. This makes discotic compounds serious candidates for applications as organic charge transport layers in a variety of devices such as field effect transistors, photovoltaic cells, and light-emitting diodes. For optimum performance, compounds are sought which display high charge carrier mobilities and a broad temperature range over which they possess liquid-crystalline mesophases. An estimate of the maximum mobility that could possibly be achieved with a given type of discotic material is therefore useful for setting realistic aims and guidelines for optimal device design and performance.

The pulse-radiolysis time-resolved microwave conductivity technique (PR-TRMC), as applied to the study of the conductive properties of discotic C96 materials, has been fully described elsewhere.^[40-43] Briefly, the bulk solid is contained in a cell consisting of a 1 cm length of Ka-band (26.5-42 GHz) waveguide, closed at one end with a metal plate ("short circuit") and flanged at the other end for connection to the microwave detection circuitry. A uniform micromolar concentration of charge carriers is produced in the sample by a nanosecond pulse of ionizing radiation (3 MeV electrons from a Van de Graaff accelerator). Any change in the conductivity of the sample resulting from the

formation of mobile charge carriers is monitored (without the need of electrode contacts) as a decrease in the microwave power reflected by the sample cell. The one-dimensional, intracolumnar charge carrier mobility is determined from the end-of-pulse conductivity per unit dose, $\Delta\sigma_{\text{eop}}/D$ (Sm^2/J), using the relationship

$$\Sigma\mu_{1D} = 3 \cdot \frac{\Delta\sigma_{\text{eop}}}{D} \cdot \frac{E_p}{W_p} \quad (1)$$

where E_p is the average energy deposited in eV per ionization event and W_p is the probability that initially formed ion-pairs survive to the end of the pulse. The value of E_p was taken to be 25 eV, and the values of W_p , which were all within the range 0.36 ± 0.12 for the present compounds, were calculated as described previously.^[40-43] The factor of 3 in Eq. (1) takes into account the fact that the organized columnar domains within the bulk samples investigated are randomly oriented and that charge transport is expected to be highly anisotropic and to occur almost exclusively along the axis of the macrocyclic stacks. The mobility sum, $\Sigma\mu = \mu(+)+\mu(-)$, is used in Eq. (1) since the PR-TRMC technique does not allow the determination of the separate contributions of the positive and negative charge carriers. The measurements were carried out on the freshly-prepared materials as received with no prior thermal treatment. Since the conductivity measurements are extremely sensitive to even trace impurities which function as trapping centers for mobile charge carriers, charge transport properties were measured for C96 derivatives (**53a,b,c**) which could be purified by column chromatography.

Figure 45 shows the mobility values as a function of temperature for the C96 derivatives. The data for **53a** display only a gradual increase with temperature with no abrupt change indicative of a phase transition. This behavior is also found for C96-C₇ (**53b**) and C96-C_{16,4} (**53c**) and has been previously reported for the HBC-PhC₁₂.^[44] This is in accordance with the fact that these compounds are already liquid crystalline at room temperature. The mobilities found for these compounds are all substantially lower than for the compounds which are crystalline solids at room temperature. This follows the general trend of

a reduced charge mobility in the mesophase of discotic materials which is attributed to the introduction of dynamic disorder within the columnar stacks on "melting" of the aliphatic side-chains. The maximum room temperature values of $\Sigma\mu_{1D}$ found for the liquid crystalline derivatives of HBC and C96 are all close to $0.2 \text{ cm}^2\text{V}^{-1}\text{s}^{-1}$, indicating no significant dependence on core size.

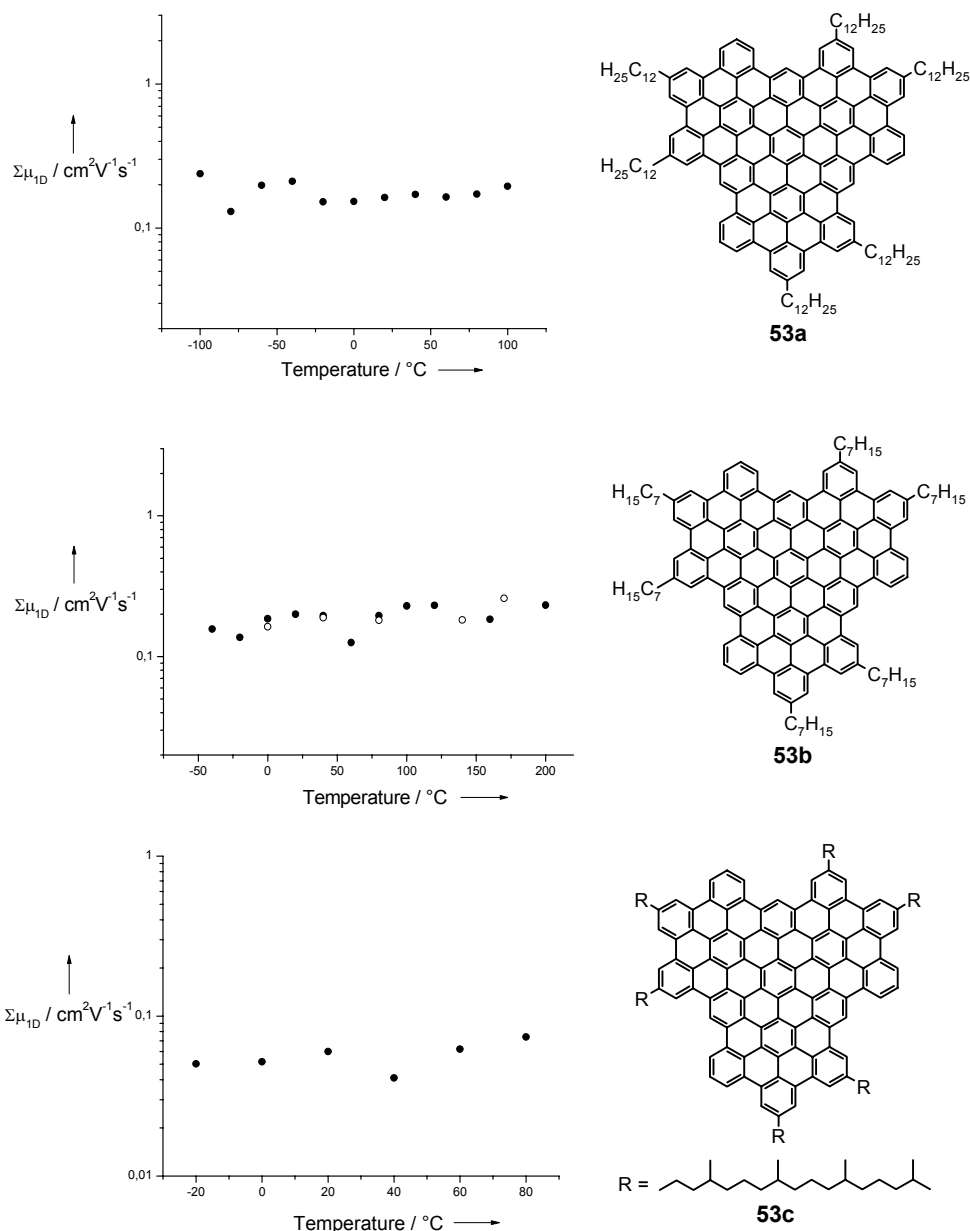


Figure 45. The temperature dependence of the one-dimensional intracolumnar charge carrier mobility for **53a,b,c**; first heating (full circles) and cooling (open circles).

Compound	T [°C]	Phase	$\Sigma\mu_{1D}$ [$\text{cm}^2\text{V}^{-1}\text{s}^{-1}$]	Calculated [c]
HBC-C ₁₂	RT	K	0.70	
	95 [a]	K	0.96	
	115 [b]	D	0.38	0.42
HBC-Ph-C ₁₂	RT	D	0.22	0.42
	100	D	0.31	
C96-C ₁₂	RT	D	0.16	1.26
	100	D	0.20	
C96-C ₇	RT	D	0.20	1.26
	100	D	0.23	
C96-C _{16,4}	RT	D	0.06	1.26
	100	D	0.08	

Table 2. Intracolumnar charge carrier mobilities $\Sigma\mu_{1D}$ in discotic HBC and C96 derivatives on heating: [a] – at about $T(K \rightarrow D) - 10$ °C; [b] – at about $T(K \rightarrow D) + 10$ °C; [c] – calculated using Eq. (2); K denotes the crystalline solid phase, D denotes columnar mesophase.

For comparative purposes, the mobility values for these compounds, given in Table 2, are for room temperature (RT) and temperatures of approximately 100 °C, *i.e.* close to the $T(K \rightarrow D) + 10$ °C temperatures for the room temperature crystalline materials (HBC-C₁₂). It can be seen that the mobilities in the mesophases of all of the C96 derivatives lie within the range ca. 0.1 to 0.3 $\text{cm}^2\text{V}^{-1}\text{s}^{-1}$. The values of $\Sigma\mu_{1D}$ for three alkyl substituted C96 derivatives **53a-c** show a tendency to decrease with increasing alkyl chain length from 0.23 to 0.20 to 0.08 $\text{cm}^2\text{V}^{-1}\text{s}^{-1}$ in going from C96-C₇ (**53b**) to C96-C₁₂ (**53a**) to C96-C_{16,4} (**53c**). A similar tendency has been found for alkoxy-substituted triphenylenes.^[41] The values found for the present compounds (**53a-c**) are approximately an order of

magnitude larger than the maximum value of $0.025 \text{ cm}^2\text{V}^{-1}\text{s}^{-1}$ previously found for discotic triphenylene derivatives,^[45] and similar to values found for HBC derivatives in the liquid crystalline phase.^[44] Moreover, the mobilities are essentially independent of temperature (over the range measured), which is of major importance with respect to applications in thin layer devices.

On the basis of the maximum values of the mobility found in the mesophase of a variety of discotic materials with different (hetero)aromatic cores, Van de Craats proposed the following empirical relationship between $\Sigma\mu_{1D}$ and the core size:^[45]

$$\Sigma\mu_{1D} = 3\exp(-83/n) \text{ [cm}^2\text{V}^{-1}\text{s}^{-1}] \quad (2)$$

The limiting, infinite core, value of $3 \text{ cm}^2\text{V}^{-1}\text{s}^{-1}$ was taken as the value found for sheet-to-sheet charge transport in graphite. The values of $\Sigma\mu_{1D}$ calculated using Eq. (2) for HBC and C96 compounds are given in the last column of Table 2. As can be seen, Eq. (2) predicts an increase by a factor of 3 in going from HBC to C96, whereas experimentally no improvement in charge carrier mobility was observed. In addition, the absolute value calculated for C96 is more than a factor of 5 larger than that actually measured. Eq. (2) is therefore clearly not supported by the present results. We conclude rather that the mobility is in fact relatively insensitive to the size of the aromatic core, at least for core sizes larger than approximately 40 carbon atoms. Although the C96 compounds studied were purified similarly to the HBC derivatives by using column chromatography, trace amounts of impurities may still be present after purification. In comparison to HBC, a larger excess of oxidant (iron(III) chloride) has to be used in the final cyclodehydrogenation reaction during the preparation of C96. Additionally, it is possible that the larger aromatic core of C96 more effectively interstitially traps traces of contaminants, which can not be removed using the purification techniques that are available to us. This may explain why no improvement of the values of $\Sigma\mu_{1D}$ is observed, since the conductivity measurements are extremely sensitive to even trace impurities which function as trapping centers for mobile charge carriers, thus canceling the advantage gained from a larger core size. On

the other hand, in recent theoretical work, consideration has been given to the influence on the charge transfer integral of lateral, longitudinal and rotational fluctuations within the columnar stacks of discotic materials.^[46-48] It was shown that charge mobilities are maximized in cofacial conformations, and they are dramatically reduced for angles of 60, 180 and 300°, as a result of the D_{3h} symmetry in case of the triphenylene molecule. Hence, deviations from cofacial packing, in order to avoid steric hindrance among lateral chains are highly detrimental to the transport properties. In the case of C96, which also possess D_{3h} symmetry, rotation of the cores will dramatically reduce the number of the core carbon atoms which can interact between adjacent stacked discs, and could be another reason for lower than expected values of $\Sigma\mu_{1D}$ being observed for C96 compounds. One of the general conclusions reached from the previously mentioned study was that "an increase in size of the conjugated core does not necessarily ensure better transport properties".^[46] The results presented here tend to support this conclusion.

2.4 Uniaxial alignment of C96-C₁₂ by solution processing

Direct processing of organic semiconductors from solution presents an important criterion for low-cost device manufacture. Additionally, an important step in the fabrication of efficient (opto-)electronic devices is control of structural order and the alignment of the ordered units of active semiconductor material, as this can improve charge carrier transport in the material significantly.^[49,50] It was shown that different device configurations require different kinds of order and therefore varied processing techniques. An efficient application in photovoltaic devices necessitates "face-on" arrangement of the molecules,^[17,51] while the "edge-on" order with uniaxial columnar orientation in the direction of the charge migration is desired in FETs.^[52-54] Langmuir-Blodgett^[55,56] and zone-crystallization techniques^[19,57] were reported as suitable methods to gain highly ordered surface layers. The solution casting onto pre-oriented poly(tetrafluoroethylene) (PTFE)

layers enables the fabrication of large aligned areas, with highly oriented discotic materials.^[58,59] Recently, using the zone-casting technique which is based on solution processing, highly ordered thin layers of HBC-C₁₂ were prepared.^[60] The optical properties of these films in polarized light could be switched reversibly from anisotropic in their crystalline state to high birefringent in the mesophase.^[61] This control of optical behavior was possible due to the highly ordered structure of these layers and the specific intracolumnar arrangement which changed from the herringbone structure in the crystalline state to the cofacial π -stacking in the mesophase. Moreover, these HBC-C₁₂ layers also revealed high field-effect properties (FET mobility up to $0.5 \times 10^{-2} \text{ cm}^2 \text{ V}^{-1} \text{ s}^{-1}$).

In this section, we demonstrate that large-area, uniaxially aligned thin films of C96-C₁₂ (**53a**) can be prepared in one processing step on untreated glass by the zone-casting technique. The results that are presented below were obtained in cooperation with Wojciech Pisula in the group of Prof. Müllen.

Zone casting was performed by using of a specially constructed apparatus, schematically presented in Figure 46. A syringe with the solution was placed into the upper heating block, whereas a glass support onto the lower block. Both blocks were thermally controlled. The solution flow was controlled by a step motor which ejects the solution at a constant flow. Another motor moves the support under a nozzle at a controlled speed causing the solution to be spread onto the support.

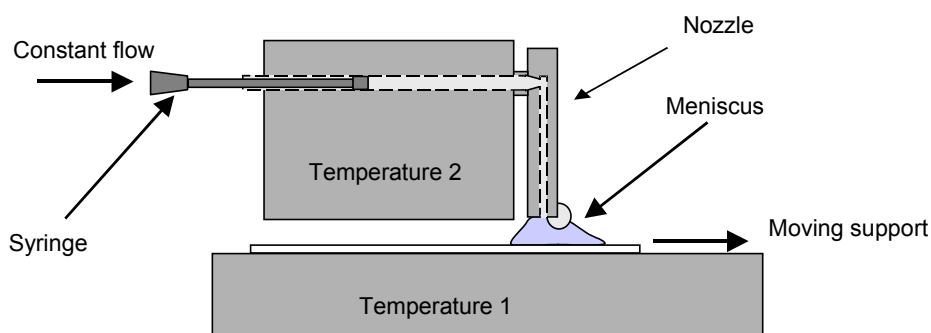


Figure 46. Schematic presentation of the zone-casting apparatus.

During this procedure, a meniscus is formed between the nozzle and the support. While the solvent evaporates, the concentration gradient changes within the meniscus. When the critical concentration is attained, the material begins to precipitate from the solution onto the moving support forming the aligned thin layer. The film morphology is controlled by the processing parameters, e.g. the polarity of the solvent, concentration, temperatures of the heating blocks, solvent flow, substrate velocity, which strongly affect the processed material. The optimal processing parameters for C96-C₁₂ were toluene solution (1 mg/ml), substrate velocity of 20 $\mu\text{m/s}$, and temperatures of 55 °C and 45 °C for the solvent and the substrate, respectively. The zone-casting was performed directly onto an untreated glass substrate.

Thin homogenous layers were obtained during the zone-cast processing of the discotic C96-C₁₂ at optimized conditions. The assignment of the optical anisotropy is one important tool in order to investigate the structure of the uniaxially oriented films.^[62] The optical anisotropy is strongly dependent on the transition dipole moment of the molecules, which in turn gives essential information about the molecular organization. Cross-polarized optical microscopy (POM) in Figure 47(a),(b) indeed exposed a high optical anisotropy of the zone-cast films. The degree of birefringence depended on the orientation of the layer's zone-casting direction axis relative to the analyzer/polarizer axis. It is obvious that the maximum birefringence appeared at angles of 45° between the deposition axis of the layers and the analyzer/polarizer axis, whereas by coinciding both axes an optically complete erasation of light was observed. This strong optical anisotropy of the layers was verified by absorption measurements in polarized light performed parallel and perpendicular to the casting direction. The absorption spectra are shown in Figure 47c. The absorption spectra of C96-C₁₂, recorded perpendicular and parallel towards the deposition direction, displayed a maximum absorption at 480 nm with a nearby shoulder at 565 nm. This is an 18 nm red shift in comparison to the absorption of C96-C₁₂ in solution. This significant absorption shift can be explained by the pronounced columnar aggregation in the solid-state film after zone-casting. A dichronic ratio of 3.04 was determined from the maximum absorption peaks, whereby the higher absorption

took place during the measurements perpendicular to the casting direction. The optical behavior observed for the zone-cast layers were similar to the results reported for thin HBC-PhC₁₂ films, which were uniaxially oriented on friction-deposited PTFE.^[62] The optical anisotropy of the layers aligned by both techniques is closely connected to the molecular arrangement and thus to the transition dipole moment which is oriented in the aromatic core. X-ray studies of bulk samples revealed an orthogonally arranged of the disc molecules towards the columnar axis.^[35] Therefore, the higher absorption of polarized light takes place perpendicular to the columnar axis, which is oriented in the casting direction, and the index of refraction parallel and perpendicular to the optical axis is different. At an angle of 45° of this optical axis to the polarizer directions, the sample imparts maximum birefringence.

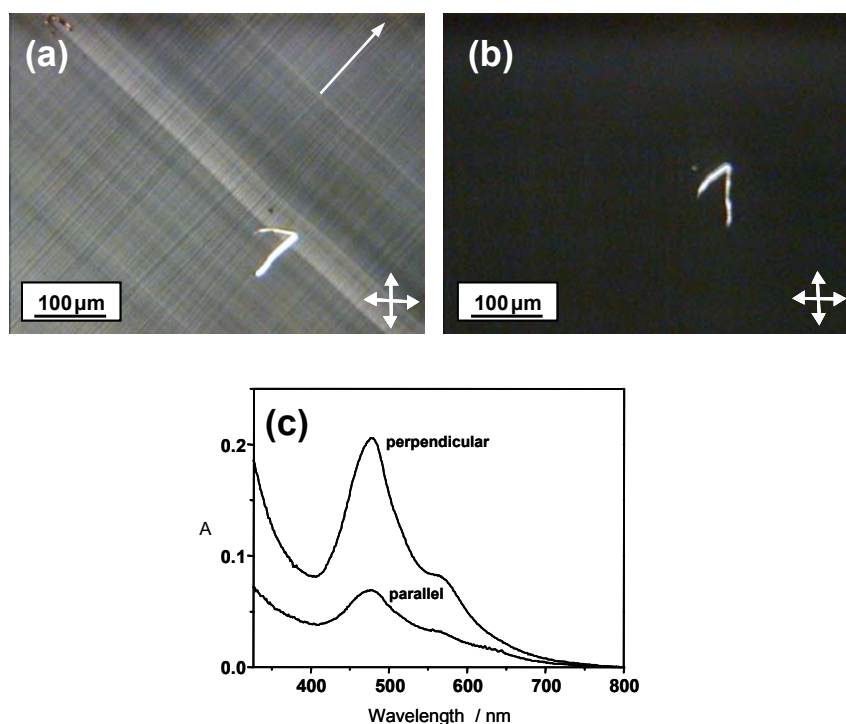


Figure 47. POM image of zone-cast C96-C₁₂ with (a) 45° and (b) 0° of the deposition direction towards the analyzer/polarizer axis. The number "1" shows that the same part of the sample and the same light intensity is used for both images. White arrow indicates the zone-casting direction; (c) UV/Vis absorption spectra in polarized light measured parallel and perpendicular to the casting direction.

In order to correlate the optical properties of the films with the supramolecular arrangement of the molecules, structure investigations by means of electron microscopy were performed. Electron diffraction enables the assignment of the intra- and intercolumnar in-plane structure within the zone-cast layers. Figure 48 presents typical electron diffraction pattern of zone-cast C₉₆-C₁₂. Distinct equatorial reflections indicate high uniaxial intercolumnar orientation in the casting direction. On the other hand, meridional peaks, corresponding to the characteristic intracolumnar distance of 0.34 nm, confirmed the orthogonal intracolumnar arrangement of the discotic molecules towards the columnar axis, also found in bulk samples. Moreover, the shape of the meridional reflections verifies also the high intracolumnar order of the molecules. The position of the first equatorial reflections peak was correlated to an intercolumnar distance of 3.26 nm for a C₉₆-C₁₂ hexagonal phase, which is in agreement with the unit cell parameters determined for extruded filaments, examined by X-ray diffraction.

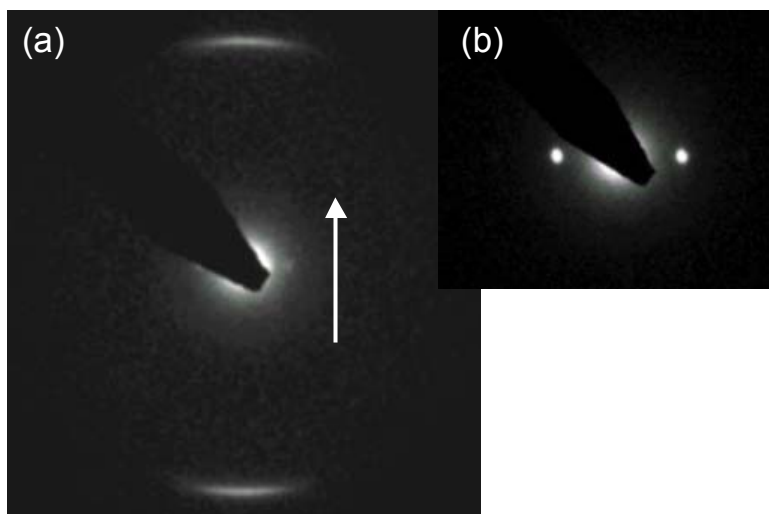


Figure 48. (a) Electron diffraction of zone-cast films of C₉₆-C₁₂; (b) magnification of the equatorial reflections from pattern in (a); arrows indicate the casting direction.

Since the electron diffraction results provide information only about the in-plane structure of the zone-cast films, additional X-ray scattering experiments performed in reflection offer information about the out-of-plane arrangement.

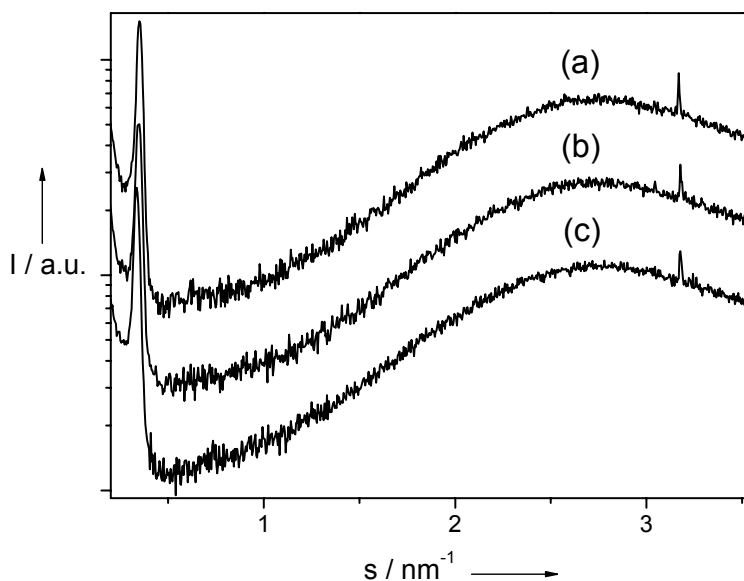


Figure 49. Temperature dependent theta-theta X-ray diffraction of zone-cast C96-C₁₂: (a) at 30 °C, (b) at 150 °C and (c) cooled back to 30 °C.

The X-ray diffraction presented in Figure 49 of zone-cast C96-C₁₂ suggests a uniform out-of-plane structure with an intercolumnar period identical to that in-plane. Furthermore, during thermal treatment no changes in the supramolecular structure were observed. This is analogous to the behavior reported for the bulk material which also did not show any temperature dependent structural transitions. Both techniques, electron diffraction pattern and X-ray diffraction, revealed only one main reflection at identical positions for the zone-cast C96-C₁₂ layers. By assuming an identical hexagonal columnar arrangement in the bulk and in the zone-cast surface layers, the appearance of the same unit cell parameter in both investigated planes might suggest strong displacement of the columnar lattice along the casting direction. A uniform hexagonal columnar order on the substrate would show reflections at a different position for both planes, but in a relationship of $\sqrt{3}$ to each other. Nevertheless, the results from electron diffraction proved that the columns were highly oriented in the deposition direction. Furthermore, the packing parameters evidently suggest that the discotic molecules were in a edge-on orientation towards the support. The aromatic cores were oriented perpendicular to the substrate and therefore the columnar axis parallel to it.

In conclusion, it was found that highly ordered surface layers of C96-C₁₂ can be obtained by the zone-casting technique. The organization of films obtained from solution depends strongly on the nucleation and growth ability of the material. The zone-cast films revealed high macroscopic uniaxial orientation of the columns with a molecular edge-on arrangement on the glass support and high intracolumnar arrangement of the discotic molecules, as confirmed by using polarized optical microscopy and structure studies performed by means of electron- and X-ray diffraction. These findings are essential for the possible application of the new C96-C₁₂ material in electronic devices, such as FETs, because of the ease with which highly ordered films can be prepared in one step from solution.

2.5 Self-assembly and electrical properties of supramolecular architectures of C96-C₁₂ studied by Scanning Force Microscopy (SFM) and Kelvin Probe Force Microscopy (KPFM)

In this section, the self-assembly of C96-C₁₂ (**53a**) from solutions onto a mica surface, using different solvents and deposition techniques is described. Moreover, attention is focussed on the growth of such a system on heterogeneous surfaces, in order to exploit surface recognition to direct the self-assembly on the tens of micrometers scale. Finally, the electrical characterization of networks of C96-C₁₂ molecules on a surface, achieved by using of Kelvin Probe Force Microscopy is also described. The results originate from a long and productive collaboration with Dr. Paolo Samori and Matteo Palma, ISOF-CNR, Bologna, Italy.

Dry thin films were prepared on muscovite mica surfaces systematically varying the solution concentration. The mica was freshly cleaved before the deposition took place. 1,2-Dichlorobenzene and chloroform were chosen as solvents, because they provide good solubility of C96-C₁₂. The temperature of

the substrate and the solution were systematically varied (up to 160 °C) during the deposition, in order to gain insight into its effect on the self-assembly at surfaces. To probe the kinetics of the process of self-assembly, the molecules were processed into thin films using three different methodologies (Figure 50):

(a) by *immersion* of the mica sample into a heated solution for 5 minutes followed by drying on a heating plate, at the same temperature as the solution for 2 hours.

(b) by *drop-casting*, by applying a 20 μl drop of solution onto the surface and letting the solvent evaporate. The time required for the complete evaporation of the solvent was a few hours (2 $\frac{1}{2}$ h) when deposition was carried out on a heating plate, or 2 days at room temperature.

(c) by *spin-coating*: a drop of solution is placed on the substrate that is rotated very fast for 30 sec. The adsorption therefore occurs very rapidly.



Figure 50. The deposition methods: (a) immersion, (b) drop-casting and (c) spin-coating.

Different methods (immersion, drop-casting and spin-coating), exploited to process the ultra-thin films from solutions onto surfaces, lead to different results. The formation of a given structure depends on the interplay between a number of parameters including the type of deposition process, the choice of the solvent,

the concentration as well as the temperature of the solution and of the substrate. These boundary conditions were systematically varied leading to three different surface morphologies:

I. a continuous layer, with a thickness ranging from 1.9 to 3.5 nm (Figure 51a). This height, being comparable with the molecule diameter, suggests an edge-on packing of the molecules at surface;

II. a percolated network of fiber-like objects, having widths of 11 ± 2 nm, heights of 2.7 ± 0.4 nm and lengths on the micrometer scale (Figure 51b);

III. broken patterns of elongated clusters with heights of 2.6 ± 0.8 nm, widths of 10 ± 2.5 nm and lengths of 200 ± 100 nm (Figure 51c).

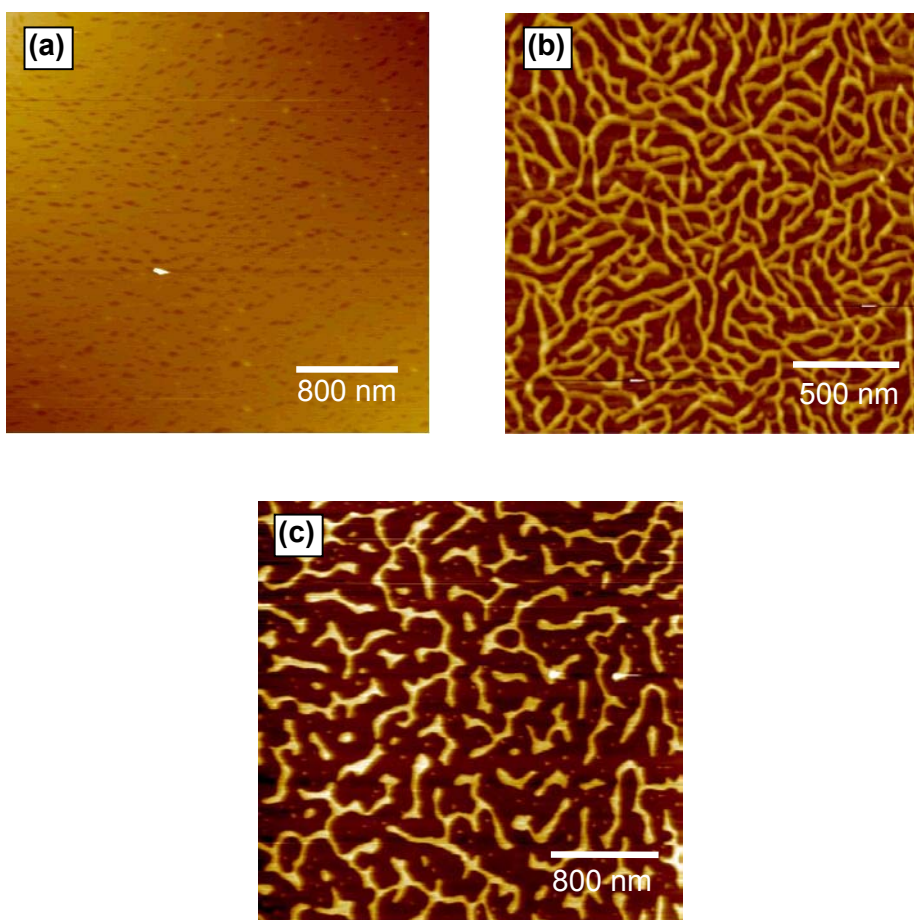


Figure 51. SFM topographical images of thin films of C96-C₁₂ adsorbed on mica by (a) drop-casting a 10^{-5} M 1,2-dichlorobenzene solution at 135 °C, (b) immersion of the substrate in a 10^{-6} M 1,2-dichlorobenzene solution at 85 °C. (c) drop-casting a 10^{-5} M chloroform solution at 45 °C.

Self-assembly from solutions is a quite complex process which involves the substrate, the solvent, the solute and the ambient atmosphere. The surface is initially coated with a uniform layer of solution. Assuming a non-uniform evaporation of the solvent, upon drying-up of the solvent, areas of uncovered dry surface are obtained.^[63] The unstable film evolves via nucleation and growth of these dry patches. At the end, the dry uncoated areas coalesce, the solvent evaporates completely and the molecules are frozen at the interface between colliding dry patches. The supramolecular arrangement depended strongly on the employed deposition method (drop-casting, immersion or spin-coating), even for the same solvent, concentration and temperature. Interestingly, the immersion method led to more uniform films on the micrometer scale.

2.5.1 C96-C₁₂ at the interface with Au electrodes

To measure the electrical behavior of molecules in a current-carrying electrical device, we need to connect them via electrodes to the outside world. Moreover, it is of prime importance to gain an insight into the properties of the molecular based architecture when interfaced to a metallic electrode. This is fundamental in order to tailor contacts, and with this in mind, we have studied the self-assembly of the C96-C₁₂ in confined spaces and its behavior when interacting with Au nanostructures.

To explore the role played by the type of substrate on the self-assembly, and to investigate interfacial recognition processes, we have produced a heterogeneous surface. A 180 μm wide mica channel located between two gold electrodes were prepared by vacuum sublimation of gold onto a freshly cleaved mica surface covered with a metallic wire. The channel was obtained by lifting off the covering wire. The thickness of the deposited gold layer was 12.1 ± 1.6 nm. This patterned surface was then used as a substrate for the deposition of a C96-C₁₂ solution. Large variations of surface morphology on mica have been observed on the tens of micrometer scale. Figure 52 shows various morphologies obtained with two different C96-C₁₂ solutions: a 10⁻⁵ M solution in chloroform drop

cast at room temperature (Figure 52b) and a 5×10^{-7} M solution in 1,2-dichlorobenzene deposited by immersion at room temperature (Figure 52c).

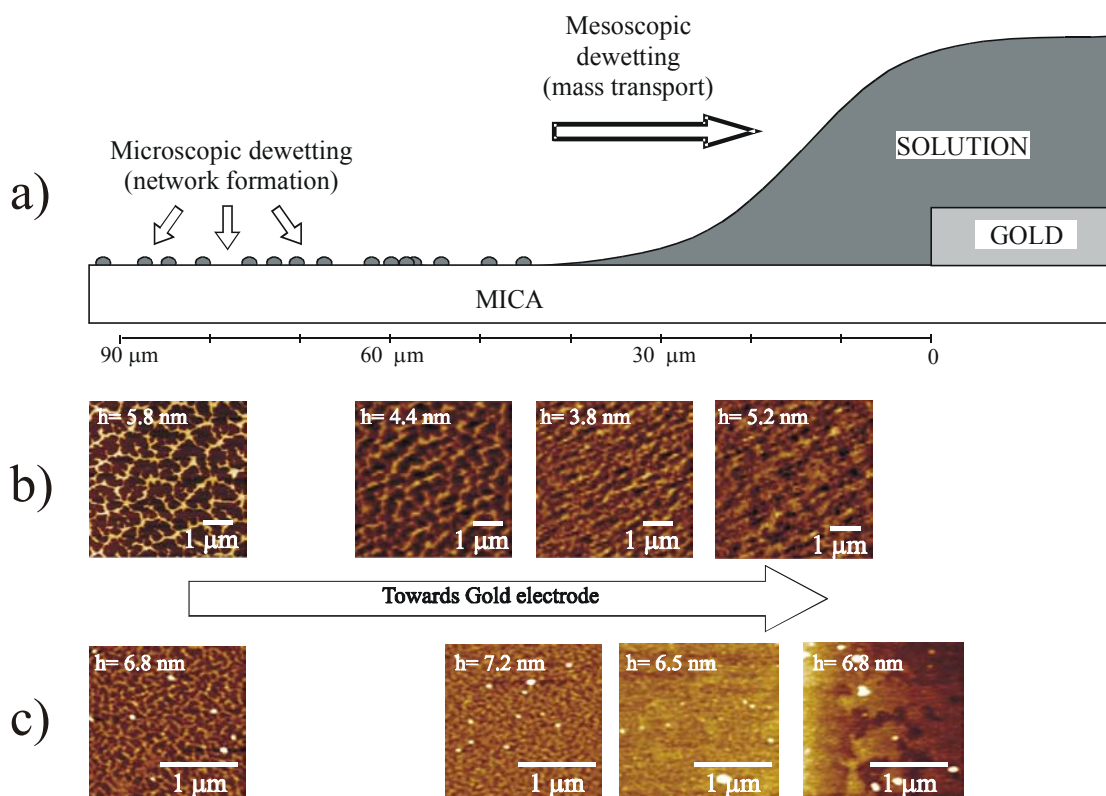


Figure 52. **a)** Schematic cartoon depicting the dewetting process. Topographical SFM image revealing **b)** different morphologies obtained on mica deposited by drop-casting a 10^{-5} M solution of C96-C₁₂ in chloroform at room temperature, at distances of 85, 55, 35 and 15 μm from the Au electrode; **c)** different morphologies obtained on mica depositing by immersion of a 5×10^{-7} M solution of C96-C₁₂ in 1,2-dichlorobenzene at room temperature, at distances of 85, 45, 25, 5 μm from the Au pattern. Image sizes and Z- ranges (h) are indicated in the images.

In both cases, at a distance of ~ 85 μm from the electrode the surface morphology was similar to that observed on a neat mica support, being characterized by the aforementioned percolated network. As the distance from the gold wall was decreased, the web density increased leading to a structure made up of

aggregates close to each other. At short distance (5 μm) from the Au electrode, flat layered areas begin to appear between the network regions, leading to a uniform monolayer of C96-C₁₂ that covered the surface near the Au wall; the layer had an average thickness of 1.4 ± 0.2 nm. This value is slightly smaller than the molecule diameter of 1.7 nm, thus suggesting an edge-on adsorption on mica with a slight tilt from the normal.

The organic solutions used in the various experiments preferentially interact better with Au rather than with mica, as confirmed by contact-angle measurements. If a drop is deposited at the Au-mica frontier, partial mass transport of the liquid towards the metal can be observed on the tens of micrometers scale by optical microscopy. This is evidenced by a rapid enlargement of the drop borders on the gold side, whereas the contact area with the mica is pinned. This suggests that the different morphologies previously observed are due to a longer retention of the solution in proximity to the gold electrode, while only an ultrathin liquid layer remains on the areas far from the electrode, which is prone to dry faster. The gold layer used in our experiments was only 12.1 ± 1.6 nm thick, while the effects of the step were visible at distances of tens of micrometers from the Au-mica interface. This suggests that the topographical effect on the surface morphology due to the Au step is negligible. Thus, the difference observed on such a mesoscale is likely due to different dewetting dynamics caused by the presence of the gold electrode, with the liquid drop slowly retreating toward the gold surface, as shown in Figure 52a. The resulting surfaces show a hybrid architecture where organic and metallic phases are in intimate contact. Hence, while Van der Waals interactions control the self-assembly process on a nanometer scale, hydrodynamic forces can govern the growth on micrometer and sub-micrometer length scales.

To have a homogeneous self-assembled structure on mica between two gold walls, a different method has been used for preparation of the C96-C₁₂ films in the confined space. This time the gold has been deposited by vacuum sublimation on top of the previously self-assembled C96-C₁₂ film consisting of fiber-like objects. For example, a film of C96-C₁₂ on mica prepared using the

immersion method from a 5×10^{-7} M 1,2-dichlorobenzene solution has been used for this purpose. On top of the spider web, 4.6 ± 1.3 nm thick gold layer has been produced by vacuum sublimation (Figure 53). This type of contact between the gold electrodes and our supramolecular nanostructures has been used to investigate the electrical properties of C96-C₁₂ architectures.

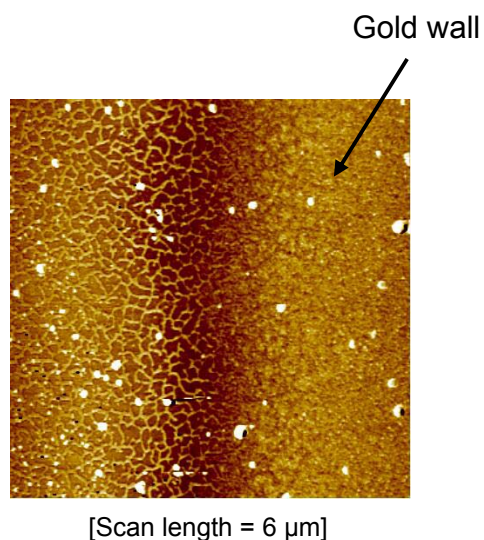


Figure 53. SFM topographical image of thin film of C96-C₁₂ (produced by immersion using 5×10^{-7} M 1,2-dichlorobenzene solution), partially covered by gold.

2.5.2 Electrical properties

Electrostatic force microscopy (EFM)^[64] and Kelvin probe force microscopy (KPFM)^[65] have been employed to study the electrical properties of different C96-C₁₂ architectures on mica. The surface charge on the sample has been mapped and absolute work function value of C96-C₁₂ nanostructures has been determined.

Recently a number of new atomic force microscopy (AFM) techniques exploiting electrically conducting probes have been developed to measure

electrostatic forces, charge distributions, voltage drops, capacitance, resistances and surface potentials on sub-100 nm length scales. These new AFM adaptations, i.e. electrostatic force microscopy, Kelvin probe microscopy, hold great promise for electrical characterization of materials since high resolution topographic imaging and electrical measurements are achieved simultaneously, providing direct correlation of electrical properties with specific topographic features.^[66]

Electrostatic Force Microscopy (EFM) maps the spatial variation of the potential-energy difference between a tip and a sample surface, which results from a non-uniform charge distribution and variations in surface work function. The work function, ϕ of an infinite metal surface is defined as the energy difference between two states of the solid.^[67] In the initial state the electron is in the highest occupied level of the neutral ground state of the solid, i.e. at the Fermi level E_F . In the final state the solid is singly ionized with the electron being at infinity in vacuum at rest, i.e. at the so called vacuum level (VL). For organic semiconductors it is reasonable to consider E_F at the midpoint of the HOMO-LUMO gap.^[68,69] For standard EFM imaging the research instrument is operated in non-contact mode with an electrically conducting cantilever. The conductive cantilever is electrically biased relative to the sample. This bias results in an electrostatic force between the tip and charge on the sample surface. This electrostatic force causes cantilever deflection. Standard EFM shows regions of relatively higher or lower surface charge on the sample.

Both AC and DC voltage bias signals can be applied simultaneously between the tip and the sample. In this case, the voltage between the tip and the sample can be expressed by the following equation:

$$V(t) = V_{dc} - \Delta\phi + V_{ac} \sin(\omega t) \quad (3)$$

where V_{dc} is the DC offset potential applied to the tip, $\Delta\phi$ is the surface potential on the sample (difference in work function between the tip and the sample), and V_{ac} and ω are the amplitude and frequency of the applied AC voltage signal, respectively.

For standard EFM imaging the conductive Si cantilever is electrically biased relative to the gold electrode previously deposited on the C96-C₁₂ fibres by vacuum sublimation. It was then possible to observe regions of relatively higher or lower surface charge on the sample. Figure 54 displays a topographical (Figure 54a) and an EFM image (Figure 54b) of C96-C₁₂ deposited on mica from a 10⁻⁵ M chloroform solution. The topographical image shows an adsorbate network having a height of 2.6 ± 0.8 nm. The typical width of the network features is 11 ± 2 nm, corresponding to several molecular diameters. Small globular co-adsorbates with a height of 5 nm are visible on top of the fiber branches (see arrows in Figure 54). In the EFM image the C96-C₁₂ network appears brighter than the surrounding flat areas, indicating that the former is more charged. On the other hand the co-adsorbates are darker. This suggests that they are more poorly charged and, importantly, provides evidence that the recorded EFM signal does not merely reflect the topography of the surface.

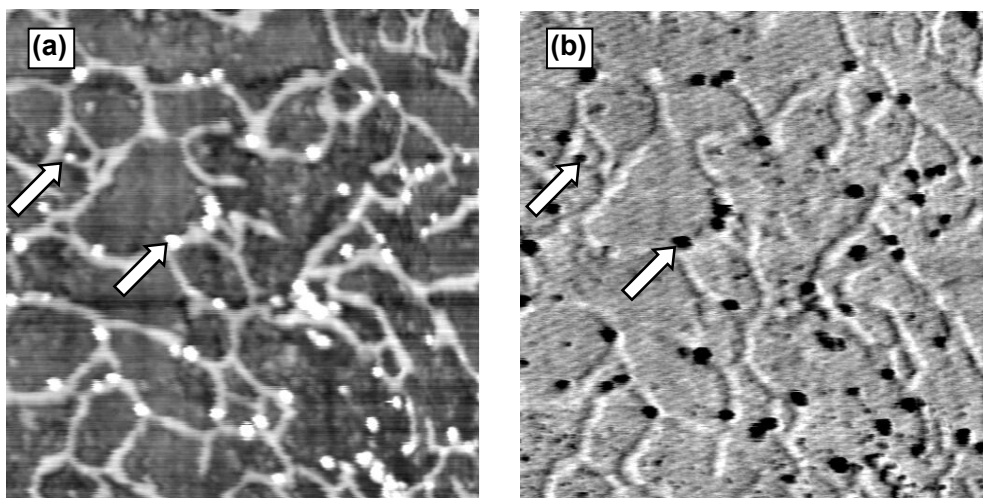


Figure 54. (a) SFM topographical and (b) EFM images of C96-C₁₂ networks deposited on mica from a 10⁻⁵ M chloroform solution. The EFM measurements were performed applying a bias of 8V to the sample. Arrows indicate impurities co-adsorbates on the network. Image size 1 μm.

The EFM yields only a qualitative indication of surface charging, and can not be applied for quantitative measurements. Thus, we implemented our system to perform KPFM microscopy.

Enhanced EFM mode, also known as Kelvin Probe Force Microscopy (KPFM) (Figure 55), provides quantitative data on surface charge.^[65,66] A feedback loop is the only additional equipment for this mode. This loop applies a variable DC offset potential (voltage) to the cantilever tip to maintain a zero electrostatic force on the tip. The potential difference that zeros the force on the tip is a measure of the surface potential difference between the tip and the sample ($F_\omega = 0 \Rightarrow \Delta\phi = V_c$). The research instrument is operated in non-contact mode with an electrically conducting tip. So the absolute work function value of semiconductor and metal surfaces can be determined knowing the work function of the tip. This can be easily obtained using a material with a well known work function value as a reference sample for the calibration.

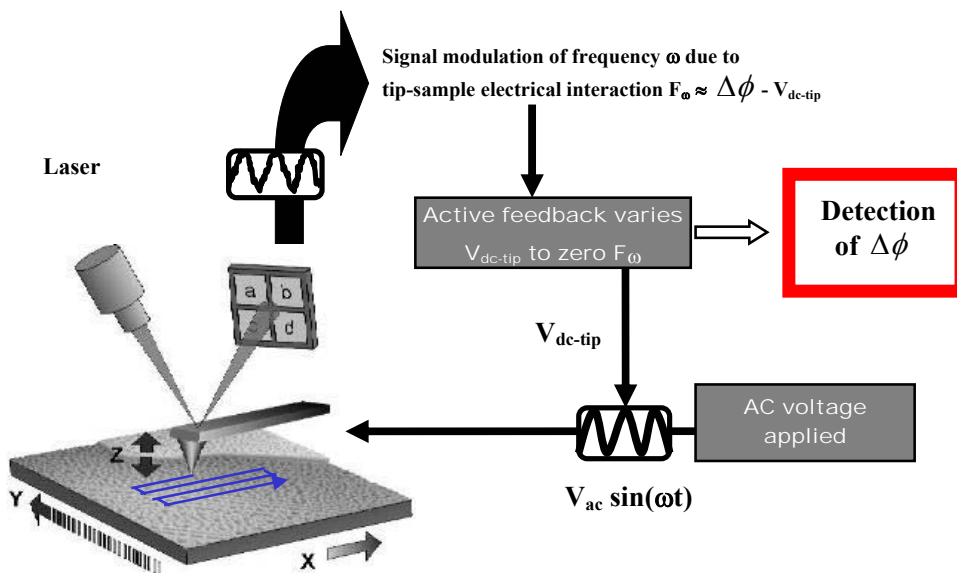


Figure 55. KPFM apparatus.

In our experiments a p-type silicon tip has been used, while HOPG has been employed as a reference sample for calibration. It is in fact easy to obtain a clean HOPG surface by simply cleaving the sample with adhesive tape. Moreover, the HOPG work function is well known to be 4.65 eV.^[70] Thus, on a freshly cleaved HOPG ($\Phi = 4.65$ eV) the surface potential (= work function difference between the tip and the sample) has been shown to be:

$$\Delta\Phi (\text{tip} - \text{HOPG}) = 225 \pm 10 \text{ mV}$$

so the silicon tip work function is:

$$\Phi (\text{tip}) = 4.65 + 0.225 = 4.875 \pm 0.010 \text{ eV}$$

This value is in reasonable agreement with that of $4.85 \pm 0.05 \text{ eV}$ for a p-type silicon. Materials with a known work function have then been studied to ensure the correct set up of the tip (Figure 56).

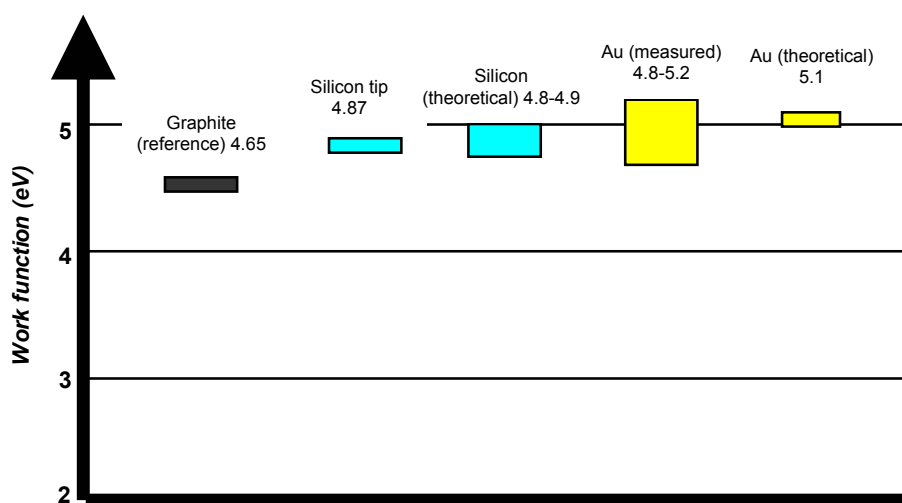


Figure 56. Work function values.

For Au surfaces ($\Phi = 5.1 \text{ eV}$) deposited by vacuum sublimation on mica, we have found (for different samples and for different zones of the same gold surface), a wide range for the experimented work function:

$$4.815 \text{ eV} \leq \Phi (\text{Au}) \leq 5.215 \text{ eV}$$

The observed variations in work function values for different gold surfaces are in good agreement with reference studies.^[71] Such effects can be caused by adsorbates or surface states since KPFM measurements are sensitive to dipole layers at the surface of the layer to be measured.^[71] It also can depend on the degree of crystallinity and on the crystal structure of the Au sample. By applying a potential bias (V_a) to the gold electrode, the surface potential of both the gold wall and the sample shifts upwards by an amount of V_a , while the difference in work functions remain constant.

Work function values for different C96-C₁₂ architectures have then been measured. The layers exhibits a surface potential of $\Delta\Phi = 1.00 \pm 0.01$ eV. Consequently the work function value for the C96-C₁₂ layer results

$$\Phi(\text{C96-C}_{12} \text{ layer}) = \Phi(\text{tip}) - \Delta\Phi = (4.88 - 1.00) \text{ eV} = 3.88 \pm 0.02 \text{ eV}.$$

Similarly, the work function of the networks and of the elongated clusters was

$$\Phi(\text{C96-C}_{12} \text{ network}) = 3.53 \pm 0.05 \text{ eV, and}$$

$$\Phi(\text{C96-C}_{12} \text{ clusters}) = 3.47 \pm 0.06 \text{ eV}.$$

The work functions of the three different types of C96-C₁₂ architectures are summarized in the graph in Figure 57.

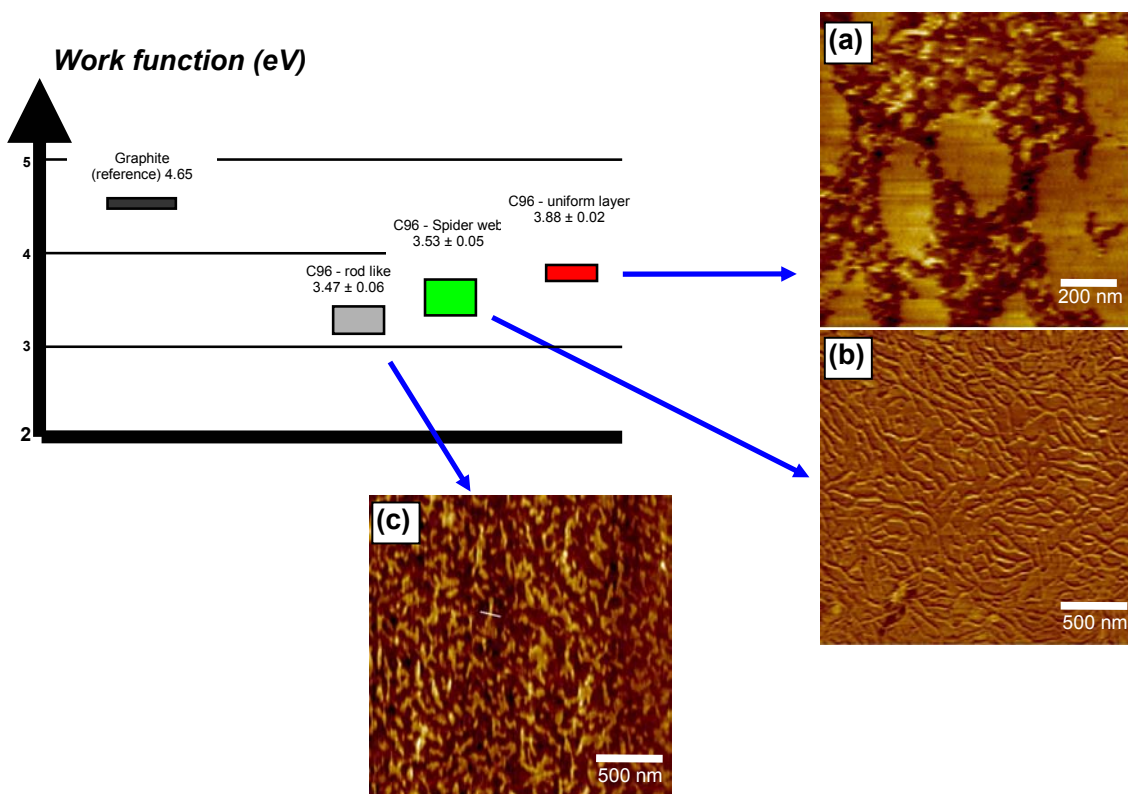


Figure 57. KPFM results and images of different C96-C₁₂ architectures: (a) layers formed by drop-casting a 10^{-5} M 1,2-dichlorobenzene solution at room temperature, (b) network obtained by immersion of mica in a 10^{-6} M 1,2-dichlorobenzene solution at 85 °C, and (c) elongated agglomerates produced by spin-coating a 10^{-5} M chloroform solution at 45 °C.

While the work function of the network was 350 mV smaller than the work function estimated for the self-assembled layers, that of the elongated clusters was found to be even lower. Noteworthy, it has been more difficult to obtain clear and reproducible KPFM imaging of clusters and of the fibers composing the continuous network because of the small cross section of these structures. It is reasonable to consider the layer work function value as a reliable result, since it is most likely that the values obtained for the fibers and for clusters are influenced by a systematic error. This is due to the long-range nature of electrostatic forces, which limits the spatial resolution attainable with the utilized tip. The measured potential is actually a weighted average over all the potentials on the surface, the derivatives of the capacitances being the weighting factors.^[72] The resolution and accuracy are limited by the capacitances between the tip and the respective surface regions, which means that the measured potential of an area will be influenced by the value of the surrounding surface potential. Therefore the determination of the work function of the network and of the clusters might be underestimated, even if the single clusters are well resolved in the image, as shown in Figure 54 where the lateral resolution is below 10 nm.

The measurement of the work function is a fundamental issue for the fabrication of devices, because the possibility to inject holes or electrons from metallic contacts into the organic layer will depend on the difference between metal and organic work functions, and on the electronic structure of their interface. The definition of work function itself is not straightforward. In its classical definition, it is the energy needed to remove an electron from the Fermi level in a metal to a point at infinite distance away outside the surface. This definition describes an "ideal" vacuum level energy for an electron at infinite distance, and is not compatible with the well-known fact that the work function is different for different faces of the same crystal. This is especially true for metal-organic interfaces. A more suitable definition for the vacuum level is the energy of an electron at rest just outside the surface.^[71] The work function we are measuring, depends strongly on the surface considered and is not a bulk parameter.^[71] The values obtained with KPFM are thus not an intrinsic characteristic of C96-C₁₂ but are very likely to depend on the local molecular

order on the surface, and can be compared with work function of other materials only considering them an average value of the whole nanostructured surface. On the other hand, the measurement of the effective work function of the material deposited on a surface in nanostructured patterns, rather than the work function of the same material in the bulk, is important for organic electronics applications.

The different morphological arrangements of C96-C₁₂ on the surface have significant differences in work function, a factor which is often mentioned in the development of nanoelectronic devices, but rarely probed on such small scales. The high resolution attainable with KPFM allows one to directly correlate, at nanometer scale, the electrical characteristics of a material with its structure. Even if the systems being considered are not regular at the molecular scale, the different arrangements observed have a strong effect on the electrical behavior of the whole system. The C96 material, deposited under different conditions on the surface, can show a variation of work function as large as 0.4 eV. The arrangement with the higher work function was found to be the layered one which is the more uniform and flat, while it is relatively easier to remove electrons from the networks. The network morphology has a higher mean curvature and surface roughness, greater disorder and may also possess a larger number of defects, e.g. missing discs, which could account for the lower work function measured.

In summary, the different arrangements of C96-C₁₂ molecules on mica were studied, along with the effect of these arrangements on the work function. It was possible to drive the self-assembly of C96-C₁₂ molecules on electrically insulating substrate toward three different surface morphologies (continuous layer, network of fiber-like objects, or elongated clusters) by tuning a variety of boundary conditions including the deposition method, the type of solvent and substrate, the concentration of the solution, and the temperature of the surface and of the solution. The formation of these three different assemblies is governed by the interplay of intramolecular, intermolecular and interfacial interactions. A key role is played by the mechanism of solvent evaporation at the surface. We have also studied the self-assembly behavior of C96-C₁₂ on mica in a confined geometry, namely in a mica channel, having a width of a hundred of micrometers,

between two hard walls of gold. The presence of the gold pattern generates a gradient of solution at different distances from the Au-mica wall, leading to different dewetting dynamics and thus different final morphologies on the tens of micrometers scale. A second approach to interface the C96-C₁₂ self-assembled fibers to the Au electrodes has been pursued by first depositing C96-C₁₂ fibers on mica and then subliming in vacuum the gold on the top, making use of a grid. This permitted us to obtain fibers that are just partially coated by gold. The rest of the fibers are exposed to air. In this way the conductive tip of SFM could be used as a counter-electrode to test the electrical properties of the nanowire architectures on the nanoscale. It has been shown that KPFM is a powerful method to simultaneously explore the morphological and electronic properties of nanoscale architectures self-assembled at surfaces, with a resolution below 10 nm and 0.05 V. We have determined the work function of C96-C₁₂ assemblies adsorbed onto the insulating mica with a high precision, and found that the work function can be lowered by depositing it in the form of interconnected networks or small islands, rather than as a continuous layer. These findings are important to improve the transport across a metallo-organic junction and more generally, to optimize the choice of the different components for the fabrication of supramolecularly engineered electronic devices. Finally, the results presented here pave the way towards KPFM measurements of the same supramolecular networks integrated in a working device, e.g. an organic transistor, with a spatial resolution of a few nanometers.

2.6 Superphenalene derivatives with lower symmetry

Desymmetrization is one of the most important concepts in synthetic chemistry. This concept covers not only the loss of symmetry through the introduction of an asymmetric centre into a molecule, but also reduction of symmetry due to constitutional, configurational and conformational modifications. This loss of symmetry affects the chemical and material properties of the

resulting compounds, as different parts of the molecule can now interact differently with other molecules or with surfaces or interfaces. Conformational desymmetrizations are particularly important in the design and preparation of functional materials. In order to reduce the melting point of discotic liquid crystals, the concept of reducing symmetry is adopted by many research groups, with the basic idea that if the molecular symmetry is reduced, then the molecules would pack less favourably in the crystal state and, therefore, the melting point will decrease. Asymmetrical substitution can have a large effect on the thermal behavior, but, also, can modify physical and electronic properties. However, the synthesis of desymmetrized materials, such as phthalocyanines^[73], porphyrins,^[74] or triphenylenes^[75-79] is not straightforward and may present a major synthetic challenge. Generally the most convenient synthetic methods for such materials rely on the undirected assembly of smaller building blocks. Using a mixture of starting components or using non-symmetrical components in such methods leads to complex statistical mixtures of isomers, which are frequently difficult to separate, and from which the desired isomers are often obtained in low yields. As a result, the best methods for making desymmetrized materials depend upon development of high-yielding synthetic steps to build the molecules up in a directed stepwise manner. Recently, new HBC derivatives with reduced symmetry were synthesized in our group, utilizing bromo or iodo substituted building blocks.^[22,33,80-83] These desymmetrized HBCs show different physical and chemical properties from their symmetrical analogs, for example their phase-transition temperature to the isotropic phase is lowered compared with symmetrical HBCs, as crystallization of the large aromatic cores within the columnar stacks is suppressed.^[81,84] In another example of their different and potentially advantageous physico-chemical properties, the ω -carboxyalkyl substituent on HBC acts as a hydrophilic anchor, such that highly-ordered Langmuir-Blodgett films can be formed at an air-water interface.^[85,86] This material also forms ionic complexes, via acid-base interaction with amino-substituted poly-siloxanes, which have been shown by X-ray diffraction experiments to possess a remarkable degree of long-range order.^[87]

The symmetry of a superphenalene can be reduced in different ways, such as core asymmetric substitution, for example, putting two or four peripheral chains in a superphenalene molecule, or side chains asymmetry by attaching alkyl chains of different length in the periphery or by changing the mode of the attachment of the peripheral chains, e.g., mixed alkyl-ester derivatives. Lateral modifications of the chemical structure will in any case very strongly disturb the three-fold rotational symmetry. We may therefore expect modified transition temperatures, but also the possibility of new supramolecular structures. Here we report our initial results on the facile synthesis of alkylated, desymmetrized superphenalene (Figure 59), and new building blocks, which can be converted into a range of useful functionalities (Figure 58).

2.6.1 Synthesis

In order to prepare superphenalene derivatives (**75**, **76**) with four and two alkyl chains at the periphery of the core, new building blocks **71a** and **72a** had to be synthesized (Figure 58).

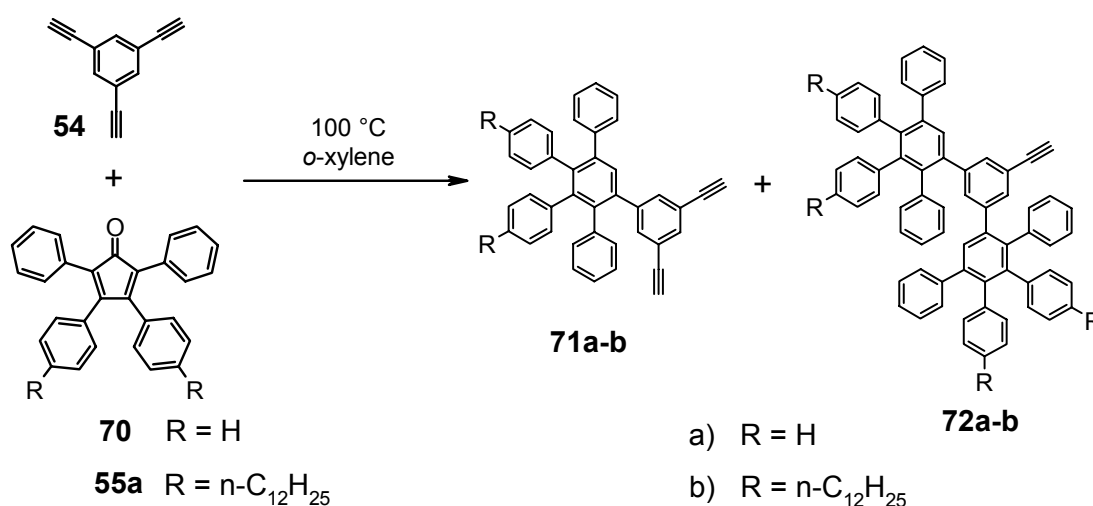


Figure 58. Synthesis of building blocks **71a-b** and **72a-b**.

Diels-Alder reaction of commercially available 1,3,5-triethynylbenzene (**54**) with one equivalent of tetraphenylcyclopentadienone (**70**), in *o*-xylene at 100 °C gave mixture of polyphenylene compounds **71a** and **72a**, which could be easily separated and purified by column chromatography. These compounds, carrying terminal triple bonds, can serve as building blocks for the introduction of new functionalities, such as bromine, iodine or ester groups, which do not hinder the cyclodehydrogenation reaction, and can be converted to a number of other different functionalities. The related building blocks **71b** and **72b**, also containing alkyl chains, which is important for solubility of the target compounds, could be prepared as well. A mixture of polyphenylene compounds **71b** and **72b**, obtained in Diels-Alder reaction of 1,3,5-triethynylbenzene (**54**) with 1.3 equivalents of 3,4-bis(4-dodecylphenyl)-2,5-diphenylcyclopentadienone (**55a**), in *o*-xylene at 100-140 °C, could be also separated by column chromatography and were isolated in 30% (**71b**) and 50% (**72b**) yield. The subsequent synthesis of asymmetric superphenalene derivatives **75** and **76** are depicted in Figure 59.

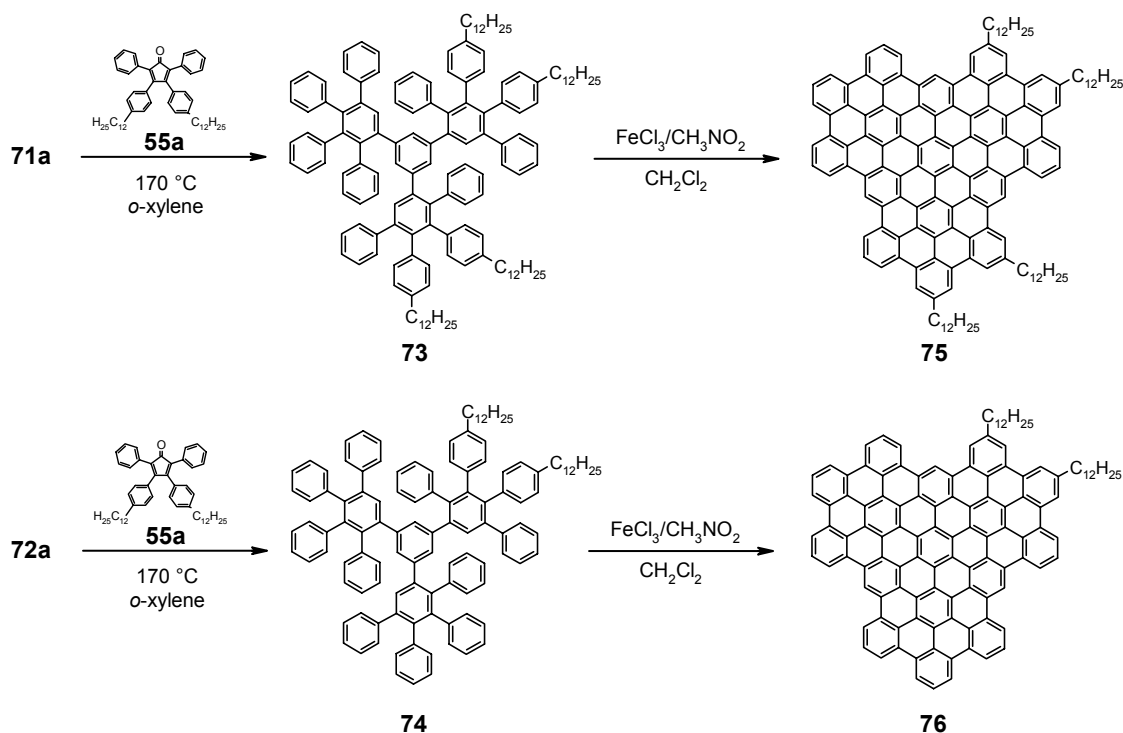


Figure 59. Synthesis of the asymmetrically alkyl substituted superphenalenes **75** and **76**.

The building blocks **71a** and **72a**, carrying terminal triple bonds, were used in a subsequent Diels-Alder reaction with an excess of 3,4-bis(4-dodecylphenyl)-2,5-diphenylcyclopentadienone (**55a**) (1.3 equiv per triple bond) in refluxing *o*-xylene, to afford the corresponding two and four alkyl substituted polyphenylene precursors **73** and **74**, in 88 and 83% yield. Both were readily soluble in organic solvents, and their purities were unequivocally confirmed by ^1H and ^{13}C NMR spectroscopy, FD mass spectrometry, and elemental analysis. The final step for this reaction sequence, the oxidative cyclodehydrogenation^[22,24] was carried out by addition of a solution of iron(III) chloride (90 equiv, i.e. 2.5 equiv per hydrogen to be removed) in nitromethane to the solution of **73** or **74** in dichloromethane. Throughout the duration of the reaction, a constant stream of argon was bubbled through the mixture to remove HCl formed *in situ*. Precipitation with methanol after 18 hours afforded the desired compounds **75** and **76** as deep red-brown solids, which were identified by MALDI-TOF mass spectrometry^[26,27] (Figure 60).

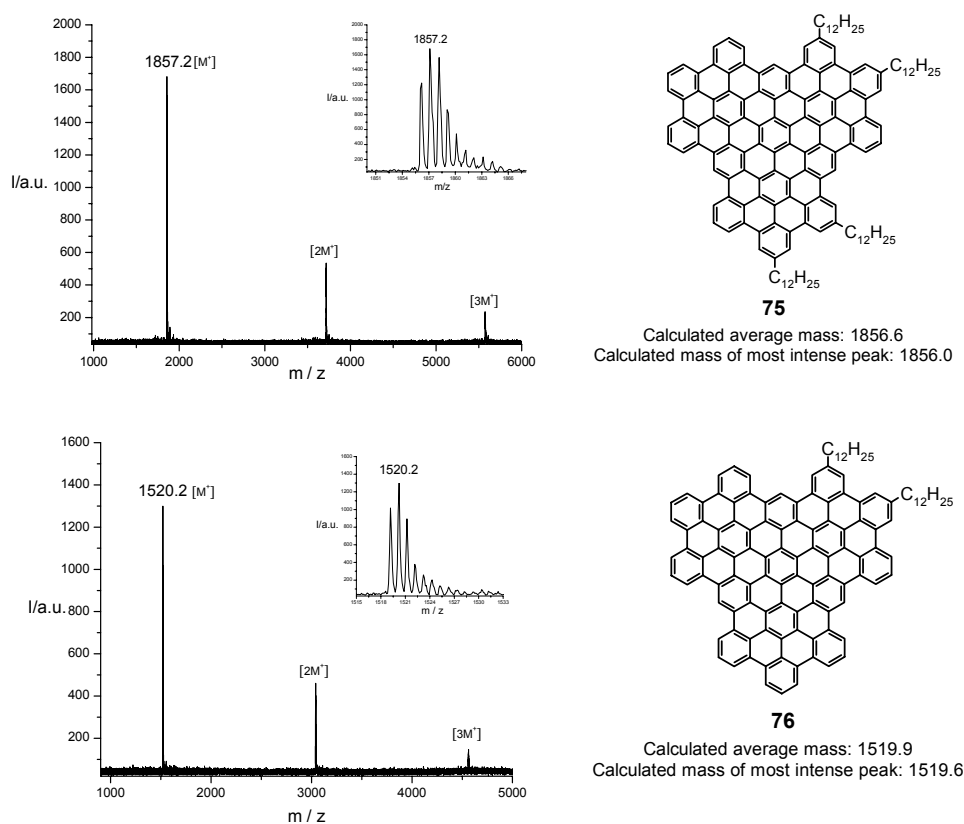


Figure 60. MALDI-TOF mass spectra of **75** and **76**.

We were astonished to find that a superphenalene disc with only four dodecyl alkyl chains (**75**) is soluble in common organic solvents after gentle heating or ultra-sonification. For further purification, **75** could be filtered through a column of silica gel with toluene. However, the poor solubility of **76** has so far precluded preparative chromatography.

The characterization of **75** with solution NMR technique was not useful. Even at elevated temperatures (up to 170 °C), it did not show any resolved signals in the aromatic region. The UV/Vis absorption spectrum of **75** shows a broad, asymmetric, featureless profile, with a low-energy tail extending to roughly 700 nm, as shown in Figure 61. Interestingly, the absorption maxima of **75** is located at 480 nm, and red shifted 18 nm compared with superphenalene with six alkyl chains (**53a**) (λ_{max} = 462 nm). This shift may be caused by different aggregate-formation of **75** in solution due to asymmetric alkyl substitution. The UV/Vis measurements of **75** in toluene or THF show no concentration dependence over the range 10^{-4} – 10^{-7} M. Likewise, a 10^{-5} M toluene solution, exhibits no temperature dependence over the range 20 – 85 °C (where 85 °C was the experimental maximum).

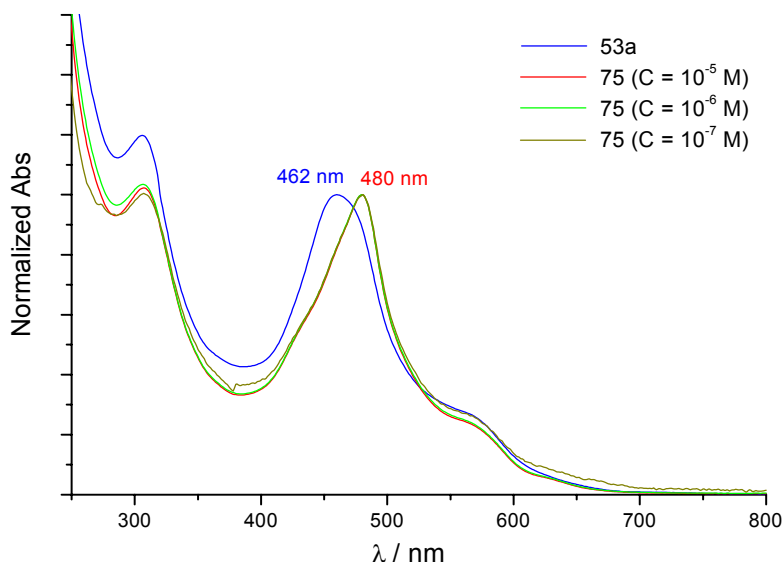


Figure 61. Normalized absorption spectra of **75** ($C = 10^{-5}$ – 10^{-7} M) and **53a** (blue line, $C = 6.3 \times 10^{-6}$ M) in THF.

2.6.2 Phase characterization

Differential scanning calorimetry (DSC), polarized optical microscopy (POM), and wide-angle X-ray diffraction (WAXD) were used to characterize the phase-forming properties of **75**. DSC of **75** did not reveal any phase transition in the interval from $-150\text{ }^{\circ}\text{C}$ to $250\text{ }^{\circ}\text{C}$. As in the case of other C96 derivatives, no clearing point was observed by POM below $550\text{ }^{\circ}\text{C}$ for **75**, indicating a thermally stable mesophase. Birefringent, shearable thin films between crossed-polarizers were observed, but no sharp changes with temperature were seen. Temperature dependent X-ray measurements were performed on an oriented sample. Orientation was obtained by extrusion of the material through a 0.7 mm orifice.^[35] The measured 2D-WAXS patterns are the same from a temperature of $30\text{ }^{\circ}\text{C}$ to $150\text{ }^{\circ}\text{C}$, and back to $30\text{ }^{\circ}\text{C}$. The diffractogram recorded at $30\text{ }^{\circ}\text{C}$ is shown in Figure 62 as a representative example.

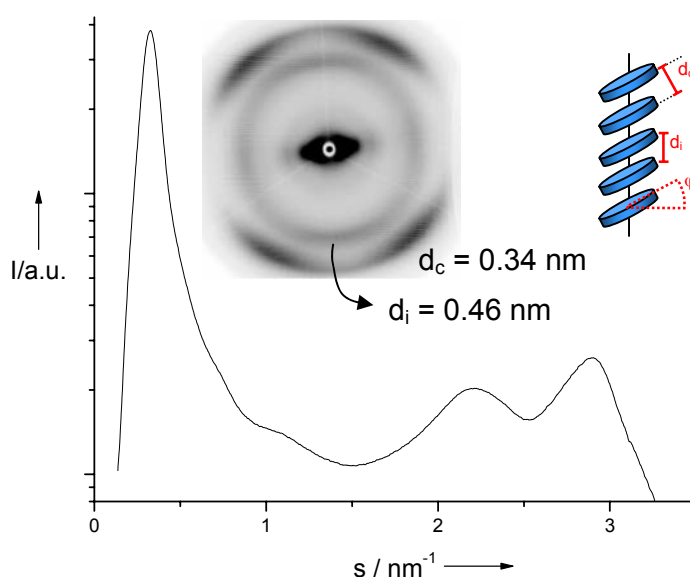


Figure 62. 2D X-ray diffraction pattern of an extruded fiber of **75** and its integrated intensity distribution, at room temperature.

Analysis of the results for **75** reveals a columnar structure with a tilted arrangement of the discs, preserved over the whole temperature range. The

molecules are tilted by an angle of $\varphi = 42^\circ$ relative to the columnar axis. The tilt angle is calculated by the equation $\varphi = \arccos(d_c/d_i)$, where d_i is the repeat distance along the column, and for **75** the value of d_i is 0.46 nm. The cofacial distance d_c is 0.34 nm, typical for the π - π -stacking distance. Hence, the asymmetric substitution of a C96 disc has strong influence on the intracolumnar arrangement of the discs, causing the tilting of the discs within the columns with the respect to the columnar axis. On the equator there is only the first-order peak recognizable, and no higher order reflections are visible. The reflexes in the equatorial direction are not resolved, even at 150 °C. The same results were obtained in Θ - Θ -X-ray measurements. Therefore, the limited diffraction data do not allow determination of the intercolumnar arrangement and the unit cell parameter.

2.6.3 Charge carrier mobility

The intracolumnar charge carrier mobilities of **75**, determined using the pulse-radiolysis time-resolved microwave conductivity technique (PR-TRMC), are shown as a function of temperature in Figure 63.

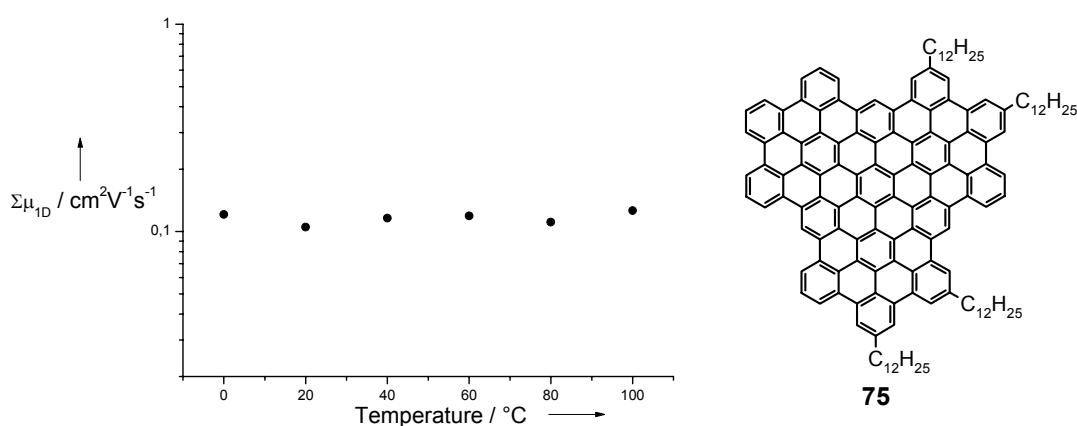


Figure 63. The temperature dependence of the one-dimensional intracolumnar charge carrier mobility of **75**, measured by the PR-TRMC technique.

The data for **75** in Figure 63 display only a gradual increase with temperature with no abrupt change indicative of a phase transition. This behavior is also found for C96-C₁₂ (**53a**), C96-C₇ (**53b**), C96-C_{16,4} (**53c**) and has been previously reported for the HBC-PhC₁₂.^[44] The values found for **75** (0.10-0.12 cm²V⁻¹s⁻¹) are slightly lower than values previously found for C96-C₁₂ (**53a**) (0.16-0.20 cm²V⁻¹s⁻¹). This can be due to columnar structure of **75** with tilted arrangement of the discs, which results in reduced orbital overlap of neighbouring discs within a columnar stack. On the other hand, non-tilted stacking of C96-C₁₂ (**53a**) increases the area of orbital overlap, which leads to a higher mobility.^[88,89]

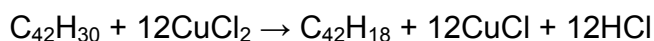
To summarize, it has been shown that the superphenalene core can be easily desymmetrized, and the facile synthesis of asymmetrically substituted C96 derivatives (**75** and **76**), with four and two alkyl chains, respectively, is presented. Critical for the synthesis of such asymmetric discs was the preparation of the mono- and di-yne building blocks **71a** and **72a**. Such building blocks (and their alkyl substituted analogues **71b** and **72b**, which were also prepared), could serve as useful starting points for the synthesis of other asymmetric C96 derivatives, bearing such functionalities as bromine, iodine or ester groups which offer many possibilities for further chemical modification. It was found that introduction of only two dodecyl alkyl chains onto the periphery of C96 core is not enough to provide any solubility, however, surprisingly, the C96 derivative with four dodecyl chains (**75**) could be dissolved upon gentle heating. Interestingly, in the solution UV/Vis spectra of **75**, a red shift was observed relative to the hexa-substituted C96-C₁₂ (**53a**). This shift may be caused by different aggregate-formation of **75** in solution, as a result of the asymmetric alkyl substitution. It has been found that the asymmetric alkyl substitution of the C96 disc has no effect on the thermal properties of the resulting compounds, as the large core size appears to be the dominant factor influencing the thermal behavior. However, the columnar packing of **75** is influenced by the symmetry of substitution at the core periphery; asymmetric substitution of C96 disc with four alkyl chains causes a tilting of the discs within the columns with respect to the columnar axis which is not observed in the case of the symmetrically substituted C96-C₁₂ (**53a**). Such a tilted

arrangement of the discs can result in reduced orbital overlap between neighbouring discs within a columnar stack, and may explain the slightly lower charge carrier mobility values of **75** relative to those previously found for C96-C₁₂ (**53a**).

2.7 Study of the oxidative cyclodehydrogenation reaction

As was pointed out in Chapter 1, intramolecular oxidative cyclodehydrogenation of oligophenylene precursors, which proceeds via a radical cation transition state, gives access to extremely large PAHs. The oxidative methods of the cyclodehydrogenation reaction are derived from the Scholl conditions^[90] and rely on Lewis-acids as reagents. A combination of aluminium(III) chloride and copper(II) trifluoromethanesulfonate in carbon disulfide has in many cases proven to be the best reagent for the planarization of unsubstituted oligophenylenes. Anhydrous iron(III) chloride is extremely efficient for the synthesis of large alkyl substituted PAHs, even up to a C132 disc, but can also be used for the preparation of unsubstituted discs. These cyclodehydrogenation conditions were adopted and modified from the work of Kovacic, who discovered that benzene could be polymerized to poly-*para*-phenylenes (PPP) by a Lewis acid and an oxidant.^[24]

The synthesis of hexa-*peri*-hexabenzocoronene (HBC, **8**) is the most investigated example of oxidative intramolecular cyclodehydrogenation.^[6,22] Starting from hexaphenylbenzene, C₄₂H₃₀ (**77**), in the presence of copper(II) salts under Lewis-acid conditions in an inert solvent, a multiple, intramolecular cyclodehydrogenation is performed with complete aromatization to the desired product, according to the general process:



The aromatization of each newly formed carbon-carbon bond leads to the elimination of two hydrogens, which are ejected as two HCl molecules. Every new carbon-carbon bond formation is associated with a cyclization which

increases the size of the PAH being formed. Recently, it was shown by Kübel that by using a smaller excess of the oxidizing agent, an intermediate product, phenyldibenzo[*fg,ij*]phenanthro[9,10,1,2,3-*pqrst*]pentaphene (**78**) could be isolated (Figure 64).^[91] Other intermediate products containing only two new carbon-carbon bonds were observed in trace amounts. The observation and isolation of intermediate products proves that oxidative cyclodehydrogenation does not occur as a concerted planarization of all phenyl rings under carbon-carbon bond formation in one step, but proceeds in separate reaction steps.

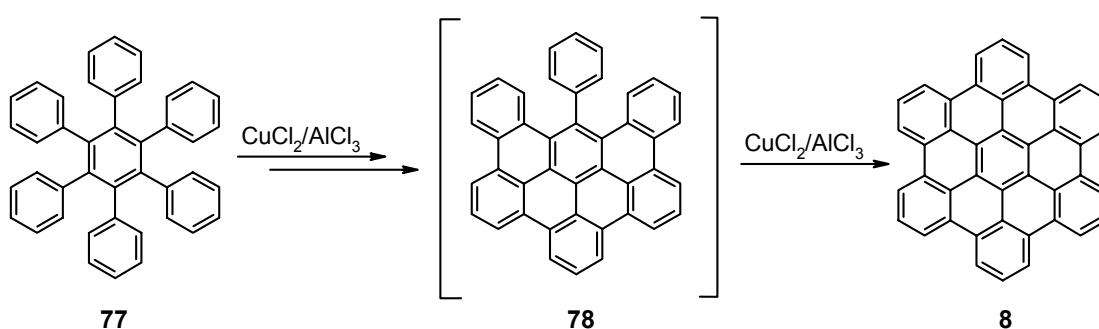


Figure 64. Oxidative cyclodehydrogenation of hexaphenylbenzene (**77**) yielding HBC (**8**) after formation of an intermediate product **78**.

In order to cast light onto the intramolecular oxidative cyclodehydrogenation of the C₉₆ precursor (C₉₆H₆₆), this reaction has been systematically studied. It should be pointed out that an additional source of complexity in the case of larger oligophenylene precursors is the greater number of sites for the formation of each new carbon-carbon bond. Thus, in the case of the C₉₆ precursor, the cyclodehydrogenation can progress from the "outside" periphery towards the "inside" of the dendrimer, or from "inside" of the dendrimer towards the periphery, or these two possibilities can occur in parallel and simultaneously. Two different pathways of the cyclodehydrogenation of C₉₆ precursor (**79**), and some of the many possible intermediates which can be formed during this reaction, are depicted in Figure 65.

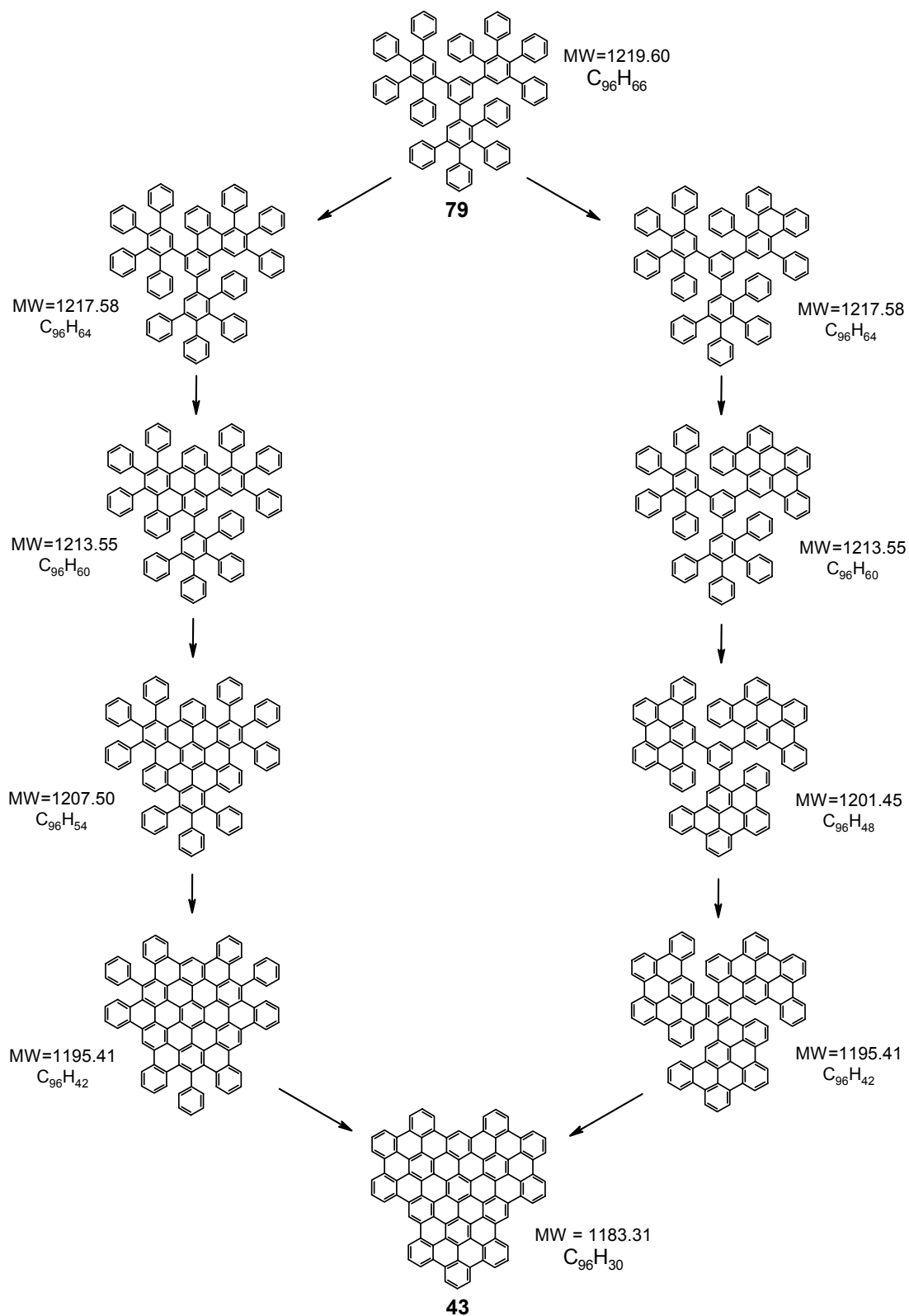


Figure 65. Two different pathways of the cyclodehydrogenation of C₉₆ precursor C₉₆H₆₆ (**79**) and some of many possible intermediates.

The most crucial factors in the planarization reaction are the stoichiometry of cyclodehydrogenation reagent employed and the reaction time. Hence, a series of cyclodehydrogenation reactions of the C96 precursor with different quantities of iron(III) chloride and different reaction times was carried out. In order to avoid complete planarization and attempt to isolate intermediates, a smaller excess or deficiency of the oxidizing agent and shorter reaction times were used. Iron(III) chloride acts as both Lewis acid and oxidizing agent, and by predissolving it in nitromethane, it can be added homogeneously to the solution of the precursor in dichloromethane at room temperature. The concentration of the dichloromethane solutions of C96 precursor used in our experiments was always the same (100 mg of precursor in 100 mL of dichloromethane). To remove hydrogen chloride formed during the reaction, a steady stream of argon was bubbled through the reaction solution. After quenching the reaction by addition of methanol, mass spectra of the resulting cyclodehydrogenation products were measured and are depicted in Figure 66. The reaction conditions including the number equivalents of iron(III) chloride per hydrogen to be removed and reaction times are noted in the figure and the calculated masses of the starting material ($C_{96}H_{66}$, MW=1219.6) and the fully closed disc ($C_{96}H_{30}$, MW=1183.3) are shown as lines. The sample preparation for MALDI-TOF was done according to the solid-state method with TCNQ as matrix.^[26,27]

Starting with a small excess of 1.5 equivalents of iron(III) chloride per hydrogen to be removed and a reaction time of one hour (experiment 1), resulted (according to the MALDI-TOF mass spectrum) in the formation of fully planarized disc $C_{96}H_{30}$ (peak at 1183 Da) and partially cyclized products (peaks at 1188 and 1198 Da). The first peak at 1183 Da is the most intense one, suggesting that the cyclodehydrogenation reaction of the $C_{96}H_{66}$ dendrimer was driven more towards the completely dehydrogenated product. Although an exact quantification of the distribution from mass spectrometry is not possible since the differently cyclized products possess different desorption probabilities, some clear conclusions can be made.

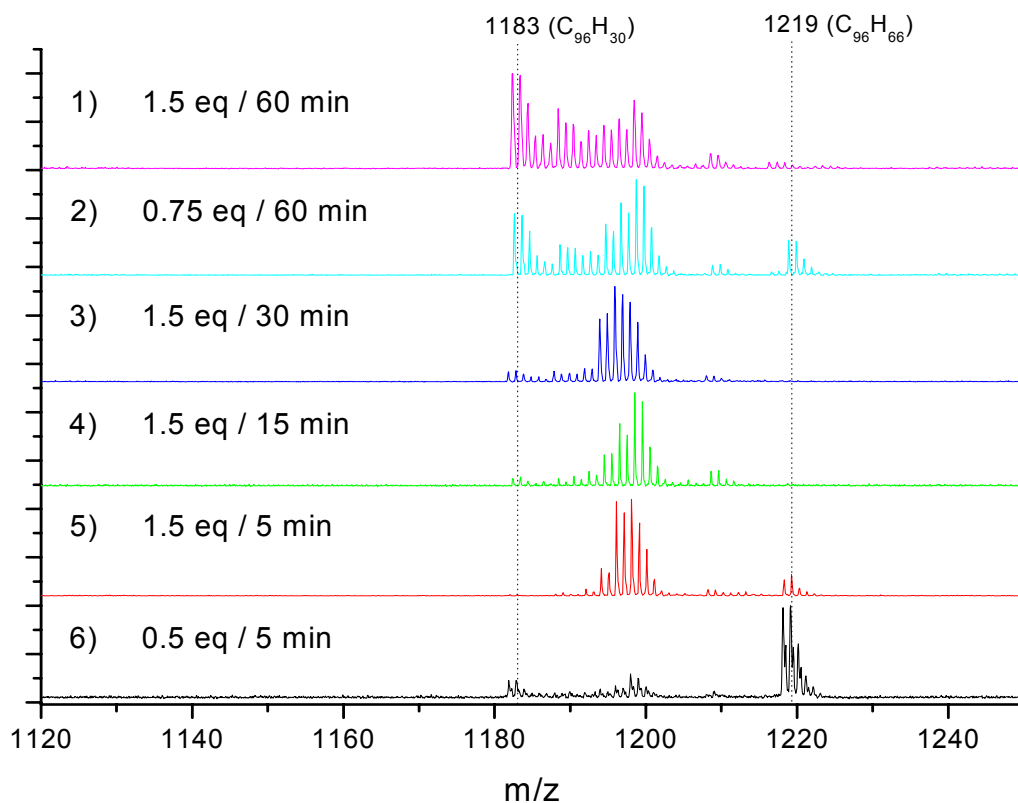


Figure 66. MALDI-TOF mass spectra of the cyclodehydrogenation products of **79** with iron(III) chloride. The vertical lines represent the calculated masses of the molecules C₉₆H₆₆ (**79**) and C₉₆H₃₀ (**43**).

Decreasing the amount of iron(III) chloride to only 0.75 equivalents (exp. 2) led to the formation of partially cyclized products (the most intense peak at 1198 Da, ten to twelve formed carbon-carbon bonds), but also to the complete cyclization (peak at 1183 Da). The peak of unreacted, starting material, at 1219 Da, was also observed. By using the same amount of iron(III) chloride (1.5 equivalents per hydrogen to be removed), but decreasing the reaction time from 60 to 5 minutes, resulted in the formation of only partially cyclized products (the most intense peaks at 1198 and 1196 Da), as shown in Figure 66, experiments 3-5. When cyclodehydrogenation was carried out with only 0.5 equivalents of iron(III) chloride per hydrogen to be removed and a reaction time of five minutes (exp. 6),

mainly starting material ($C_{96}H_{66}$ dendrimer) was observed, along with very small amounts of completely and partially cyclized products.

The mixtures obtained in previously described cyclodehydrogenation reactions (experiments 3-5) were subjected to preparative column chromatography (done separately for every experiment). The insoluble, completely cyclized material ($C_{96}H_{30}$ disc, **43**) did not move through the column, while two soluble fractions, with masses of ≈ 1196 and 1210 Da, could be separated and recovered. The isotopically resolved MALDI-TOF mass spectra and UV/Vis spectra of these fractions are shown in Figure 67.

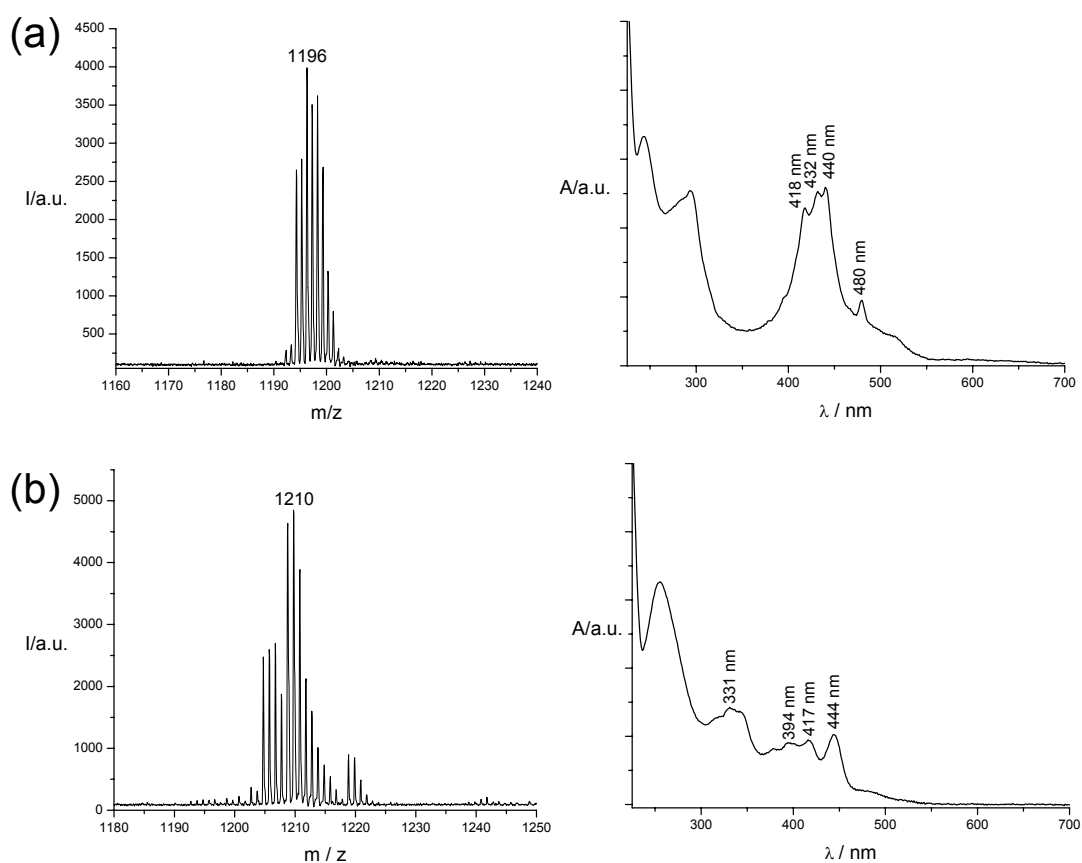


Figure 67. MALDI-TOF mass spectra and UV/Vis spectra (in THF) of two isolated fractions (experiment 4).

However, analytical HPLC and mass spectrometry showed that the isolated fractions are not pure, single compounds, but rather mixtures of three or four inseparable intermediates which differ by probably only one or two carbon-carbon

bonds. This makes it impossible to determine the molecular structure of isolated intermediates. For example, many different intermediate structures can be drawn, possessing the molecular mass of 1196 Da and different graphitic fragments. The ^1H NMR measurements in 1,1,2,2-tetrachloroethane, of this fraction showed overlapped multiple peaks between 7.0 and 8.0 ppm and several low field signals between 8.0 and 10.0 ppm, suggesting the formation of larger aromatic fragments. Since the UV/Vis spectra of isolated fractions differ from the UV/Vis spectra of existing well-defined graphitic molecules,^[1,31,92,93] it was not possible to make any conclusions about the structure of intermediate compounds based on UV/Vis measurements.

In conclusion, by using different reaction conditions (amount of iron(III) chloride and reaction time), partially cyclized products could be observed during the oxidative cyclodehydrogenation of the C96 precursor. This suggests that cyclodehydrogenation does not occur in one step, as a concerted planarization of all phenyl rings under carbon-carbon bond formation, but likely proceeds in many separate reaction steps. However, intermediates could not be isolated as single, pure compounds, and their structures unambiguously identified. This lack of definitive information on the intermediates precludes us from hypothesizing an exact mechanism for this complex, stepwise, oxidative cyclodehydrogenation reaction.

2.8 Literature

- [1] M. D. Watson, A. Fechtenkötter, K. Müllen, *Chem. Rev.* **2001**, *101*, 1267-1300.
- [2] V. S. Iyer, M. Wehmeier, J. D. Brand, M. A. Keegstra, K. Müllen, *Angew. Chem. Int. Ed. Engl.* **1997**, *36*, 1604-1607.
- [3] F. Morgenroth, K. Müllen, *Tetrahedron* **1997**, *53*, 15349-15366.
- [4] F. Morgenroth, E. Reuther, K. Müllen, *Angew. Chem. Int. Ed. Engl.* **1997**, *36*, 631-634.
- [5] M. Müller, C. Kübel, F. Morgenroth, V. S. Iyer, K. Müllen, *Carbon*, **1998**, *36*, 827-831.
- [6] M. Müller, C. Kübel, K. Müllen, *Chem. Eur. J.* **1998**, *4*, 2099-2109.

- [7] H. C. Brown, E. F. Knights, C. G. Scouten, *J. Am. Chem. Soc.* **1974**, *96*, 7765-7770.
- [8] H. C. Brown, R. Liotta, C. G. Scouten, *J. Am. Chem. Soc.* **1976**, *98*, 5297-5301.
- [9] A. Suzuki, R. S. Dhillon, *Top. Curr. Chem.* **1986**, *130*, 23-88.
- [10] N. Miyaoura, T. Ishiyama, M. Ishikawa, A. Suzuki, *Tetrahedron Lett.* **1986**, *27*, 6369-6372.
- [11] N. Miyaoura, T. Ishiyama, H. Sasaki, M. Satoh, A. Suzuki, *J. Am. Chem. Soc.* **1989**, *111*, 314-321.
- [12] N. Miyaoura, A. Suzuki, *Chem. Rev.* **1995**, *95*, 2457-2483.
- [13] U. M. Wiesler, *Dissertation*, Johannes-Gutenberg Universität, Mainz, **2000**.
- [14] M. A. Ogliaruso, M. G. Romaneli, E. I. Becker, *Chem. Rev.* **1965**, *65*, 261-367.
- [15] A. Fechtenkötter, K. Saalwächter, M. A. Harbison, K. Müllen, H. W. Spiess, *Angew. Chem. Int. Ed. Engl.* **1999**, *38*, 3036-3042.
- [16] A. Fechtenkötter, N. Tchebotareva, M. Watson, K. Müllen, *Tetrahedron* **2001**, *57*, 3769-3783.
- [17] C. Y. Liu, A. Fechtenkötter, M. D. Watson, K. Müllen, A. J. Bard, *Chem. Mater.* **2003**, *15*, 124-130.
- [18] A. Fechtenkötter, *Dissertation*, Johannes-Gutenberg Universität, Mainz, **2001**.
- [19] W. Pisula, M. Kastler, D. Wasserfallen, T. Pakula, K. Müllen, *J. Am. Chem. Soc.* **2004**, *126*, 8074-8075.
- [20] M. Kastler, *Dissertation in preparation*, Johannes-Gutenberg Universität, Mainz.
- [21] H. J. Barber, R. Slack, *J. Chem. Soc.* **1944**, 612-615.
- [22] S. Ito, M. Wehmeier, J. D. Brand, C. Kübel, R. Epsch, J. P. Rabe, K. Müllen, *Chem. Eur. J.* **2000**, *6*, 4327-4342.
- [23] T. Weil, *Dissertation*, Johannes-Gutenberg Universität, Mainz, **2001**.
- [24] P. Kovacic, M. B. Jones, *Chem. Rev.* **1987**, *87*, 357-379.
- [25] PC Spartan Pro, Ver.1.0, Wavefunction Inc., Irvine, CA, **2000**.
- [26] L. Przybilla, J. D. Brand, K. Yoshimura, H. J. Räder, K. Müllen, *Anal. Chem.* **2000**, *72*, 4591-4597.
- [27] K. Yoshimura, L. Przybilla, S. Ito, J. D. Brand, M. Wehmeier, H. J. Räder, K. Müllen, *Macromol. Chem. Phys.* **2001**, *202*, 215-222.
- [28] V. S. Iyer, K. Yoshimura, V. Enkelmann, R. Epsch, J. P. Rabe, K. Müllen, *Angew. Chem. Int. Ed. Engl.* **1998**, *37*, 2696-2699.
- [29] I. Fischbach, *Dissertation*, Johannes-Gutenberg Universität, Mainz, **2003**.
- [30] M. A. Biasutti, J. Rommens, A. Vaes, S. De Feyter, F. D. De Schryver, P. Herwig, K. Müllen, *Bull. Soc. Chim. Belg.* **1997**, *106*, 659-664.
- [31] C. Simpson, *Dissertation*, Johannes-Gutenberg Universität, Mainz, **2003**.
- [32] A. Tracz, D. Wostek, I. Kucinska, J. K. Jeszka, M. Watson, K. Müllen, T. Pakula, in *NATO Sci. Ser. II*, **2002**, *59*, 315-318.
- [33] P. Samori, X. Yin, N. Tchebotareva, Z. Wang, T. Pakula, F. Jäckel, M. D. Watson, A. Venturini, K. Müllen, J. P. Rabe, *J. Am. Chem. Soc.* **2004**, *126*, 3567-3575.

- [34] L. Gherghel, C. Kübel, G. Lieser, H. J. Räder, K. Müllen, *J. Am. Chem. Soc.* **2002**, *124*, 13130-13138.
- [35] I. Fischbach, T. Pakula, P. Minkin, A. Fechtenkötter, K. Müllen, H. W. Spiess, K. Saalwächter, *J. Phys. Chem. B* **2002**, *106*, 6408-6418.
- [36] G. R. Desiraju, A. Gavezotti, *Acta Cryst.* **1989**, *B45*, 473-482.
- [37] C. A. Hunter, K. R. Lawson, J. Perkins, C. J. Urch, *J. Chem. Soc. Perkin. Trans.* **2001**, *2*, 651-669.
- [38] B. Glüsen, A. Kettner, J. H. Wendorff, *Mol. Cryst. Liq. Cryst. A* **1997**, *303*, 115-120.
- [39] N. Boden, R. J. Bushby, A. N. Cammidge, A. El-Mansoury, P. S. Martin, Z. Lu, *J. Mater. Chem.* **1999**, *9*, 1391-1402.
- [40] P. G. Schouten, J. M. Warman, M. P. de Haas, C. F. van Nostrum, G. H. Gelinck, R. J. M. Nolte, M. J. Copyn, J. W. Zwikker, M. K. Engel, M. Hanack, Y. H. Chang, W. T. Ford, *J. Am. Chem. Soc.* **1994**, *116*, 6880-6894.
- [41] J. M. Warman, A. M. van de Craats, *Mol. Cryst. Liq. Cryst.* **2003**, *396*, 41- 72.
- [42] P. G. Schouten, J. M. Warman, M. P. de Haas, *J. Phys. Chem.* **1993**, *97*, 9863-9870.
- [43] P. G. Schouten, J. M. Warman, G. H. Gelinck, M. J. Copyn, *J. Phys. Chem.* **1995**, *99*, 11780-11793.
- [44] A. M. van de Craats, J. M. Warman, A. Fechtenkötter, J. D. Brand, M. A. Harbison, K. Müllen, *Adv. Mater.* **1999**, *11*, 1469-1472.
- [45] A. M. van de Craats, J. M. Warman, *Adv. Mater.* **2001**, *13*, 130-133.
- [46] J. Cornil, V. Lemaure, J. P. Calbert, J. L. Bredas, *Adv. Mater.* **2002**, *14*, 726-729.
- [47] K. Senthilkumar, F. C. Grozema, F. M. Bickelhaupt, L. D. A. Siebbeles, *J. Chem. Phys.* **2003**, *119*, 9809-9817.
- [48] V. Lemaure, D. A. da Silva Filho, V. Coropceanu, M. Lehmann, Y. Geerts, J. Piris, M. G. Debije, A. M. van de Craats, K. Senthilkumar, L. D. A. Siebbeles, J. M. Warman, J. L. Brédas, J. Cornil, *J. Am. Chem. Soc.* **2004**, *126*, 3271-3279.
- [49] H. Sirringhaus, R. J. Wilson, R. H. Friend, M. Inbasekaran, W. Wu, E. P. Woo, M. Grell, D. D. C. Bradley, *Appl. Phys. Lett.* **2000**, *77*, 406-408.
- [50] H. Sirringhaus, P. J. Brown, R. H. Friend, M. M. Nielsen, K. Bechgaard, B. M. W. Langeveld-Voss, A. J. H. Spiering, R. A. J. Janssen, E. W. Meijer, P. Herwig, D. M. de Leeuw, *Nature* **1999**, *401*, 685-688.
- [51] K. Hatsusaka, K. Ohta, I. Yamamoto, H. Shirai, *J. Mater. Chem.* **2001**, *11*, 423-433.
- [52] X. L. Chen, A. J. Lovinger, Z. Bao, J. Sapjeta, *Chem. Mater.* **2001**, *13*, 1341-1348.
- [53] Y. Y. Noh, J. J. Kim, Y. Yoshida, K. Yase, *Adv. Mater.* **2003**, *15*, 699-702.
- [54] K. Xiao, Y. Liu, G. Yu, D. Zhu, *Appl. Phys. A* **2003**, *77*, 367-370.
- [55] V. V. Tsukruk, J. H. Wendorff, O. Karthaus, H. Ringsdorf, *Langmuir* **1993**, *9*, 614-618.

- [56] B. W. Laursen, K. Norgaard, N. Reitzel, J. B. Simonsen, C. B. Nielsen, J. Als-Nielsen, T. Bjornholm, T. I. Sølling, M. M. Nielsen, O. Bunk, K. Kjaer, N. Tchebotareva, M. D. Watson, K. Müllen, J. Piris, *Langmuir* **2004**, *20*, 4139-4146.
- [57] C. Y. Liu, A. J. Bard, *Chem. Mater.* **2000**, *12*, 2353-2362.
- [58] A. M. van de Craats, N. Stutzmann, O. Bunk, M. M. Nielsen, M. Watson, K. Müllen, H. D. Chanzy, H. Sirringhaus, R. H. Friend, *Adv. Mater.* **2003**, *15*, 495-499.
- [59] O. Bunk, M. M. Nielsen, T. I. Sølling, A. M. van de Craats, N. Stutzmann, *J. Am. Chem. Soc.* **2003**, *125*, 2252-2258.
- [60] A. Tracz, J. K. Jeszka, M. D. Watson, W. Pisula, K. Müllen, T. Pakula, *J. Am. Chem. Soc.* **2003**, *125*, 1682-1683.
- [61] J. Piris, W. Pisula, A. Tracz, T. Pakula, K. Müllen, J. M. Warman, *Liq. Cryst.* **2004**, *31*, 993-996.
- [62] J. Piris, M. G. Debije, N. Stutzmann, A. M. Van de Craats, M. D. Watson, K. Müllen, J. M. Warman, *Adv. Mater.* **2003**, *15*, 1736-1740.
- [63] E. Rabani, D. R. Reichman, P. L. Geissler, L. E. Brus, *Nature* **2003**, *426*, 271-274.
- [64] B. D. Terris, J. E. Stern, D. Rugar, H. J. Mamin, *Phys. Rev. Lett.* **1989**, *63*, 2669-2672.
- [65] J. M. R. Weaver, D. W. Abraham, *J. Vac. Sci. Technol. B*, **1991**, *9*, 1559-1561.
- [66] M. Fujihira, *Annu. Rev. Mater. Sci.* **1999**, *29*, 353-380.
- [67] K. Wandelt, *Appl. Surf. Sci.* **1997**, *111*, 1-10.
- [68] H. Ishii, N. Hayashi, E. Ito, Y. Washizu, K. Sugi, Y. Kimura, M. Niwano, Y. Ouchi, K. Seki, *Phys. Stat. Sol. (a)*, **2004**, *201*, 1075-1094.
- [69] J. Janata, *Phys. Chem. Chem. Phys.* **2003**, *5*, 5155-5158.
- [70] C. Sommerhalter, T. W. Matthes, T. Glatzel, A. Jäger-Waldau, M. C. Lux-Steiner, *Appl. Phys. Lett.* **1999**, *75*, 286-288.
- [71] H. Ishii, K. Sugiyama, E. Ito, K. Seki, *Adv. Mater.* **1999**, *11*, 605-625.
- [72] H. O. Jacobs, F. F. Knapp, S. Müller, A. Stemmer, *Ultramicroscopy*, **1997**, *69*, 39-49.
- [73] G. de la Torre, C. G. Claessens, T. Torres, *Eur. J. Org. Chem.* **2000**, 2821-2830.
- [74] A. K. Burrell, D. L. Officer, P. G. Plieger, D. C. W. Reid, *Chem. Rev.* **2001**, *101*, 2751-2796.
- [75] N. H. Tinh, M. C. Bernaud, G. Sigaud, C. Destrade, *Mol. Cryst. Liq. Cryst.* **1981**, *65*, 307-316.
- [76] R. C. Borner, R. F. W. Jackson, *J. Chem. Soc. Chem. Commun.* **1994**, 845-846.

- [77] A. N. Cammidge, H. Gopee, *J. Mater. Chem.* **2001**, *11*, 1-11.
- [78] J. A. Rego, S. Kumar, H. Ringsdorf, *Chem. Mater.* **1996**, *8*, 1402-1409.
- [79] S. Kumar, M. Manickam, S. K. Varshney, D. S. Shankar Rao, S. Krishna Prasad, *J. Mater. Chem.* **2000**, *10*, 2483-2489.
- [80] J. D. Brand, C. Kübel, S. Ito, K. Müllen, *Chem. Mater.* **2000**, *12*, 1638-1647.
- [81] N. Tchebotareva, X. Yin, M. D. Watson, P. Samori, J. P. Rabe, K. Müllen, *J. Am. Chem. Soc.* **2003**, *125*, 9734-9739.
- [82] N. Tchebotareva, *Dissertation*, Johannes-Gutenberg Universität, Mainz, **2003**.
- [83] J. Wu, *Dissertation*, Johannes-Gutenberg Universität, Mainz, **2004**.
- [84] Z. Wang, M. D. Watson, J. Wu, K. Müllen, *Chem. Commun.* **2004**, 336-337.
- [85] N. Reitzel, T. Hassenkam, K. Balashev, T. R. Jensen, P. B. Howes, K. Kjaer, A. Fechtenkötter, N. Tchebotareva, S. Ito, K. Müllen, T. Bjørnholm, *Chem. Eur. J.* **2001**, *7*, 4894-4901.
- [86] S. Kubowitz, U. Pietsch, M. D. Watson, N. Tchebotareva, K. Müllen, A. F. Thünemann, *Langmuir*, **2003** *19*, 5036-5041.
- [87] A. F. Thünemann, D. Ruppelt, S. Ito, K. Müllen, *J. Mater. Chem.* **1999**, *9*, 1055-1057.
- [88] C. A. Hunter, J. K. M. Sanders, *J. Am. Chem. Soc.* **1990**, *112*, 5525-5534.
- [89] A. M. van de Craats, *Dissertation*, University of Technology, Delft, The Netherlands, **2000**.
- [90] R. Scholl, C. Seer, R. Weitzenböck, *Chem. Ber.* **1910**, *43*, 2202-2209.
- [91] C. Kübel, K. Eckhardt, V. Enkelmann, G. Wegner, K. Müllen, *J. Mater. Chem.* **2000**, *10*, 879-886.
- [92] F. Dötz, J. D. Brand, S. Ito, L. Gherghel, K. Müllen, *J. Am. Chem. Soc.* **2000**, *122*, 7707-7717.
- [93] F. Dötz, *Dissertation*, Johannes-Gutenberg Universität, Mainz, **2000**.

CHAPTER 3

Control of the Homeotropic Order of Discotic Columnar Systems

3.1 Introduction

In order to get high efficiency, the various device configurations require specific modes of order between the electrodes, accomplished by different processing techniques. In field-effect transistors, the main charge transport takes place parallel to the insulating substrate and therefore requires an edge-on arrangement of the discotic molecules. In general, edge-on arrangement is the preferred alignment of columnar mesophases. Langmuir-Blodgett,^[1-3] zone-casting technique,^[4,5] zone-crystallization^[6,7] or solution casting onto pre-oriented PTFE^[8-10] are suitable methods to obtain highly ordered surface layers with the desired columnar orientation. On the other hand, optimized photovoltaic devices require, in addition to an optimal acceptor-donor interaction,^[11] a face-on arrangement and migration of charges foremost perpendicular to the substrate. Different discotic systems reveal spontaneous face-on arrangement inducing macroscopic homeotropic alignment with the columnar axis perpendicular to the substrate. The surface affinity of the molecules can be modified by changing the chemical nature of the aromatic core or of the side chains.^[12,13] During solution processing of alkylated HBC on molybdenum disulfide^[14] or highly oriented pyrolytic graphite,^[15] the interaction between the aromatic core with the surfaces plays an important role during the alignment leading to monolayer formation with molecules lying flat on the substrate. On the other hand, examples of homeotropic alignment of triphenylenes^[16,17] and phthalocyanines^[18] bearing heteroatoms in the side chains imply a strong influence of the substituents on the arrangement of the molecules.

Homeotropic alignment in micrometer thick films can only be achieved thermally by cooling columnar materials from the melt. However, this approach did not work initially with a number of derivatives of hexa-*peri*-hexabenzocoronene (HBC). The major problem was that the isotropization temperatures (T_i) of the materials were often above 400 °C, which was much higher than the on-set of decomposition (decomposition starts at 300 °C by cleavage of alkyl chains).^[19,20] Recently, it was shown that the substitution of a HBC core by 3,7,11,15-tetramethylhexadecanyl (HBC-C_{16,4}) led to an effectively lowering of T_i to 231 °C.^[21] The lowered processing temperature allowed homeotropic alignment of this material between two ITO surfaces and the investigation of the relationship between photoconductivity and columnar order. Short circuit photocurrents were 5 times higher at better-ordered regions compared to those in poorly oriented parts. Unsymmetrical substitution of a pyrene unit covalently tethered to an alkylated HBC core is another concept for decreasing T_i .^[22] It has been shown that the introduction of bulky and space filling dove-tailed side chains with the branching site directly at the HBC aromatic core leads to a drastic decrease of T_i .^[7] Similar effects have also been reported previously for other smaller discotic systems.^[23,24]

The exact mechanism leading to homeotropic order is still unknown. The example of HBC-C_{16,4} shows that molecular affinity towards the surfaces is not a prerequisite for face-on arrangement. On the other hand, the increase of attraction towards specific surfaces has been reported for other discotic systems.^[16-18] These results prompted us to combine the two advantageous properties discussed above: substitution of the discs with branched alkyl chains and insertion of a heteroatoms, such as oxygen, into these alkyl chains which might have an influence on the mesomorphic properties of discotic liquid crystalline HBC and C96. In the following pages of this chapter, synthesis, characterization, as well as homeotropic self-assembly (results obtained in cooperation with W. Pisula in the group of Prof. Müllen) of such alkyl-ether derivatives are presented.

3.2 Synthesis of hexa-alkylether substituted HBC and C96 discs

Two HBC derivatives, namely, hexa(3-(2-decyltetradecyloxy)propyl)-HBC (**86a**) and hexa(3-(3,7-dimethyloctyloxy)propyl)-HBC (**86b**), substituted at the periphery by six branched alkyl ether chains, were synthesized. These chains, 3-(2-decyltetradecyloxy)propene (**82a**) and 3-(3,7-dimethyloctyloxy)propene (**82b**) were prepared by Williamson ether synthesis (Figure 68) between commercially available allyl chloride (**81**) and the corresponding alcohol (**80a-b**) in 79 and 78% yield, respectively. The synthesis was carried out in aqueous sodium hydroxide solution at 45 °C and in the presence of the phase-transfer catalyst tetrabutylammonium hydrogen sulphate (TBAH).^[25-28]

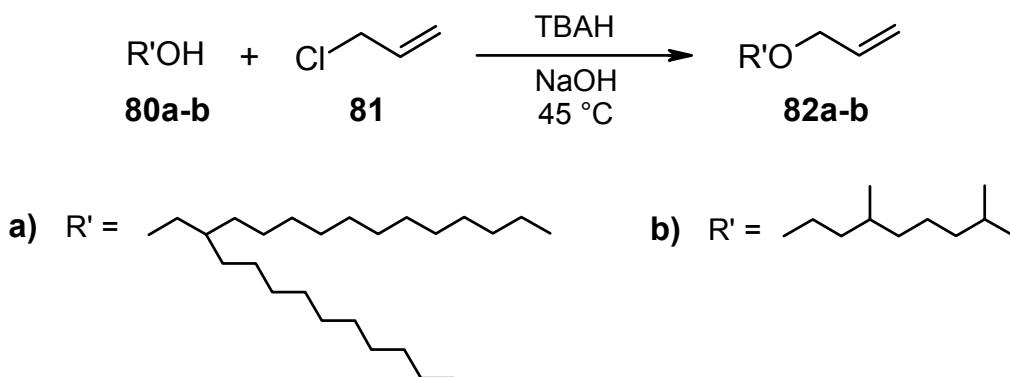


Figure 68. Synthesis of 3-(2-decyltetradecyloxy)propene (**82a**) and 3-(3,7-dimethyloctyloxy)propene (**82b**).

The following steps, leading to the hexa(3-(2-decyltetradecyloxy)propyl)-HBC (**86a**) and hexa(3-(3,7-dimethyloctyloxy)propyl)-HBC (**86b**) are depicted in Figure 69.

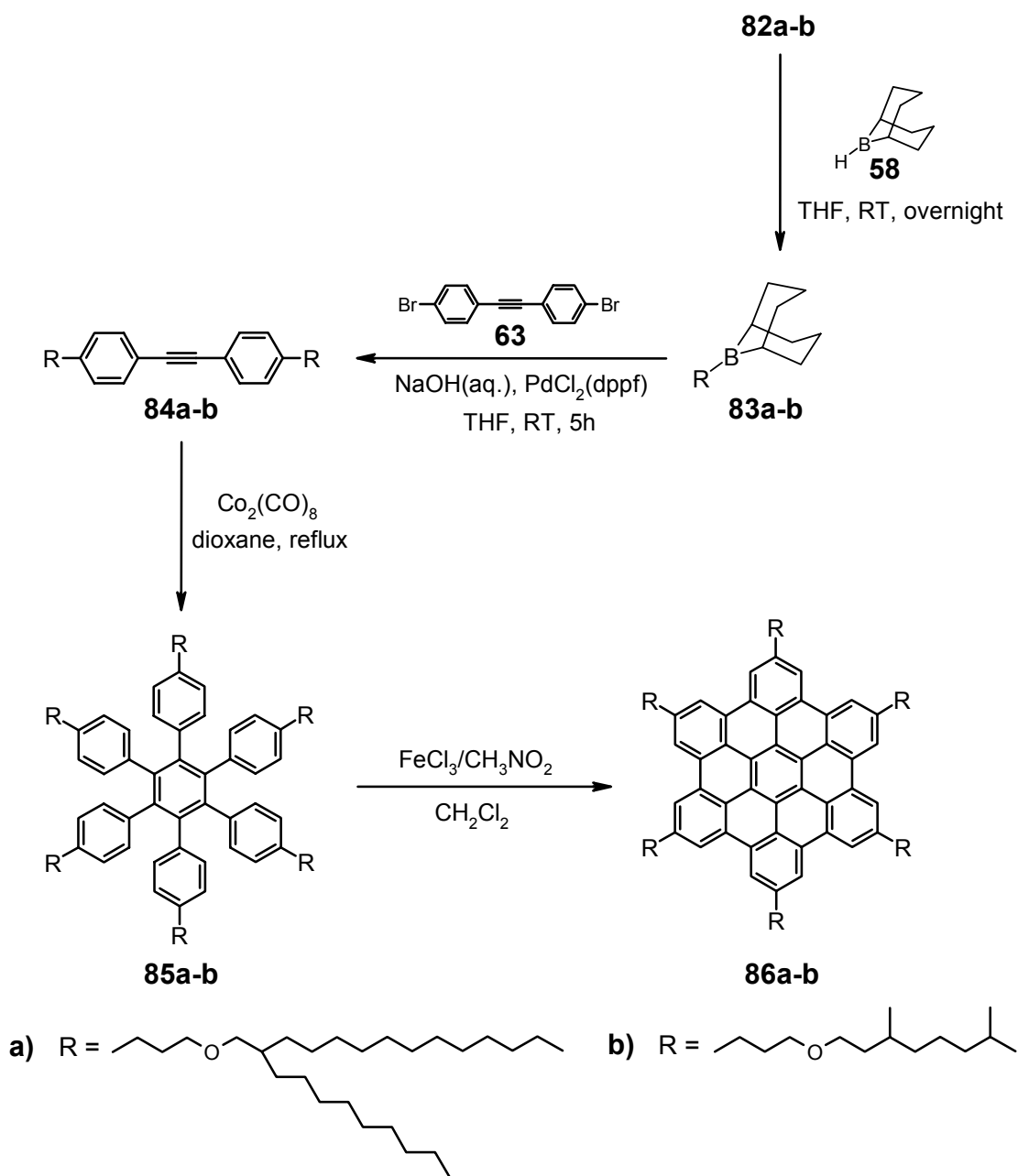


Figure 69. Synthesis of hexa(3-(2-decyltetradecyloxy)propyl)-HBC (**86a**) and hexa(3-(3,7-dimethyloctyloxy)propyl)-HBC (**86b**).

The disubstituted diphenylacetylenes **84a-b** were easily synthesized in a one-pot reaction from 4,4'-dibromodiphenylacetylene (**63**), prepared according to a

literature procedure.^[29] First, hydroboration^[30-35] of **82a-b** with 9-borabicyclo[3.3.1]nonane in THF (9-BBN, **58**) at room temperature, overnight, gave the corresponding intermediate organoboranes **83a-b**, which were then directly used in the subsequent Suzuki coupling^[36-41] with 4,4'-dibromodiphenylacetylene (**63**), in the presence of catalytic PdCl₂(dppf). Reaction was complete after 5 hours at room temperature, and the corresponding disubstituted diphenylacetylenes **84a-b** were isolated in 65 and 60% yield, respectively, following column chromatographic purification. Co₂(CO)₈ mediated cyclotrimerization^[42] of **84a-b** yielded hexaphenylbenzene derivatives **85a-b** in 80% yield, after workup. The final step for this reaction sequence was the oxidative planarization of the six pendant phenyl rings in **85a-b** with concurrent loss of twelve hydrogens. The cyclodehydrogenation^[43] was carried out by adding a solution of iron(III) chloride in nitromethane to the hexaphenylbenzene precursors **85a-b** in dichloromethane to afford the hexa(3-(2-decyltetradecyloxy)propyl)-HBC (**86a**) and hexa(3-(3,7-dimethyloctyloxy)propyl)-HBC (**86b**), where the oxygen atoms are located at the δ position of the alkyl chain. While the cyclodehydrogenation of **85b** to **86b** was achieved under standard conditions for alkylated HBCs (36 equiv of iron(III) chloride, and 45 min reaction time), cyclodehydrogenation of **85a** to the desired HBC **86a** required a larger excess of oxidant (60-70 equiv) and longer reaction time (2-3 hours). Isolated yields after workup were in the order of 80%. The resulting HBC derivatives are yellow in the bulk state, show very good solubility in common organic solvents, and have been characterized by ¹H and ¹³C NMR, and MALDI-TOF mass spectrometry. The ¹H NMR spectra of **86a-b** in solution, at 25 and 100 °C, are shown in Figure 70. As can be seen in Figure 70, on heating from 25 °C to 100 °C, the relevant aromatic signals experience a downfield shift of $\Delta\delta = 0.29$ (from $\delta = 8.67$ to $\delta = 8.96$) for **86a** and $\Delta\delta = 0.23$ (from $\delta = 8.41$ to $\delta = 8.64$) for **86b**. A somewhat less pronounced shift to low fields can be observed for the protons of the alkyl side chains. It is clear that an increase in the temperature leads to smaller aggregates in solution, a phenomenon widely observed in the HBC and other disc-like systems.^[44-50]

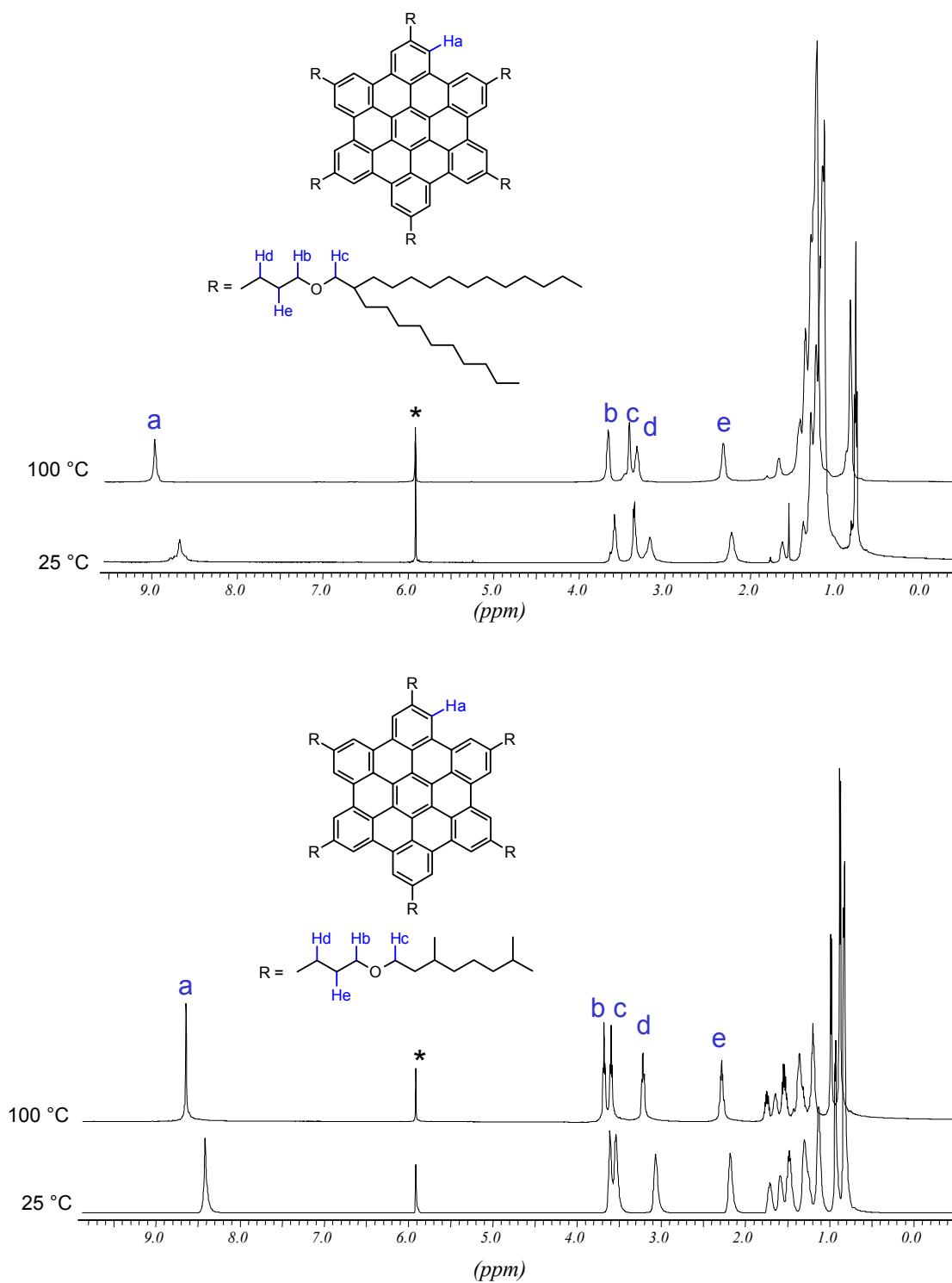


Figure 70. ^1H NMR spectra of hexa(3-(2-decyltetradecyloxy)propyl)-HBC (**86a**) and hexa(3-(3,7-dimethyloctyloxy)propyl)-HBC (**86b**) in $\text{tetrachloroethane-d}_4$ (*) at 25 and 100 °C.

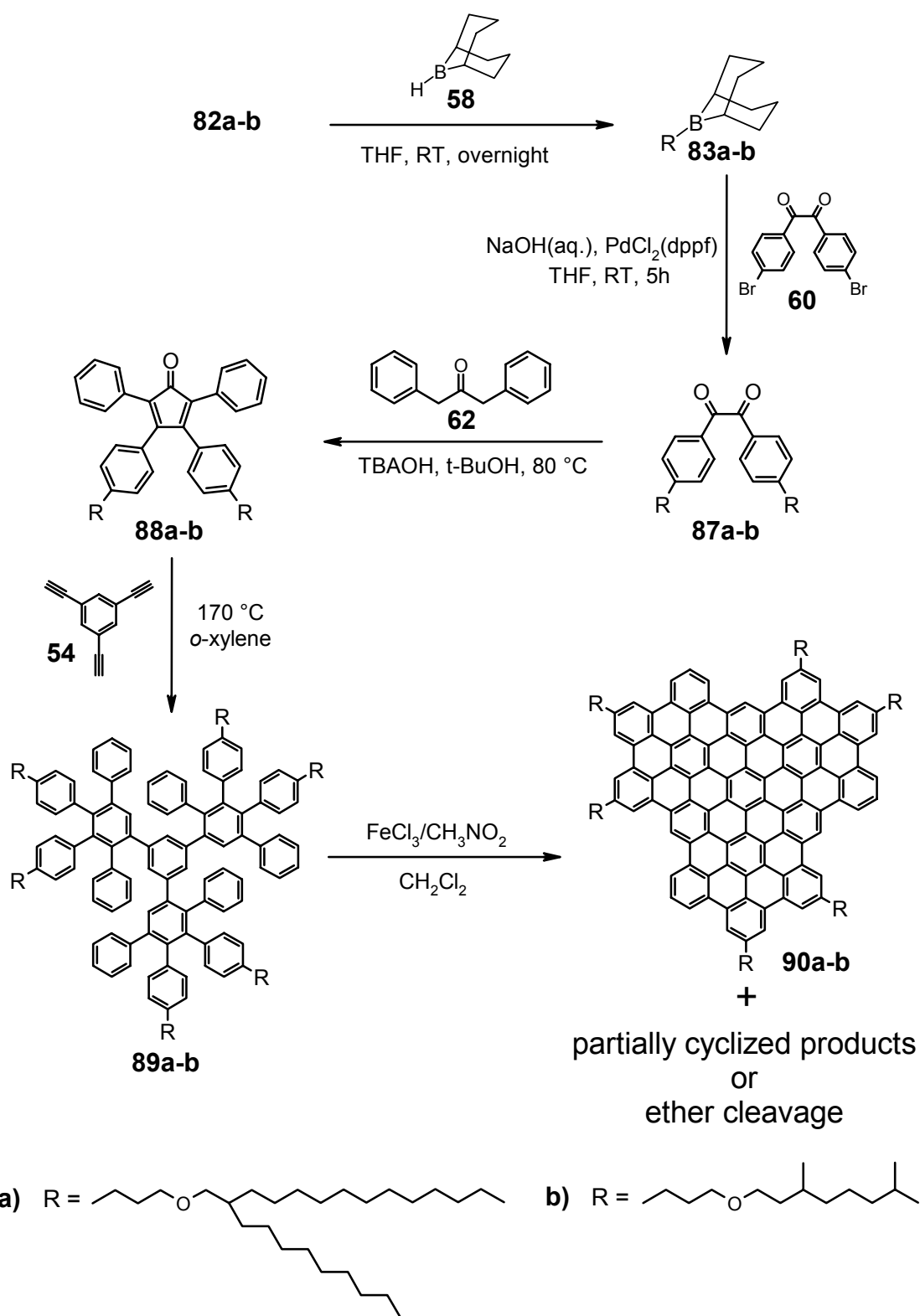


Figure 71. Synthetic pathway to alkyl ether substituted C₉₆ precursors **89a-b** and attempted cyclodehydrogenation.

The synthesis of alkyl ether substituted C96 precursors (**89a-b**) is outlined in Figure 71. First, hydroboration^[30-35] of 3-(2-decyltetradecyloxy)propene (**82a**) and 3-(3,7-dimethyloctyloxy)propene (**82b**) with 9-borabicyclo[3.3.1]nonane (**58**) in THF at room temperature, overnight, gave the corresponding intermediate organoboranes **83a-b**, which were then directly used in the subsequent Suzuki coupling^[36-41] with 4,4'-dibromobenzil (**60**), in the presence of catalytic PdCl₂(dppf). Reactions were complete after 5 hours at room temperature, and 4,4'-bis[3-(2-decyltetradecyloxy)propyl]benzil (**87a**) and 4,4'-bis[3-(3,7-dimethyloctyloxy)propyl]benzil (**87b**) were isolated in 75 and 60% yield, respectively, after workup. They were reacted in the next step, in a double Knoevenagel condensation with commercially available 1,3-diphenyl-2-propanone (**62**) to afford 3,4-bis{4-[3-(2-decyltetradecyloxy)propyl]phenyl}-2,5-diphenylcyclopentadienone (**88a**) and 3,4-bis{4-[3-(3,7-dimethyloctyloxy)propyl]phenyl}-2,5-diphenylcyclopentadienone (**88b**), as dark purple, viscous oils in 64 and 71% yield, respectively, after purification by column chromatography.^[51] Diels-Alder reaction of commercially available 1,3,5-triethynylbenzene (**54**) with excess (3.6 equiv) of **88a-b**, in *o*-xylene at 170 °C, gave the corresponding alkyl ether substituted C96 precursors **89a-b**. The workup of these first generation dendrimers was by evaporation of the solvent, followed by column chromatography to afford colorless, highly viscous oils (**89a-b**), in 95 and 78% yield, respectively.

The key step on the path to C96-derivatives **90a-b** is the oxidative cyclodehydrogenation of the oligophenylene precursors **89a-b**. In a typical cyclization experiment the precursor **89a**, or **89b** was dissolved in dichloromethane, and a solution of iron(III) chloride (90-108 equiv) in nitromethane was added dropwise at room temperature. After 18 hours, the mixture was precipitated in methanol. However, in the case of **89a** and **89b**, this standard synthetic protocol did not give just the desired compounds **90a-b**, but also mixture of number of partially cyclized products. Unfortunately, the desired C96-derivatives could not be separated and isolated as pure compounds. Therefore, the reaction conditions were modified. Slightly increasing the amount of oxidant (108-180 equiv) and prolongation of reaction time led to the desired product but still the presence of partially cyclized products, and in some cases

ether cleavage were observed. On the other hand, use of enormous amounts of iron(III) chloride (such as 250 equiv) or a very long reaction time led to complete ether cleavage. Unfortunately, the alkyl ether C96-derivatives could not be prepared as clean compounds.

3.3 Phase characterization of hexa-alkylether substituted HBCs

3.3.1 Thermal phase characterization

In order to detect phase transitions and to determine the corresponding transition temperatures and enthalpies, differential scanning calorimetry (DSC) was performed on HBC derivatives **86a-b** (Figure 72).

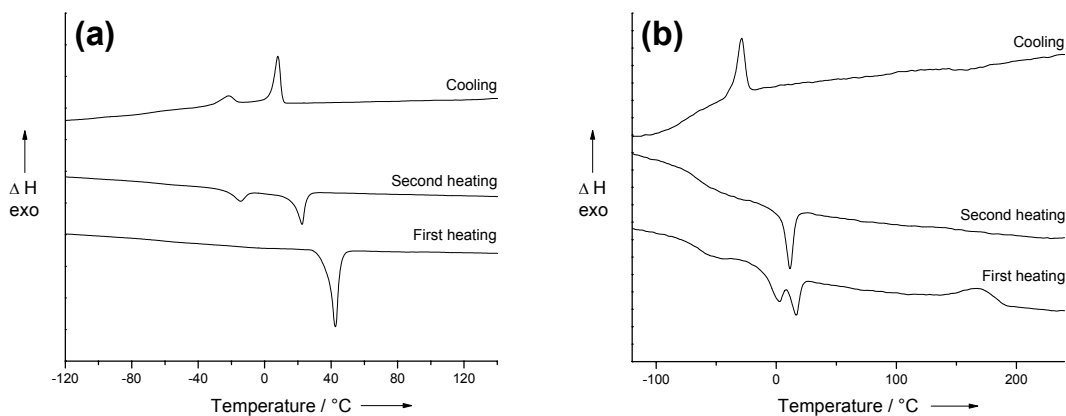


Figure 72. Differential scanning calorimetry traces of (a) **86a** and (b) **86b** (10 K/min).

It was found that the phase behavior of the investigated HBC compounds differs significantly, indicating a strong dependence of the thermal behavior on the length of the side chains. Both compounds investigated were assigned to a plastic crystalline phase in their low temperature phase. At room temperature

these materials possess a waxy and soft consistency. The significant lowering of the isotropization temperature was observed for compound **86a**, which is substituted by the very long side chains (Figure 72a). During the first heating cycle the isotropic phase transition of this material was found at 42 °C. The second heating showed this isotropization temperature lower at 22 °C. Additionally, prior to this transition, a new exothermic peak at -15 °C appeared representing a solid-solid transition which was confirmed by rheology measurements (Figure 73).

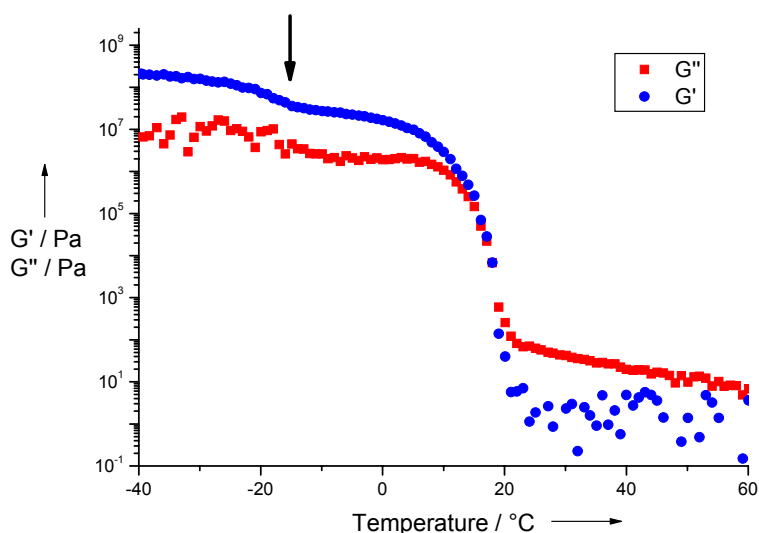


Figure 73. Storage (circle symbols) and loss (square symbols) moduli of **86a** recorded as a function of temperature during cooling. Arrow indicates the solid-solid transition.

The dynamic mechanical experiments revealed a change in shear storage modulus from more than 10⁸ Pa to 10⁷ Pa. The material entered the isotropic state at 18 °C and became liquid with a viscosity of approximately $\eta = 7$ Pa s. By shortening the alkyl chains, the T_i of **86b** increased to ~370 °C, and the material showed a broad disordered columnar phase from 0 °C. The results are summarized in Table 3.

Compound	Temperature [°C]	Enthalpy [kJmol ⁻¹]	Phase transition
86a	-15 (-21)	22.0 (19.4)	Col _x – Col _p
	42 [*] , 22 (14)	57.8 (65.3)	Col _p – I
86b	0 (-38)	17.6 (18.2)	Col _p – Col _{hd}
	~370 (~340)	-	Col _{hd} – I

Table 3. Thermal behavior determined by DSC of the HBC derivatives **86a-b**. The recrystallization temperatures and the enthalpies during cooling are given in brackets. List of abbreviations: (*) – first heating, Col_x – unassigned columnar phase, Col_p – plastic crystalline phase, Col_{hd} – disordered columnar phase, I – isotropic phase.

In order to obtain further information about the relationship between the molecular structure and supramolecular order, optical textures were investigated by means of polarized optical microscopy (POM). Thereby, the crystallization from the isotropic state was studied only for **86a**, because the isotropization temperature of **86b** was too high. Therefore first, the samples were placed on one glass slide and heated to the isotropic state. **86a** revealed a characteristic fan-shaped optical textures as presented in Figure 74.

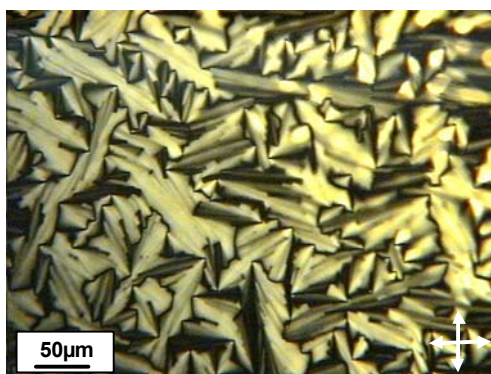


Figure 74. Characteristic optical texture of **86a** crystallized as a thin film on one surface at a cooling rate of 1 °C/min.

3.3.2 Structure investigation by X-ray scattering

The supramolecular organization of columnar systems is particularly important for one-dimensional charge carrier mobility. Therefore, the intra- and intercolumnar arrangement was investigated by both powder X-ray diffraction of bulk materials and 2D-WAXS experiments of extruded filaments.^[52] The pronounced macroscopic alignment of columns within the filaments was indicated by the intense and sharp equatorial reflections corresponding to the intercolumnar arrangement, strongly correlated to the thermal phase of the compounds.

Figure 75 exhibits typical intensity distributions for both the disordered isotropic state and for the highly ordered crystalline phase of **86a**. The unit cell derived from the reflection positions was assigned to a two-dimensional lateral orthorhombic lattice with packing parameters $a = 3.52$ nm and $b = 3.17$ nm. This arrangement was recovered after cooling the sample from the isotropic state.

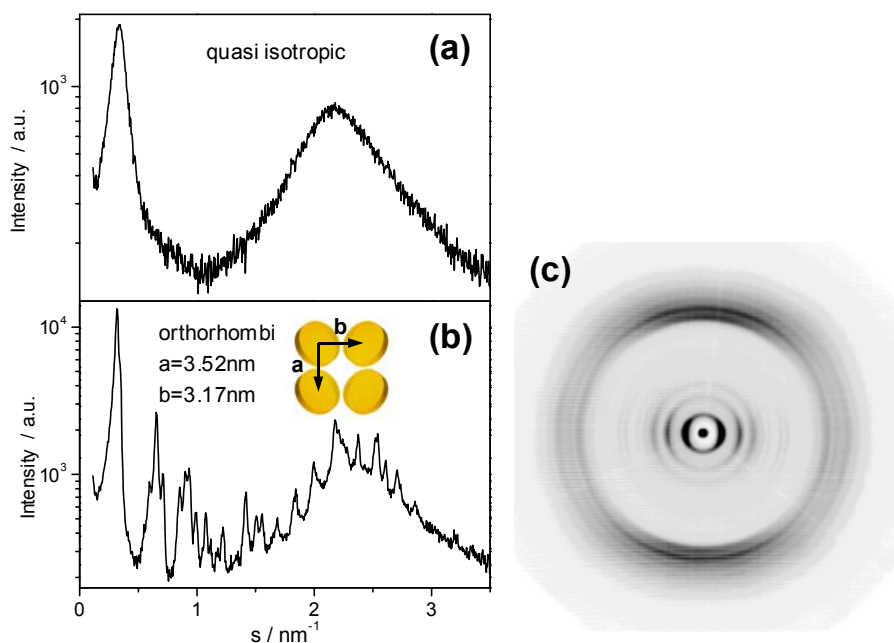


Figure 75. Intensity distribution of a powder X-ray diffraction for **86a** in (a) isotropic phase, (b) plastic crystalline phase, and (c) characteristic 2D-WAXS pattern for an extruded filament of **86a**.

From 2D-WAXS results (Figure 75c) it was possible to determine the intracolumnar arrangement of the discotic molecules. The meridional reflections related to a π - π stacking correlation distance of 0.47 nm are characteristic of an intracolumnar period with molecules tilted towards the columnar axis. Furthermore, a second off-meridional peak which was weakly split was determined as corresponding to 0.44 nm. It indicated a slight tilting of the disc to the columnar axis with a small angle, atypical for discotic molecules and suggests a strong influence of the long side chains on the intracolumnar packing. The solid-solid phase transition at -15 °C was not accompanied by any structural change; both solid-state phases confirmed a tilted arrangement of the discs to the columnar axes and an identical intercolumnar arrangement. For the sample heated to the isotropic state, a small angle reflection appeared corresponding to a distance of 2.99 nm, as derived from the maximum peak in the X-ray diffraction in Figure 75a. A reflection of this kind can be attributed to position correlation of molecular aggregates possessing electron density contrast between the aromatic core stacks and the aliphatic substituents. Assuming only nearest neighbor relation, the correlation distance should be taken as $d = \frac{1.23}{S_{\max}}$.^[53] This value allows one to estimate the number of stacking molecules consisting in the aggregate as a spherical unit of volume $\frac{\pi}{6}d^3$ which is related to the molecular mass M by the following equation:

$$\frac{\pi}{6}d^3 = \frac{M \cdot n}{\rho \cdot N_A} \quad (4)$$

where n is the number of molecules, ρ is the density assumed here 1 g/cm³ for both nanophases (the aromatic core and the alkyl shell) and N_A is Avogadro's number. For this relationship, the most probable stacking number of nearly 5 molecules was calculated suggesting that the molecules in the isotropic state are not isolated, but form aggregates consisting of several discs.

In contrast to **86a**, compound **86b** revealed a strong structural dependence on thermal treatment. Both powder diffraction pattern (Figure 76a and c) of **86b** as obtained from solution and thermally treated suggested an

orthorhombic two-dimensional unit cell, but significantly different in the packing parameters. After cooling back to the plastic crystalline phase, unit cell parameters a and b decreased approximately 1 nm implying a significantly enhanced intercolumnar packing triggered by the reorganization of molecules during exposure to the higher temperature phase. In that Col_{hd} state the intercolumnar arrangement changed in comparison to the low temperature phase and was assigned to a hexagonal disordered columnar state with the unit cell $a = 2.78$ nm, as implied by the large number of higher order reflexes with a reflection distribution corresponding to a relationship $1 : \sqrt{3} : 2 : \sqrt{7}$ (Figure 76b). These reflections were also in this state intensive and sharp, in contrast to the meridional peaks which became more diffuse and unclear with an added distinct amorphous halo. In addition, the off-meridian reflections are also apparent in this state verifying the tilted arrangement of the discs within the columns.

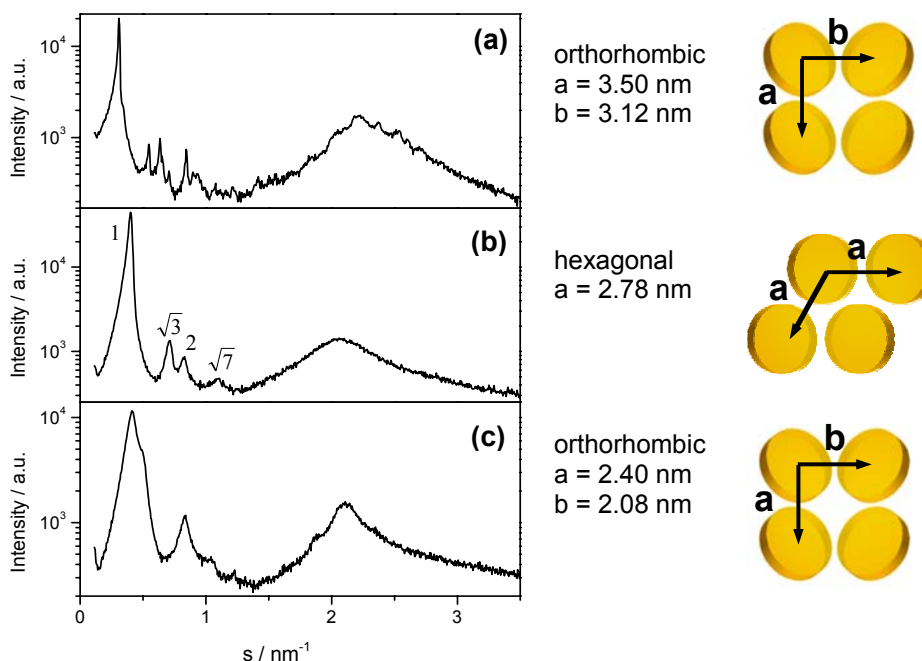


Figure 76. Powder diffraction of **86b** as obtained from solution **(a)**, in the Col_{hd} phase **(b)** and cooled back to the plastic crystalline phase **(c)**.

The 2D-WAXS pattern in Figure 77 shows that the meridional reflections were broad and fuzzy indicating that the correlation of the tilting discs was relatively weak. During cooling, the degree of intracolumnar order improved, typical for a more ordered phase plastic crystalline phase, leading to an increase in intensity of the off-meridian reflections which corresponded to molecular tilting towards the columnar axes.

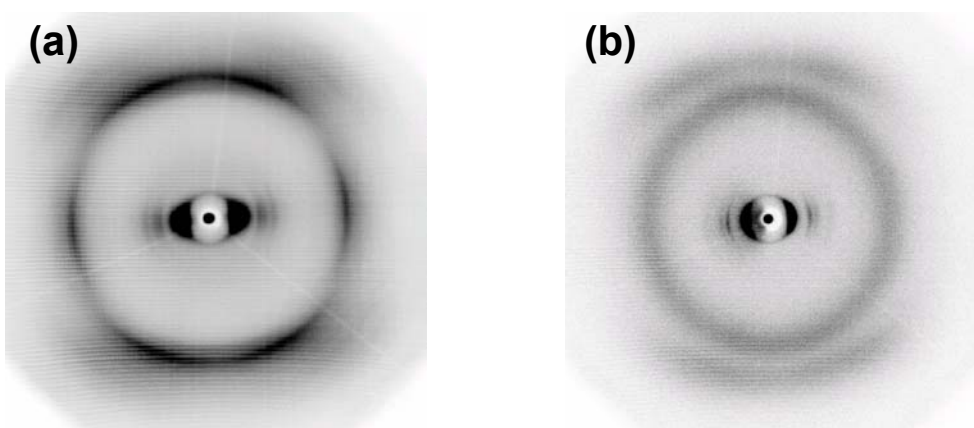


Figure 77. Characteristic 2D-WAXS pattern of **86b** as extruded filament **(a)** in the plastic crystalline phase and **(b)** in the Col_d phase.

3.3.3 Homeotropic arrangement

Small discotic systems like triphenylenes and phthalocyanines bearing alkoxy groups at their core periphery, spontaneously form homeotropic order when crystallized from the isotropic state,^[16-18] whereas on the other hand, the successful alignment of HBC-C_{16,4}^[21] proved that these specific peripheral units are not essential for this orientation procedure. Therefore, the control of homeotropic supramolecular order by the introduction of heteroatoms into the side chains was investigated.

When slowly crystallized from their isotropic state between two polar surfaces as a thin film, both compounds **86a-b** revealed identical self-assembly behavior. The images from the optical microscope are presented in Figures 78 and 79.

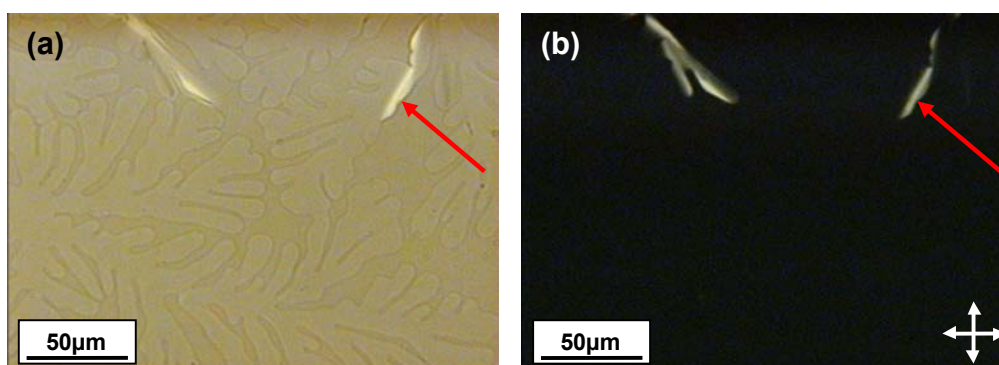


Figure 78. Optical microscopy images of **86a** during crystallization between two glass slides **(a)** without and **(b)** with cross-polarizers. Red arrow indicates defects in homeotropic order.

In each case, first a dendritic texture appeared close to the corresponding recrystallization temperature. When cross-polarizers were applied the image became black. This observation is characteristic of the homeotropic phase where the columnar axis is perpendicular to the substrate. Since the light propagation coincides with the optical axis, the transmitted light intensity is always zero for all positions of the sample with respect to the analyzer/polarizer axis. Only some parts of the film show birefringence due to homeotropic packing defects as indicated by a red arrow in Figure 78.

Both compounds **86a** and **86b** revealed a similar 2D hexagonal WAXS pattern when crystallized between the two aluminum foils. The first order reflection for **86a** arose at 3.55 nm, but of poorer pattern quality resulting in a less distinct packing correlation. The characteristic room temperature 2D-WAXS pattern of **86b** in Figure 79c exhibited a hexagonal intercolumnar distance of 2.78 nm being in good agreement with the unit cell parameters determined for the bulk

mesophase of this compound and verifying the stability of this ordering at room temperature.

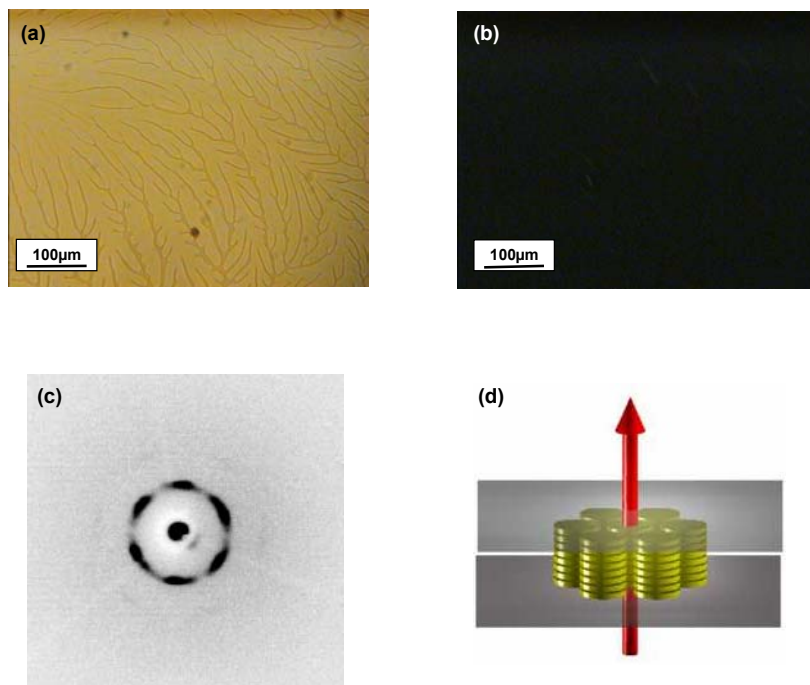


Figure 79. Optical microscopy images of **86b** homeotropically aligned during controlled crystallization between two glass slides **(a)** without and **(b)** with cross-polarizers; **(c)** 2D-WAXS pattern of **86b** at room temperature crystallized between two thin aluminum foils, the most essential intermediate 2θ range of 2° - 10° is presented; **(d)** schematic presentation of the homeotropic alignment between two surfaces during the X-ray experiment, the discs represent the molecules and the red arrow assign the X-ray beam direction.

This is in contrast to observations monitored by POM for **86b** crystallized between two glass slides at room temperature. After reaching the homeotropic phase, further crystallization caused the dendritic structures to touch each other and more birefringent defects appeared (Figure 80). First, these defects emerged at the dendritic frontlines and upon further decreasing the temperature also appeared within these structures. Finally, at approximately 50°C the whole optical texture changed with a significant increase in birefringence indicating a transition in the supramolecular organization from a loss of the homeotropic order

to an edge-on arrangement. This phenomenon is in contrast to the 2D-WAXS results which displayed a markedly homeotropic alignment for compound **86b** at room temperature.

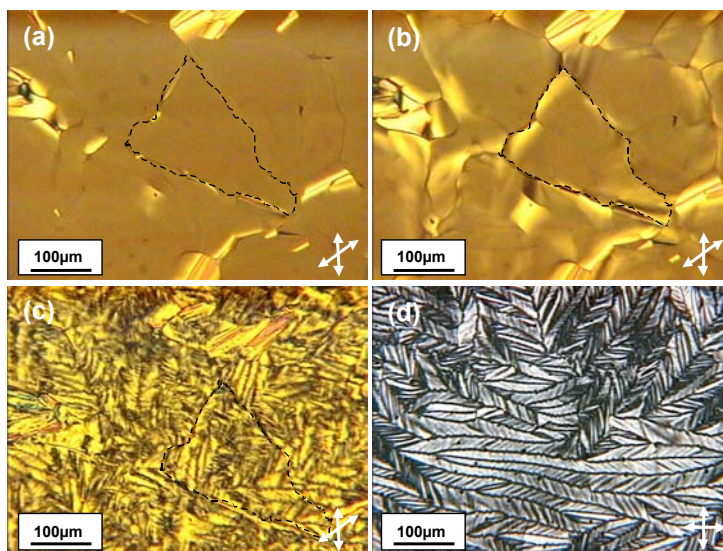


Figure 80. Optical microscopy images of **86b** crystallized at 1 °C/min from the isotropic state; Images **(a) – (c)** taken with an angle analyzer/polarizer axis of 45°, **(a)** at 350 °C, **(b)** at 290 °C and **(c)** 100 °C (dashed lines indicate the same part); **(d)** cross-polarized image of a randomly chosen position of the sample after keeping it for 24 hours at room temperature.

Since both surfaces, glass and aluminium have similar surface polarities, another factor was assumed to have a significant influence on the supramolecular order. In general, each phase transition involves a considerable structural change, which in turn is associated with a density alternation and an alternation in macroscopic dimensions of the sample. A thermal phase transition induces changes in supramolecular order towards a more thermodynamically favourable organization for given molecules. If aluminium foils can be considered as flexible surfaces (while glass slides as fixed surfaces, limiting the volume), then one can assume that during the crystallization they can compensate for the density and macroscopic changes maintaining the homeotropic orientation. Therefore, the stability of this characteristic alignment can be regarded as a mechanical problem in some systems.

Summarizing the results obtained in this chapter, one concludes that by varying the molecular design of HBC derivatives it was possible to significantly influence the desired properties of the material, making it promising for potential application in photovoltaic devices. In order to obtain a highly processible compound the isotropization temperature had to be lowered significantly. Therefore, the aggregation of the molecules had to be reduced by overcoming the π - π interaction of the aromatic cores. The introduction of bulky and space filling side chains induces strong steric interactions at the core periphery and dominates the stacking ability of the discs. Although the branching site is not directly at the aromatic core, the substitution of very long alkyl chains induces a drastic lowering of the isotropization temperature. In particular, for compound **86a** the T_i decreased to room temperature leading to a complete suppression of the liquid crystalline phase. The introduction of strong steric interaction by using long side chains thus influences the stacking behavior of the molecules generating intracolumnar disorder. X-ray scattering experiments showed that especially in the liquid crystalline phase, the exceptionally long side chains occupy a large volume due to their high mobility in the periphery and disturb the strong interaction between the aromatic cores. The molecules then possess high lateral rotation and longitudinal mobility maintaining the tilted arrangement towards the columnar axis instead of changing their packing to a characteristic orthogonal arrangement.^[52] The disturbed π - π interaction and increased intracolumnar disorder could have a dramatic influence on the charge carrier mobility along the columns. This suggestion has to be proven by additional experiments such as time-of-flight measurements.

Indeed, the introduction of ether groups in the side chains essentially improves the affinity of the HBC derivatives investigated toward face-on arrangement at the corresponding surface and facilitated a control of the homeotropic alignment. The presence of these polar ether units in the HBC core periphery has a fundamental influence on the self-organization behavior of the molecules on polar surfaces. During controlled crystallization between two glass or aluminum surfaces, the materials formed a homeotropic phase which appeared at cooling rates of even 20 °C/min proving the high attraction of the

polar groups to this kind of surfaces. It was quite surprising that the desired alignment of the sample was obtained by such simple thermal treatment, since the heteroatoms at the δ position of the side chains are not positioned directly at the aromatic core. Due to a strong affinity for studied HBC compounds to the applied surfaces, the side chain architecture seems to be most important for the processibility of the material, rather than for the alignment mechanism. An additional factor is an appropriate viscosity of the isotropic phase, which was proven by rheology measurements. During the processing procedure, the interaction of the first molecules with the surface plays a crucial role. Upon further decreasing the temperature, the crystallization progresses and other molecules stack upon the pre-arranged discs at the surface creating in this way the desired macroscopic order.

Further research activities in our group have resulted in new HBC derivatives whose thermal properties can be effectively controlled by dove-tailed alkyl ether chains (prepared by B. El Hamaoui), and investigations concerning their phase behavior and surface interaction are currently underway (W. Pisula).

3.4 Literature

- [1] O. Karthaus, H. Ringsdorf, V. V. Tsukruk, J. H. Wendorff, *Langmuir* **1992**, *8*, 2279-2283.
- [2] N. Reitzel, T. Hassenkam, K. Balashev, T. R. Jensen, P. B. Howes, K. Kjaer, A. Fechtenkötter, N. Tchebotareva, S. Ito, K. Müllen, T. Bjørnholm, *Chem. Eur. J.* **2001**, *7*, 4894-4901.
- [3] Smolenyak, R. Peterson, K. Nebesny, M. Torker, D. F. O'Brien, N. R. Armstrong, *J. Am. Chem. Soc.* **1999**, *121*, 8628-8636.
- [4] A. Tracz, J. K. Jeszka, M. D. Watson, W. Pisula, K. Müllen, T. Pakula, *J. Am. Chem. Soc.* **2003**, *125*, 1682-1683.
- [5] J. Piris, W. Pisula, A. Tracz, T. Pakula, K. Müllen, J. Warman, *Liq. Cryst.* **2004**, *31*, 993-996.
- [6] C. Y. Liu, A. J. Bard, *Chem. Mater.* **2000**, *12*, 2353-2362.
- [7] W. Pisula, M. Kastler, D. Wasserfallen, T. Pakula, K. Müllen, *J. Am. Chem. Soc.* **2004**, *126*, 8074-8075.

- [8] A. M. van de Craats, N. Stutzmann, O. Bunk, M. M. Nielsen, M. Watson, K. Müllen, H. D. Chanzy, H. Siringhaus, R. H. Friend, *Adv. Mater.* **2003**, *15*, 495-499.
- [9] O. Bunk, M. M. Nielsen, T. I. Solling, A. M. van de Craats, N. Stutzmann, *J. Am. Chem. Soc.* **2003**, *125*, 2252-2258.
- [10] S. Zimmermann, J. H. Wendorff, C. Weder, *Chem. Mater.* **2002**, *14*, 2218-2223.
- [11] L. Schmidt-Mende, A. Fechtenkötter, K. Müllen, E. Moons, R. H. Friend, J. D. MacKenzie, *Science* **2001**, *293*, 1119-1122.
- [12] H.-T. Jung, S. O. Kim, Y. K. Ko, D. K. Yoon, S. D. Hudson, V. Percec, M. N. Holerca, W.-D. Cho, P. E. Mosier, *Macromolecules* **2002**, *35*, 3717-3721.
- [13] N. Boden, R. J. Bushby, P. S. Martin, S. D. Evans, R. W. Owens, D. A. Smith, *Langmuir* **1999**, *15*, 3790-3797.
- [14] R. Friedlein, X. Crispin, D. Simpson, M. D. Watson, F. Jäckel, W. Osikowicz, S. Marciniak, M. P. d. Jong, P. Samori, S. K. M. Jönsson, M. Fahlman, K. Müllen, J. P. Rabe, W. R. Salaneck, *Phys. Rev. B* **2003**, *68*, 195414.
- [15] P. Samori, M. Keil, R. Friedlein, J. Birgerson, M. Watson, K. Müllen, W. R. Salaneck, J. P. Rabe, *J. Phys. Chem. B* **2001**, *105*, 11114-11119.
- [16] N. Terasawa, H. Monobe, K. Kiyohara, Y. Shimizu, *Chem. Commun.* **2003**, 1678-1679.
- [17] A. N. Cammidge, H. Gopee, *J. Mater. Chem.* **2001**, *11*, 2773-2783.
- [18] K. Hatsusaka, K. Ohta, I. Yamamoto, H. Shirai, *J. Mater. Chem.* **2001**, *11*, 423-433.
- [19] P. Herwig, C. W. Kayser, K. Müllen, H. W. Spiess, *Adv. Mater.* **1996**, *8*, 510-513.
- [20] S. Ito, M. Wehmeier, J. D. Brand, C. Kubel, R. Epsch, J. P. Rabe, K. Müllen, *Chem. Eur. J.* **2000**, *6*, 4327-4342.
- [21] C. Y. Liu, A. Fechtenkötter, M. D. Watson, K. Müllen, A. J. Bard, *Chem. Mater.* **2003**, *15*, 124-130.
- [22] N. Tchegotareva, X. M. Yin, M. D. Watson, P. Samori, J. P. Rabe, K. Müllen, *J. Am. Chem. Soc.* **2003**, *125*, 9734-9739.
- [23] P. G. Schouten, J. F. van der Pol, J. W. Zwikker, W. Drenth, S. J. Picken, *Mol. Cryst. Liq. Cryst.* **1991**, *195*, 291-305.
- [24] T. Sauer, G. Wegner, *Mol. Cryst. Liq. Cryst.* **1988**, *162*, 97-118.
- [25] C. Brondino, B. Boutevin, Y. Hervaud, N. Pelaprat, A. Manseri, *J. Fluorine Chem.* **1996**, *76*, 193-200.
- [26] B. Boutevin, B. Youssef, S. Boileau, A. M. Garnault, *J. Fluorine Chem.* **1987**, *35*, 399-410.
- [27] D. B. Sharp, T. M. Patrick, *J. Org. Chem.* **1961**, *26*, 1389-1394.
- [28] L. W. Devaney, G. W. Panian, *J. Am. Chem. Soc.* **1953**, *75*, 4836-4837.
- [29] H. J. Barber, R. J. Slack, *R. J. Chem. Soc.* **1944**, 612-615.
- [30] H. C. Brown, E. F. Knights, C. G. Scouten, *J. Am. Chem. Soc.* **1974**, *96*, 7765-7770.
- [31] H. C. Brown, R. Liotta, C. G. Scouten, *J. Am. Chem. Soc.* **1976**, *98*, 5297-5301.
- [32] R. Liotta, H. C. Brown, *J. Org. Chem.* **1977**, *42*, 2836-2839.

- [33] H. C. Brown, R. Liotta, G. W. Kramer, *J. Org. Chem.* **1978**, *43*, 1058-1063.
- [34] A. Suzuki, *Acc. Chem. Res.* **1982**, *15*, 178-184.
- [35] A. Suzuki, R. S. Dhillon, *Top. Curr. Chem.* **1986**, *130*, 23-88.
- [36] N. Miyauro, T. Ishiyama, M. Ishikawa, A. Suzuki, *Tetrahedron Lett.* **1986**, *27*, 6369-6372.
- [37] N. Miyauro, T. Ishiyama, H. Sasaki, M. Satoh, A. Suzuki, *J. Am. Chem. Soc.* **1989**, *111*, 314-321.
- [38] M.R. Netherton, C. Dai, K. Neuschütz, G. C. Fu, *J. Am. Chem. Soc.* **2001**, *123*, 10099-10100.
- [39] N. Miyauro, A. Suzuki, *Chem. Rev.* **1995**, *95*, 2457-2483.
- [40] A. Suzuki, *J. Organomet. Chem.* **1999**, *576*, 147-168.
- [41] A. Suzuki, *Metal-Catalyzed Cross-Coupling Reactions*, F. Diederich, P. J. Stang, (Eds.), Wiley-VCH, New York, **1998**, Chapter 2.
- [42] K. P. C. Vollhardt, *Acc. Chem. Res.* **1977**, *10*, 1-8.
- [43] P. Kovacic, M. B. Jones, *Chem. Rev.* **1987**, *87*, 357-379.
- [44] J. S. Zhang, J. S. Moore, *J. Am. Chem. Soc.* **1992**, *114*, 9701-9702.
- [45] A. S. Shetty, J. S. Zhang, J. S. Moore, *J. Am. Chem. Soc.* **1996**, *118*, 1019-1027.
- [46] S. L. Lahiri, J. L. Thompson, J. S. Moore, *J. Am. Chem. Soc.* **2000**, *122*, 11315-11319.
- [47] S. Höger, K. Bonrad, A. Mourran, U. Beginn, M. Möller, *J. Am. Chem. Soc.* **2001**, *123*, 5651-5659.
- [48] Y. Tobe, N. Utsumi, K. Kawabata, A. Nagano, K. Adachi, S. Araki, M. Sonoda, K. Hirose, K. Naemura, *J. Am. Chem. Soc.* **2002**, *124*, 5350-5364.
- [49] A. Fechtenkötter, *Dissertation*, Johannes-Gutenberg Universität, Mainz, **2001**.
- [50] J. Wu, *Dissertation*, Johannes-Gutenberg Universität, Mainz, **2004**.
- [51] M. A. Ogliaruso, M. G. Romanelli, E. I. Becker, *Chem. Rev.* **1965**, *65*, 261-367.
- [52] I. Fischbach, T. Pakula, P. Minkin, A. Fechtenkötter, K. Müllen, H. W. Spiess, K. Saalwächter, *J. Phys. Chem. B* **2002**, *106*, 6408-6418.
- [53] A. Guinier, *X-ray Diffraction in Crystals, Imperfect Crystals and Amorphous Bodies*; W. H. Freeman & Co.: San Francisco, CA, **1963**.

CHAPTER 4

Synthesis and Properties of Dendronized Superphenalenes

4.1 Introduction

π - π Stacking interactions between aromatic units are important non-covalent intermolecular forces that contribute to self-assembly and molecular recognition in a variety of supramolecular systems including nucleic acids,^[1-3] discotic liquid crystals,^[4] molecular crystals,^[5-7] and various protein and enzyme-substrate complexes.^[8] The nature of the π - π interactions has been thoroughly studied theoretically^[9-14] and experimentally^[15-19] for many years, and one important goal is that scientists may one day employ molecular stacking interactions to build controlled nanoscale structures.

The spontaneous formation of molecular assemblies extending over several tens of nanometers is a characteristic feature of liquid crystals. Of particular interest are discotic liquid crystals displayed by flat disc-shaped molecules, which organize spontaneously into one-dimensional stacks within the mesophase, and where the stacks form a two-dimensional lattice.^[20,21] Such materials have been considered for use as organic hole or electron conducting pathways in organic light-emitting diodes, field-effect transistors or in photovoltaic devices.^[22,23] High one-dimensional charge carrier mobilities have been observed in discotic liquid-crystalline materials based on phthalocyanines,^[24] triphenylenes^[25] and hexa-*peri*-hexabenzocoronenes (HBCs).^[26] Their π - π interactions in solution play an important role in promoting self-assembly in solid films, which is relevant to their electronic or optoelectronic properties. The self-assembly behavior of disc-like molecules, such as porphyrins and phthalocyanines has been studied by concentration and temperature dependent

UV/Vis spectroscopy, ^1H NMR spectroscopy and vapor pressure osmometry (VPO).^[27-30]

Unsubstituted, large polycyclic aromatic hydrocarbons (PAHs), such as a hexa-*peri*-hexabenzocoronene or superphenalene are characterized by strong intermolecular cohesion due to the strong π - π interactions between aromatic units, which results in extremely high thermally stable, non-melting, insoluble solids.^[31-34] Attachment of flexible substituents onto the periphery improves the solubility and lowers the melting point. Melting leads to remarkably stable discotic mesophases with columnar superstructures.^[35] Hence, alkyl or alkylphenyl substituted HBCs exhibit columnar mesophases with large phase widths, a high order parameter and high charge carrier mobilities.^[26,35] These properties qualify HBCs as particularly promising candidates for applications in organic electronic and optoelectronic devices.^[36-38] The self-assembly behavior of HBC-based materials in the bulk and on surfaces has been intensively studied by various techniques such as X-ray diffraction, solid-state NMR spectroscopy and scanning probe microscopy.^[39-41] Very recently, the solution self-assembly behavior of HBC derivatives was studied.^[42] The high tendency of hexadodecyl-substituted HBC to aggregate was determined by concentration and temperature-dependent ^1H NMR spectroscopic measurements and nonlinear least-squares analysis of the experimental data. It was found that rigid dendrons, introduced around the HBC core, suppress the π - π interactions of the cores to a certain extent, and a slow (with respect to the NMR time scale) monomer-dimer equilibrium was observed. This equilibrium was further controlled by temperature, concentration, and solvent to afford discrete monomeric or dimeric species. "Moving" the dendron arms closer to the HBC core gave a molecule which exists only as a nonaggregated monomer. This concept of employing dendritic substituents to effect steric isolation of a functional core (e.g., porphyrin, phthalocyanine, fullerene, etc.) is being actively studied by a number of groups.^[43-50]

Alkyl substituted superphenalene (C96) derivatives show very strong tendency to aggregate in solution as described in Chapter 2. Therefore, the steric isolation of the superphenalene core represents an interesting challenge and could lead to materials which are useful as a models for studying substituent

effects on the π - π interactions. Herein, shape-persistent, polyphenylene dendrons,^[51,52] of various size, have been peripherally attached to the superphenalene core in an attempt to modify the self assembly of these discotic molecules. Molecular structures and three-dimensional models of such dendronized superphenalenes (compounds **91** and **92**) are shown in Figure 81.

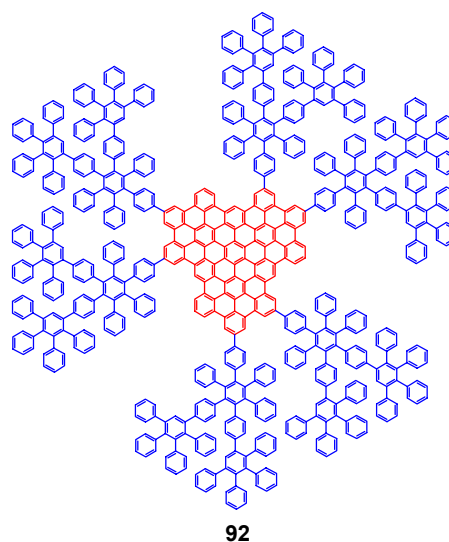
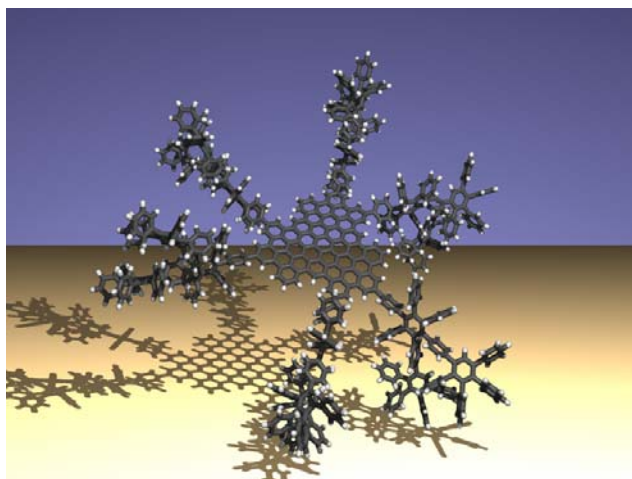
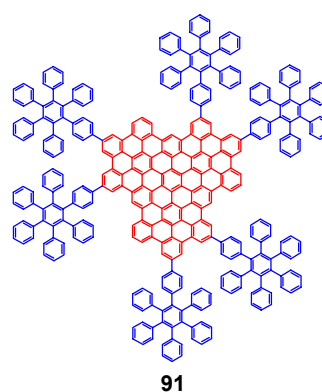
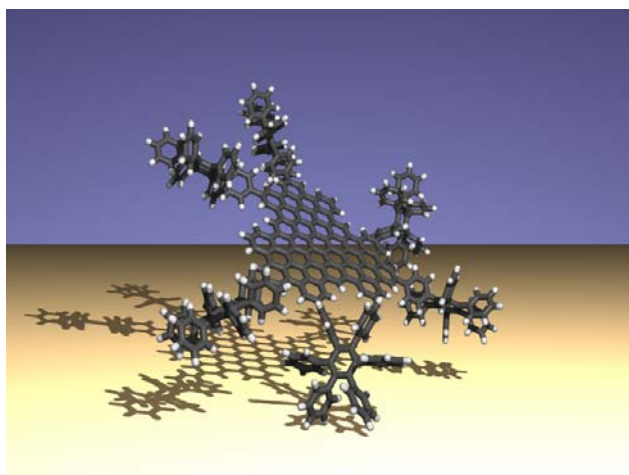


Figure 81. Molecular structures and three-dimensional models^[53] of the dendronized superphenalenes **91** and **92**.

The bulky substituents are expected to dramatically diminish or even completely eliminate the π - π stacking of the superphenalene cores. Less aggregated or nonaggregated superphenalenes are desirable to further understand structure-property relationships. In the following pages of this chapter, synthesis, characterization as well as aggregation behavior of dendronized superphenalene derivatives are described.

4.2 Synthesis and structural characterization

4.2.1 Synthesis of hexa(4-iodophenyl)-C96

A new synthetic concept for the synthesis of new HBC derivatives, based on novel functionalizable mesogenic building blocks, has been recently developed by J. Wu in our group.^[54] Thus, hexa(4-iodophenyl)-*peri*-hexabenzocoronene, prepared by rational multistep synthesis, acts as an HBC building block with versatile reactive sites, which can be converted into a range of useful functionalities.^[42,55,56] Inspired by this new concept, we have synthesized analogous hexa(4-iodophenyl)-C96, which could then be further functionalized and used for the synthesis of dendronized superphenalenes **91** and **92**. The synthesis of the key building block, hexa(4-iodophenyl)-C96 (**97**), is outlined in Figure 82. 3,4-Bis[4'-(4''-trimethylsilylphenyl)phenyl]-2,5-diphenylcyclopentadienone (**94**) was prepared by Suzuki coupling^[57] between 3,4-bis(4-bromophenyl)-2,5-diphenylcyclopentadienone (**67**) and an excess of commercially available 4-(trimethylsilyl)phenylboronic acid (**93**) in 93% yield, after workup. The Diels-Alder reaction of commercially available 1,3,5-triethynylbenzene (**54**) with excess (3.6 equiv) of **94** in *o*-xylene at 170 °C gave 1,3,5-tris{3',4'-di[4''-(4'''-trimethylsilylphenyl)phenyl]-2',5'-diphenylphenyl}benzene (**95**) in 87% yield. Compound **95** was then treated with iodine monochloride in chloroform to afford the target precursor 1,3,5-tris{3',4'-di[4''-(4'''-iodophenyl)phenyl]-2',5'-diphenylphenyl}benzene (**96**) in 92% yield. All

these soluble compounds were fully characterized by NMR and mass spectrometry techniques.

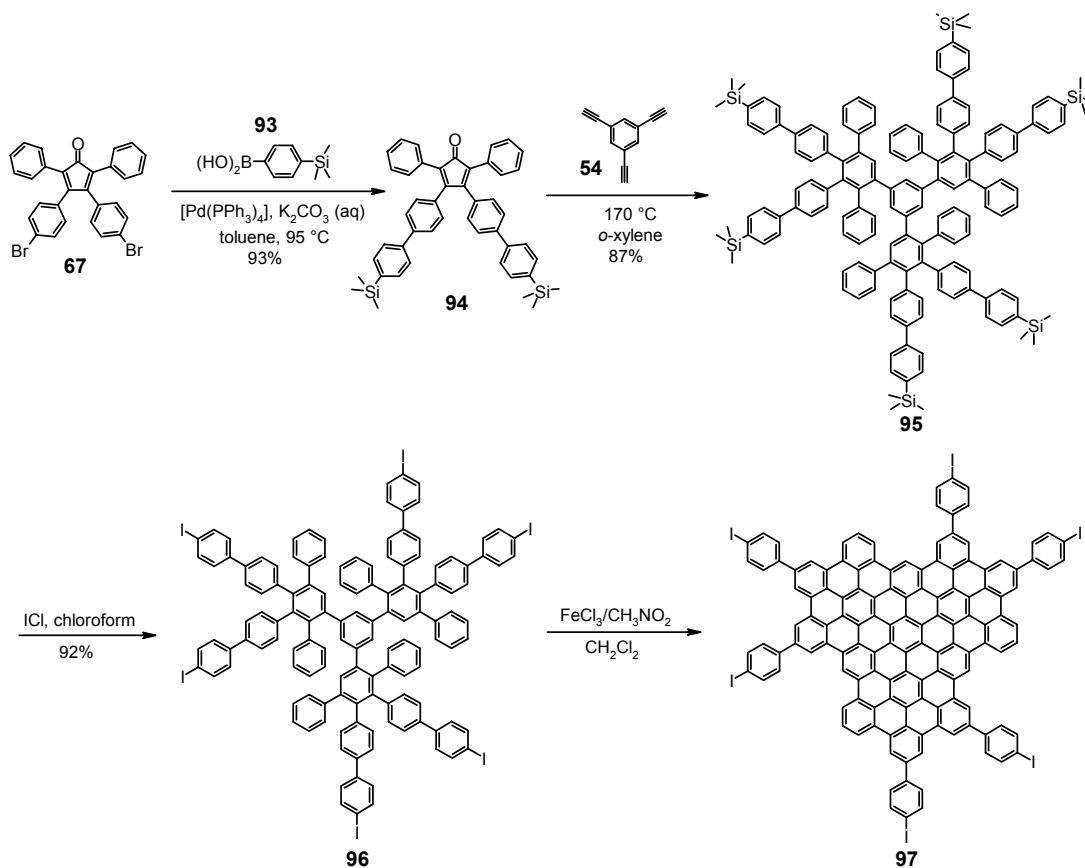


Figure 82. Synthesis of hexa(4-iodophenyl)-C96 (**97**).

The subsequent cyclodehydrogenation was again the most crucial step of the whole synthesis. The previously successfully employed system of iron(III) chloride/nitromethane in dichloromethane was applied again. It was found that three equivalents of iron(III) chloride per hydrogen to be removed and 18 hours reaction resulted in the formation of the desired product. Compound **97** was identified by MALDI-TOF mass spectrometry (solid-state analyte-in-matrix preparation)^[58,59] which reveals a single species with isotopic distribution in accord with that calculated for compound **97** (Figure 83). Upon quenching of the reaction solution by addition of methanol, **97** precipitated as dark-brown solid

which was collected by filtration and was washed thoroughly with methanol until the solvent showed no more trace of yellow color from the iron salts. The poor solubility of **97** has so far precluded preparative chromatography.

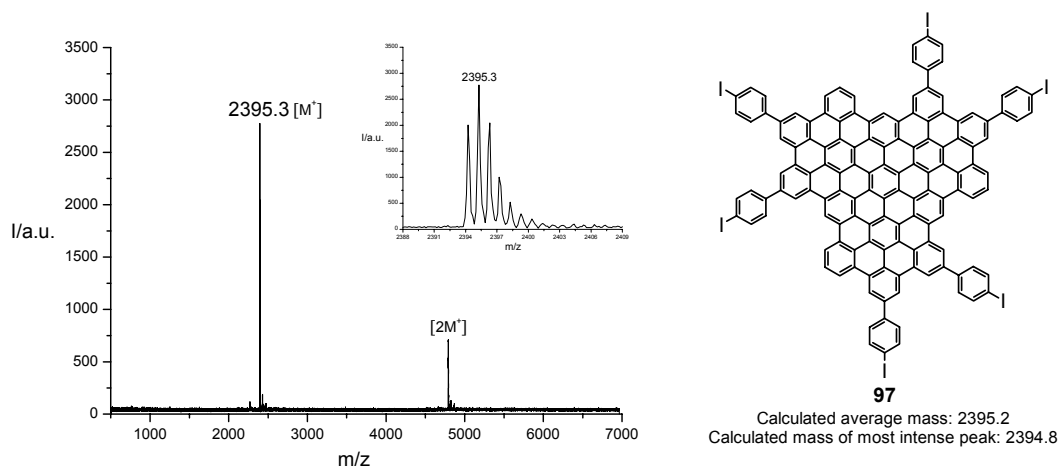


Figure 83. MALDI-TOF mass spectrum of hexa(4-iodophenyl)-C96 (**97**); inset shows isotopic distribution.

4.2.2 Functionalization of hexa(4-iodophenyl)-C96 by Hagihara-Sonogashira coupling reaction towards dendronized superphenalenes

Surprisingly, despite the virtual insolubility of hexa(4-iodophenyl)-C96 (**97**), palladium-catalyzed Hagihara-Sonogashira coupling reaction^[60] with terminal acetylene groups works smoothly, thus providing a versatile method of functionalization. Hexa(4-iodophenyl)-C96 (**97**) was converted by a six-fold Hagihara-Sonogashira coupling with phenylacetylene (**98**) into the insoluble hexa[4-(ethynylphenyl)phenyl]-C96 (**99**) in quantitative yield (Figure 84). A solid-state MALDI-TOF mass spectrum of compound **99** indicates quantitative conversion, even though both the starting material and product are insoluble, proving the high reactivity of the building block **97**.

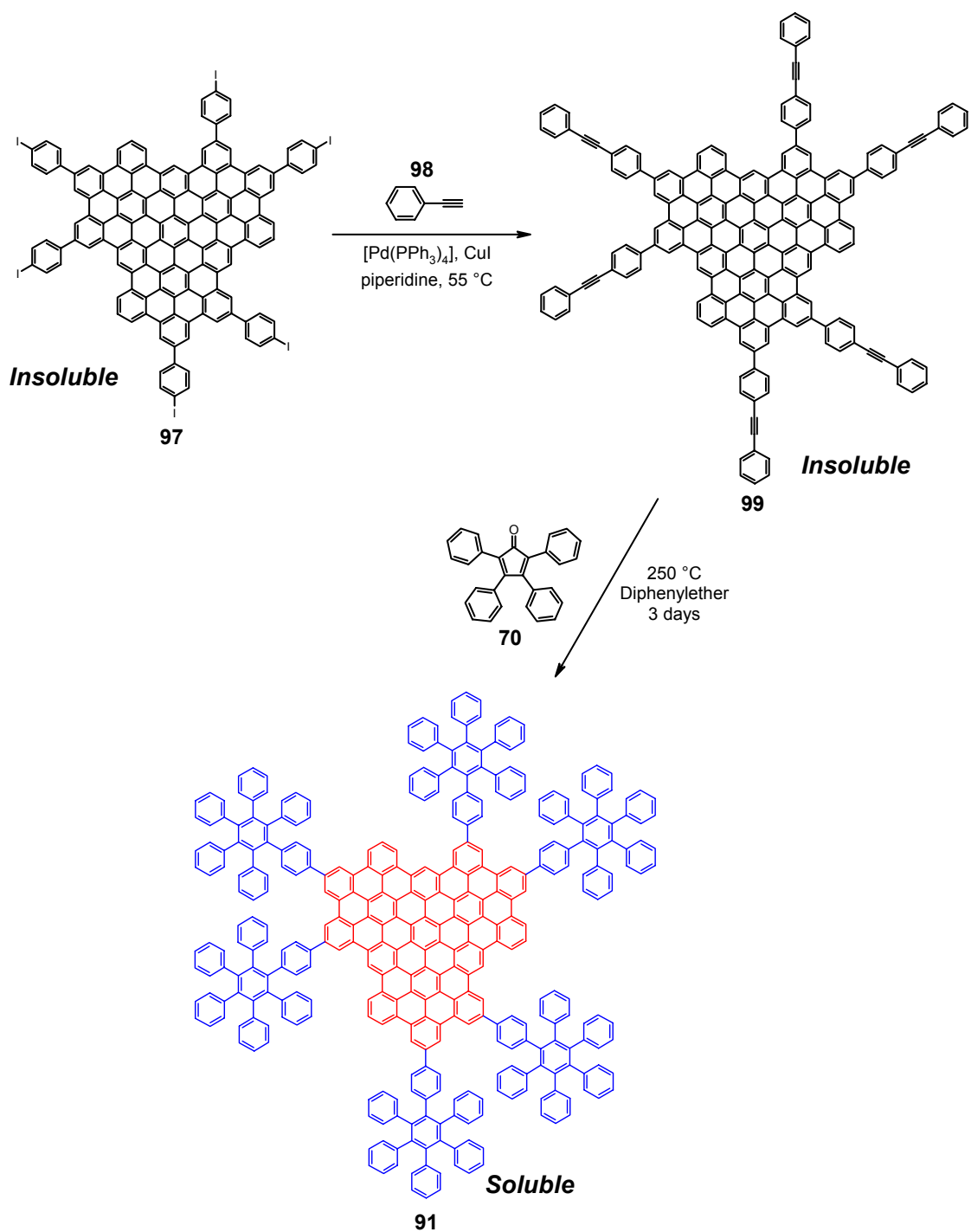


Figure 84. Synthesis of dendronized superphenalene **91**.

The subsequent Diels-Alder reaction between **99** and a large excess (24 equiv) of commercially available tetraphenylcyclopentadienone (**70**) proceeded in

diphenylether at 250 °C. The reaction was monitored by MALDI-TOF mass spectrometry, and after three days came to completion. After cooling, methanol was added to the reaction mixture, and the precipitate was collected by filtration and washed with methanol. The desired product, dendronized superphenalene **91** readily dissolves in common organic solvents at room temperature, and was isolated in 84% yield after purification by column chromatography. The MALDI-TOF mass spectrum of **91** is shown in Figure 85.

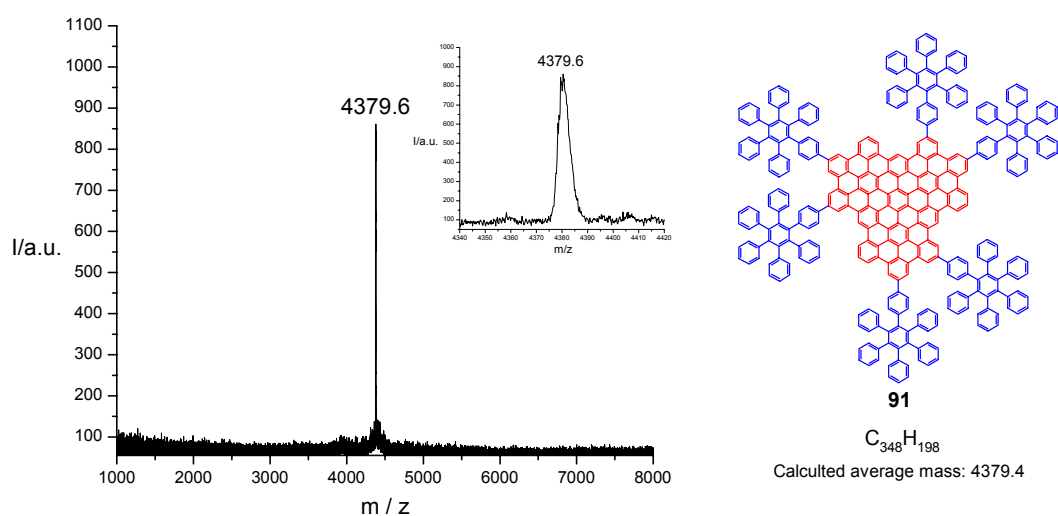


Figure 85. MALDI-TOF mass spectrum of dendronized superphenalene **91**.

The build-up of dendronized superphenalene **92**, with larger dendrons (second generation) around the core, required preparation of tetraphenylcyclopentadienone (**102**) with corresponding dendrons. This compound was synthesized according to the procedure described in the PhD thesis of U. M. Wiesler (Figure 86).^[61,62] The starting material, 4,4'-diethynylbenzil (**100**), was prepared via a Hagihara-Sonogashira coupling^[60] of triisopropylsilylacetylene and 4,4'-dibromobenzil, followed by deprotection with KF in DMF. After a Diels-Alder cycloaddition with an excess of tetraphenylcyclopentadienone (**70**) in refluxing *o*-xylene, the benzyl **101** was obtained as a pale yellow amorphous powder. The Knoevenagel condensation of compound **101** with 1,3-diphenylacetone (**62**) in the presence of

tetrabutylammonium hydroxide leads to the corresponding cyclopentadienone **102** in 85% yield.

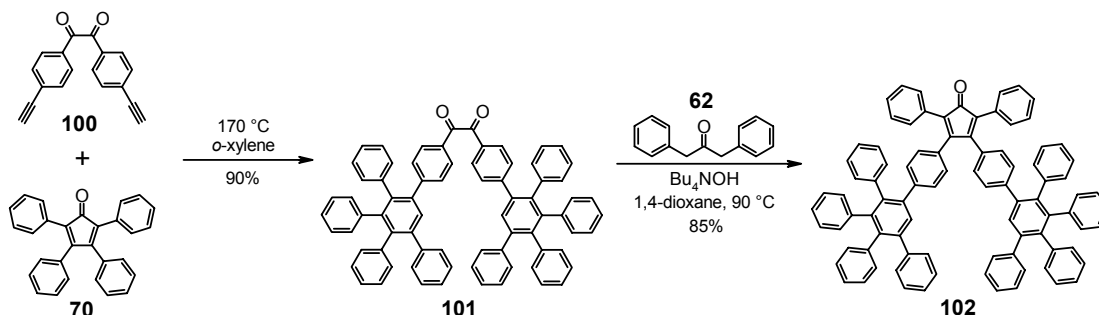


Figure 86. Synthesis of a dendronized cyclopentadienone **102**, according to U. M. Wiesler.^[61,62]

The following final step, a Diels-Alder reaction between **99** and large excess (18 equiv) of **102** required a higher temperature and longer reaction time, due to apparent steric hindrance and much greater crowding of the phenyl rings (Figure 87).^[63-65]

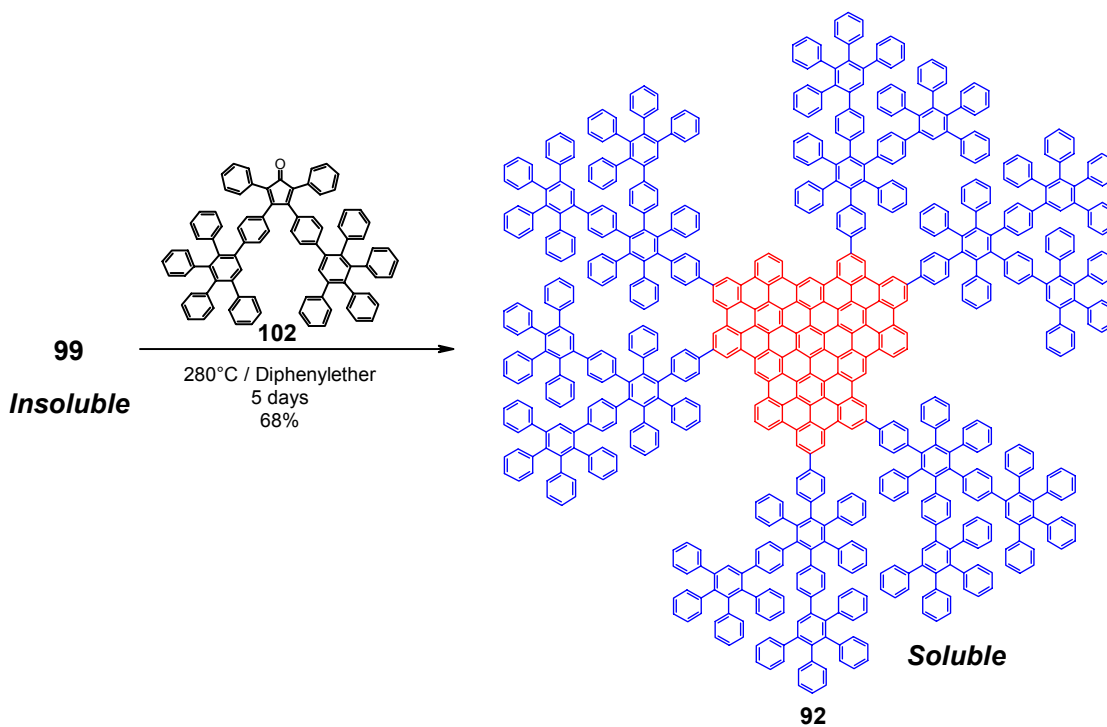


Figure 87. Synthesis of dendronized superphenalene **92**.

Thus, reaction had to proceed in diphenylether at temperature of 280 °C using a thermostatically-controlled heating mantle. The reaction was monitored by MALDI-TOF mass spectrometry, and was at completion after five days. After cooling, methanol was added to the reaction mixture, and the precipitate was collected by filtration and washed with methanol. The desired product, dendronized superphenalene **92** readily dissolves in common organic solvents at room temperature, and was isolated in 68% yield after purification by column chromatography. The MALDI-TOF mass spectrum of **92** is shown in Figure 88.

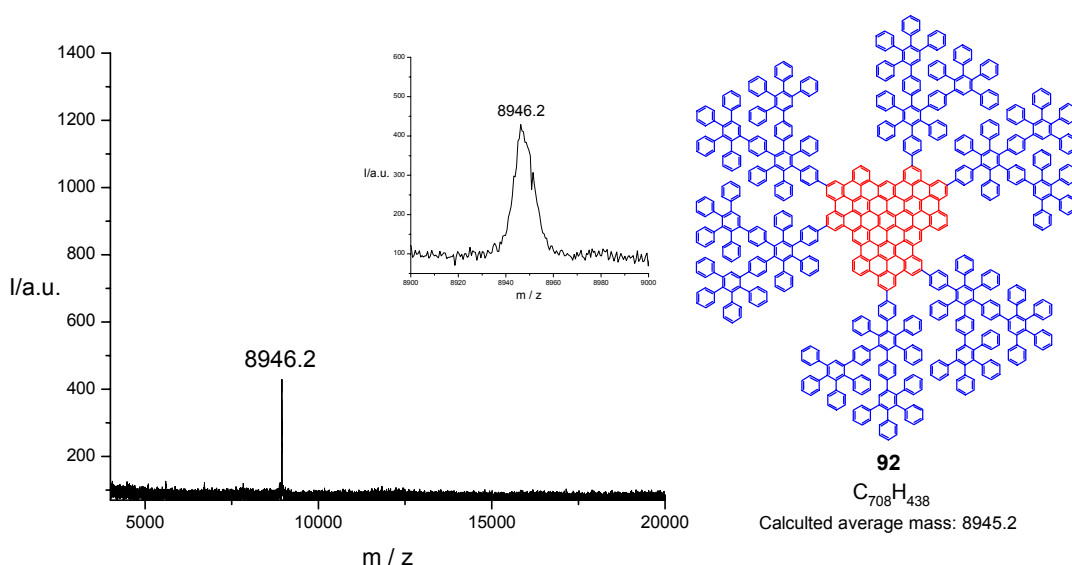


Figure 88. MALDI-TOF mass spectrum of dendronized superphenalene **92**.

Although both dendronized superphenalenes **91** and **92** readily dissolve in common organic solvents at room temperature, their ^1H NMR spectra are not very informative. To illustrate this, the ^1H NMR spectra of **91** and **92** in tetrachloroethane- d_4 are shown in Figure 89. In all the ^1H NMR spectra of compounds **91** and **92**, regardless of the solvent, concentration and temperature, resonances arising from the phenyl rings of the dendrons could be observed, but not those of the protons on the aromatic core.

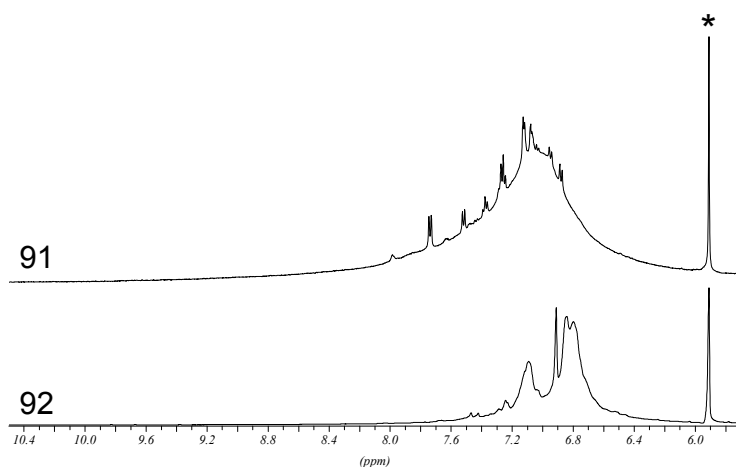


Figure 89. ^1H NMR (aromatic region only) of **91** and **92** in tetrachloroethane- d_4 ($*$).

These observations may be explained by several factors, one being low molecular mobility due to large size of **91** and **92**, which leads to a broadening of the signals. In the case of **91**, the sharp peaks probably arise from the outer sphere protons, due to the higher mobility of these phenyl rings and their better interactions with the solvent. The intense, broad signal under the sharp peaks arises from non-averaged anisotropy of the disc and the phenyl rings close to the core. In the case of **92**, the signals of the outer sphere protons are not as well resolved (as **91**), likely due to the higher density of the phenyl rings in the second generation dendrons, their lower symmetry and lower molecular mobility.

4.3 UV/Vis absorption and fluorescence measurements

The aggregation of PAH discs has a great influence, not only on their order, but also on the photophysical and electronic properties of each disc.^[66-68] Hence, studying the photophysical properties of HBC- C_{12} in solution by steady state and time-resolved spectroscopy showed that due to aggregation, both

absorption and emission bands changed as a function of concentration. This is in contrast to the HBC with six bulky *tert*-butyl groups which does not self-assemble, and consequently shows no concentration dependence.^[69]

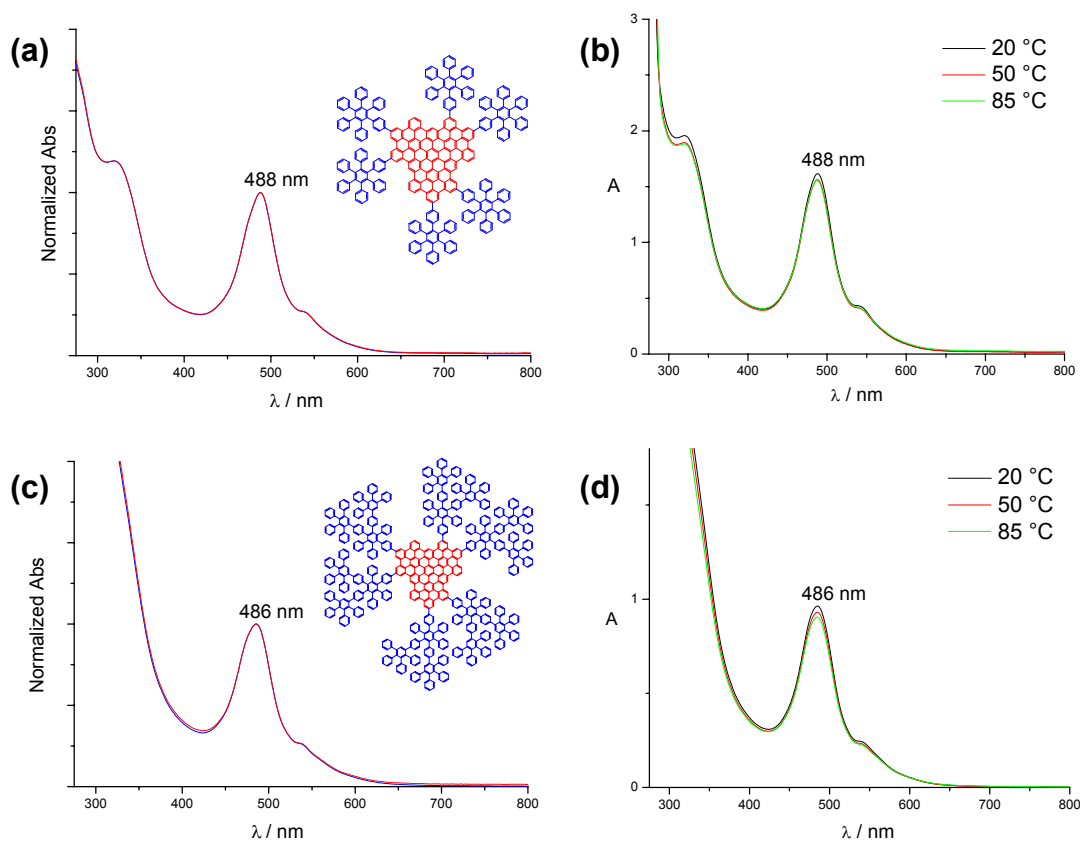


Figure 90. Normalized UV-Vis absorption spectra of (a) **91** and (c) **92** in THF; $C = 10^{-5}$ M (blue line) and 10^{-6} M (red line); temperature dependent UV/Vis spectra of (b) **91** and (d) **92** in 1.1×10^{-5} M toluene solution.

UV/Vis absorption spectra of **91** and **92** measured with varying concentration or temperature are shown in Figure 90. The UV/Vis absorption spectra of **91** and **92**, measured in THF and toluene in the concentration range 10^{-4} - 10^{-7} M, show a broad, featureless profile, but no concentration or solvent dependence. The broad bands are probably the result of many close excited electronic states with a small energy difference, thus overlapping each other. The maximum absorptions of **91** ($\lambda_{\max} = 488$ nm) and **92** ($\lambda_{\max} = 486$ nm) are red

shifted relative to C96-C₁₂ (**53a**, λ_{\max} = 462 nm), which can be explained as a consequence of extended conjugation between the dendrons and superphenalene core. It should be pointed out that going to higher dendrimer generation, i.e. from **91** to **92**, has no significant influence upon the absorption maximum. The variable temperature UV/Vis measurements in 10⁻⁵ M toluene solution did not show any temperature dependence over the range of 20 – 85 °C (85 °C was the upper experimental limit; small variations in the absorbance are within the limit of experimental error).

Solid-state absorption spectra of C96-C₁₂ (**53a**) and dendronized superphenalenes **91** and **92** have been recorded from films prepared by spin-coating from 10⁻³ M toluene solutions onto quartz substrates at room temperature, and are depicted in Figure 91.

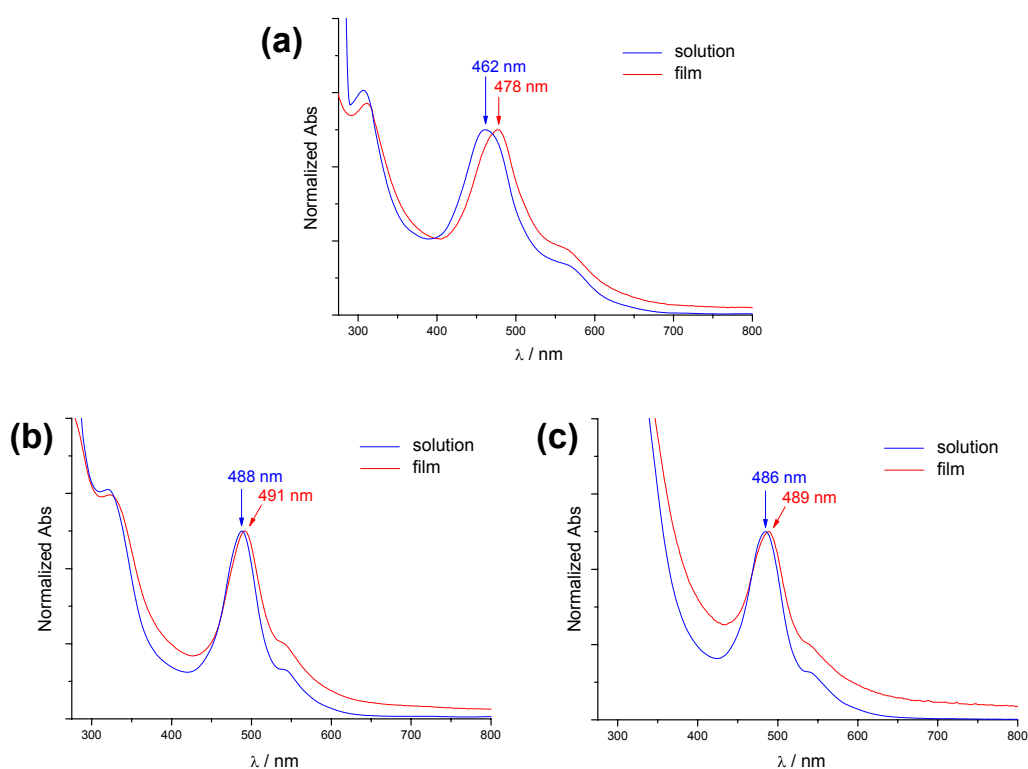


Figure 91. Solid-state UV/Vis absorption spectra of (a) C96-C₁₂ (**53a**), (b) **91** and (c) **92**, recorded from films, prepared by spin-coating from 10⁻³ M toluene solutions at room temperature; for comparison, their solution UV/Vis spectra are also shown (all spectra are normalized at λ_{\max}).

The absorption spectrum of the film of C96-C₁₂ (**53a**) displayed a maximum of absorption at 478 nm, as shown in Figure 91a. This is a 16 nm bathochromic shift in comparison to the absorption of C96-C₁₂ in solution. This significant absorption shift can be explained by the pronounced columnar aggregation in the solid-state film after spin-coating. The absorption maximum of dendronized superphenalenes **91** and **92** in the film is essentially not shifted compared to that in solution (only a shift of 2-3 nm is observed), and this can be ascribed to the inability of the superphenalene core to π -stack in the dendronized superphenalenes.

The fluorescence spectra of dendronized superphenalenes **91** and **92** measured by varying concentration or temperature are shown in Figure 92. In general, compounds **91** and **92** showed similar fluorescence spectra when excited at 488 and 486 nm, respectively, giving rise to emission bands centered at 674 nm, significantly red-shifted compared to C96-C₁₂ (\approx 570 nm). Going to the higher dendrimer generation has no influence upon the maximum in the emission spectra, while the fluorescence intensity slightly decreases. In the emission spectra of C96-C₁₂, the appearance of a low energy tail (at about 640 nm) was observed upon decreasing the concentration, although the exact reason for this is currently not known (Chapter 2). On the other hand, the fluorescence measurements of the dendronized superphenalenes **91** and **92** in THF or toluene solution, did not show any concentration dependence, over the range 10^{-5} – 5×10^{-8} M (Figure 92a,c). Also, the variation of temperature over the range 300 – 400K has no influence on the fluorescence spectrum of **91** and **92** in 1,2-dichlorobenzene, as shown in Figure 92b,d (only a small change in fluorescence intensity was observed, but this is within experimental error). The absence of change in the UV/Vis and fluorescence spectra of **91** and **92** with concentration and temperature appears consistent with the assumption that six bulky dendritic substituents around the core suppress the π - π stacking of the cores to some extent, thus leading to less- or non-aggregated species. However, the lack of clear results from the NMR and light-scattering experiments, preclude definite conclusions from being made with regard to the extent of aggregation. This study

also shows that in contrast to smaller discs, such as HBC, where the self-assembly behavior could be effectively controlled by introduction of bulky substituents as shown by ^1H NMR, self assembly of larger discs, such as superphenalene is far more difficult to control due to the inadequacy of analytical methods available for its study.

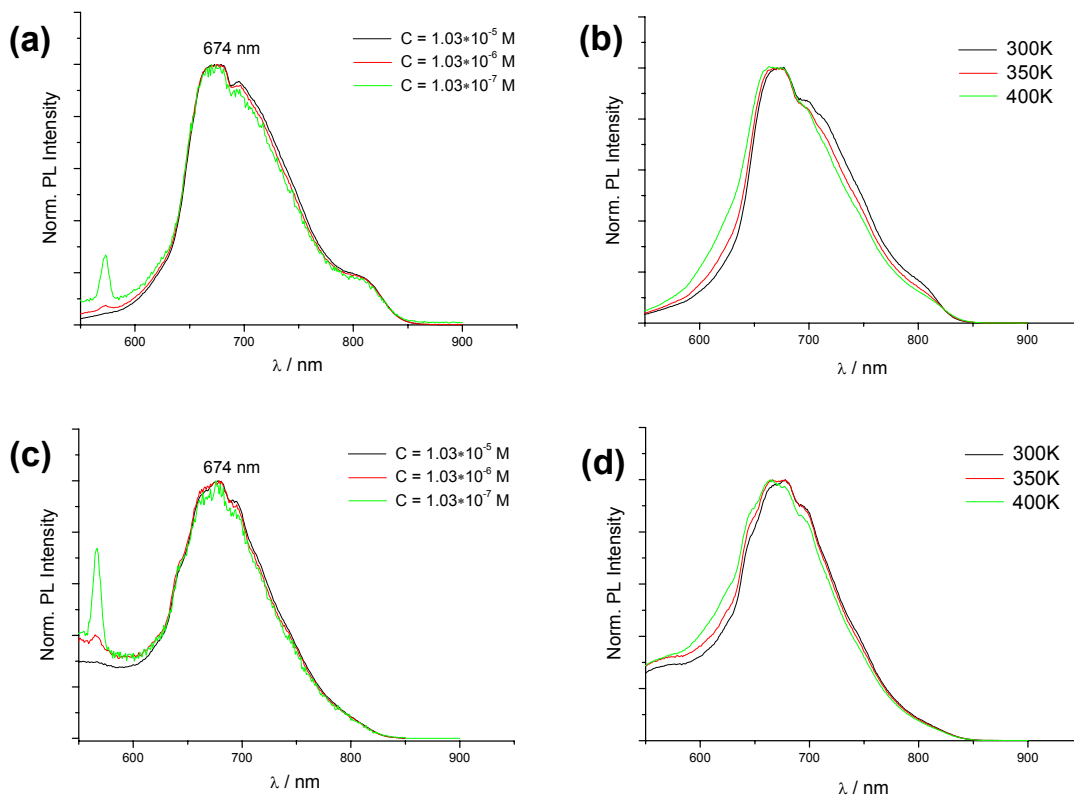


Figure 92. Concentration dependent fluorescence spectra of (a) **91** and (c) **92** in THF, and temperature dependent fluorescence spectra of (b) **91** and (d) **92** in 10^{-5} M 1,2-dichlorobenzene solution (excited at 488 and 486 nm, respectively; spectra are normalized at the emission maximum).

Summarizing the results described in this chapter, the insoluble building block, hexa(4-iodophenyl)-C96 (**97**), carrying six reactive sites, can be prepared by a rational approach, and despite its virtual insolubility, **97** could be easily and quantitatively functionalized by a subsequent standard transition metal-catalyzed

coupling reaction. In general, this allows functionalization of the superphenalene core as a final step, which greatly broadens the scope of functionalities that may be introduced around the discs, thus paving the way to new materials based on superphenalene. The principle was demonstrated through the preparation of dendronized superphenalenes **91** and **92**, with bulky dendritic substituents around the core, which were expected to lead to the steric isolation and diminished π - π interactions of the cores. Here, although insoluble, **97** could be quantitatively converted by Hagihara-Sonogashira coupling with phenylacetylene into the also insoluble hexa[4-(ethynylphenyl)phenyl]-C96 (**99**). The carbon-carbon triple bond of **99** provides active sites for further functionalization by Diels-Alder reaction, leading to the dendronized superphenalenes **91** and **92**. Despite their good solubility in common organic solvents, in ^1H NMR spectra, regardless of the solvent, concentration and temperature, resonances arising from the mobile phenyl rings of the dendrons could be observed, but not those of the protons on the aromatic core, which are effected by low molecular mobility. UV/Vis and fluorescence spectroscopic measurements have been applied to probe the influence of the surrounding polyphenylene dendrimer shell upon the self-assembly properties of the superphenalene core. The dendronized superphenalenes **91** and **92** show red shifted absorption spectra relative to that of the alkylated C96-C₁₂. UV/Vis measurements in solution exhibited no dependence on concentration and temperature. Solid-state UV/Vis spectra of **91** and **92** are essentially identical to those measured in solution, and thus stands in contrasts to the alkylated C96-C₁₂ which shows a significant red shift on moving from solution to film. These observations are consistent with the known aggregation properties of C96-C₁₂ in the bulk by virtue of strong π - π stacking, an interaction that is hindered by the presence of bulky dendritic substituents on **91** and **92**. Similarly to the solution UV/Vis experiments, fluorescence measurements displayed a red shift relative to that of the alkylated C96-C₁₂, and no dependence on concentration and temperature. However, the results from optical and NMR experiments do not provide sufficient information to be able to quantify the degree of self-assembly of **91** and **92** in solution.

4.4 Literature

- [1] W. Saenger, *Principles of Nucleic Acid Structure*, Springer-Verlag, New York, **1984**, 132-140.
- [2] M. Petersheim, D. H. Turner, *Biochemistry*, **1983**, *22*, 256-263.
- [3] K. M. Guckian, B. A. Schweitzer, R. X. F. Ren, C. J. Sheils, P. L. Paris, D. C. Tahmassebi, E. T. Kool, *J. Am. Chem. Soc.* **1996**, *118*, 8182-8183.
- [4] D. Demus, J. W. Goodby, G. W. Gray, H. W. Spiess, V. Vill, (eds.) *Handbook of Liquid Crystals*, Vol. 2B, Wiley-VCH, Weinheim, **1998**.
- [5] G. R. Desiraju, *Crystal Engineering: Design of Organic Solids*, Elsevier, Amsterdam, **1989**.
- [6] P. W. Carter, S. G. DiMaggio, J. D. Porter, A. Streitwieser, *J. Phys. Chem.*, **1993**, *97*, 1085-1096.
- [7] J. Brey, K. Kratzer, H. Yersin, *J. Am. Chem. Soc.* **2000**, *122*, 2548-2555.
- [8] J. P. DiNitto, P. W. Huber, *Biochemistry*, **2001**, *40*, 12645-12653.
- [9] C. A. Hunter, J. K. M. Sanders, *J. Am. Chem. Soc.* **1990**, *112*, 5525-5534.
- [10] G. Ravishanker, D. L. Beveridge, *J. Am. Chem. Soc.* **1985**, *107*, 2565-2566.
- [11] W. L. Jorgensen, D. L. Severance, *J. Am. Chem. Soc.* **1990**, *112*, 4768-4777.
- [12] P. Linse, *J. Am. Chem. Soc.* **1992**, *114*, 4366-4373.
- [13] P. Hobza, H. L. Selzle, E. W. Schlag, *J. Am. Chem. Soc.* **1994**, *116*, 3500-3506.
- [14] C. Janiak, *J. Chem. Soc. Dalton Trans.* **2000**, 3885-3896.
- [15] J. H. Williams, *Acc. Chem. Res.* **1993**, *26*, 593-598.
- [16] R. Laatikainen, J. Ratilainen, R. Sebastian, H. Santa, *J. Am. Chem. Soc.* **1995**, *117*, 11006-11010.
- [17] F. Cozzi, M. Cinquini, R. Annunziata, T. Dwyer, J. S. Siegel, *J. Am. Chem. Soc.* **1992**, *114*, 5729-5733.
- [18] E. E. Tucker, S. D. Christian, *J. Phys. Chem.*, **1979**, *83*, 426-427.
- [19] K. Miyamura, A. Mihara, T. Fujii, Y. Gohshi, Y. Ishii, *J. Am. Chem. Soc.* **1995**, *117*, 2377-2378.
- [20] S. Chandrasekhar, *Liquid Crystals*, 2nd ed., Cambridge University Press, Cambridge, **1992**.
- [21] H. Stegmeyer, *Liquid Crystals*, Springer-Verlag, New York, **1994**.
- [22] R. J. Bushby, O. R. Lozman, *Curr. Opin. Coll. Inter. Sci.* **2002**, *7*, 343-354.
- [23] R. J. Bushby, O. R. Lozman, *Curr. Opin. Sol. State Mater. Sci.* **2003**, *6*, 569-578.
- [24] P. G. Schouten, J. M. Warman, M. P. de Haas, C. F. van Nostrum, G. H. Gelinck, R. J. M. Nolte, M. J. Copyn, J. W. Zwikker, M. K. Engel, M. Hanack, Y. H. Chang, W. T. Ford, *J. Am. Chem. Soc.* **1994**, *116*, 6880-6894.

- [25] D. Adam, P. Schuhmacher, J. Simmerer, L. Häussling, K. Siemensmeyer, K. H. Etzbach, H. Ringsdorf, D. Haarer, *Nature* **1994**, *371*, 141-143.
- [26] A. M. van de Craats, J. M. Warman, A. Fechtenkötter, J. D. Brand, M. A. Harbison, K. Müllen, *Adv. Mater.* **1999**, *11*, 1469-1472.
- [27] J. W. Schutte, M. Sluyters-Rehbach, J. H. Sluyters, *J. Phys. Chem.* **1993**, *97*, 6069-6073.
- [28] R. D. Parina, D. J. Halko, J. H. Swinehart, *J. Phys. Chem.* **1972**, *76*, 2343-2348.
- [29] K. M. Kadish, D. Sazou, Y. M. Liu, A. Saoiabi, M. Ferhat, R. Guillard, *Inorg. Chem.* **1988**, *27*, 686-690.
- [30] K. Kano, K. Fukuda, H. Wakami, R. Nishiyabu, R. F. Pasternack, *J. Am. Chem. Soc.* **2000**, *122*, 7494-7502.
- [31] M. Müller, C. Kübel, K. Müllen, *Chem. Eur. J.* **1998**, *4*, 2099-2109.
- [32] F. Dötz, J. D. Brand, S. Ito, L. Gherghel, K. Müllen, *J. Am. Chem. Soc.* **2000**, *122*, 7707-7717.
- [33] M. D. Watson, A. Fechtenkötter, K. Müllen, *Chem. Rev.* **2001**, *101*, 1267-1300.
- [34] C. D. Simpson, J. D. Brand, A. J. Berresheim, L. Przybilla, H. J. Räder, K. Müllen, *Chem. Eur. J.* **2002**, *8*, 1424-1429.
- [35] C. D. Simpson, J. Wu, M. D. Watson, K. Müllen, *J. Mater. Chem.* **2004**, *14*, 494-504.
- [36] L. Schmidt-Mende, A. Fechtenkötter, K. Müllen, E. Moons, R. H. Friend, J. D. MacKenzie, *Science* **2001**, *293*, 1119-1122.
- [37] A. M. van de Craats, N. Stutzmann, O. Bunk, M. M. Nielsen, M. Watson, K. Müllen, H. D. Chanzy, H. Sirringhaus, R. H. Friend, *Adv. Mater.* **2003**, *15*, 495-499.
- [38] J. Piris, M. G. Debije, N. Stutzmann, A. M. Van de Craats, M. D. Watson, K. Müllen, J. M. Warman, *Adv. Mater.* **2003**, *15*, 1736-1740.
- [39] I. Fischbach, T. Pakula, P. Minkin, A. Fechtenkötter, K. Müllen, H. W. Spiess, K. Saalwächter, *J. Phys. Chem. B* **2002**, *106*, 6408-6418.
- [40] S. P. Brown, I. Schnell, J. D. Brand, K. Müllen, H. W. Spiess, *J. Am. Chem. Soc.* **1999**, *121*, 6712-6718.
- [41] P. Samori, A. Fechtenkötter, F. Jäckel, T. Böhme, K. Müllen, J. P. Rabe, *J. Am. Chem. Soc.* **2001**, *123*, 11462-11467.
- [42] J. Wu, A. Fechtenkötter, J. Gauss, M. D. Watson, M. Kastler, C. Fechtenkötter, M. Wagner, K. Müllen, *J. Am. Chem. Soc.* **2004**, *126*, 11311-11321.
- [43] S. Hecht, J. M. J. Fréchet, *Angew. Chem. Int. Ed.* **2001**, *40*, 75-91.
- [44] M. Kimura, T. Shiba, M. Yamazaki, K. Hanabusa, H. Shirai, N. Kobayashi, *J. Am. Chem. Soc.* **2001**, *123*, 5636-5642.
- [45] C. A. Kernag, D. V. McGrath, *Chem. Commun.* **2003**, 1048-1049.
- [46] A. C. H. Ng, X. Li, D. K. P. Ng, *Macromolecules*, **1999**, *32*, 5292-5298.
- [47] M. Brewis, G. J. Clarkson, M. Helliwell, A. M. Holder, N. B. McKeown, *Chem. Eur. J.* **2000**, *6*, 4630-4636.
- [48] N. Kobayashi, *Curr. Opin. Sol. State Mater. Sci.* **1999**, *4*, 345-353.

- [49] C. J. Hawker, K. L. Wooley, J. M. J. Fréchet, *J. Chem. Soc. Chem. Commun.* **1994**, 925-926.
- [50] K. L. Wooley, C. J. Hawker, J. M. J. Fréchet, F. Wudl, G. Srdanov, S. Shi, C. Li, M. Kao, *J. Am. Chem. Soc.* **1993**, *115*, 9836-9837.
- [51] U. M. Wiesler, T. Weil, K. Müllen, *Top. Curr. Chem.* **2001**, *212*, 2-40.
- [52] A. J. Berresheim, M. Müller, K. Müllen, *Chem. Rev.* **1999**, *99*, 1747-1785.
- [53] PC Spartan Pro, Ver.1.0.5. Wavefunction Inc., Irvine, CA, **2000**.
- [54] J. Wu, M. D. Watson, K. Müllen, *Angew. Chem. Int. Ed.* **2003**, *42*, 5329-5333.
- [55] J. Wu, M. D. Watson, L. Zhang, Z. Wang, K. Müllen, *J. Am. Chem. Soc.* **2004**, *126*, 177-186.
- [56] J. Wu, M. Baumgarten, M. G. Debije, J. Warman, K. Müllen, *Angew. Chem. Int. Ed.* **2004**, *43*, 5331-5335.
- [57] N. Miyaura, A. Suzuki, *Chem. Rev.* **1995**, *95*, 2457-2483.
- [58] L. Przybilla, J. D. Brand, K. Yoshimura, H. J. Räder, K. Müllen, *Anal. Chem.* **2000**, *72*, 4591-4597.
- [59] K. Yoshimura, L. Przybilla, S. Ito, J. D. Brand, M. Wehmeier, H. J. Räder, K. Müllen, *Macromol. Chem. Phys.* **2001**, *202*, 215-222.
- [60] S. Takahashi, Y. Kuroyama, K. Sonogashira, N. Hagihara, *Synthesis* **1980**, 627-630.
- [61] U. M. Wiesler, K. Müllen, *Chem. Commun.* **1999**, 2293-2294.
- [62] T. Weil, U. M. Wiesler, A. Herrmann, R. Bauer, J. Hofkens, F. C. De Schryver, K. Müllen, *J. Am. Chem. Soc.* **2001**, *123*, 8101-8108.
- [63] L. Tong, D. M. Ho, N. J. Vogelaar, C. E. Schutt, R. A. Pascal, Jr., *J. Am. Chem. Soc.* **1997**, *119*, 7291-7302.
- [64] R. A. Pascal, Jr., N. Hayashi, D. M. Ho, *Tetrahedron* **2001**, *57*, 3549-3555.
- [65] X. Shen, D. M. Ho, R. A. Pascal, Jr., *J. Am. Chem. Soc.* **2004**, *126*, 5798-5805.
- [66] A. Bayer, J. Hübner, J. Kopitzke, M. Oestreich, W. Rühle, J. H. Wendorf, *J. Phys. Chem. B* **2001**, *105*, 4596-4602.
- [67] S. Marguet, D. Markovitsi, P. Millié, H. Sigal, *J. Phys. Chem. B* **1998**, *102*, 4697-4710.
- [68] A. J. Fleming, J. N. Coleman, A. B. Dalton, A. Fechtenkötter, M. D. Watson, K. Müllen, H. J. Byrne, W. J. Blau, *J. Phys. Chem. B* **2003**, *107*, 37-43.
- [69] M. A. Biasutti, J. Rommens, A. Vaes, S. De Feyter, F. D. De Schryver, P. Herwig, K. Müllen, *Bull. Soc. Chim. Belg.* **1997**, *106*, 659-664.

CHAPTER 5

Graphitic Molecules with Partial "Zig-Zag" Periphery

5.1 Introduction

Molecular size, symmetry, and the nature of the periphery have a great influence on the electronic properties as well as the two- and three-dimensional superstructures of the graphite discs.^[1-14] According to the Clar classification, graphitic molecules with "armchair" and "cove" peripheries, as shown in Figure 93 (A,B), are all-benzenoid PAHs.^[1] Within the Clar-type topologies, one expects a lowering of the HOMO-LUMO gap upon increasing the size of the molecules. However, the HOMO-LUMO energy gap of PAHs depends not only upon the size, but also upon the nature of the periphery. Namely, in addition to the linear topologies A and B (Figure 93), Stein and Brown considered two other peripheral structures, C and D, in their theoretical work.^[15]

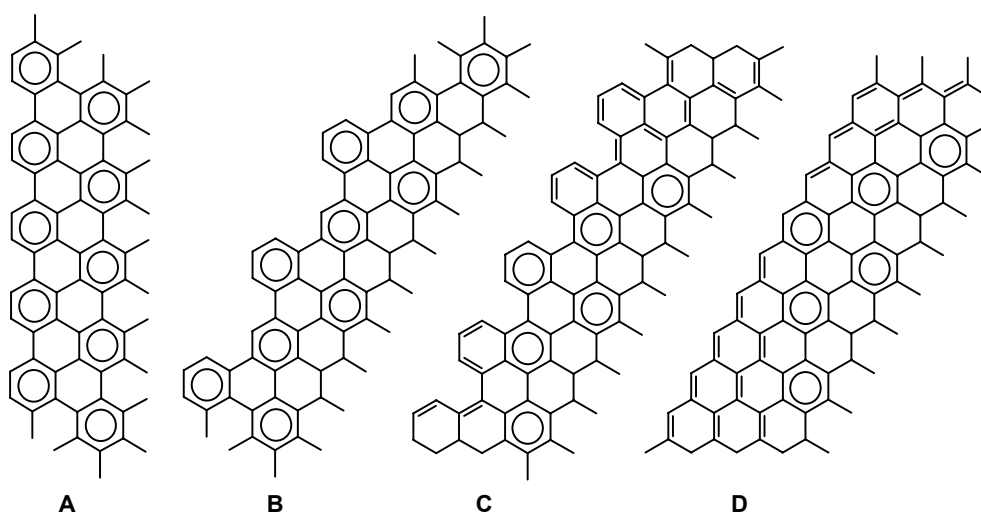


Figure 93. Peripheral topologies of large PAHs: all-benzenoid (A,B), acene-like (C), and quinoidal (D).

These structures are typical for polycyclic aromatics and according to the Clar model, must lead to the products with higher energy. Topology C, formed from [4]helicene-like units, forces the double bonds that are not part of an electron sextet into an acene-like configuration, whereas the "zig-zag" topology of the remaining double bonds in topology D gives a quinoidal character. It was shown that, in particular, a "zig-zag" periphery is predicted to lead to a lower HOMO-LUMO gap than the "armchair" periphery, and also to higher reactivity.^[15]

Because of its hexagonal symmetry, hexa-*peri*-hexabenzocoronene (**8**, Figure 94) serves as an intriguing homologue of benzene. The idea of using HBC as the starting point of "superbenzene" chemistry of molecular graphite subunits suggests a series of further structural modifications, such as variation of its edge-structure. In this chapter, results which promise the establishment of a new family of graphitic molecules with "reactive" double bond, are presented. As was pointed out above, the integration of "zig-zag" edges should dramatically influence, not only its electronic properties, but also its two- and three-dimensional self-assembly behavior (due to the changing of symmetry).

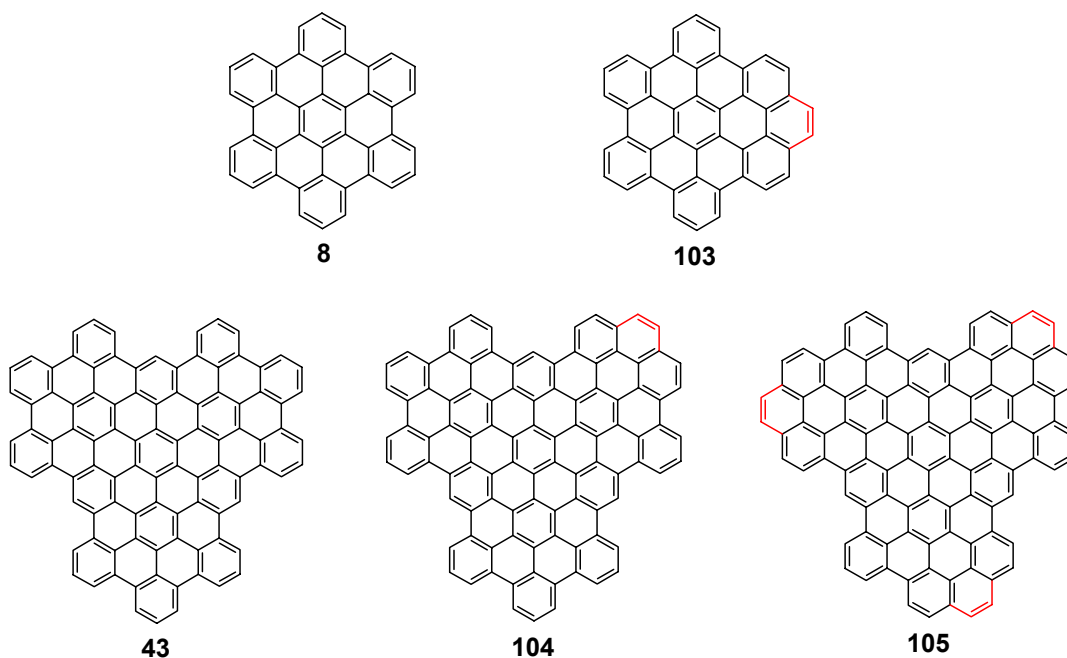


Figure 94. Molecular structure of HBC (**8**), superphenalene (**43**), and target compounds, with partial "zig-zag" periphery.

5.2 Synthesis

Whereas cyclotrimerization of phenyl-substituted ethynes is restricted to the preparation of polyphenylene precursors with six-fold symmetry, Diels-Alder [4+2] cycloaddition of tetraphenylcyclopentadienone with diarylacetylenes is a well-established method to construct polyphenylene derivatives.^[16-21] Therefore, the key design element here is to incorporate a "zig-zag" edge into the cyclopentadienones. Recently, Z. Wang, in the group of Prof. Müllen, found that pyrene-4,5-dione derivatives form unique helical columnar arrangements in single crystals,^[22] and that their Knoevenagel condensation with benzil gives the desired building block, 1,3-diphenylcyclopenta[e]pyren-2-one (**106**, Figure 95).

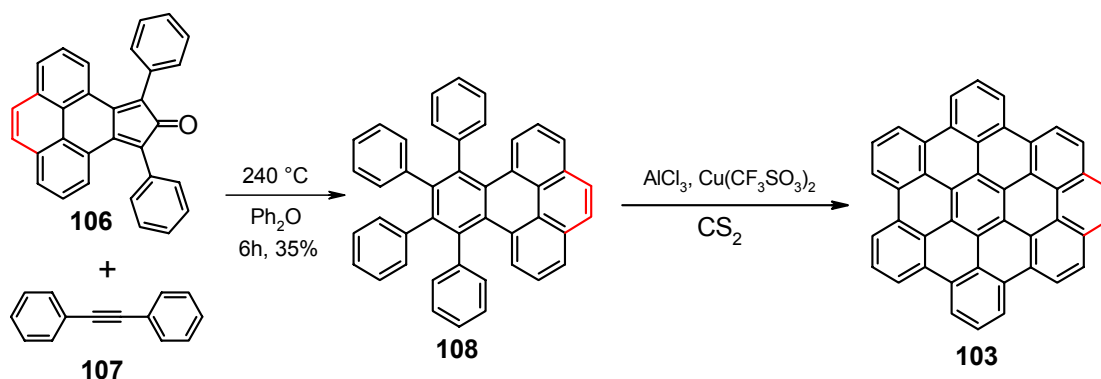


Figure 95. Synthetic route to "zig-zag" HBC (**103**).

Diels-Alder reaction of 1,3-diphenylcyclopenta[e]pyren-2-one^[23,24] (**106**, prepared by Z. Wang) with commercially available diphenylacetylene (**107**) resulted in the corresponding 9,10,11,12-tetraphenyl-benzo[e]pyrene (**108**) in relatively low yield (35%), probably because of the thermal decomposition of **106** during cycloaddition process (240 °C). Cyclodehydrogenation^[5,6] of the unsubstituted **108** proceeded smoothly with copper(II) trifluoromethanesulfonate and aluminium(III) chloride to give the desired planar PAH **103** with one additional "zig-zag" edge. The vanishing solubility of **103** precludes solution ¹H NMR and ¹³C NMR characterization; however, MALDI-TOF mass spectrometry (solid-state

analyte in TCNQ matrix preparations),^[25,26] reveals a single species with isotopic distribution in accord to that calculated for compound **103**, proving the loss of exactly 10 hydrogen atoms during the formation of five new carbon-carbon bonds (Figure 96).

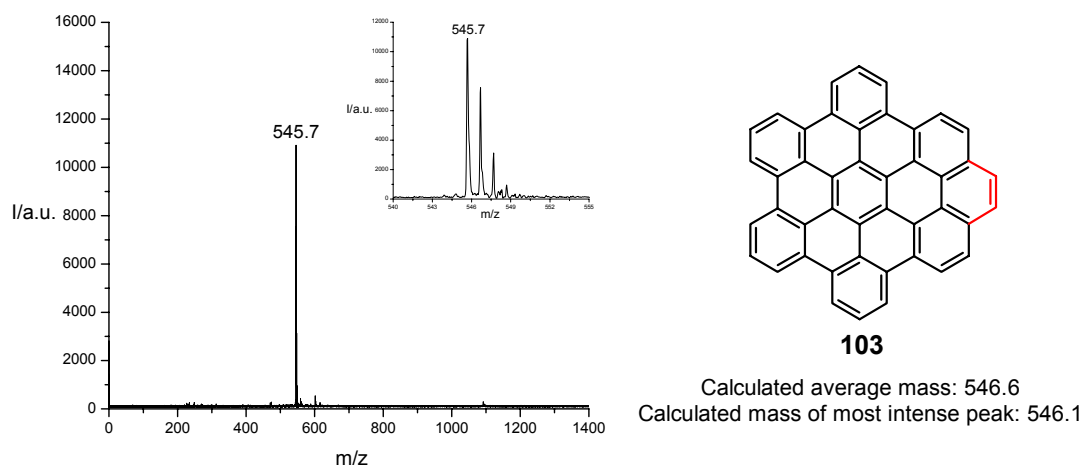


Figure 96. MALDI-TOF mass spectrum of "zig-zag" HBC (**100**); inset shows isotopic distribution.

To demonstrate the versatility of our "molecular Lego", we have synthesized superphenalene "zig-zag" derivatives, **104** and **105**, with one and three additional "zig-zag" edges, respectively (Figure 97). The two key steps toward the graphitic discs **104** and **105** are the synthesis of the polyphenylene precursors (**109** and **110**) and the subsequent oxidative cyclodehydrogenation. Three-fold Diels-Alder cycloaddition of commercially available 1,3,5-triethynylbenzene (**54**) with excess (4.4 equiv) of 1,3-diphenylcyclopenta[*e*]pyren-2-one (**106**) in refluxing *o*-xylene, gave the propeller-like precursor 1,3,5-tris(9',12'-diphenyl-benzo[*e*]pyren-11'-yl)benzene (**110**) in 70% yield, after work up. The previously described building block **72a** (Chapter 2) with one terminal triple bond was used for the synthesis of polyphenylene precursor **109**. The Diels-Alder reaction of **72a** with excess (1.3 equiv) of 1,3-diphenylcyclopenta[*e*]pyren-2-one (**106**) in refluxing *o*-xylene gave 1-(9',12'-diphenyl-benzo[*e*]pyren-11'-yl)-3,5-di(2',3',4',5'-tetraphenylphenyl)benzene

(**109**) in 74% yield, after work up. The structure and purity of precursors **109** and **110** were confirmed by ^1H and ^{13}C NMR spectroscopy, FD mass spectrometry, and elemental analysis. As the 2D-representation of **109** and **110** suggests, they could be cleanly cyclodehydrogenated to a graphitic molecules **104** ($\text{C}_{98}\text{H}_{30}$) and **105** ($\text{C}_{102}\text{H}_{30}$) with a more extended "zig-zag" character (Figure 97).

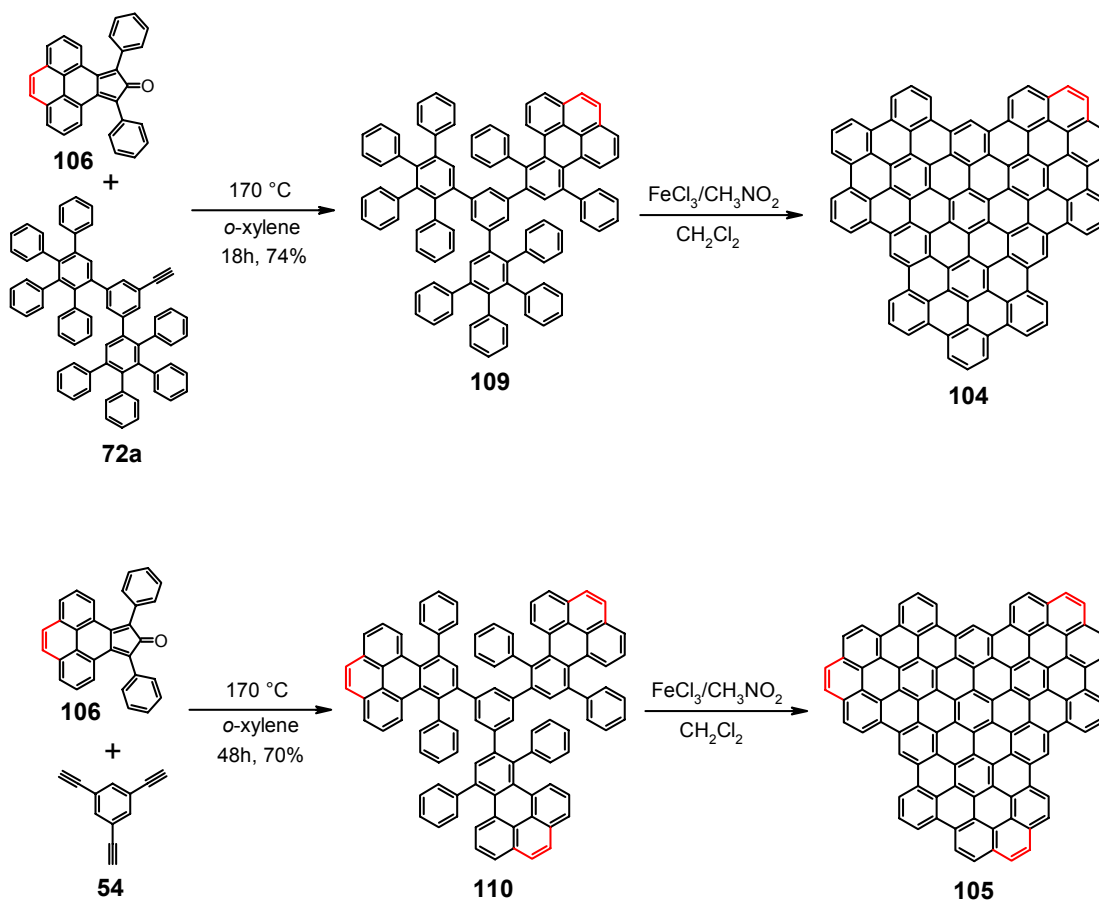


Figure 97. Synthetic routes to "zig-zag" superphenalenes **104** and **105**.

Again, the subsequent final cyclodehydrogenation step was the most crucial one of the whole synthesis. The MALDI-TOF mass spectrometry, using a solid-state sample preparation method with TCNQ as matrix, played a major role in the control of the reactions and the determination of the degree of cyclodehydrogenation.^[5,6] The planarization was first attempted using the system

of aluminium(III) chloride and copper(II) trifluoromethanesulfonate in carbon disulfide, as has been successfully employed for the synthesis of **103**. However, reaction of precursor **109** with three equivalents (and 48 hours reaction time) or six equivalents (and 24 hours) of aluminium(III) chloride per hydrogen to be removed, resulted in the formation of the desired, fully planarized disc **104**, and significant amounts of partially cyclized products. In the case of precursor **110**, use of three equivalents of aluminium(III) chloride (and 28 hours) also resulted in the formation of the desired product **105** and a significant amount of partially cyclized compounds. Increasing the amount of aluminium(III) chloride led to **105** and significant amounts of chlorinated side-products.

The attention was therefore redirected to the iron(III) chloride/nitromethane system in a dichloromethane solution of the precursor. For precursor **109**, reaction with smaller amounts of iron(III) chloride (three or four equivalents per hydrogen to be removed) results in the formation of $C_{98}H_{30}$ disc **104**, but partially cyclized products were also observed. It turns out that 5.5 equivalents of iron(III) chloride per hydrogen to be removed and 24 hours reaction resulted in the best results, leading to the formation of **104**, as shown in the MALDI-TOF mass spectrum in Figure 98. Use of larger amounts of oxidant (more than six equivalents) and the same reaction time led to complete planarization, but also a significant amount of chlorinated products was observed. Oxidative cyclodehydrogenation of precursor **110** required a shorter reaction time and smaller excess of iron(III) chloride. However, it should be pointed out that chlorination, as a side-reaction occurred easily and was difficult to completely eliminate. The optimum conditions for this molecule were three equivalents of iron(III) chloride and 10 hours reaction time, leading to the MALDI-TOF mass spectrum depicted in Figure 98. The isotopically resolved molecular ion peak of $C_{102}H_{30}$ PAH (**105**) is by far the predominant product, however small amounts of chlorinated, side-products are observed.

The PAHs **104** and **105** were precipitated as dark red-brown materials upon addition of methanol to the cyclodehydrogenation reaction solution, collected by filtration and washed with methanol until the solvent showed no more trace of yellow color from iron salts. After drying, the resulting powders

have a black color, since the color of the product is very dependent on the morphology, which is likely influenced by the sample treatment. Due to the very poor solubility of new graphite discs (**104** and **105**), NMR characterization failed. Elemental analysis of such kinds of insoluble graphite discs can not provide reliable information about the elemental composition because of the incomplete combustion during these measurements. Alternatively, as was pointed out above, isotope-resolved MALDI-TOF mass spectrometry using a solid-state sample preparation method, played a major role in the proof of identity of these large PAHs.

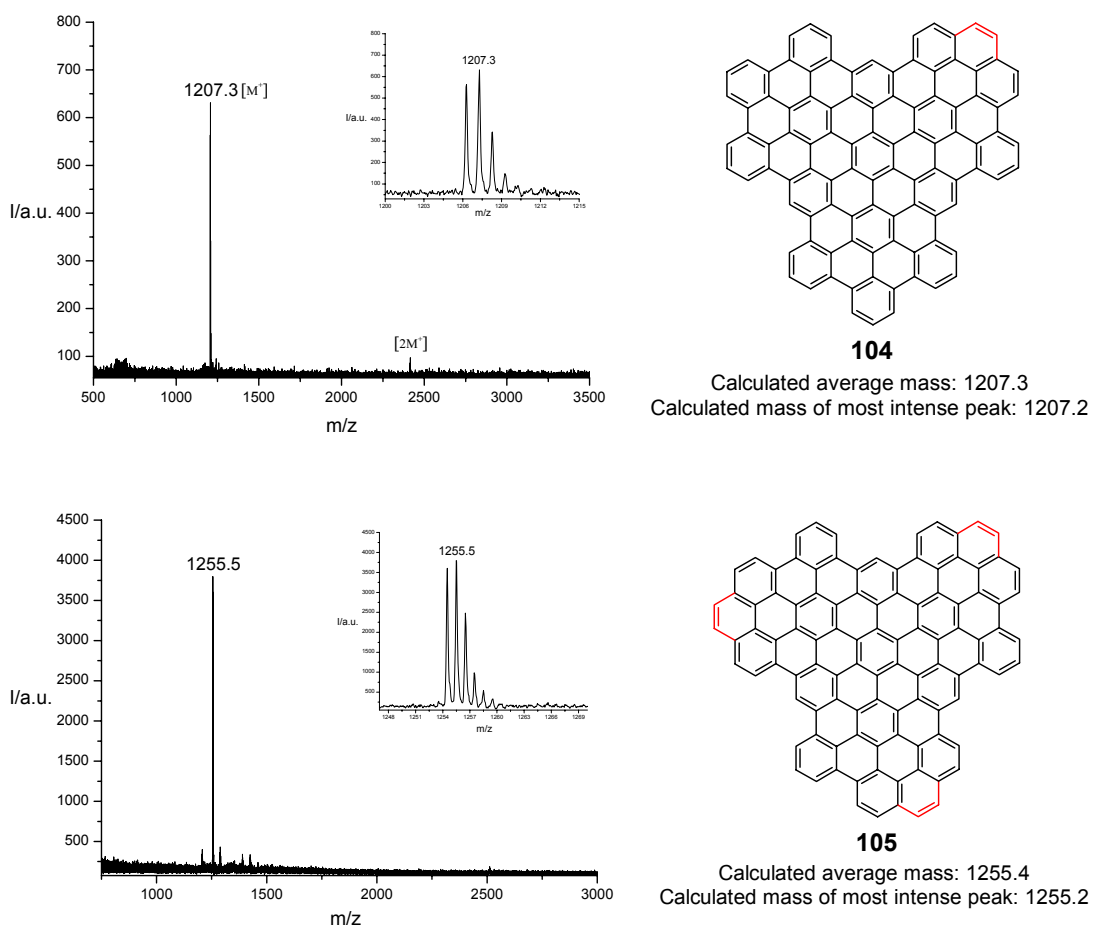


Figure 98. MALDI-TOF mass spectra of "zig-zag" superphenelenes **104** and **105**; inset shows isotopic distribution.

5.3 UV/Vis and fluorescence characterization

Ultralarge, unsubstituted PAHs show very poor solubility in all the usual solvents, which can be attributed to the extensive planarity and the consequent packing behavior of these large aromatics. Although a new "zig-zag" HBC (**103**) shows a very poor solubility, refluxing of a small amount of **103** in 1,2,4-trichlorobenzene (1 mg/1L) gave a solution of sufficient concentration to record its absorption and fluorescence spectra in solution. After the solution had cooled back down to room temperature, the measurements were conducted. The resulting spectra are shown in Figure 99.

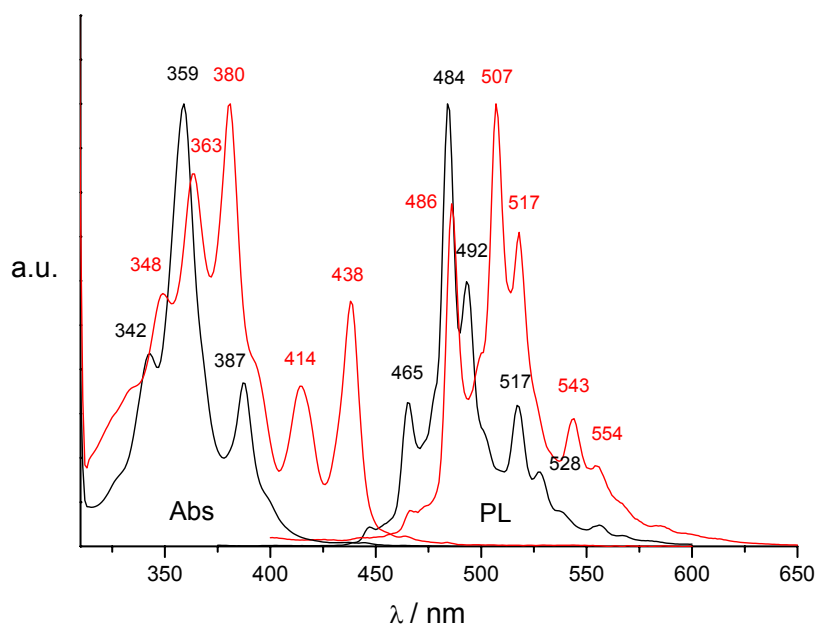


Figure 99. Normalized UV/Vis absorption and fluorescence spectra of HBC (**8**; black line) and "zig-zag" HBC (**103**; red line), recorded at room temperature in 1,2,4-trichlorobenzene solution.

A UV/Vis absorption spectrum of **103** recorded in 1,2,4-trichlorobenzene clearly shows three types (groups) of bands (α , p (or L_b , L_a ^[27]) and β (B_a , B_b ^[27])) which are typical for aromatic hydrocarbons (Figure 99).^[1] The absorption maximum of **103** ($\lambda_{\max} = 380\text{nm}$) shows a significant bathochromic shift with

respect to the corresponding band of **8** ($\lambda_{\text{max}} = 359 \text{ nm}$) ($0 \rightarrow 0$ band of the $S_0 \rightarrow \beta$ transition, assignments based upon calculations). Reducing the symmetry increases the intensity of $0 \rightarrow 0$ band of the α (or L_b) transition (486 nm) which is otherwise very weak (symmetry forbidden) for the D_{6h} symmetric unsubstituted HBC, as shown in the profile of the emission spectra. Interestingly, there is also a characteristic band at 438 nm that is not found in the all-benzenoid analogue. ZINDO-CIS quantum chemical calculations (performed by Prof. F. Negri, University of Bologna, Italy) were carried out to estimate excitation energies and oscillator strengths at the B3LYP/3-21G equilibrium structure of this molecule, and it was found that a net, remarkable transition dipole moment is associated with the $0 \rightarrow 0$ band of the $S_0 \rightarrow L_a$ (or $S_0 \rightarrow p$) transition. The wavefunction composition of this state provides an explanation: the (H \rightarrow L) excitation dominates the L_a state of "zig-zag" HBC, thus breaking the perfect cancellation of transition dipole moment which occurs in HBC, owing to the identical weights of the two (H \rightarrow L) and (H-1 \rightarrow L+1) excitations. It is clear that this is a result of strong electronic perturbation in these orbitals, both in shape and energy, induced by two additional π -centres.

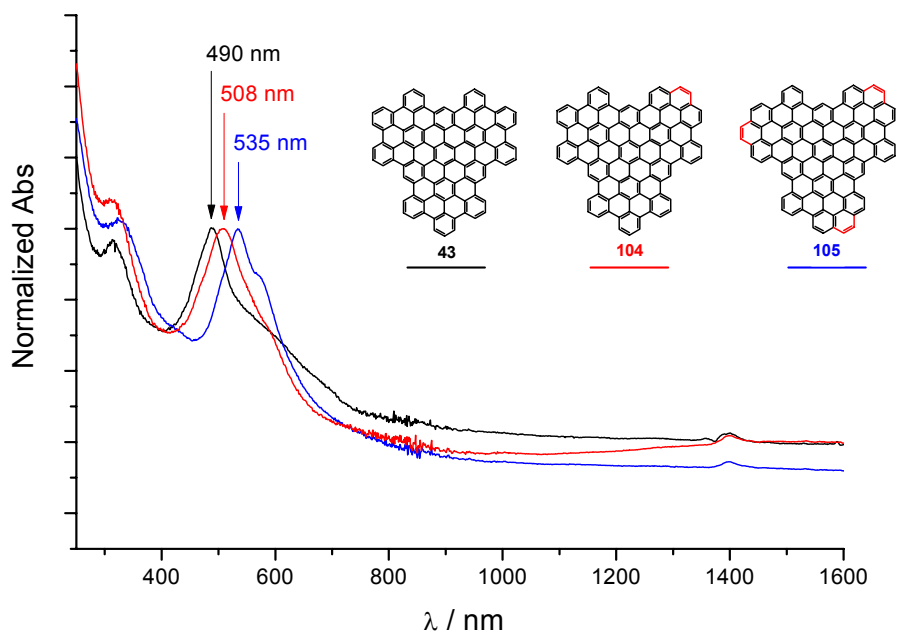


Figure 100. Solid-state UV/Vis spectra of **43** (black line), **104** (red line) and **105** (blue line).

In contrast to "zig-zag" HBC (**103**), "zig-zag" superphenalenes **104** and **105** were refluxed in 1,2,4-trichlorobenzene for 24 h, but UV/Vis spectra could not be measured from these solutions. Thus, the only possibility to study these properties for large unsubstituted PAHs **104** and **105** is the measurement in thin films (solid-state characterization). Thin films were prepared mechanically by simply smearing samples on a quartz substrate. The resulting UV/Vis spectra of thin films of **43**, **104** and **105** are shown in Figure 100. They show a broad, featureless profile, with low-energy tails extending to roughly 750 nm. As a consequence of the integration of additional "zig-zag" edges, the absorption maximum (β band) of **104** ($\lambda_{\text{max}} = 508$ nm) and **105** ($\lambda_{\text{max}} = 535$ nm) shows a significant bathochromic shift (18 and 45 nm, respectively) when compared to their parent superphenalene PAH (**43**) without a "zig-zag" edge ($\lambda_{\text{max}} = 490$ nm). In contrast to the smaller HBC core, the integration of "zig-zag" edges did not cause the appearance of new visible bands in UV/Vis spectra. The "zig-zag" superphenalene core, carrying solubilizing substituents could lead to new processible materials with a broader absorption range that more effectively captures solar radiation, thus providing greater photovoltaic performance.

5.4 Synthesis and characterization of soluble "zig-zag" superphenalene

One of the difficulties in dealing with larger PAHs is the fact that with increasing the size of the core, the solubility of these compounds decreases dramatically.^[5] Alkyl substitution is a prerequisite for the solubilization of large PAHs and it is also important for the formation of liquid crystalline phases.^[5,13] In order to acquire more spectroscopic information and gain more insight into the two- and three-dimensional self-assembly behavior of these new graphitic molecules, we have focused our attention on the synthesis and characterization of a soluble derivative of **104**. Presumably, the introduction of six *tert*-butyl groups is not enough to solubilize large PAH^[7] such as **104**, and we have

synthesized soluble "superphenalene" with an additional "zig-zag" edge **113**, by incorporating long dodecyl alkyl chains, as shown in Figure 101.

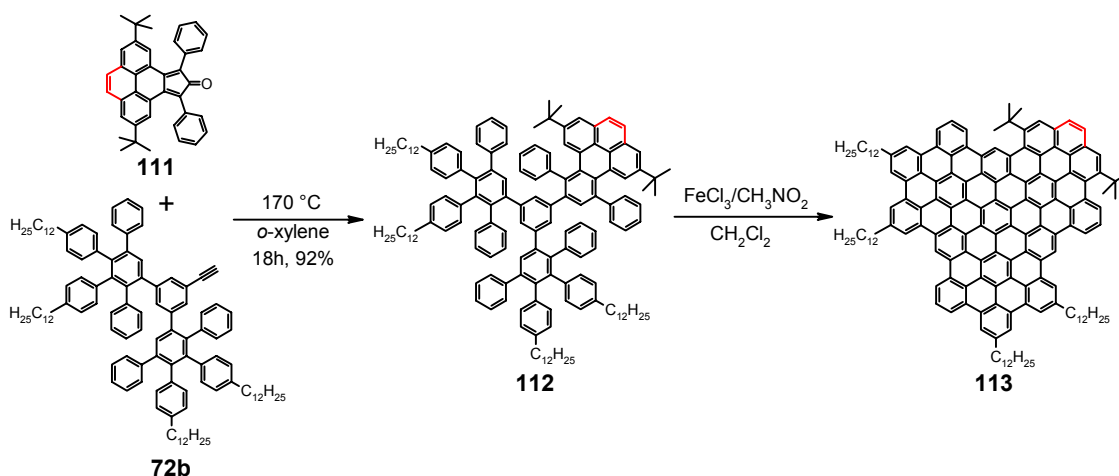


Figure 101. Synthesis of the soluble "zig-zag" superphenalene derivative **113**.

Following the construction principle described for **104**, the polyphenylene precursor **112**, bearing four dodecyl alkyl chains, was synthesized by a Diels-Alder reaction between **72b** (building block with one terminal triple bond, previously described in Chapter 2) and excess (1.3 equiv) of 2,7-di-*tert*-butyl-9,11-diphenyl-cyclopenta[*e*]pyren-10-one (**111**; prepared by Z. Wang) in refluxing *o*-xylene. The reaction resulted in the formation of **112** in nearly quantitative yield, probably because *tert*-butyl groups kinetically stabilize the cyclopentadienone. The final, key step for the synthesis of **113** is the oxidative cyclodehydrogenation of **112**. Using anhydrous iron(III) chloride as oxidant and Lewis acid, we obtained **113**, as waxy red-brown solid in 71 % yield, after workup (filtration through a short pad of silica gel with toluene). Compound **113** was identified by MALDI-TOF mass spectrometry, proving the success of the cyclodehydrogenation reaction (Figure 102).

Compound **113** is soluble in common organic solvents, such as dichloromethane, THF, and toluene. However, in the ¹H NMR spectra of compound **113**, regardless of the solvent and temperature used, resonances arising from the mobile alkyl side chains could be resolved, but not those of the protons on the aromatic core, because of their low mobility.

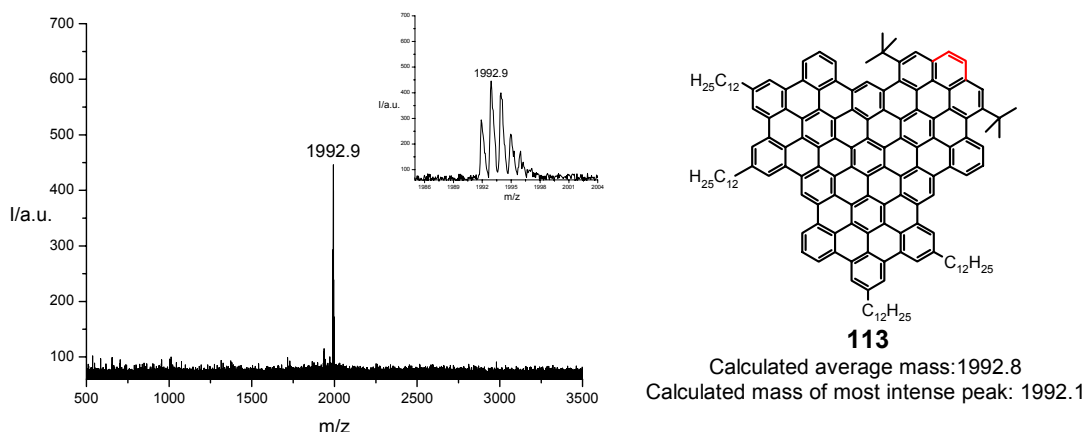


Figure 102. MALDI-TOF mass spectra of **113**; inset shows isotopic distribution.

The UV/Vis absorption spectrum of **113** in toluene (Figure 103) shows a broad, featureless profile ($\lambda_{\text{max}} = 474$ nm) with a low-energy tail extending to 700 nm. The maximum absorption is shifted 12 nm, relative to C₉₆-C₁₂ (**53a**, $\lambda_{\text{max}} = 462$ nm), as would be expected with the integration of two additional π -centers. The UV/Vis measurements of **113** in toluene or THF show no concentration dependence over the range $10^{-4} - 10^{-7}$ M (Figure 103). Likewise, a 1.4×10^{-5} M toluene solution exhibits no temperature dependence over the range 20 – 85 °C (where 85 °C was the upper experimental limit) as shown in Figure 103.

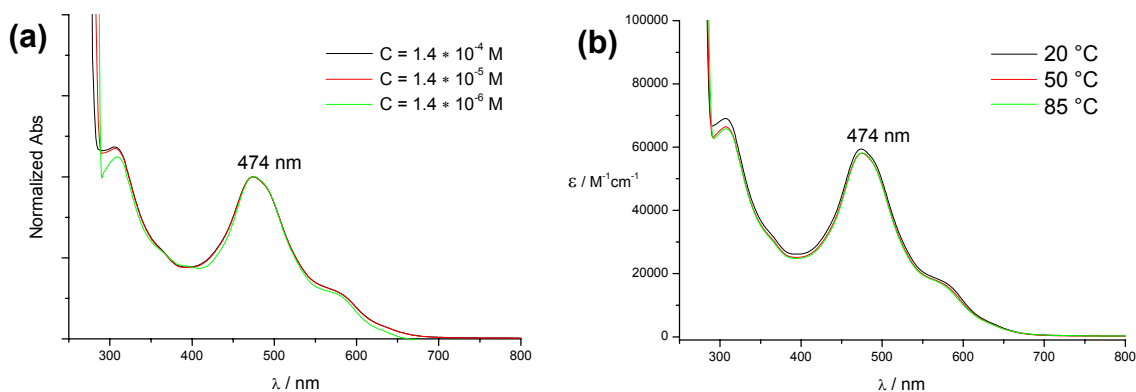


Figure 103. (a) Concentration dependent UV/Vis absorption spectra of **113** in toluene (normalized at 474 nm), and (b) temperature dependent UV/Vis absorption spectra in 1.4×10^{-5} M toluene solution.

Solid samples of **113** were characterized by differential scanning calorimetry (DSC), polarized optical microscopy (POM) and wide-angle X-ray scattering (WAXS). Compound **113** showed no recognizable transitions in the DSC analysis in the measured range from $-150\text{ }^{\circ}\text{C}$ to $250\text{ }^{\circ}\text{C}$. The liquid-crystalline character of **113** was confirmed by the observation of birefringent, shearable thin films between crossed-polars, but no sharp changes with temperature were seen. Temperature dependent X-ray measurements were performed on an oriented sample. Orientation was obtained by extrusion of the material through a 0.7 mm orifice.^[28] The measured 2D-WAXS diffraction patterns are the same from a temperature of $30\text{ }^{\circ}\text{C}$ to $150\text{ }^{\circ}\text{C}$, and back to $30\text{ }^{\circ}\text{C}$. Therefore the diffractogram recorded at $30\text{ }^{\circ}\text{C}$ is shown in Figure 104 as a representative example.

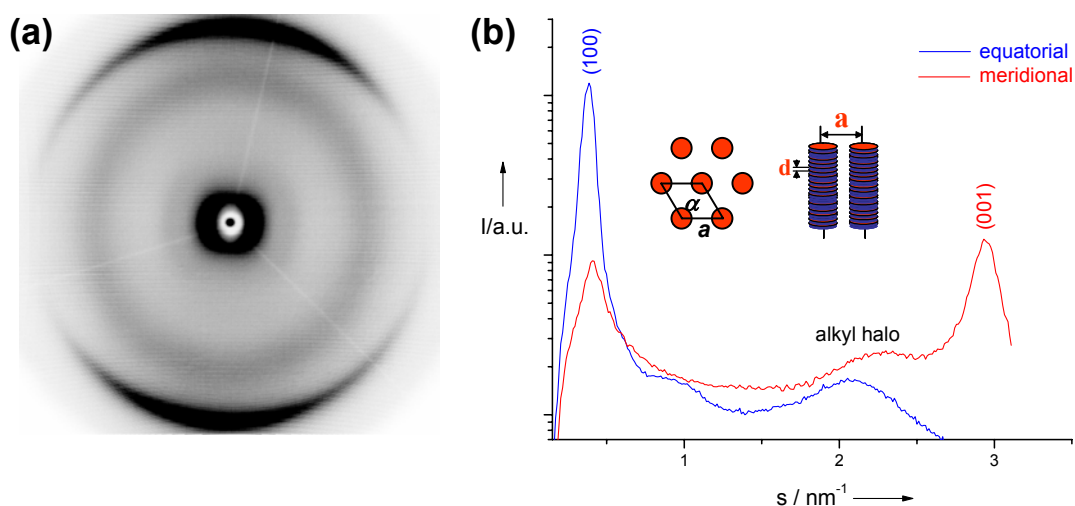


Figure 104. (a) 2D-WAXS diffractogram of an extruded fiber of **113** and (b) its intensity distributions along the equator and meridian.

On the equator, the first-order peak is recognizable, however no well-resolved higher order reflections are visible. The reflexes in the equatorial direction are not resolved even at $150\text{ }^{\circ}\text{C}$. At small angles along the equator, the presence of only a single peak makes the assignment of a unit cell difficult. It can be clearly seen that the 100 peak is asymmetric, with a shoulder on the larger diffraction angle side, and upon closer inspection, as the most probably, hexagonal unit cell can

be assumed with a unit cell parameter of $a = 3.03$ nm. The evenly distributed circular halo at $d = 0.5$ nm is caused by the amorphous alkyl chains. The meridional reflexes ($d = 0.34$ nm, labeled 001) are relatively intense, suggesting long-range intracolumnar order. Tilting of the cores, often observed in columnar discotics and planar π -systems in general, is completely suppressed at room temperature in the case of **113**.^[29,30] These results are also in contrast to the results obtained for asymmetric C96 derivative **75** (substituted with four dodecyl alkyl chains on periphery), where tilting of the discs within the columns was observed. This suggests that additional "zig-zag" edge with two additional *tert*-butyl groups in **113** have a big influence on the packing behavior of the molecule. In the absence of tilting, favorable orbital interactions might be achieved instead by lateral disc offset (graphite-like stacking).

Further research activities of Z. Wang in the group of Prof. Müllen have resulted in the successful synthesis of soluble "zig-zag" HBC derivative (**114**, Figure 105), achieved by introduction of six *tert*-butyl groups. The good solubility of **114** allows further derivatization to probe the chemical reactivity unique to the "zig-zag" motif. The selective oxidation of the "zig-zag" edge to its corresponding diketo structure (**115**) was achieved by using ruthenium dioxide/sodium periodate in aqueous *N,N*-dimethylformamide, which provides a potentially versatile building block for new giant graphene molecules.

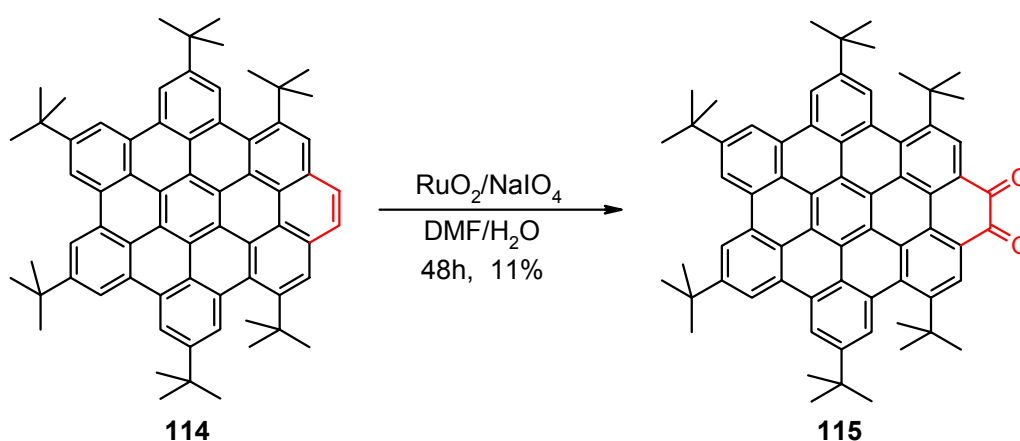


Figure 105. The selective oxidation of the "zig-zag" edge of **114**, according to Z. Wang.

In order to probe the reactivity of the "zig-zag" edge of superphenalene disc, we have tried to selectively oxidize the "zig-zag" edge of **113** under the same conditions as used for **114** (with ruthenium dioxide / sodium periodate). However, according to the MALDI-TOF mass spectrometry measurements, the desired product with a corresponding diketo structure could not be obtained.

To theoretically estimate the reactivity of these "zig-zag" discs towards electrophilic reaction (oxidation), we have performed simple calculations based on semi-empirical methods (RHF/AM1, Austin Model) without including extended configuration interaction (CIS).^[31] Although such an approach does not account for the electron-electron correlation energies, it still provides a quick tool to compare the location of the frontier orbitals in these different cores. Figure 106 shows both the frontier orbitals (HOMO-LUMO) and the electronic potential surface derived for compounds **8**, **103**, **43**, and **104**. Clearly, increasing the π -conjugation and in absence of substituents, we observed the expected decrease in the HOMO relative energies in going from HBC (**8**) to "zig-zag" C96 (**104**). A comparison between the HOMO distribution of HBC (**8**) and "zig-zag" HBC (**103**) shows that there is a considerable delocalization of the HOMO onto the double "zig-zag" bond of **103** (Figure 106a,b). The size of the lobes on the additional carbon atoms (see orbitals, Figure 106b) indicates an increased amount of π -charge, and hence a greater probability of oxidation reaction at these sites (marked with black arrow in the figure) in comparison to the other carbon atoms with the same sign. In agreement with this, the electronic distribution of the potential energy surface shows that while it is highly symmetric in the case of HBC (**8**), this is not so for "zig-zag" HBC (**103**). Although such a comparison qualitatively indicates the most probable position at which the oxidation reaction can occur, it does not give any indication of the kinetics of the process. Although a small amount of asymmetry is retained in the case of the larger "zig-zag" superphenalene core (see black arrow on Figure 106d), such a clear difference in the localization of the HOMO orbital in the "zig-zag" periphery is not observed. Therefore, this would be in agreement with the lower tendency for the larger

system to undergo facile oxidation with a mild oxidant, such as ruthenium dioxide/sodium periodate.

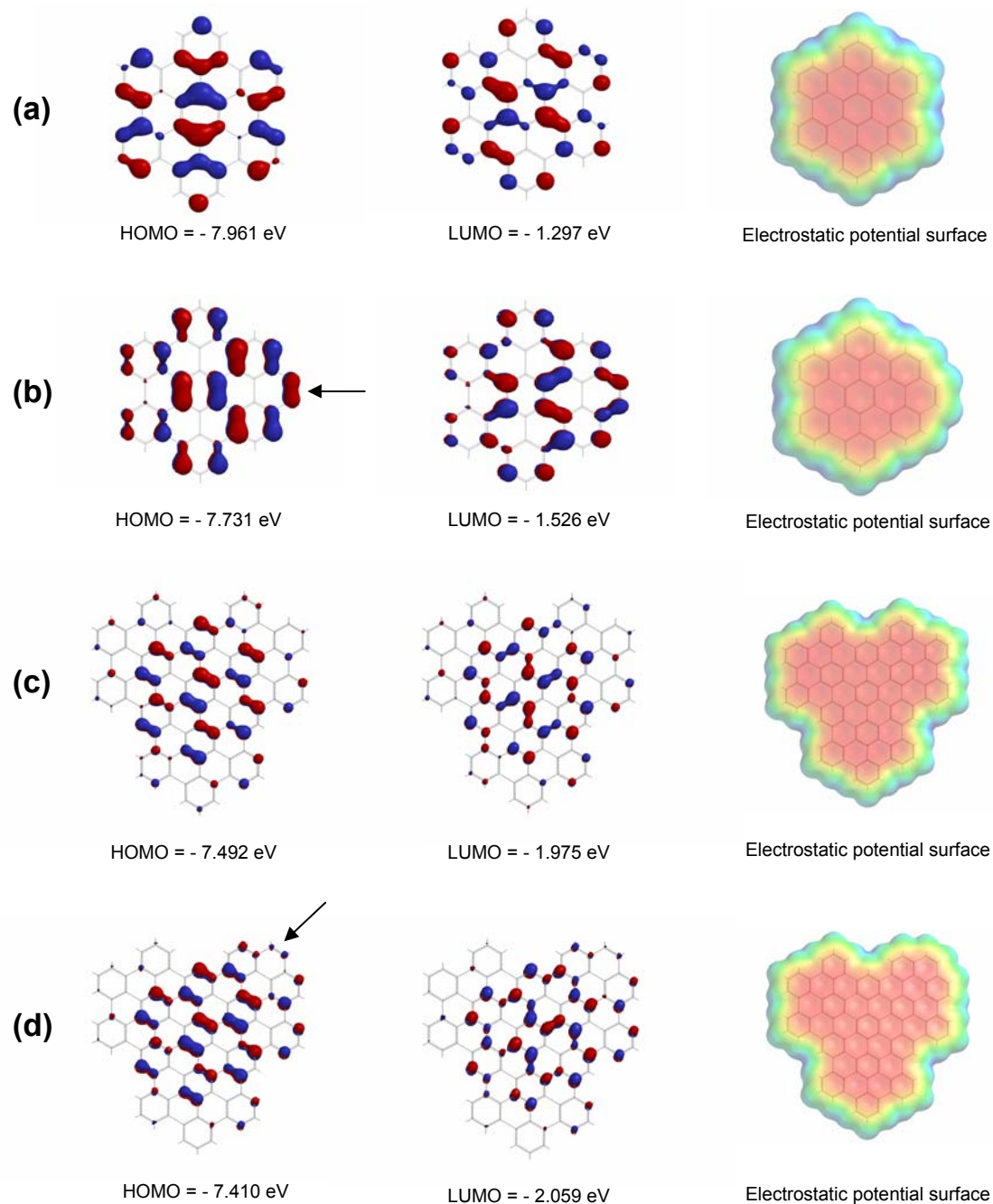


Figure 106. Frontier orbitals and electrostatic potential surfaces of **8**, **103**, **43**, and **104**, calculated semi-empirically (AM1).

In conclusion, a new synthetic protocol providing entry to novel polycyclic aromatics with partial "zig-zag" periphery and possessing dramatically different electronic properties has been developed. The task of designing the suitable precursors (**108**, **109** and **110**) is simplified by the introduction of "zig-zag" edge into the cyclopentadienone (**106**). Cyclododehydrogenation of these precursors, using aluminium(III) chloride or iron(III) chloride led to the new graphitic molecules (**103**, **104**, **105**), with partial "zig-zag" periphery. Integration of "zig-zag" edges has a strong influence on the electronic properties of new molecules, as was manifested in the UV/Vis and fluorescence spectra. This is the result of a strong electronic perturbation induced by additional π -centres, which increase the size and lower the symmetry of the molecules. In addition to serving as interesting theoretical models for graphite, they also provide reactive sites for further functionalization, e.g., preparation of their corresponding K-region oxide. It was shown that the selective oxidation of the "zig-zag" edge of **114** to its corresponding diketo structure (**115**) could be achieved by using ruthenium dioxide/sodium periodate, while in the case of the larger disc **113**, the corresponding diketo structure could not be obtained under the same conditions. This experimental observation has been substantiated through theoretical studies, which show considerable delocalization of the HOMO onto the "zig-zag" bond of smaller disc **103**, while no such clear delocalization onto the "zig-zag" periphery of larger disc **104** was observed. As was seen for **113**, the attachment of long alkyl chains onto PAHs cores such as **103** and **105**, should confer liquid crystalline properties upon them, and further exploration of this topic is currently underway within the group of Prof. Müllen.

5.5 Literature

- [1] E. Clar, *Polycyclic Hydrocarbons*, Academic Press, New York, **1964**.
- [2] J. R. Dias, *Handbook of Polycyclic Hydrocarbons, Part A: Benzenoid Hydrocarbons*, Elsevier, Amsterdam, **1987**.

- [3] M. Zander, *Polycyclische Aromaten: Kohlenwasserstoffe und Fullerene*, B. G. Teubner, Stuttgart, **1995**.
- [4] R. G. Harvey, *Polycyclic Aromatic Hydrocarbons*, Wiley-VCH, New York, **1997**.
- [5] M. D. Watson, A. Fechtenkötter, K. Müllen, *Chem. Rev.* **2001**, *101*, 1267-1300.
- [6] M. Müller, C. Kübel, K. Müllen, *Chem. Eur. J.* **1998**, *4*, 2099-2109.
- [7] V. S. Iyer, M. Wehmeier, J. D. Brand, M. A. Keegstra, K. Müllen, *Angew. Chem. Int. Ed. Engl.* **1997**, *36*, 1604-1607.
- [8] F. Dötz, J. D. Brand, S. Ito, L. Gherghel, K. Müllen, *J. Am. Chem. Soc.* **2000**, *122*, 7707-7717.
- [9] V. S. Iyer, K. Yoshimura, V. Enkelmann, R. Epsch, J. P. Rabe, K. Müllen, *Angew. Chem. Int. Ed. Engl.* **1998**, *37*, 2696-2699.
- [10] C. D. Simpson, J. D. Brand, A. J. Beresheim, L. Przybilla, H. J. Räder, K. Müllen, *Chem. Eur. J.* **2002**, *8*, 1424-1429.
- [11] S. Ito, M. Wehmeier, J. D. Brand, C. Kübel, R. Epsch, J. P. Rabe, K. Müllen, *Chem. Eur. J.* **2000**, *6*, 4327-4342.
- [12] P. Samori, N. Severin, C. D. Simpson, K. Müllen, J. P. Rabe, *J. Am. Chem. Soc.* **2002**, *124*, 9454-9457.
- [13] C. D. Simpson, J. Wu, M. D. Watson, K. Müllen, *J. Mater. Chem.* **2004**, *14*, 494-504.
- [14] C. Simpson, *Dissertation*, Johannes-Gutenberg Universität, Mainz, **2003**.
- [15] S. E. Stein, R. L. Brown, *J. Am. Chem. Soc.* **1987**, *109*, 3721-3729.
- [16] A. J. Berresheim, M. Müller, K. Müllen, *Chem. Rev.* **1999**, *99*, 1747-1785.
- [17] F. Morgenroth, K. Müllen, *Tetrahedron* **1997**, *53*, 15349-15366.
- [18] U. M. Wiesler, T. Weil, K. Müllen, *Top. Curr. Chem.* **2001**, *212*, 1-40.
- [19] R. A. Pascal, Jr., N. Hayashi, D. M. Ho, *Tetrahedron*, **2001**, *57*, 3549-3555.
- [20] N. Smyth, D. van Engen, R. A. Pascal, Jr. *J. Org. Chem.* **1990**, *55*, 1937-1940.
- [21] L. Tong, D. M. Ho, N. J. Vogelaar, C. E. Schutt, R. A. Pascal, Jr. *J. Am. Chem. Soc.* **1997**, *119*, 7291-7302.
- [22] Z. Wang, V. Enkelmann, F. Negri, K. Müllen, *Angew. Chem. Int. Ed. Engl.* **2004**, *43*, 1972-1975.
- [23] R. A. Pascal, Jr., W. D. McMillan, D. Van Engen, R. G. Eason, *J. Am. Chem. Soc.* **1987**, *109*, 4660-4665.
- [24] H. M. Duong, M. Bendikov, D. Steiger, Q. Zhang, G. Sonmez, J. Yamada, F. Wudl, *Org. Lett.* **2003**, *5*, 4433-4436.
- [25] L. Przybilla, J. D. Brand, K. Yoshimura, H. J. Räder, K. Müllen, *Anal. Chem.* **2000**, *72*, 4591-4597.
- [26] K. Yoshimura, L. Przybilla, S. Ito, J. D. Brand, M. Wehmeir, H. J. Räder, K. Müllen, *Macromol. Chem. Phys.* **2001**, *202*, 215-222.
- [27] J. R. Platt, *J. Chem. Phys.* **1949**, *17*, 484-496.

- [28] I. Fischbach, T. Pakula, P. Minkin, A. Fechtenkötter, K. Müllen, H. W. Spiess, *J. Phys. Chem. B* **2002**, *106*, 6408-6418.
- [29] G. R. Desiraju, A. Gavezotti, *Acta Crystallogr. Sect. B* **1989**, *45*, 473-482.
- [30] C. A. Hunter, K. R. Lawson, J. Perkins, C. J. Urch, *J. Chem. Soc. Perkin. Trans. 2* **2001**, 651-669.
- [31] PC Spartan Pro, Ver.1.0, Wavefunction Inc., Irvine, CA, **2000**.

CHAPTER 6

Summary

The results of the present work "New discotic liquid crystals based on large polycyclic aromatic hydrocarbons as materials for molecular electronics" can be summarized as follows:

I. A series of new columnar discotic liquid crystalline materials based on the superphenalene (C₉₆) core was synthesized (Figure 107). Hence, the scope of our straightforward synthetic approach to discotic liquid crystals based on large all-benzenoid PAHs has been expanded.

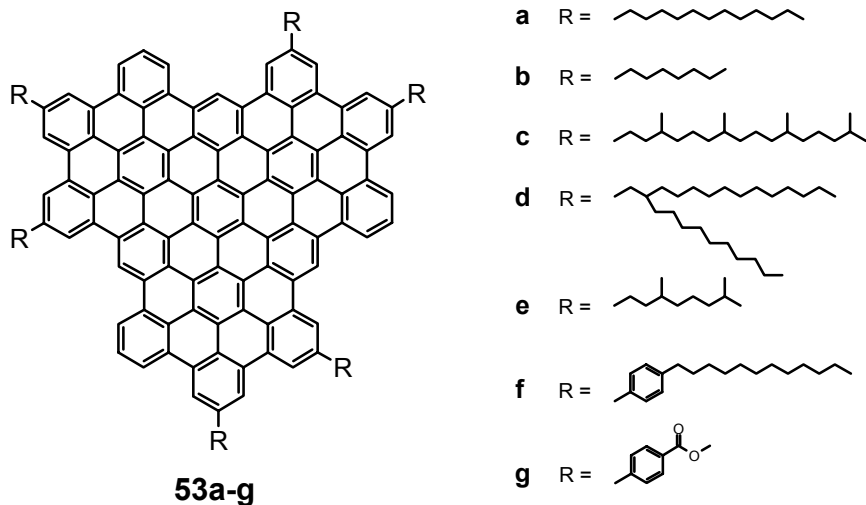


Figure 107. Molecular structures of superphenalene (C₉₆) derivatives **53a-g**.

The hexasubstituted superphenalene discs **53a-g** were prepared by oxidative cyclodehydrogenation of suitable oligophenylene precursors with iron(III) chloride. These precursors were built-up via Diels-Alder reaction of the

1,3,5-triethynylbenzene core with corresponding cyclopentadienones. It should be pointed out that the only proof of structure and purity of **53a-g** available is MALDI-TOF mass spectrometry. Superphenalene derivatives **53a-d** are soft, waxy materials, readily dissolve in common organic solvents at room temperature (in contrast to **53e,f** which show poor solubility). Their remarkable solubility can be explained by inefficient side-chain packing around self-assembled columns, which are otherwise well developed. Good solubility allowed purification by column chromatography, of high importance for applications in devices where purity of materials plays a crucial role. The maximum absorption ($\lambda_{\text{max}} \approx 460$ nm) of the new compounds is shifted, relative to HBC ($\lambda_{\text{max}} \approx 360$ nm), to a position within the visible spectrum that could lead to more effective photovoltaic performance. Characterization of solid samples of **53a-d** by DSC, polarized optical microscopy and wide-angle X-ray scattering (WAXS) showed liquid-crystalline character of these materials.

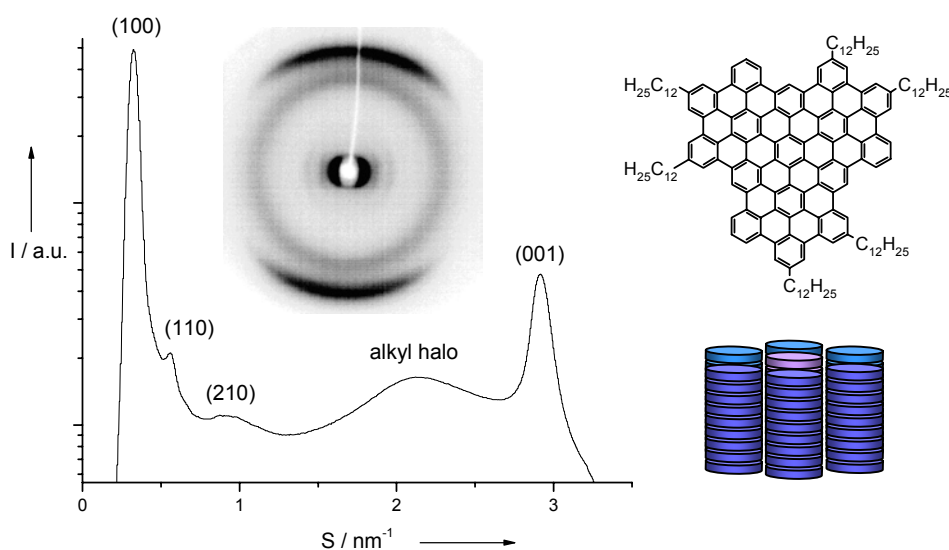


Figure 108. 2D X-ray diffraction pattern of an extruded fiber of **53a** and its integrated intensity distribution.

Temperature-dependent 2D-WAXS measurements reveal hexagonally packed columnar mesophases with disc planes perpendicular to the columnar axes (with the exception of **53d** where is tilting of the discs observed, attributed to the large

steric demand of long dove-tail substituents). There was no abrupt change in the diffraction patterns with temperature. The meridional reflexes are relatively intense, suggesting long-range intracolumnar order (Figure 108).

The one-dimensional, intracolumnar charge carrier mobilities of superphenalene derivatives **53a-c** were determined using the pulse-radiolysis time-resolved microwave conductivity technique (PR-TRMC). The mobility values for these compounds lie within the range ca. 0.1 to 0.3 $\text{cm}^2\text{V}^{-1}\text{s}^{-1}$ and they are approximately an order of magnitude larger than the maximum value of 0.025 $\text{cm}^2\text{V}^{-1}\text{s}^{-1}$ previously found for discotic triphenylene derivatives, and similar to values found for HBC derivatives in the liquid crystalline phase. Moreover, the mobilities are essentially independent of temperature (over the range measured), of major importance with respect to applications in organic electronic devices.

Good solubility and the fact that these new superphenalene derivatives were found to be liquid crystalline at room temperature ensured the formation of highly ordered films necessary for the implementation in organic molecular devices. We have shown that large-area, uniaxially aligned thin films of C96-C₁₂ (**53a**) could be prepared in one processing step on untreated glass by the zone-casting technique (Figure 109).

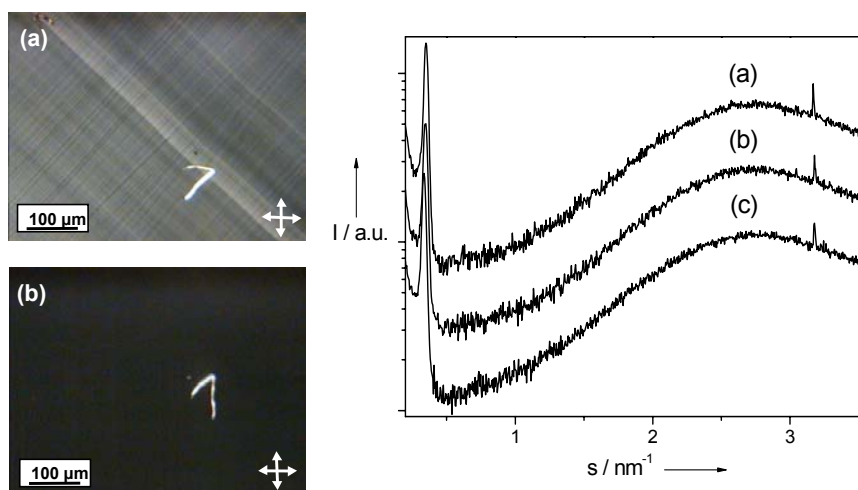


Figure 109. POM image of zone-cast C96-C₁₂ with (a) 45° and (b) 0° of the deposition direction towards the analyzer/polarizer axis, and temperature dependent theta-theta X-ray diffraction zone-cast C96-C₁₂ at 30 °C (a), 150 °C (b) and cooled back to 30 °C (c).

The self-assembly of C96-C₁₂ from solution onto a mica surface and a heterogeneous, mica-gold surface, using different solvents and deposition techniques such as immersion, drop-casting and spin-coating, was investigated. Varying a number of parameters including the type of deposition method, the choice of the solvent, the concentration, as well as the temperature of the solution and of the substrate, various types of supramolecular arrangements have been obtained. The work function (Φ) values of different C96-C₁₂ architectures have than been measured by employing Kelvin Probe Force Microscopy (KPFM). It was found that different morphological arrangements of C96-C₁₂ on the surface exhibit significant differences (as large as 0.4 eV) in work function ($\Phi(\text{layer}) = 3.88$ eV; $\Phi(\text{fibers}) = 3.53$ eV; $\Phi(\text{rods}) = 3.47$ eV); i.e. the measured work function depends strongly on the surface considered and it is not a bulk parameter. The values obtained with KPFM are thus not an intrinsic characteristic of C96-C₁₂ but very likely depend on the local molecular order on the surface, which is correlated with the molecular packing density and with the presence of defects of the self-assembled arrangement. On the other hand, the measurement of the effective work function of the material deposited on a surface in nanostructured patterns, rather than the work function of the same material in the bulk, is more important for organic electronics applications.

The symmetry of superphenalene could be reduced by unsymmetric substitution of the core with two and four alkyl chains. Desymmetrization has no effect on the thermal properties of the resulting compounds, but the columnar packing (tilting of the discs) and electronic properties (red shift in UV/Vis spectrum) are affected, when compared with those of the analogous symmetrical compounds.

II. HBC derivatives, such as **86a-b**, substituted at the periphery by six branched alkyl ether chains were synthesized (Figure 110). It was shown that effective lowering of isotropisation temperature could be achieved by introduction of bulky and space filling side chains (such as in **86a**, $T_i = 22$ °C), which induce strong steric interactions at the core periphery and dominate the stacking ability of the

discs. Additionally, the introduction of ether groups within the side chains enhances the affinity of the discotic molecules towards polar surfaces, resulting in homeotropic self-assembly when the compounds are processed from the isotropic state between two surfaces (Figure 110). These results are important for the design of photovoltaic cells based on HBC derivatives.

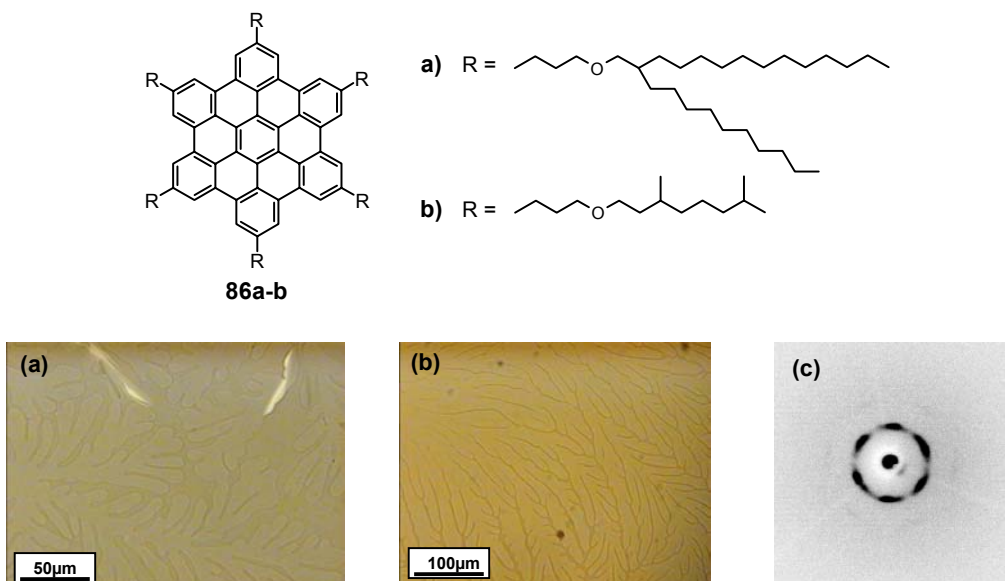


Figure 110. Molecular structures of alkyl ether substituted HBCs **86a-b**; **(a)**, **(b)** optical microscopy images of **86a** and **86b** respectively, homeotropically aligned during controlled crystallization between two glass slides; **(c)** 2D-WAXS pattern of **86b** at room temperature crystallized between two thin aluminium foils.

III. A new, important building block, hexa(4-iodophenyl)-C96 (**97**), carrying six reactive sites was prepared by a rational approach and despite its virtual insolubility, could be easily and quantitatively functionalized by a subsequent palladium-catalyzed Hagihara-Sonogashira coupling reaction. Generally, this concept allows functionalization of the core as a final step, which greatly broadens the scope of functionalities that may be introduced around the discs, thus paving the way to new materials based on superphenalene. The principle was demonstrated through the preparation of dendronized superphenalenes **91**

and **92** with the bulky dendritic substituents around the core, resulting in the suppression of π - π stacking of the cores to some extent, as a result of enhanced steric hindrance (Figure 111).

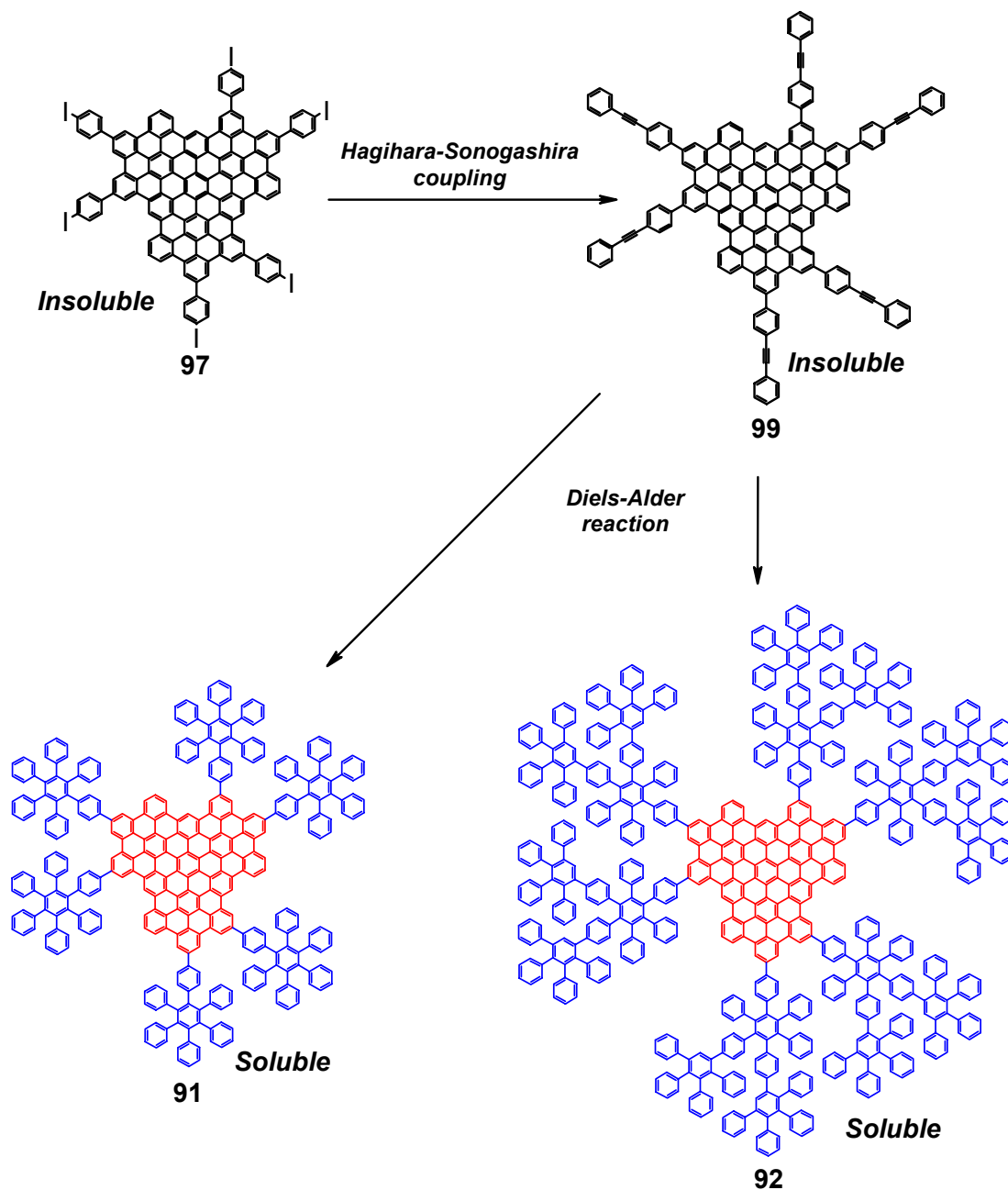


Figure 111. Synthesis of dendronized superphenalenes **91** and **92** via the insoluble hexa(4-iodophenyl)-C₉₆ building block (**97**).

IV. A new family of graphitic molecules with partial "zig-zag" periphery has been established (Figure 112). A key question in relation to change in edge-structure was the introduction of "zig-zag" periphery into polyphenylene precursors. It was found that 1,3-diphenylcyclopenta[*e*]pyren-2-one is a suitable candidate for the introduction of a "zig-zag" fragment, and the corresponding polyphenylene precursors could be efficiently prepared and planarized using aluminium(III) chloride or iron(III) chloride, to the desired molecules **103**, **104**, and **105**.

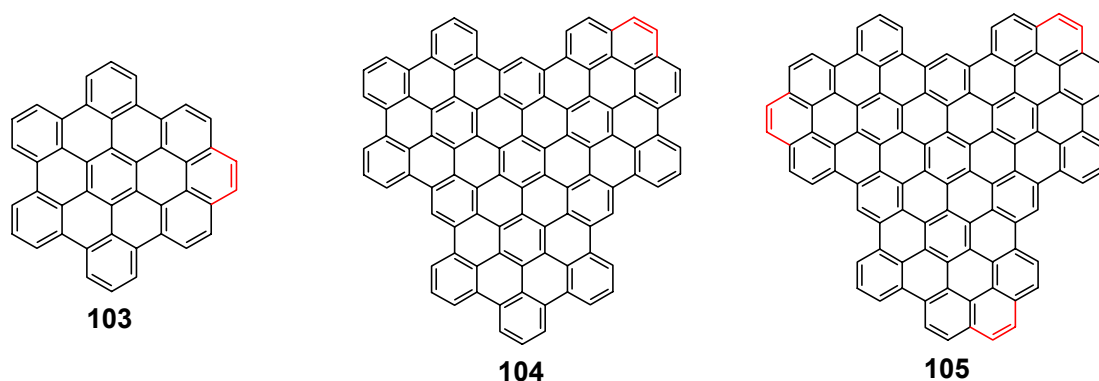


Figure 112. New graphitic molecules with partial "zig-zag" periphery.

The integration of "zig-zag" edges showed a strong influence on the electronic properties of the new molecules, leading to a significant bathochromic shift with respect to the parent PAHs (HBC and superphenalene). Attaching long alkyl chains to the PAH core **104** led to new liquid crystalline materials. In addition to serving as interesting theoretical models for graphite, these new graphitic molecules also provide reactive sites for further functionalization (e.g. preparation of their corresponding K-region oxide), a current avenue of study in the group of Prof. Müllen.

CHAPTER 7

Experimental Section

7.1 General methods

NMR spectroscopy:

^1H NMR and ^{13}C NMR spectra were recorded in CD_2Cl_2 , $\text{C}_2\text{D}_2\text{Cl}_4$, THF- d_8 , CDCl_3 or o -DCB- d_4 on a Bruker DPX 250, Bruker AMX 300, Bruker DRX 500 or Bruker DRX 700 spectrometer with use of the solvent proton or carbon signal as an internal standard.

Mass spectrometry:

FD mass spectra were obtained on a VG Instruments ZAB 2-SE-FPD spectrometer. MALDI-TOF mass spectra were measured on a Bruker Reflex II-TOF spectrometer using a 337 nm nitrogen laser and 7,7,8,8-tetracyanoquinodimethane (TCNQ) as matrix. The mass instrument is not dedicated to isotopic measurements, and the deviations of relative intensities of peaks, from those calculated, can be more than 10%.

UV/Vis spectroscopy:

UV/Vis spectra were recorded at room temperature on a Perkin-Elmer Lambda 9 spectrophotometer.

Fluorescence spectroscopy:

Fluorescence spectra were recorded on a SPEX-Fluorolog II (212) spectrometer.

Melting points:

Melting points were determined using a Büchi B-545 apparatus in open capillaries and are uncorrected.

Elemental analysis:

Elemental analyses^[*] were carried out on a Foss Heraeus Vario EL as a service of the Institute for Organic Chemistry, Johannes-Gutenberg-University of Mainz.

[*] Because of the high carbon content of large, non-alkylated PAHs, combustion may be incomplete (soot formation), resulting in values lower than expected for the carbon content.

Differential scanning calorimetry (DSC) and thermogravimetric analysis (TGA):

DSC was measured on a Mettler DSC 30 with heating and cooling rates of 10 °C/min in the range from -150 °C to 250 °C. For TGA a Mettler TG 50 thermogravimetric analyzer was used.

Polarization microscopy:

A Zeiss Axiophot with a nitrogen flushed Linkam THM 600 hot stage was used to perform polarization microscopy.

X-ray:

Powder X-ray diffraction experiments were performed using a Siemens D 500 Kristalloflex diffractometer with a graphite-monochromatized CuK_α X-ray beam, emitted from a rotating Rigaku RV-300 anode. 2D WAXS measurements of oriented filaments were conducted using a rotating anode (Rigaku 18 kW) X-ray beam (CuK_α, pinhole collimation, double graphite monochromator) and CCD camera. The patterns were recorded with vertical orientation of the filament axis and with the beam perpendicular to the filament.

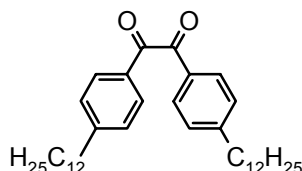
7.2 Materials

Chemicals and solvents:

The chemicals and solvents were obtained from the companies ABCR, Lancaster, Merck, Riedel-de Haen, Sigma-Aldrich, Fluka and Strem and used as obtained, unless otherwise mentioned. THF was freshly distilled over potassium prior to use, in reactions.

Chromatography:

Preparative column chromatography was performed on silica gel from Merck with a particle size of 0.063-0.200 mm (Geduran Si 60). For analytical thin layer chromatography (TLC) silica gel coated substrates 60 F₂₅₄ from Merck were used. Compounds were detected by fluorescence quenching at 254 nm and self-fluorescence at 366 nm.

8.3 Syntheses**4,4'-Didodecylbenzil (61a)**

A synthesis of this compound has been previously reported in the PhD thesis of M. Wehmeier, a new improved procedure is described here.

In a dry 500 mL two-necked round bottom flask, 167.4 mL of a 0.5 M THF solution of 9-borabicyclo[3.3.1]nonane (9-BBN) was added slowly to 12.8 g (76.04 mmol) of 1-dodecene under an argon atmosphere, and the resulting mixture was stirred overnight at room temperature. To this solution, 20.0 mL of 3 M aqueous NaOH solution was added via syringe and then, after 15 min, 7.0 g (19.0 mmol) of 4,4'-dibromobenzil and 0.78 g (0.96 mmol) of [PdCl₂(dppf)]·CH₂Cl₂, respectively. The reaction mixture was stirred under argon at room temperature for further 5 hours. The product was extracted with dichloromethane, and the organic phase washed with water three times and dried over magnesium sulfate. After evaporating the solvent, the residue was purified by column chromatography (silica gel, petroleum ether/dichloromethane 7:3) to afford 7.5 g **61a** (72% yield) as a pale yellow oil, which solidified upon standing.

¹H NMR (500 MHz, C₂D₂Cl₄): δ = 7.80 (d, ³J(H,H) = 8.2 Hz, 4H, Ar-H), 7.25 (d, ³J(H,H) = 7.9 Hz, 4H, Ar-H), 2.60 (t, ³J(H,H) = 7.6 Hz, 4H, α-CH₂), 1.60-1.50 (m, 4H, β-CH₂), 1.28-1.12 (m, 36H, CH₂), 0.81 (t, ³J(H,H) = 6.9 Hz, 6H, CH₃).

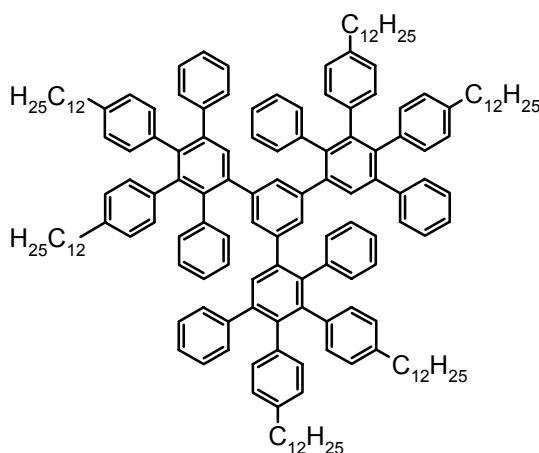
¹³C NMR (125 MHz, C₂D₂Cl₄): δ = 194.89 (C=O), 151.58, 130.97, 130.35, 129.43, 36.52, 32.21, 31.27, 29.94, 29.84, 29.73, 29.65, 29.57, 23.02, 14.52.

MS (FD, 8 kV): *m/z* (%): 546.8 (100) [*M*⁺] (calcd for C₃₈H₅₈O₂: 546.9).

m.p.: 46 °C

EA: calcd (%) for C₃₈H₅₈O₂: C 83.46, H 10.69; found: C 83.00, H 11.29.

1,3,5-Tris[3',4'-di(4''-dodecylphenyl)-2',5'-diphenylphenyl]benzene (**56a**)



76 mg (0.51 mmol) of 1,3,5-triethynylbenzene and 1.31 g (1.82 mmol) of 3,4-bis(4-dodecylphenyl)-2,5-diphenylcyclopentadienone (**55a**) were dissolved in 4 mL of *o*-xylene under an argon atmosphere and the resultant mixture heated for 18 h at 170 °C. After cooling, the solvent was removed under reduced pressure and the residue purified by column chromatography (silica gel, petroleum ether/dichloromethane 5:1) to afford 1.10 g (97% yield) **56a**, as a colorless solid.

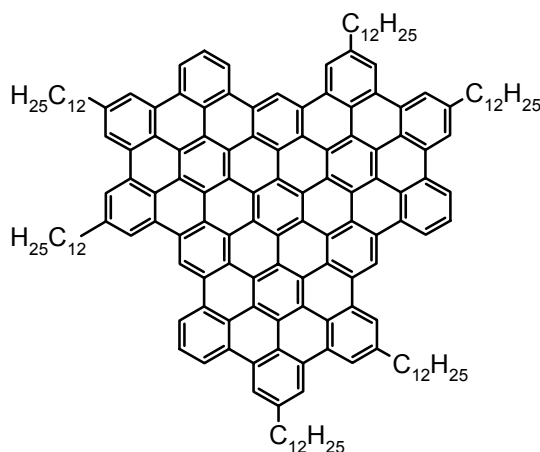
¹H NMR (500 MHz, C₂D₂Cl₄, 60 °C): δ = 7.10-7.02 (m, 15H, Ar-H), 6.75-6.49 (m, 45H, Ar-H), 2.32 (t, ³J(H,H) = 7.3 Hz, 6H, α-CH₂), 2.27 (t, ³J(H,H) = 7.3 Hz, 6H, α-CH₂), 1.44-1.04 (m, 120H, CH₂), 0.83 (t, ³J(H,H) = 6.9 Hz, 18H, CH₃).

^{13}C NMR (125 MHz, $\text{C}_2\text{D}_2\text{Cl}_4$, 60 °C): δ = 142.26, 141.77, 140.71, 140.55, 140.42, 139.74, 139.40, 139.31, 139.16, 137.94, 137.64, 132.07, 131.66, 131.60, 131.29, 130.46, 130.00, 127.40, 126.97, 126.67, 126.06, 125.61, 35.58, 35.52, 32.15, 31.34, 31.32, 29.94, 29.89, 29.72, 29.57, 29.05, 28.95, 22.92, 14.37.

MS (FD, 8 kV): m/z (%): 2229.8 (100) [M^+] (calcd for $\text{C}_{168}\text{H}_{210}$: 2229.6).

EA: calcd (%) for $\text{C}_{168}\text{H}_{210}$: C 90.51, H 9.49; found: C 90.45, H 9.36.

Hexadodecyl-C96 (53a)



0.35 g (0.16 mmol) of 1,3,5-tris[3',4'-di(4''-dodecylphenyl)-2',5'-diphenylphenyl]benzene (**56a**) was dissolved in 150 mL dichloromethane in a 500 mL two-necked round bottom flask. A constant stream of argon was bubbled into the solution through a glass capillary. A solution of 2.29 g (14.1 mmol) iron(III) chloride in 15 mL nitromethane was then added dropwise via syringe. Throughout the duration of the reaction, a constant stream of argon was bubbled through the mixture to remove HCl formed *in situ*. Fresh dichloromethane was added intermittently to replace that which had evaporated. After 18 h, the reaction was quenched with 200 mL methanol and the precipitate collected by filtration and washed with methanol. The residue was dried and purified by column chromatography (first column: silica gel, water/THF 7:3 → 100%THF;

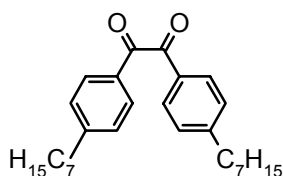
second column: silica gel, toluene) to afford 0.25 g (73 % yield) **53a** as a dark red-brown waxy solid.

MALDI-TOF MS (TCNQ): m/z (%) = 2191.4 (61), 2192.4 (100), 2193.4 (92), 2194.4 (62), 2195.4 (30), 2196.4 (15); calcd for $C_{168}H_{174}$: 2191.4 (53), 2192.4 (100), 2193.4 (94), 2194.4 (59), 2195.4 (27), 2196.4 (10).

UV/Vis (THF, $C = 4.42 \cdot 10^{-6}$ M): λ_{\max} (ϵ) = 462 nm (56817 $M^{-1}cm^{-1}$).

EA: calcd (%) for $C_{168}H_{174}$: C 92.00, H 8.00; found: C 91.60, H 8.09.

4,4'-Diheptylbenzil (**61b**)



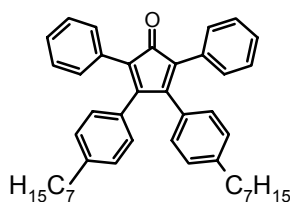
In a dry 250 mL two-necked round bottom flask 72.0 mL of a 0.5 M THF solution of 9-borabicyclo[3.3.1]nonane (9-BBN) was added slowly to 3.2 g (32.6 mmol) of 1-heptene under argon atmosphere, and the resulting mixture stirred overnight at room temperature. To this solution, 16.3 mL of 3 M aqueous NaOH solution was added via syringe and then, after 15 min, 3.0 g (8.15 mmol) of 4,4'-dibromobenzil and 0.35 g (0.43 mmol) of $[PdCl_2(dppf)] \cdot CH_2Cl_2$, respectively. The reaction mixture was stirred under argon, at room temperature for further 2 hours. The product was extracted with dichloromethane, and the organic phase washed with water three times and dried over magnesium sulfate. After evaporating the solvent, the residue was purified by column chromatography (silica gel, petroleum ether/dichloromethane 6:4) to afford 2.4 g **61b** (73% yield) as a yellow oil.

1H NMR (500 MHz, $C_2D_2Cl_4$): δ = 7.79 (d, $^3J(H,H) = 7.9$ Hz, 4H, Ar-H), 7.25 (d, $^3J(H,H) = 8.2$ Hz, 4H, Ar-H), 2.60 (t, $^3J(H,H) = 7.8$ Hz, 4H, α - CH_2), 1.62-1.48 (m, 4H, β - CH_2), 1.35-1.12 (m, 16H, CH_2), 0.80 (t, $^3J(H,H) = 6.9$ Hz, 6H, CH_3).

^{13}C NMR (62.5 MHz, $\text{C}_2\text{D}_2\text{Cl}_4$): δ = 194.93 (C=O), 151.61, 130.92, 130.37, 129.44, 36.52, 32.03, 31.29, 29.53, 29.39, 22.97, 14.49.

MS (FD, 8 kV): m/z (%): 406.6 (100) [M^+] (calcd for $\text{C}_{28}\text{H}_{38}\text{O}_2$: 406.6).

3,4-Bis(4-heptylphenyl)-2,5-diphenylcyclopentadienone (**55b**)

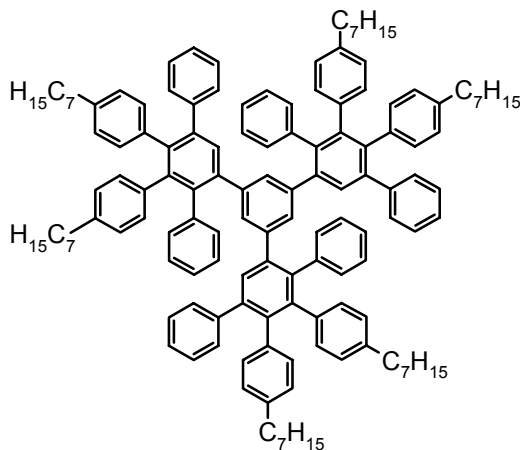


1.90 g (4.7 mmol) of 4,4'-diheptylbenzil (**61b**) and 0.98 g (4.7 mmol) of 1,3-diphenyl-2-propanone were dissolved in 15 mL *tert*-butanol under argon, then heated to 80 °C, after which 3.2 mL of a 0.8 M solution of tetrabutylammoniumhydroxide in methanol was injected quickly. After 25 minutes, the reaction was quenched by adding of water. The product was extracted with dichloromethane, the organic phase washed with water three times and dried over magnesium sulfate. After evaporation of the solvent, the residue was purified by column chromatography (silica gel, petroleum ether/dichloromethane 6:4) to afford 2.4 g **55b** (89 % yield) as a purple oil.

^1H NMR (500 MHz, $\text{C}_2\text{D}_2\text{Cl}_4$): δ = 7.24-7.12 (m, 10H, Ar-H), 6.90 (d, $^3\text{J}(\text{H},\text{H}) = 7.9$ Hz, 4H, Ar-H), 6.73 (d, $^3\text{J}(\text{H},\text{H}) = 8.2$ Hz, 4H, Ar-H), 2.49 (t, $^3\text{J}(\text{H},\text{H}) = 7.5$ Hz, 4H, α -CH₂), 1.56-1.45 (m, 4H, β -CH₂), 1.30-1.08 (m, 16H, CH₂), 0.82 (t, $^3\text{J}(\text{H},\text{H}) = 6.7$ Hz, 6H, CH₃).

^{13}C NMR (125 MHz, $\text{C}_2\text{D}_2\text{Cl}_4$): δ = 201.27 (C=O), 155.37, 143.80, 131.37, 130.44, 129.91, 129.62, 128.31, 128.15, 127.56, 124.94, 35.98, 32.14, 31.25, 29.41, 29.32, 22.96, 14.52.

MS (FD, 8 kV): m/z (%): 581.8 (100) [M^+] (calcd for $\text{C}_{43}\text{H}_{48}\text{O}$: 580.9).

1,3,5-Tris[3',4'-di(4''-heptylphenyl)-2',5'-diphenylphenyl]benzene (56b)

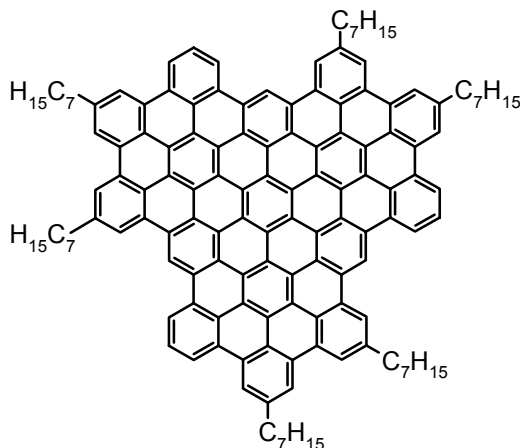
158 mg (1.05 mmol) of 1,3,5-triethynylbenzene and 2.20 g (3.79 mmol) of 3,4-bis(4-heptylphenyl)-2,5-diphenylcyclopentadienone (**55b**) were dissolved in 10 mL of *o*-xylene under an argon atmosphere and the resultant mixture was heated for 22 h at 160 °C. After cooling, the solvent was removed under reduced pressure and the residue purified by column chromatography (silica gel, petroleum ether/dichloromethane 4:1) to afford 1.77 g (93% yield) **56b**, as a colorless solid.

¹H NMR (700 MHz, C₂D₂Cl₄, 130 °C): δ = 7.14-7.06 (m, 15H, Ar-H), 6.87-6.55 (m, 45H, Ar-H), 2.37 (t, ³J(H,H) = 7.3 Hz, 6H, α-CH₂), 2.33 (t, ³J(H,H) = 7.3 Hz, 6H, α-CH₂), 1.47-1.37 (m, 12H, β-CH₂), 1.33-1.10 (m, 48H, CH₂), 0.89 (t, ³J(H,H) = 6.8 Hz, 18H, CH₃).

¹³C NMR (175 MHz, C₂D₂Cl₄): δ = 142.51, 141.91, 140.73, 140.53, 139.81, 139.52, 139.49, 139.41, 138.16, 137.86, 132.06, 131.70, 131.67, 130.99, 130.43, 130.10, 127.25, 126.84, 126.79, 126.53, 125.96, 125.55, 35.50, 35.45, 31.91, 31.07, 29.12, 28.93, 28.86, 22.63, 13.89.

MS (FD, 8 kV): *m/z* (%): 1809.4 (100) [*M*⁺] (calcd for C₁₃₈H₁₅₀: 1808.7).

EA: calcd (%) for C₁₃₈H₁₅₀: C 91.64, H 8.36; found: C 91.10, H 8.49.

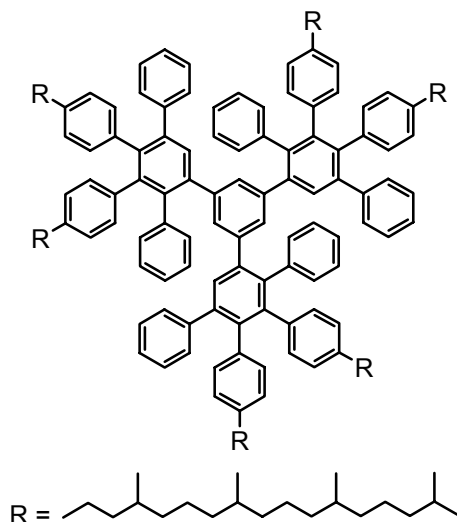
Hexaheptyl-C96 (53b)

375 mg (0.21 mmol) of 1,3,5-tris[3',4'-di(4''-heptylphenyl)-2',5'-diphenylphenyl]benzene (**56b**) was dissolved in 150 mL of dichloromethane in a 500 mL two-necked round bottom flask. A constant stream of argon was bubbled into the solution through a glass capillary. A solution of 3.03 g (18.7 mmol) iron(III) chloride in 20 mL nitromethane was then added dropwise via syringe. Throughout the duration of the reaction, a constant stream of argon was bubbled through the mixture to remove HCl formed *in situ*. Fresh dichloromethane was added intermittently to replace that which had evaporated. After 16 h, the reaction was quenched with 200 mL methanol and the precipitate collected by filtration and washed with methanol. The residue was dried and purified by column chromatography (silica gel, toluene) to afford 220 mg (60 % yield) **53b** as a dark red-brown waxy solid.

MALDI-TOF MS (TCNQ): m/z (%) = 1771.3 (68), 1772.3 (100), 1773.3 (59), 1774.3 (46), 1775.3 (22), 1776.3 (18); calcd for C₁₃₈H₁₁₄: 1770.9 (64), 1771.9 (100), 1772.9 (77), 1773.9 (39), 1774.9 (15), 1775.9 (5).

UV/Vis (THF, C = 6.06 · 10⁻⁶ M): λ_{\max} (ϵ) = 462 nm (52152 M⁻¹cm⁻¹).

EA: calcd (%) for C₁₃₈H₁₁₄: C 93.52, H 6.48; found: C 93.32, H 6.14.

1,3,5-Tris{3',4'-di[4''-(3,7,11,15-tetramethylhexadecyl)phenyl]-2',5'-diphenylphenyl}benzene (56c)

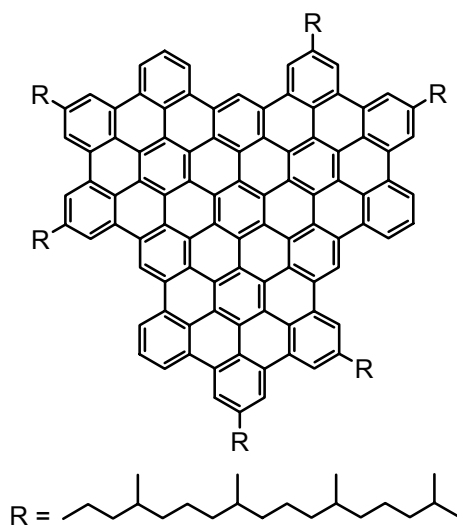
30 mg (0.20 mmol) of 1,3,5-triethynylbenzene and 0.69 g (0.72 mmol) of 3,4-bis[4-(3,7,11,15-tetramethylhexadecyl)phenyl]-2,5-diphenylcyclopentadienone (**55c**) were dissolved in 10 mL of *o*-xylene under an argon atmosphere and the resultant mixture heated for 22 h at 160 °C. After cooling, the solvent was removed under reduced pressure and the residue purified by column chromatography (silica gel, petroleum ether/dichloromethane 5:1) to afford 0.49 g (85% yield) **56c**, as a colorless highly viscous oil.

¹H NMR (700 MHz, C₂D₂Cl₄): δ = 7.12-6.98 (m, 15H, Ar-H), 6.78-6.45 (m, 45H, Ar-H), 2.38-2.20 (m, 12H, α-CH₂), 1.48-1.40 (m, 6H, CH), 1.38-0.90 (m, 138H, CH, CH₂); 0.83-0.75 (m, 72H, CH₃), 0.75-0.70 (m, 18H, CH₃).

¹³C NMR (175 MHz, C₂D₂Cl₄, 100 °C): δ = 142.40, 141.81, 140.71, 140.63, 140.47, 140.06, 139.74, 139.42, 139.29, 138.00, 137.72, 132.04, 131.69, 131.65, 131.08, 130.42, 130.03, 127.29, 126.88, 126.79, 126.51, 125.98, 125.56, 39.67, 38.79, 37.73, 33.17, 33.03, 32.44, 28.13, 24.90, 24.66, 22.76, 19.93.

MS (FD, 8 kV): *m/z* (%): 2902.2 (100) [*M*⁺] (calcd for C₂₁₆H₃₀₆: 2902.8).

EA: calcd (%) for C₂₁₆H₃₀₆: C 89.37, H 10.63; found: C 89.26, H 10.68.

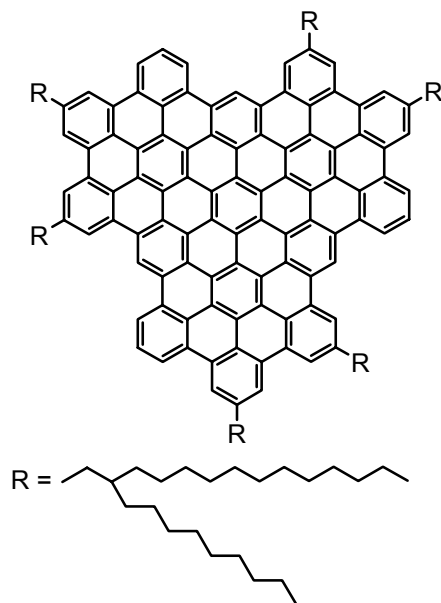
Hexa(3,7,11,15-tetramethylhexadecyl)-C96 (53c)

250 mg (0.086 mmol) of 1,3,5-tris{3',4'-di[4''-(3,7,11,15-tetramethylhexadecyl)phenyl]-2',5'-diphenylphenyl}benzene (**56c**) was dissolved in 120 mL dichloromethane in a 500 mL two-necked round bottom flask. A constant stream of argon was bubbled into the solution through a glass capillary. A solution of 1.26 g (7.77 mmol) iron(III) chloride in 9 mL of nitromethane was then added dropwise via syringe. Throughout the duration of the reaction, a constant stream of argon was bubbled through the mixture to remove HCl formed *in situ*. Fresh dichloromethane was added intermittently to replace that which had evaporated. After 16 h, the reaction was quenched with 200 mL methanol and the precipitate was collected by filtration and washed with methanol. The residue was dried and purified by column chromatography (silica gel, toluene) to afford 160 mg (65 % yield) **53c** as a dark red-brown waxy solid.

MALDI-TOF MS (TCNQ): m/z (%) = 2864.1 (44), 2865.1(86), 2866.1(100), 2867.1(79), 2868.1(51), 2869.1(32), 2870.1 (18); calcd for $C_{216}H_{270}$: 2864.1 (34), 2865.1 (82), 2866.1 (100), 2867.1 (81), 2868.1 (49), 2869.1 (23), 2870.1 (9).

UV/Vis (THF, $C = 5.67 \cdot 10^{-6}$ M): λ_{max} (ϵ) = 463 nm (65104 $M^{-1}cm^{-1}$).

EA: calcd (%) for $C_{216}H_{270}$: C 90.51, H 9.49; found: C 90.31, H 9.56.

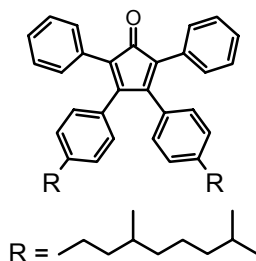
Hexa(2-decyltetradecyl)-C96 (53d)

110 mg (0.034 mmol) of 1,3,5-tris{3',4'-di[4''-(2-decyltetradecyl)phenyl]-2',5'-diphenyl-phenyl}benzene (**56d**) was dissolved in 100 mL dichloromethane in a 250 mL two-necked round bottom flask. A constant stream of argon was bubbled into the solution through a glass capillary. A solution of 0.5 g (3.08 mmol) iron(III) chloride in 5 mL of nitromethane was then added dropwise via syringe. Throughout the duration of the reaction, a constant stream of argon was bubbled through the mixture to remove HCl formed *in situ*. Fresh dichloromethane was added intermittently to replace that which had evaporated. After 18 h, the reaction was quenched with methanol and the precipitate was collected by filtration and washed with methanol. The residue was dried and purified by column chromatography (silica gel, toluene) to afford 82 mg (75 % yield) **53d** as a dark red-brown waxy solid.

MALDI-TOF MS (TCNQ): m/z (%) = 3201.3 (36), 3202.3 (82), 3203.3 (100), 3204.3 (90), 3205.3 (62), 3206.3 (37), 3207.3 (26), 3208.3 (20); calcd for $C_{240}H_{318}$: 3200.5 (27), 3201.5 (74), 3202.5 (100), 3203.5 (90), 3204.5 (60), 3205.5 (32), 3206.5 (14), 3207.5 (5).

UV/Vis (THF, $C = 5.48 \cdot 10^{-6}$ M): λ_{max} (ϵ) = 473 nm (103896 $M^{-1}cm^{-1}$).

EA: calcd (%) for $C_{240}H_{318}$: C 89.99, H 10.01; found: C 89.92, H 10.05.

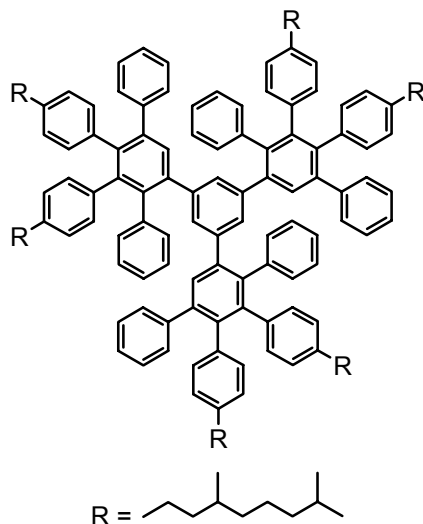
3,4-Bis[4-(3,7-dimethyloctyl)phenyl]-2,5-diphenylcyclopentadienone (55e)

2.60 g (5.30 mmol) of 4,4'-bis(3,7-dimethyloctyl)benzil (**66e**) and 1.12 g (5.30 mmol) of 1,3-diphenyl-2-propanone were dissolved in 20 mL *tert*-butanol under argon, then heated to 80 °C, after which 3.64 mL of a 0.8 M solution of tetrabutylammoniumhydroxide in methanol was injected quickly. After 25 minutes, the reaction was quenched by addition of water. The product was extracted with dichloromethane, the organic phase washed with water three times and dried over magnesium sulfate. After evaporation of the solvent, the residue was purified by column chromatography (silica gel, petroleum ether/dichloromethane 7:3) to afford 2.60 g **55e** (74 % yield) as a purple oil.

¹H NMR (250 MHz, C₂D₂Cl₄): δ = 7.24-7.12 (m, 10H, Ar-H), 6.90 (d, ³J(H,H) = 8.2 Hz, 4H, Ar-H), 6.73 (d, ³J(H,H) = 7.9 Hz, 4H, Ar-H), 2.62-2.36 (m, 4H, α-CH₂), 1.60-0.95 (m, 20H, CH, CH₂), 0.87-0.75 (m, 18H, CH₃).

¹³C NMR (62.5 MHz, C₂D₂Cl₄): δ = 201.26 (C=O), 155.35, 144.10, 131.37, 130.44, 130.18, 129.66, 128.31, 128.11, 127.55, 124.96, 39.57, 38.69, 37.43, 33.59, 32.66, 28.21, 25.04, 23.08, 22.99, 19.94.

MS (FD, 8 kV): *m/z* (%): 665.1 (100) [*M*⁺] (calcd for C₄₉H₆₀O: 665.0).

1,3,5-Tris{3',4'-di[4''-(3,7-dimethyloctyl)phenyl]-2',5'-diphenylphenyl}benzene(56e)

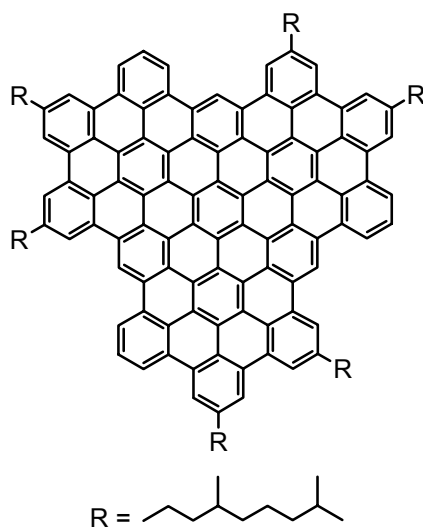
171 mg (1.14 mmol) of 1,3,5-triethynylbenzene and 2.50 g (3.76 mmol) of 3,4-bis[4-(3,7-dimethyloctyl)phenyl]-2,5-diphenyl-cyclopentadienone (**55e**) were dissolved in 15 mL of *o*-xylene under an argon atmosphere and the resultant mixture was heated for 18 h at 170 °C. After cooling, the solvent was removed under reduced pressure and the residue purified by column chromatography (silica gel, petroleum ether/dichloromethane 5:1) to afford 2.15 g (91% yield) **56e**, as a colorless solid.

¹H NMR (500 MHz, C₂D₂Cl₄, 120 °C): δ = 7.14-7.04 (m, 15H, Ar-H), 6.84-6.52 (m, 45H, Ar-H), 2.45-2.25 (m, 12H, α-CH₂), 1.58-1.48 (m, 6H, CH), 1.46-1.00 (m, 54H, CH, CH₂), 0.86 (d, ³J(H,H) = 6.4 Hz, 36H, CH₃), 0.82-0.76 (m, 18H, CH₃).

¹³C NMR (125 MHz, C₂D₂Cl₄, 60 °C): δ = 142.27, 141.76, 140.70, 140.55, 140.43, 140.02, 139.67, 139.30, 139.18, 137.89, 137.60, 132.07, 131.69, 131.63, 131.30, 130.46, 129.99, 127.40, 126.98, 126.92, 126.62, 126.05, 125.61, 39.64, 38.84, 38.79, 37.41, 33.17, 33.10, 32.32, 32.18, 28.15, 24.92, 24.88, 22.97, 22.90, 19.87.

MS (FD, 8 kV): *m/z* (%): 2061.2 (100) [*M*⁺] (calcd for C₁₅₆H₁₈₆: 2061.2).

EA: calcd (%) for C₁₅₆H₁₈₆: C 90.90, H 9.10; found: C 90.93, H 9.00.

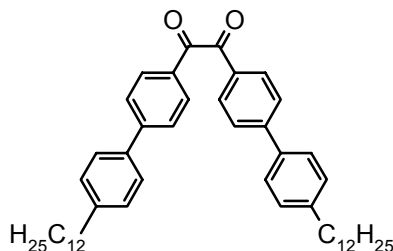
Hexa(3,7-dimethyloctyl)-C96 (53e)

350 mg (0.17 mmol) of 1,3,5-tris{3',4'-di[4''-(3,7-dimethyloctyl)phenyl]-2',5'-diphenylphenyl}benzene (**56e**) was dissolved in 150 mL of dichloromethane in a 500 mL two-necked round bottom flask. A constant stream of argon was bubbled into the solution through a glass capillary. A solution of 2.48 g (15.3 mmol) iron(III) chloride in 18 mL of nitromethane was then added dropwise via syringe. Throughout the whole reaction, a constant stream of argon was bubbled through the mixture to remove HCl formed *in situ*. Fresh dichloromethane was added intermittently to replace that which had evaporated. The reaction was stirred for 18 h and then quenched by adding 200 mL of methanol. The precipitate was collected by filtration, washed with methanol, and dried under vacuum to afford 320 mg (93% yield) **53e** as a dark brown solid.

MALDI-TOF MS (TCNQ): m/z (%) = 2023.0 (56), 2024.0 (100), 2025.0 (82), 2026.0 (47), 2027.0 (26), 2028.0 (17); calcd for $C_{156}H_{150}$: 2023.2 (57), 2024.2 (100), 2025.2 (87), 2026.2 (51), 2027.2 (22), 2028.2 (8).

UV/Vis (THF): λ_{max} = 462 nm

EA: calcd (%) for $C_{156}H_{150}$: C 92.53, H 7.47; found: C 91.36, H 8.22.

4,4'-Bis(4-dodecylphenyl)benzil (66f)

5.0 g (7.50 mmol) of 4,4'-bis(4-dodecylphenyl)diphenylacetylene (**65f**) and 0.95 g (3.75 mmol) iodine were dissolved in 50 mL of DMSO and stirred overnight at 155 °C under an argon atmosphere. After cooling, the reaction mixture was poured into 50 mL of 4% aqueous sodium thiosulfate solution and stirred 30 min. The product was extracted with chloroform, the organic phase washed three times with water and dried over magnesium sulfate. After evaporation of the solvent, the residue was purified by column chromatography (silica gel, petroleum ether/dichloromethane 6:4) to afford 3.7 g (71% yield) **66f** as a yellow powder.

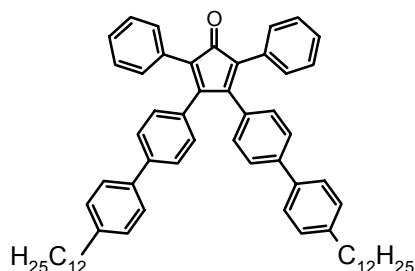
¹H NMR (500 MHz, C₂D₂Cl₄): δ = 7.98 (d, ³J(H,H) = 8.2 Hz, 4H, Ar-H), 7.68 (d, ³J(H,H) = 8.2 Hz, 4H, Ar-H), 7.50 (d, ³J(H,H) = 7.6 Hz, 4H, Ar-H), 7.23 (d, ³J(H,H) = 7.6 Hz, 4H, Ar-H), 2.58 (t, ³J(H,H) = 6.8 Hz, 4H, α-CH₂), 1.65-1.50 (m, 4H, β-CH₂), 1.35-1.10 (m, 36H, CH₂), 0.81 (t, ³J(H,H) = 6.7 Hz, 6H, CH₃).

¹³C NMR (125 MHz, C₂D₂Cl₄): δ = 194.56 (C=O), 147.84, 144.28, 136.72, 131.61, 130.86, 129.49, 127.69, 127.52, 35.95, 32.23, 31.63, 29.99, 29.92, 29.82, 29.68, 23.04, 14.56.

MS (FD, 8 kV): *m/z* (%): 698.0 (100) [*M*⁺] (calcd for C₅₀H₆₆O₂: 699.1).

m.p.: 119 °C

EA: calcd (%) for C₅₀H₆₆O₂: C 85.91, H 9.52; found: C 85.90, H 9.66.

3,4-Bis[4'-(4''-dodecylphenyl)phenyl]phenyl-2,5-diphenylcyclopentadienone (55f)

2.5 g (3.58 mmol) of 4,4'-bis(4-dodecylphenyl)benzil (**66f**) and 0.75 g (3.58 mmol) of 1,3-diphenyl-2-propanone were dissolved in 5 mL of *tert*-butanol under argon and heated to 85 °C. A solution prepared from 2.65 mL of a 0.8 M solution of tetrabutylammoniumhydroxide in methanol and 1.30 mL of *tert*-butanol was injected quickly. After 15 minutes, the reaction was quenched by addition of water. The product was extracted with dichloromethane, the organic phase washed with water three times and dried over magnesium sulfate. After evaporation of the solvent, the residue was purified by column chromatography (silica gel, petroleum ether/dichloromethane 1:1) to afford 2.4 g **55f** (77 % yield) as a purple powder.

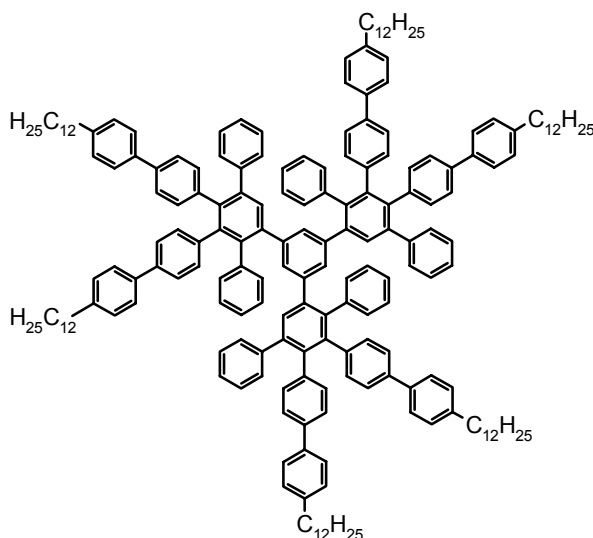
¹H NMR (500 MHz, C₂D₂Cl₄): δ = 7.47 (d, ³J(H,H) = 7.9 Hz, 4H, Ar-H), 7.40 (d, ³J(H,H) = 7.9 Hz, 4H, Ar-H), 7.28-7.20 (br, 10H, Ar-H), 7.17 (d, ³J(H,H) = 7.9 Hz, 4H, Ar-H), 6.95 (d, ³J(H,H) = 7.9 Hz, 4H, Ar-H), 2.53 (t, ³J(H,H) = 7.5 Hz, 4H, α-CH₂), 1.62-1.50 (m, 4H, β-CH₂), 1.35-1.15 (m, 36H, CH₂), 0.81 (t, ³J(H,H) = 6.7 Hz, 6H, CH₃).

¹³C NMR (125 MHz, C₂D₂Cl₄): δ = 200.90 (C=O), 154.56, 143.15, 140.90, 137.24, 131.69, 131.14, 130.49, 130.34, 129.30, 128.47, 127.82, 126.91, 126.34, 125.57, 35.86, 32.23, 31.73, 29.99, 29.96, 29.92, 29.83, 29.66, 23.03, 14.56.

MS (FD, 8 kV): *m/z* (%): 873.1 (100) [*M*⁺] (calcd for C₆₅H₇₆O: 873.3).

m.p.: 116 °C

EA: calcd (%) for C₆₅H₇₆O: C 89.40, H 8.77; found: C 89.45, H 8.86.

1,3,5-Tris{3',4'-di[4''-(4'''-dodecylphenyl)phenyl]-2',5'-diphenylphenyl} benzene (56f)

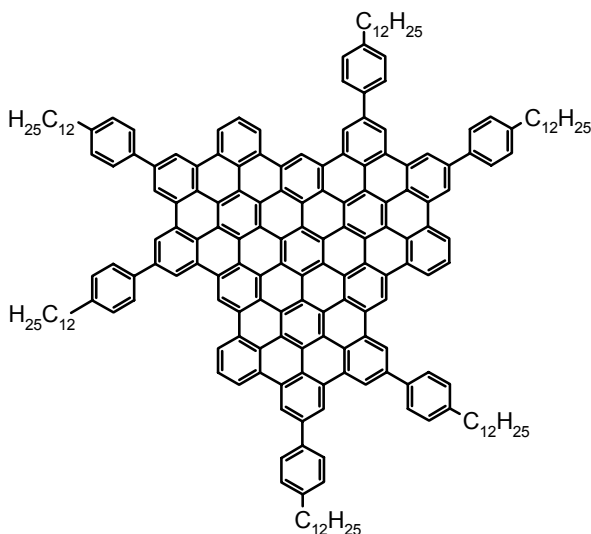
52 mg (0.35 mmol) of 1,3,5-triethynylbenzene and 1.0 g (1.15 mmol) of 3,4-bis[4'-(4''-dodecylphenyl)phenyl]-2,5-diphenylcyclopentadienone (**55f**) were dissolved in 5 mL of *o*-xylene under an argon atmosphere and the resultant mixture heated for 18 h at 170 °C. After cooling, the solvent was removed under reduced pressure and the residue purified by column chromatography (silica gel, petroleum ether/dichloromethane 3:2) to afford 0.9 g (97% yield) **56f**, as a colorless solid.

¹H NMR (500 MHz, C₂D₂Cl₄, 100 °C): δ = 7.36-7.26 (m, 12H, Ar-H), 7.18-7.04 (m, 40H, Ar-H), 6.90-6.68 (m, 32H, Ar-H), 2.55 (t, ³J(H,H) = 7.4 Hz, 12H, α-CH₂), 1.62-1.52 (m, 12H, β-CH₂), 1.35-1.20 (m, 108H, CH₂); 0.86 (t, ³J(H,H) = 6.7 Hz, 18H, CH₃).

¹³C NMR (125 MHz, C₂D₂Cl₄, 100 °C): δ = 142.17, 142.06, 142.00, 141.34, 140.90, 140.79, 140.70, 140.43, 139.70, 139.48, 139.34, 138.94, 138.29, 138.24, 137.91, 137.62, 132.27, 132.22, 132.06, 131.51, 130.41, 130.16, 128.83, 128.79, 127.56, 127.16, 126.78, 126.33, 125.90, 125.27, 124.99, 35.72, 32.08, 31.39, 29.81, 29.78, 29.74, 29.66, 29.54, 29.45, 22.80, 14.17.

MS (FD, 8kV): *m/z* (%): 2686.5 (100) [*M*⁺] (calcd for C₂₀₄H₂₃₄: 2686.1).

EA: calcd (%) for C₂₀₄H₂₃₄: C 91.22, H 8.78; found: C 90.82, H 8.61.

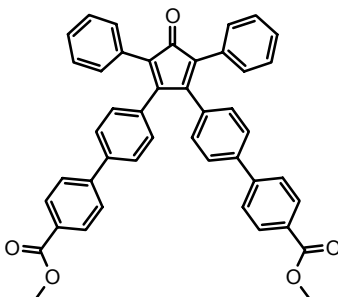
Hexa(4-dodecylphenyl)-C96 (53f)

250 mg (0.093 mmol) of 1,3,5-tris{3',4'-di[4''-(4'''-dodecylphenyl)phenyl]-2',5'-diphenylphenyl}benzene (**56f**) was dissolved in 150 mL of dichloromethane in a 500 mL two-necked round bottom flask. A constant stream of argon was bubbled into the solution through a glass capillary. A solution of 1.36 g (8.38 mmol) iron(III) chloride in 10 mL of nitromethane was then added dropwise via syringe. Throughout the duration of the reaction, a constant stream of argon was bubbled through the mixture to remove HCl formed *in situ*. Fresh dichloromethane was added intermittently to replace that which had evaporated. The reaction was stirred for 17 h and then quenched by addition of 200 mL of methanol. The precipitate was collected by filtration, washed with methanol, and dried under vacuum to afford 220 mg (89% yield) **53f** as a dark brown solid.

MALDI-TOF MS (TCNQ): m/z (%) = 2646.9 (63), 2647.9 (95), 2648.9 (100), 2649.9 (75), 2650.9 (54), 2652.0 (31), 2653.0 (27); calcd for $C_{204}H_{198}$: 2647.5 (38), 2648.5 (87), 2649.5 (100), 2650.5 (76), 2651.5 (43), 2652.5 (19), 2653.5 (7).

UV/Vis (THF): λ_{max} = 474 nm

EA: calcd (%) for $C_{204}H_{198}$: C 92.47, H 7.53; found: C 91.08, H 8.04.

3,4-Bis[4'-(4''-methoxycarbonylphenyl)phenyl]-2,5-diphenylcyclopentadienone (55g)

4.5 g (8.3 mmol) of 3,4-bis(4-bromophenyl)-2,5-diphenylcyclopentadienone (**67**) and 10.0 g (55.6 mmol) of (4-methoxycarbonylphenyl)boronic acid were dissolved in 166 mL toluene under argon atmosphere, then 83 mL of 1M aqueous potassium carbonate solution and 1.25 g (1.1 mmol) of tetrakis(triphenylphosphine)palladium(0) added. The resultant mixture was heated under argon for 26 h at 95 °C. After cooling, the product was extracted with dichloromethane, the organic phase washed with water three times, then dried over magnesium sulfate. After evaporation of the solvent, the residue was purified by column chromatography (silica gel, petroleum ether/dichloromethane 1:9) to afford 3.6 g (67% yield) **55g** as a purple powder.

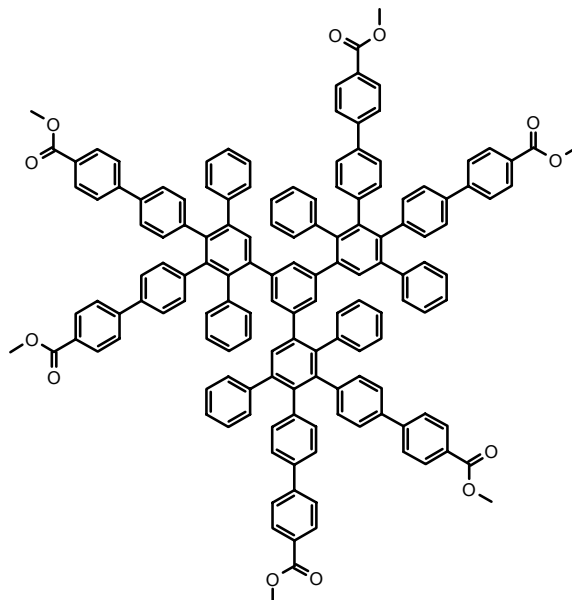
¹H NMR (700 MHz, C₂D₂Cl₄): δ = 7.99 (d, ³J(H,H) = 7.7 Hz, 4H, Ar-H), 7.60 (d, ³J(H,H) = 8.6 Hz, 4H, Ar-H), 7.43 (d, ³J(H,H) = 8.5 Hz, 4H, Ar-H), 7.26-7.16 (m, 10H, Ar-H), 6.99 (d, ³J(H,H) = 7.7 Hz, 4H, Ar-H), 3.84 (s, 6H, CH₃).

¹³C NMR (175 MHz, C₂D₂Cl₄): δ = 200.67 (C=O, cyclopentadienone), 167.16 (C=O, ester), 154.04, 144.71, 139.89, 132.90, 130.85, 130.47, 130.42, 129.41, 128.55, 128.01, 127.18, 127.02, 126.03, 52.64 (CH₃).

MS (FD, 8 kV): *m/z* (%): 652.5 (100) [*M*⁺] (calcd for C₄₅H₃₂O₅: 652.7).

m.p.: 225 °C

EA: calcd (%) for C₄₅H₃₂O₅: C 82.80, H 4.94; found: C 82.78, H 4.91.

1,3,5-Tris{3',4'-di[4''-(4'''-methoxycarbonylphenyl)phenyl]-2',5'-diphenylphenyl}benzene (56g)

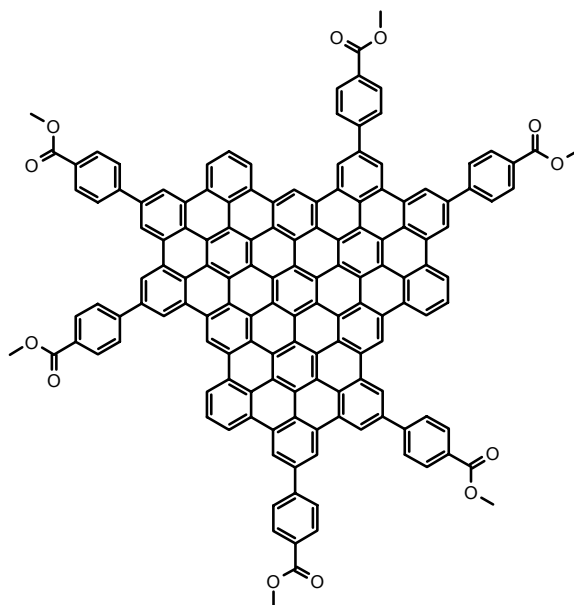
102 mg (0.68 mmol) of 1,3,5-triethynylbenzene and 1.6 g (2.45 mmol) of 3,4-bis[4'-(4''-methoxycarbonylphenyl)phenyl]-2,5-diphenylcyclopentadienone (**55g**) were dissolved in 10 mL of *o*-xylene under an argon atmosphere and the resultant mixture heated for 20 h at 160 °C. After cooling, the solvent was removed under reduced pressure and the residue purified by column chromatography (silica gel, hexane/ethylacetate 7:3 to ethylacetate) to afford 1.34 g (97% yield) **56g**, as a colorless solid.

¹H NMR (700 MHz, C₂D₂Cl₄): δ = 7.92-7.84 (m, 12H, Ar-H), 7.44 (d, ³J(H,H) = 7.7 Hz, 6H, Ar-H), 7.42 (d, ³J(H,H) = 7.7 Hz, 6H, Ar-H), 7.17-7.02 (m, 27H, Ar-H), 6.88-6.60 (m, 33H, Ar-H), 3.81 (s, 18H, CH₃).

¹³C NMR (175 MHz, C₂D₂Cl₄, 100 °C): δ = 166.97 (C=O), 145.51, 145.45, 141.88, 141.03, 140.98, 140.94, 140.60, 140.55, 140.21, 139.44, 138.66, 137.08, 136.82, 132.41, 132.37, 131.99, 131.62, 130.34, 130.19, 130.09, 130.06, 129.15, 127.62, 127.21, 126.83, 126.80, 126.50, 126.04, 125.78, 125.52, 52.04 (CH₃).

MS (FD, 8 kV): *m/z* (%): 2024.0 (100) [*M*⁺] (calcd for C₁₄₄H₁₀₂O₁₂: 2024.4).

EA: calcd (%) for C₁₄₄H₁₀₂O₁₂: C 85.44, H 5.08; found: C 85.22, H 5.07.

Hexa(4-methoxycarbonylphenyl)-C96 (53g)

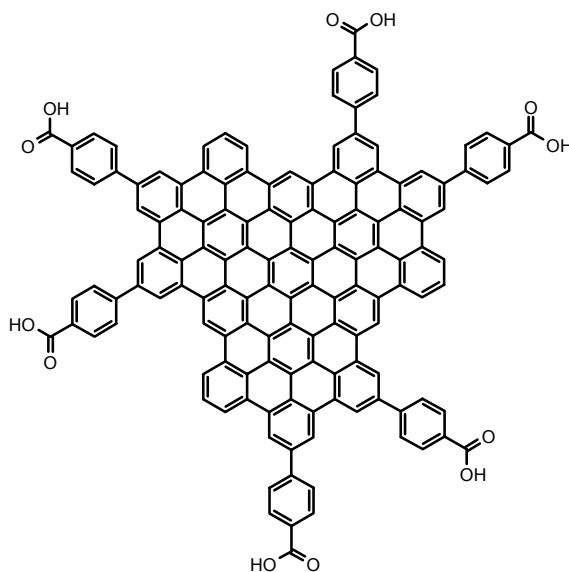
0.5 g (0.25 mmol) of 1,3,5-tris{3',4'-di[4''-(4'''-methoxycarbonylphenyl)phenyl]-2',5'-diphenylphenyl}benzene (**56g**) was dissolved in 200 mL of dichloromethane in a 500 mL two-necked round bottom flask. A constant stream of argon was bubbled into the solution through a glass capillary. A solution of 5.7 g (35.1 mmol) iron(III) chloride in 35 mL of nitromethane was then added dropwise via syringe. Fresh dichloromethane was added intermittently to replace that which had evaporated. After 4 h, a condenser was attached to the flask and the argon bubbling rate reduced. The reaction mixture was stirred for a further 20 h and then quenched by addition of methanol. The precipitate was collected by filtration, washed with methanol, and dried under vacuum to afford 0.47 g of a solid product. MALDI-TOF MS indicated that the reaction had not proceeded to completion. The previously isolated product was treated with another 5.7 g (35.1 mmol) of iron(III) chloride following the procedure as described above. Finally, 0.45 g (92% yield) of the desired product **53g** was obtained as a dark red-brown solid.

MALDI-TOF MS (TCNQ): m/z (%) = 1986.9 (63), 1987.9 (100), 1988.9 (87), 1989.9 (46), 1990.9 (24), 1991.8 (9); calcd for $C_{144}H_{66}O_{12}$: 1986.5 (62), 1987.5 (100), 1988.5 (82), 1989.5 (45), 1990.5 (19), 1991.5 (6).

UV/Vis (CH₂Cl₂, C = 5.09 · 10⁻⁶ M): λ_{max} (ε) = 465 nm (36027 M⁻¹cm⁻¹).

EA*: calcd (%) for C₁₄₄H₆₆O₁₂: C 87.00, H 3.35; found: C 81.67, H 3.15.

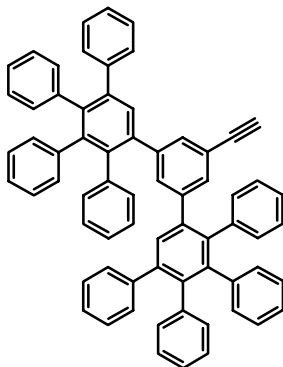
Hexa(4-carboxyphenyl)-C96 (69)



0.2 g (0.10 mmol) of hexa(4-methoxycarbonylphenyl)-C96 (**53g**) was dissolved in 150 mL of dry THF under an argon atmosphere and a solution of 0.34 g (6.06 mmol) of potassium hydroxide in 3 mL of water was added. The resulting mixture was refluxed for 3 days. After cooling, the solvent was removed, the residue dissolved in 100 mL of water, and the solution was acidified with 2 M hydrochloric acid. The precipitate was collected by filtration, washed with 350 mL of water, and dried under vacuum to afford 0.18 g (94% yield) **69** as a red-brown solid.

MALDI-TOF MS (TCNQ): *m/z* (%) = 1902.6 (83), 1903.6 (100), 1904.6 (81), 1905.6 (58), 1906.5 (20), 1907.4 (10); calcd for C₁₃₈H₅₄O₁₂: 1902.4 (65), 1903.4 (100), 1904.4 (78), 1905.4 (42), 1906.4 (17), 1907.4 (6).

EA*: calcd (%) for C₁₃₈H₅₄O₁₂: C 87.06, H 2.86; found: C 81.00, H 3.23.

1,3-Di(2',3',4',5'-tetraphenylphenyl)-5-ethynylbenzene (72a)

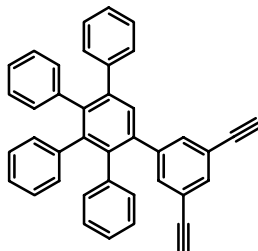
1.50 g (9.99 mmol) of 1,3,5-triethynylbenzene and 3.84 g (9.99 mmol) of tetraphenylcyclopentadienone were dissolved in 10 mL of *o*-xylene under an argon atmosphere and heated at 100 °C for 4 hours. After cooling to room temperature, methanol was added to the reaction mixture, and the precipitate was collected by filtration and washed with methanol. The residue (mixture of **72a** and **71a**) was purified by column chromatography (silica gel, petroleum ether/dichloromethane 7:3) to afford 1.39 g (16 % yield) **72a** as a white solid.

¹H NMR (250 MHz, C₂D₂Cl₄): δ = 7.15-6.94 (m, 15H, Ar-H), 6.87-6.60 (m, 30H, Ar-H), 2.81(s, 1H, CH).

¹³C NMR (175 MHz, C₂D₂Cl₄, 140 °C): δ= 142.11, 142.06, 141.71, 141.07, 140.62, 140.35, 140.08, 139.95, 139.77, 139.56, 132.72, 131.78, 131.00, 130.26, 127.54, 127.06, 126.88, 126.62, 126.31, 125.92, 125.62, 125.37, 120.95, 84.37, 76.34.

MS (FD, 8 kV): *m/z* (%): 863.4 (100) [*M*⁺] (calcd for C₆₈H₄₆: 863.1).

EA: calcd (%) for C₆₈H₄₆: C 94.63, H 5.37; found: C 94.59, H 5.32.

1-(2',3',4',5'-Tetraphenylphenyl)-3,5-diethynylbenzene (71a)

Compound **71a** was prepared as described above for compound **72a** (in the same reaction as a co-product). Purification by column chromatography (silica gel, petroleum ether/dichloromethane 7:3) afforded 0.62 g (12% yield) **71a** as a white solid.

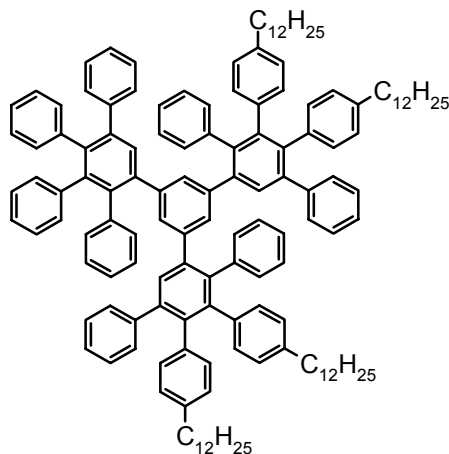
¹H NMR (500 MHz, C₂D₂Cl₄): δ = 7.41 (s, 1H, Ar-H), 7.33 (s, 1H, Ar-H), 7.25-7.21 (br, 2H, Ar-H), 7.13-7.05 (br, 5H, Ar-H), 6.95-6.68 (m, 15H, Ar-H), 2.95 (s, 2H, CH).

¹³C NMR (125 MHz, C₂D₂Cl₄): δ = 142.63, 142.11, 141.74, 141.03, 140.25, 140.16, 139.99, 139.48, 139.45, 138.71, 134.29, 133.64, 131.72, 131.65, 131.17, 130.20, 127.91, 127.38, 127.18, 126.89, 126.56, 126.18, 125.82, 125.54, 121.87, 82.98, 78.15.

MS (FD, 8 kV): *m/z* (%): 506.5 (100) [*M*⁺] (calcd for C₄₀H₂₆: 506.6).

m.p.: 96 °C

EA: calcd (%) for C₄₀H₂₆: C 94.83, H 5.17; found: C 94.75, H 5.08.

1,3-Di[3',4'-di(4''-dodecylphenyl)-2',5'-diphenylphenyl]-5-(2',3',4',5'-tetraphenylphenyl)benzene (73)

0.20 g (0.39 mmol) of 1-(2',3',4',5'-tetraphenylphenyl)-3,5-diethynylbenzene (**71a**) and 0.66 g (0.92 mmol) of 3,4-bis(4-dodecylphenyl)-2,5-diphenylcyclopentadienone (**55a**) were dissolved in 3 mL of *o*-xylene under an argon atmosphere and the resultant mixture was heated for 10 h at 170 °C. After cooling, solvent was removed under reduced pressure and the residue purified by column chromatography (silica gel, petroleum ether/dichloromethane 3:1) to afford 0.66 g (88% yield) **73**, as a colorless solid.

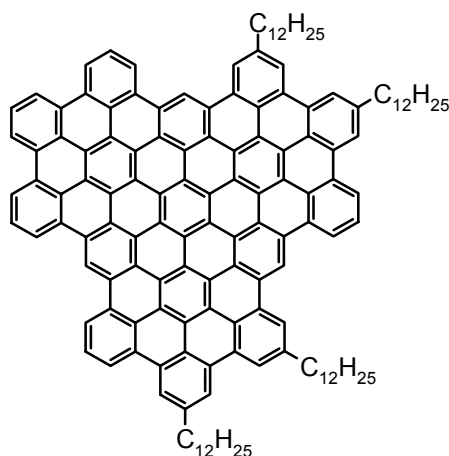
¹H NMR (500 MHz, CD₂Cl₂): δ = 7.22-7.05 (m, 15H, Ar-H), 6.95-6.55 (m, 47H, Ar-H), 2.40 (t, ³J(H,H) = 7.5 Hz, 4H, α-CH₂), 2.36 (t, ³J(H,H) = 7.3 Hz, 4H, α-CH₂), 1.50-0.95 (m, 80H, CH₂), 0.90 (t, ³J(H,H) = 6.6 Hz, 12H, CH₃).

¹³C NMR (125 MHz, CD₂Cl₂): δ = 142.31, 142.12, 141.84, 141.08, 141.05, 140.87, 140.79, 140.68, 140.59, 140.56, 140.47, 140.15, 139.77, 139.51, 139.44, 138.09, 137.80, 132.19, 132.11, 131.90, 131.87, 131.72, 131.69, 131.55, 130.49, 130.13, 130.06, 127.75, 127.71, 127.36, 127.30, 127.22, 127.16, 126.94, 126.88, 126.60, 126.49, 126.16, 126.03, 125.92, 125.64, 35.71, 35.65, 32.37, 31.64, 30.15, 30.09, 29.92, 29.80, 29.32, 29.22, 23.12, 14.29.

MS (FD, 8 kV): *m/z* (%): 1893.9 (100) [*M*⁺] (calcd for C₁₄₄H₁₆₂: 1892.9).

m.p.: 198 °C

EA: calcd (%) for C₁₄₄H₁₆₂: C 91.37, H 8.63; found: C 91.34, H 8.74.

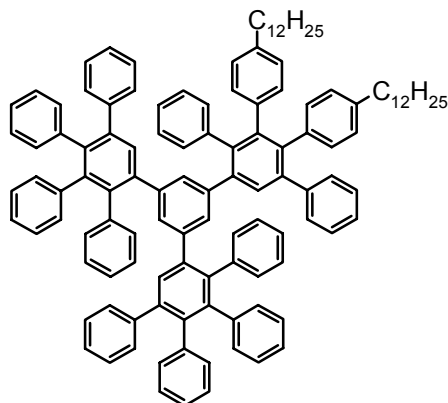
Tetradodecyl-C96 (75)

350 mg (0.18 mmol) of 1,3-di[3',4'-di(4''-dodecylphenyl)-2',5'-diphenylphenyl]-5-(2',3',4',5'-tetraphenylphenyl)benzene (**73**) was dissolved in 200 mL of dichloromethane in a 500 mL two-necked round bottom flask. A constant stream of argon was bubbled into the solution through a glass capillary. A solution of 2.7 g (16.6 mmol) iron(III) chloride in 18 mL of nitromethane was then added dropwise via syringe. Throughout the duration of the reaction, a constant stream of argon was bubbled through the mixture to remove HCl formed *in situ*. Fresh dichloromethane was added intermittently to replace that which had evaporated. After 18 h, the reaction was quenched with 200 mL of methanol and the precipitate collected by filtration and washed with methanol. The residue was then redissolved in toluene and filtered through a short pad of silica gel to afford 225 mg (65 % yield) **75** as a dark red-brown solid.

MALDI-TOF MS (TCNQ): m/z (%) = 1856.2 (73), 1857.2 (100), 1858.2 (93), 1859.2 (51), 1860.2 (32), 1861.1 (19); calcd for C₁₄₄H₁₂₆: 1855 (62), 1856 (100), 1857 (81), 1858.0 (43), 1859.0 (17), 1860.0 (5).

UV/Vis (THF, C = 5.78 · 10⁻⁶ M): λ_{\max} (ϵ) = 480 nm (64160 M⁻¹cm⁻¹).

EA: calcd (%) for C₁₄₄H₁₂₆: C 93.16, H 6.84; found: C 92.94, H 6.95.

1-[3',4'-Di(4''-dodecylphenyl)-2',5'-diphenylphenyl]-3,5-di(2',3',4',5'-tetraphenylphenyl)benzene (74)

0.3 g (0.35 mmol) of 1,3-di(2',3',4',5'-tetraphenylphenyl)-5-ethynylbenzene (**72a**) and 0.3 g (0.42 mmol) of 3,4-bis(4-dodecylphenyl)-2,5-diphenyl cyclopentadienone (**55a**) were dissolved in 3 mL of *o*-xylene under an argon atmosphere and the resultant mixture heated for 10 h at 170 °C. After cooling, the solvent was removed under reduced pressure and the obtained residue was purified by column chromatography (silica gel, petroleum ether/dichloromethane 7:3) to afford 0.45 g (83% yield) **74**, as a white powder.

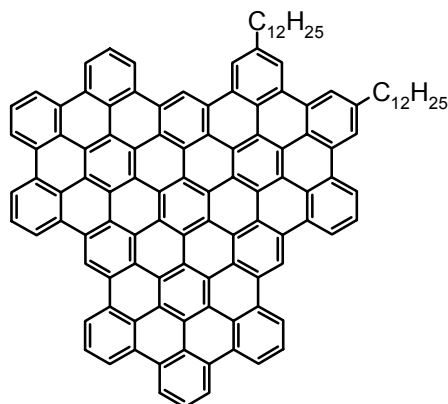
¹H NMR (500 MHz, C₂D₂Cl₄): δ = 7.14-6.95 (m, 15H, Ar-H), 6.85-6.45 (m, 49H, Ar-H), 2.30 (t, ³J(H,H) = 6.9 Hz, 2H, α-CH₂), 2.25 (t, ³J(H,H) = 6.9 Hz, 2H, α-CH₂), 1.40-0.95 (m, 40H, CH₂), 0.81 (t, ³J(H,H) = 6.0 Hz, 6H, CH₃).

¹³C NMR (125 MHz, C₂D₂Cl₄): δ = 142.17, 141.96, 141.77, 141.41, 140.77, 140.63, 140.55, 140.50, 140.38, 140.32, 139.77, 139.42, 139.31, 139.12, 138.96, 137.83, 137.55, 132.08, 132.00, 131.85, 131.78, 131.65, 131.42, 130.46, 130.41, 130.03, 129.95, 127.55, 127.48, 127.14, 127.03, 126.73, 126.27, 126.13, 125.79, 125.64, 125.56, 125.28, 35.62, 35.55, 32.23, 31.45, 31.43, 30.03, 29.99, 29.82, 29.68, 29.10, 28.99, 23.03, 14.53.

MS (FD, 8 kV): *m/z* (%): 1556.7 (100) [*M*⁺] (calcd for C₁₂₀H₁₁₄: 1556.3).

m.p.: 235 °C

EA: calcd (%) for C₁₂₀H₁₁₄: C 92.62, H 7.38; found: C 92.66, H 7.45.

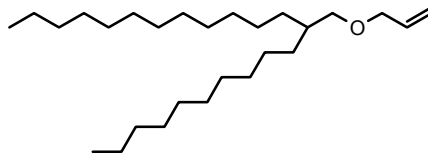
Didodecyl-C96 (76)

250 mg (0.16 mmol) of 1-[3',4'-di(4''-dodecylphenyl)-2',5'-diphenylphenyl]-3,5-di(2',3',4',5'-tetraphenylphenyl)benzene (**74**) was dissolved in 150 mL of dichloromethane in a 500 mL two-necked round bottom flask. A constant stream of argon was bubbled into the solution through a glass capillary. A solution of 2.35 g (14.5 mmol) iron(III) chloride in 15 mL of nitromethane was then added dropwise via syringe. Throughout the duration of the reaction, a constant stream of argon was bubbled through the mixture to remove HCl formed *in situ*. Fresh dichloromethane was added intermittently to replace that which had evaporated. The reaction was stirred for 18 h and then quenched by addition of 200 mL of methanol. The precipitate was collected by filtration, washed with methanol, and dried under vacuum to afford 230 mg (94% yield) **76** as a dark brown solid.

MALDI-TOF MS (TCNQ): m/z (%) = 1519.2 (78), 1520.2 (100), 1521.2 (69), 1522.2 (29), 1523.3 (20), 1524.3 (15); calcd for C₁₂₀H₇₈: 1518.6 (74), 1519.6 (100), 1520.6 (67), 1521.6 (30), 1522.6 (10), 1523.6 (3).

UV/Vis (solid state): λ_{max} = 485 nm.

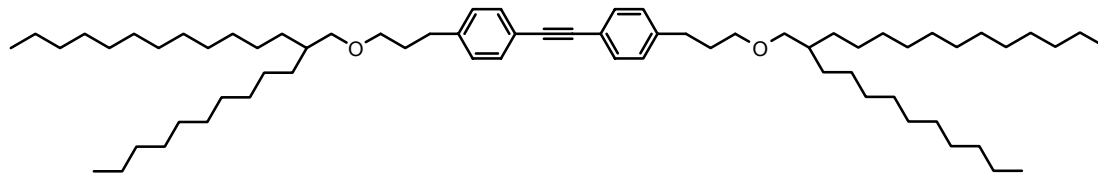
EA: calcd (%) for C₁₂₀H₇₈: C 94.83, H 5.17; found: C 94.08, H 5.84.

3-(2-Decyltetradecyloxy)propene (82a)

Into a 500 mL three-necked round bottom flask, equipped with a condenser, a magnetic stirring bar and dropping funnel, was introduced a mixture of 53.7 g (151.4 mmol) of 2-decyl-1-tetradecanol, 130 mL of 6 M aqueous NaOH solution and 5.14 g (15.1 mmol) of tetrabutylammonium hydrogen sulphate, while 34.8 g (454.7 mmol) of allyl chloride were added dropwise with stirring at 30 °C. The resulting mixture was heated to 45 °C and stirred in an inert atmosphere overnight. After cooling, the product was extracted with petroleum ether, washed three times with water, and the solvent removed under reduced pressure. Purification using column chromatography on silica gel with petroleum ether as the eluent afforded 47.5 g **82a** (79% yield) as a colorless liquid.

¹H NMR (250 MHz, CDCl₃): δ = 5.98-5.80 (m, 1H, =CH–), 5.30-5.18 (m, ³J(H,H)_{trans} = 17.1 Hz, 1H, C=CH₂), 5.17-5.07 (m, ³J(H,H)_{cis} = 10.3 Hz, 1H, C=CH₂), 3.93 (d, ³J(H,H) = 5.7 Hz, 2H, O–CH₂–), 3.27 (d, ³J(H,H) = 5.7 Hz, 2H, O–CH₂–), 1.62-1.42 (br, 1H, CH), 1.35-1.15 (br, 40H, CH₂) 0.86 (t, ³J(H,H) = 6.5 Hz, 6H, CH₃).

¹³C NMR (62.5 MHz, CDCl₃): δ = 135.29, 116.33, 73.67 (O–CH₂–), 71.95 (O–CH₂–), 38.35, 31.94, 31.47, 30.08, 29.68, 29.38, 26.88, 22.70, 14.10.

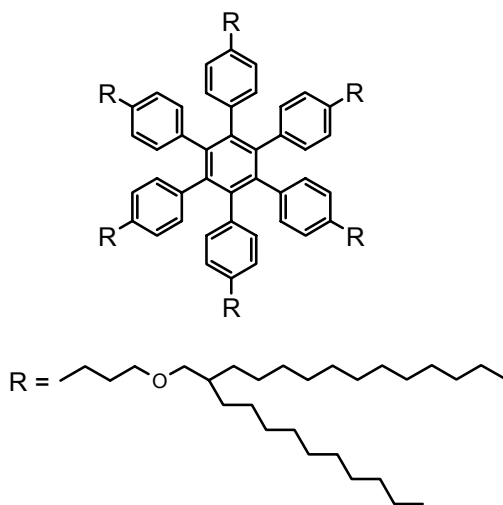
4,4'-Bis[3-(2-decyltetradecyloxy)propyl]diphenylacetylene (84a)

To 7.05 g (17.86 mmol) of 3-(2-decyltetradecyloxy)propene (**82a**) in a dry 100 mL two-necked round bottom flask, was slowly added 39.3 mL of a 0.5 M THF solution of 9-borabicyclo[3.3.1]nonane (9-BBN) under an argon atmosphere, and the resulting mixture stirred overnight at room temperature. 9 mL of a 3 M aqueous NaOH solution was added via syringe and then, after 15 min, 1.5 g (4.46 mmol) of 4,4'-dibromodiphenylacetylene (**63**) and 183 mg (0.22 mmol) of [PdCl₂(dppf)]·CH₂Cl₂ were added. The reaction mixture was stirred at room temperature for a further 5 hours. The product was extracted with dichloromethane, the organic phase washed with water three times and dried over magnesium sulfate. After evaporating the solvent, the residue was purified by column chromatography (silica gel, petroleum ether/dichloromethane 7:3) to afford 2.8 g **84a** (65% yield) as a colorless oil.

¹H NMR (250 MHz, C₂D₂Cl₄): δ = 7.37 (d, ³J(H,H) = 7.9 Hz, 4H, Ar-H), 7.11 (d, ³J(H,H) = 8.2 Hz, 4H, Ar-H), 3.30 (t, ³J(H,H) = 6.0 Hz, 4H, O-CH₂-), 3.18 (d, ³J(H,H) = 5.7 Hz, 4H, O-CH₂-), 2.62 (t, ³J(H,H) = 7.4 Hz, 4H, α-CH₂), 1.85-1.73 (m, 4H, β-CH₂), 1.53-1.39 (br, 2H, CH), 1.32-1.09 (br, 80H, CH₂), 0.80 (t, ³J(H,H) = 6.3 Hz, 12H, CH₃).

¹³C NMR (125 MHz, C₂D₂Cl₄): δ = 143.00, 131.86, 128.88, 120.87, 89.36, 74.42 (O-CH₂-), 70.01 (O-CH₂-), 38.46, 32.61, 32.24, 31.79, 31.40, 30.44, 30.03, 29.68, 27.17, 23.03, 14.53.

MS (FD, 8 kV): *m/z* (%): 968.0 (100) [*M*⁺] (calcd for C₆₈H₁₁₈O₂: 967.7).

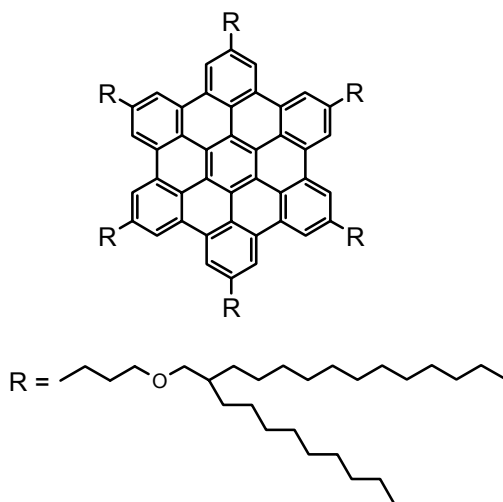
Hexa{4-[3-(2-decyltetradecyloxy)propyl]phenyl}benzene (85a)

In a 250 mL two-necked round bottom flask equipped with a reflux condenser, a solution of 2.5 g (2.58 mmol) of 4,4'-bis[3-(2-decyltetradecyloxy)propyl] diphenylacetylene (**84a**) and 100 mL of dioxane was degassed several times. 90 mg (0.26 mmol) of $\text{Co}_2(\text{CO})_8$ was then added under argon, and the resulting mixture heated at reflux for 5h. After cooling, the solvent was evaporated under vacuum and the residue purified by column chromatography (silica gel, petroleum ether/dichloromethane 7:3), yielding 2.0 g **85a** (80% yield) as colorless oil.

$^1\text{H NMR}$ (700 MHz, $\text{C}_2\text{D}_2\text{Cl}_4$): δ = 6.61 (d, $^3\text{J}(\text{H,H}) = 7.7$ Hz, 12H, Ar-H), 6.55 (d, $^3\text{J}(\text{H,H}) = 7.7$ Hz, 12H, Ar-H), 3.10-3.02 (m, 24H, O-CH₂-), 2.38-2.32 (m, 12H, α -CH₂), 1.60-1.54 (m, 12H, β -CH₂), 1.47-1.40 (m, 6H, CH), 1.26-1.16 (br, 240H, CH₂), 0.82 (t, $^3\text{J}(\text{H,H}) = 6.8$ Hz, 36H, CH₃).

$^{13}\text{C NMR}$ (175 MHz, $\text{C}_2\text{D}_2\text{Cl}_4$): δ = 140.28, 138.80, 138.26, 131.72, 126.75, 74.36 (O-CH₂-), 69.66 (O-CH₂-), 38.53, 32.24, 31.95, 31.73, 31.42, 30.46, 30.04, 29.68, 27.15, 23.02, 14.51;

MS (FD, 8 kV): m/z (%): 2903.3 (100) [M^+] (calcd for $\text{C}_{204}\text{H}_{354}\text{O}_6$: 2903.1).

Hexa[3-(2-decyltetradecyloxy)propyl]hexa-*peri*-hexabenzocoronene (86a)

A 250 mL two necked round bottom flask was charged with 0.15 g (0.052 mmol) of hexa{4-[3-(2-decyltetradecyloxy)propyl]phenyl}benzene (**85a**) and 100 mL of dichloromethane. Using a glass capillary, a constant stream of argon was bubbled through the solution. Then, 0.60 g (3.70 mmol) of iron(III) chloride dissolved in 5 mL of nitromethane was added dropwise using a syringe. After 3 hours, the reaction was quenched with a large excess of methanol. The product was extracted with dichloromethane and concentrated under reduced pressure. The residue was redissolved in toluene and filtered through a short pad of silica gel and dried under vacuum to afford 0.12 g **86a** (80% yield) as a yellow waxy solid.

¹H NMR (700 MHz, C₂D₂Cl₄): δ = 8.81 (s, 12H, Ar-H), 3.59 (t, ³J(H,H) = 6.0 Hz, 12H, O-CH₂-), 3.36 (d, ³J(H,H) = 6.0 Hz, 12H, O-CH₂-), 3.27-3.17 (br, 12H, α -CH₂), 2.28-2.20 (m, 12H, β -CH₂), 1.65-1.58 (m, 6H, CH), 1.42-1.05 (m, 240H, CH₂), 0.77 (t, ³J(H,H) = 7.3 Hz, 36H, CH₃).

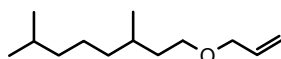
¹³C NMR (125 MHz, C₂D₂Cl₄): δ = 140.46, 130.28, 123.76, 122.09, 120.14, 74.83 (O-CH₂-), 70.70 (O-CH₂-), 38.55, 33.93, 32.52, 32.21, 31.85, 30.54, 30.08, 29.67, 27.27, 23.00, 14.49.

MALDI-TOF MS (TCNQ): m/z (%) = 2888.2 (51), 2889.1 (94), 2890.3 (100), 2891.3 (88), 2892.2 (56), 2893.2 (27), 2894.4 (11); calcd for $C_{204}H_{342}O_6$: m/z (%) = 2888.7 (37), 2889.7 (86), 2890.7 (100), 2891.7 (77), 2892.7 (45), 2893.7 (21), 2894.7 (8).

UV/Vis (THF, $C = 5.56 \cdot 10^{-6}$ M): λ_{\max} (ϵ) = 344 (75567), 360 (174883), 390 nm ($55056 \text{ M}^{-1}\text{cm}^{-1}$).

EA: calcd (%) for $C_{204}H_{342}O_6$: C 84.76, H 11.92; found: C 84.02, H 11.60.

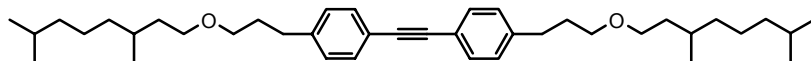
3-(3,7-Dimethyloctyloxy)propene (**82b**)



Into a 500 mL three-necked round bottom flask, equipped with a condenser, a magnetic stirring bar and dropping funnel, was introduced a mixture of 30.0 g (189.5 mmol) of 3,7-dimethyl-1-octanol, 160 mL of 6 M aqueous NaOH solution and 6.40 g (18.8 mmol) of tetrabutylammonium hydrogen sulphate, while 43.5 g (568.4 mmol) of allyl chloride were added dropwise with stirring at 30 °C. The resulting mixture was heated to 45 °C and stirred in an inert atmosphere overnight. After cooling, the product was extracted with dichloromethane, washed three times with water, and the solvent removed under reduced pressure. Purification using column chromatography (silica gel, petroleum ether/dichloromethane 9:1) afforded 29.5 g **82b** (78% yield) as a colorless liquid.

$^1\text{H NMR}$ (250 MHz, CDCl_3): δ = 5.97-5.79 (m, 1H, =CH-), 5.29-5.17 (m, $^3\text{J}(\text{H,H})_{\text{trans}} = 17.2$ Hz, 1H, C=CH₂), 5.17-5.07 (m, $^3\text{J}(\text{H,H})_{\text{cis}} = 10.3$ Hz, 1H, C=CH₂), 3.92 (d, $^3\text{J}(\text{H,H}) = 5.7$ Hz, 2H, O-CH₂-), 3.47-3.37 (m, 2H, O-CH₂-), 1.68-1.01 (m, 10H, CH, CH₂), 0.85 (d, $^3\text{J}(\text{H,H}) = 6.3$ Hz, 3H, CH₃), 0.83 (d, $^3\text{J}(\text{H,H}) = 6.6$ Hz, 6H, CH₃).

$^{13}\text{C NMR}$ (62.5 MHz, CDCl_3): δ = 135.10, 116.51, 71.77 (O-CH₂-), 68.70 (O-CH₂-), 39.25, 37.36, 36.76, 29.86, 27.92, 24.64, 22.65, 22.55, 19.64.

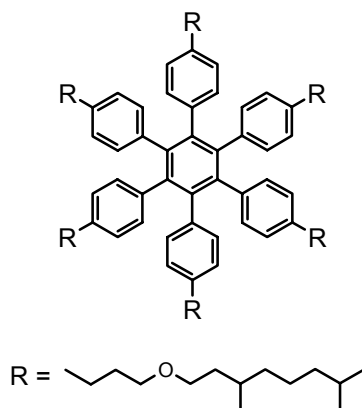
4,4'-Bis[3-(3,7-dimethyloctyloxy)propyl]diphenylacetylene (84b)

To 4.72 g (23.8 mmol) of 3-(3,7-dimethyloctyloxy)propene (**82b**) in a dry 100 mL two-necked round bottom flask, was slowly added 52.5 mL of a 0.5 M THF solution of 9-borabicyclo[3.3.1]nonane (9-BBN) under argon atmosphere, and the resulting mixture stirred overnight at room temperature. 12 mL of a 3 M aqueous NaOH solution was added via syringe and then, after 15 min, 2.0 g (5.95 mmol) of 4,4'-dibromodiphenylacetylene (**63**) and 250 mg (0.31 mmol) of [PdCl₂(dppf)]·CH₂Cl₂ were added. The reaction mixture was stirred at room temperature for another 5 hours. The product was extracted with dichloromethane, the organic phase washed with water three times and dried over magnesium sulfate. After evaporating the solvent, the residue was purified by column chromatography (silica gel, petroleum ether/dichloromethane 7:3) to afford 2.1 g **84b** (60% yield) as a colorless oil.

¹H NMR (700 MHz, C₂D₂Cl₄): δ = 7.41 (d, ³J(H,H) = 7.7 Hz, 4H, Ar-H), 7.13 (d, ³J(H,H) = 7.7 Hz, 4H, Ar-H), 3.42–3.32 (m, 8H, O–CH₂–), 2.65 (t, ³J(H,H) = 7.3 Hz, 4H, α-CH₂), 1.86–1.80 (m, 4H, β-CH₂), 1.61–1.54 (m, 2H, CH), 1.54–1.46 (m, 4H, CH₂), 1.38–1.04 (m, 14H, CH, CH₂), 0.88–0.82 (m, 18H, CH₃).

¹³C NMR (175 MHz, C₂D₂Cl₄): δ = 142.88, 131.88, 128.85, 120.94, 89.39, 69.89 (O–CH₂–), 69.47 (O–CH₂–), 39.62, 37.70, 37.08, 32.60, 31.41, 30.26, 28.25, 25.00, 23.07, 22.98, 20.09.

MS (FD, 8 kV): *m/z* (%): 575.5 (100) [*M*⁺] (calcd for C₄₀H₆₂O₂: 574.9).

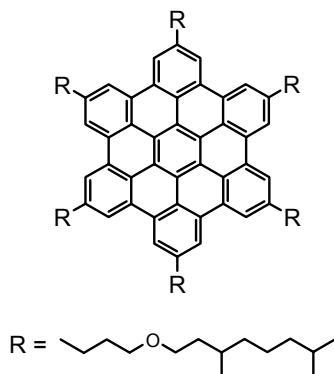
Hexa{4-[3-(3,7-dimethyloctyloxy)propyl]phenyl}benzene (85b)

In a 100 mL two-necked round bottom flask equipped with a reflux condenser, a solution of 0.63 g (1.10 mmol) of 4,4'-bis[3-(3,7-dimethyloctyloxy)propyl] diphenylacetylene (**84b**) and 50 mL of dioxane was degassed several times. 40 mg (0.12 mmol) of $\text{Co}_2(\text{CO})_8$ was then added under argon, and the resulting mixture heated at reflux for 5h. After cooling, the solvent was evaporated under vacuum and the residue purified by column chromatography (silica gel, petroleum ether/dichloromethane 8:2), yielding 0.50 g **85b** (80% yield) as colorless oil.

$^1\text{H NMR}$ (500 MHz, $\text{C}_2\text{D}_2\text{Cl}_4$, 100 °C): δ = 6.66 (d, $^3\text{J}(\text{H,H}) = 7.3$ Hz, 12H, Ar-H), 6.59 (d, $^3\text{J}(\text{H,H}) = 7.3$ Hz, 12H, Ar-H), 3.36-3.10 (m, 24H, O-CH₂-), 2.43-2.33 (m, 12H, α -CH₂), 1.65-1.45 (m, 30H, CH, CH₂), 1.35-1.05 (m, 42H, CH, CH₂), 0.91-0.78 (m, 54H, CH₃).

$^{13}\text{C NMR}$ (125 MHz, $\text{C}_2\text{D}_2\text{Cl}_4$): δ = 140.26, 138.81, 138.16, 131.71, 126.74, 69.57 (O-CH₂-), 69.33 (O-CH₂-), 39.60, 37.72, 37.11, 31.92, 31.36, 30.22, 28.24, 24.98, 23.07, 22.96, 20.04.

MS (FD, 8 kV): m/z (%): 1725.3 (100) [M^+] (calcd for $\text{C}_{120}\text{H}_{186}\text{O}_6$: 1724.8).

Hexa[3-(3,7-dimethyloctyloxy)propyl]hexa-*peri*-hexabenzocoronene (86b)

A 250 mL two-necked round bottom flask was charged with 0.25 g (0.14 mmol) of hexa{4-[3-(3,7-dimethyloctyloxy)propyl]phenyl}benzene (**85b**) and 100 mL of dichloromethane. Using a glass capillary, a constant stream of argon was bubbled through the solution. Then, 0.85 g (5.24 mmol) of iron(III) chloride dissolved in 8 mL of nitromethane was added dropwise using a syringe. After 45 minutes, the reaction was quenched with methanol and the product was extracted with dichloromethane and concentrated under reduced pressure. The resulting solid was reprecipitated from dichloromethane and methanol and dried under vacuum to afford 0.20 g **86b** (81% yield) as a yellow waxy solid.

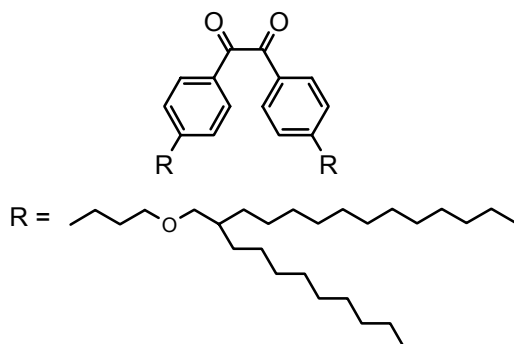
¹H NMR (500 MHz, C₂D₂Cl₄, 100 °C): δ = 8.64 (s, 12H, Ar-H), 3.67 (t, ³J(H,H) = 6.1 Hz, 12H, O-CH₂-), 3.59 (t, ³J(H,H) = 6.9 Hz, 12H, O-CH₂-), 3.21 (t, ³J(H,H) = 7.4 Hz, 12H, α-CH₂), 2.34-2.22 (m, 12H, β-CH₂), 1.79-1.70 (m, 6H, CH), 1.69-1.60 (m, 6H, CH), 1.60-1.48 (m, 12H, CH₂), 1.40-1.12 (m, 36H, CH₂), 0.98 (d, ³J(H,H) = 6.7 Hz, 18H, CH₃), 0.87 (d, ³J(H,H) = 6.4 Hz, 36H, CH₃).

¹³C NMR (125 MHz, C₂D₂Cl₄): δ = 139.92, 129.88, 123.35, 121.60, 119.67, 70.73 (O-CH₂-), 69.93 (O-CH₂-), 39.65, 37.87, 37.23, 33.86, 32.49, 30.48, 28.27, 25.05, 23.10, 23.00, 20.20;

MALDI-TOF MS (TCNQ): *m/z* (%) = 1711.5 (79), 1712.5 (100), 1713.5 (82), 1714.5 (37), 1715.5 (15), 1716.4 (8); calcd for C₁₂₀H₁₇₄O₆: *m/z* (%) = 1711.3 (73), 1712.3 (100), 1713.3 (69), 1714.3 (31), 1715.4 (11), 1716.4 (3).

UV/Vis (THF, C = 5.63 · 10⁻⁶ M): λ_{max} (ε) = 343 (83333), 359 (193141), 389 nm (61834 M⁻¹cm⁻¹).

EA: calcd (%) for C₁₂₀H₁₇₄O₆: C 84.15, H 10.24; found: C 84.06, H 10.29.

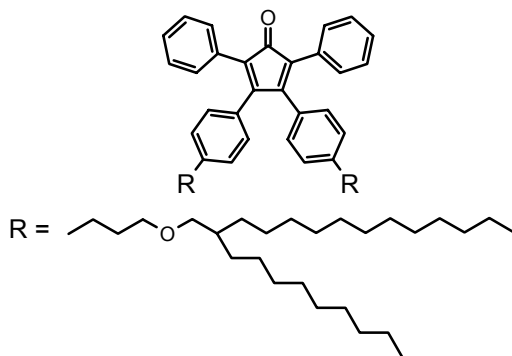
4,4'-Bis[3-(2-decyltetradecyloxy)propyl]benzil (87a)

To 13.3 g (33.69 mmol) of 3-(2-decyltetradecyloxy)propene (**82a**) in a dry 250 mL two-necked round bottom flask was slowly added 75.0 mL of a 0.5 M THF solution of 9-borabicyclo[3.3.1]nonane (9-BBN) under an argon atmosphere, and the resulting mixture stirred overnight at room temperature. 17.0 mL of 3 M aqueous NaOH solution was added via syringe, and after 15 min 3.1 g (8.42 mmol) of 4,4'-dibromobenzil and 0.35 g (0.43 mmol) of [PdCl₂(dppf)]·CH₂Cl₂ were added, respectively. The reaction mixture was stirred at room temperature for another 5 hours. The product was extracted with dichloromethane, the organic phase washed with water three times and dried over magnesium sulfate. After evaporating the solvent, the residue was purified by column chromatography (silica gel, petroleum ether/dichloromethane 3:2) to afford 6.3 g **87a** (75% yield) as a colorless oil.

¹H NMR (500 MHz, C₂D₂Cl₄): δ = 7.80 (d, ³J(H,H) = 7.6 Hz, 4H, Ar-H), 7.27 (d, ³J(H,H) = 7.9 Hz, 4H, Ar-H), 3.30 (t, ³J(H,H) = 6.0 Hz, 4H, O-CH₂-), 3.18 (d, ³J(H,H) = 5.8 Hz, 4H, O-CH₂-), 2.69 (t, ³J(H,H) = 7.5 Hz, 4H, α-CH₂), 1.85-1.76 (m, 4H, β-CH₂), 1.51-1.42 (m, 2H, CH), 1.30-1.10 (br, 80H, CH₂), 0.80 (t, ³J(H,H) = 5.8 Hz, 12H, CH₃).

¹³C NMR (125 MHz, C₂D₂Cl₄): δ = 194.70 (C=O), 150.84, 131.20, 130.34, 129.47, 74.51 (O-CH₂-), 69.88 (O-CH₂-), 38.52, 33.02, 32.19, 31.84, 31.31, 31.15, 30.38, 29.97, 29.93, 29.61, 27.17, 22.97, 14.44.

MS (FD, 8 kV): *m/z* (%): 998.7 (100) [*M*⁺] (calcd for C₆₈H₁₁₈O₄: 999.7).

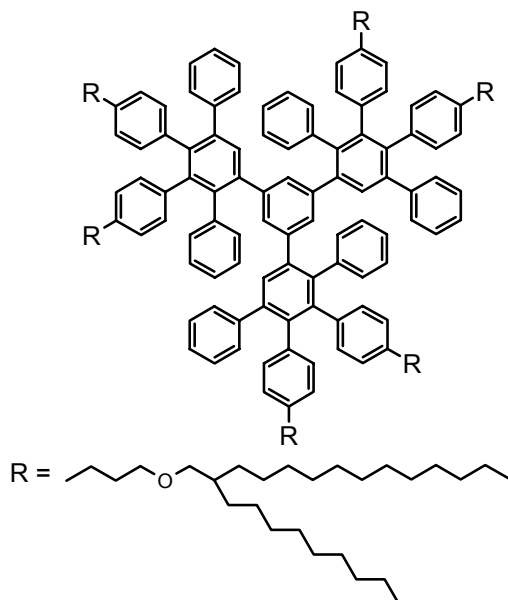
**3,4-Bis{4-[3-(2-decyltetradecyloxy)propyl]phenyl}-2,5-diphenyl
cyclopentadienone (88a)**

6.0 g (6.0 mmol) of 4,4'-bis[3-(2-decyltetradecyloxy)propyl]benzil (**87a**) and 1.26 g (6.0 mmol) of 1,3-diphenyl-2-propanone were dissolved in 20 mL of *tert*-butanol under argon, heated to 80 °C, and then 4.1 mL of a 0.8 M solution of tetrabutylammoniumhydroxide in methanol was quickly injected. After 35 minutes, the reaction was quenched by addition of water. The product was extracted with dichloromethane, the organic phase washed with water three times and dried over magnesium sulfate. After evaporating the solvent, the residue was purified by column chromatography (silica gel, petroleum ether/dichloromethane 1:1) to afford 4.5 g **88a** (64 % yield) as a purple oil.

¹H NMR (500 MHz, C₂D₂Cl₄): δ = 7.24-7.13 (m, 10H, Ar-H), 6.91 (d, ³J(H,H) = 7.9 Hz, 4H, Ar-H), 6.74 (d, ³J(H,H) = 7.9 Hz, 4H, Ar-H), 3.25 (t, ³J(H,H) = 6.0 Hz, 4H, O-CH₂-), 3.16 (d, ³J(H,H) = 5.8 Hz, 4H, O-CH₂-), 2.56 (t, ³J(H,H) = 7.3 Hz, 4H, α-CH₂), 1.82-1.72 (m, 4H, β-CH₂), 1.51-1.42 (br, 2H, CH), 1.35-1.12 (br, 80H, CH₂), 0.80 (t, ³J(H,H) = 6.6 Hz, 12H, CH₃).

¹³C NMR (125 MHz, C₂D₂Cl₄): δ = 201.19 (C=O), 155.21, 143.10, 131.30, 130.43, 129.69, 128.32, 128.24, 127.59, 125.07, 74.41 (O-CH₂-), 69.99 (O-CH₂-), 38.45, 32.41, 32.23, 31.72, 31.24, 30.44, 30.02, 29.67, 27.13, 23.03, 14.53.

MS (FD, 8 kV): *m/z* (%): 1172.7 (100) [*M*⁺] (calcd for C₈₃H₁₂₈O₃: 1173.9).

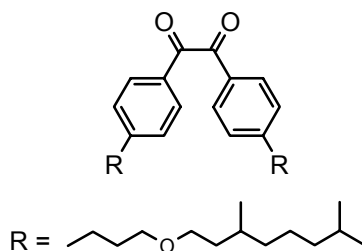
1,3,5-Tris{3',4'-di[4''-(3-(2-decyltetradecyloxy)propyl)phenyl]-2',5'-diphenylphenyl}benzene (89a)

57 mg (0.38 mmol) of 1,3,5-triethynylbenzene and 1.60 g (1.36 mmol) of 3,4-bis{4-[3-(2-decyltetradecyloxy)propyl]phenyl}-2,5-diphenylcyclopentadienone (**88a**) were dissolved in 10 mL of *o*-xylene and heated under an argon atmosphere for 17 h at 170 °C (oil bath temperature). After cooling to room temperature, the solvent was removed under reduced pressure and the residue purified by column chromatography (silica gel, petroleum ether/dichloromethane 7:3) to afford 1.30 g (95% yield) **89a** as a colorless, highly viscous oil.

¹H NMR (700 MHz, C₂D₂Cl₄): δ = 7.12-6.98 (m, 15H, Ar-H), 6.76-6.46 (m, 45H, Ar-H), 3.12-3.00 (m, 24H, O-CH₂-), 2.42-2.30 (m, 12H, α-CH₂), 1.66-1.52 (m, 12H, β-CH₂), 1.47-1.39 (m, 6H, CH), 1.30-1.05 (br, 240H, CH₂), 0.80 (t, ³J(H,H) = 6.8 Hz, 36H, CH₃).

¹³C NMR (175 MHz, C₂D₂Cl₄): δ = 142.15, 141.63, 140.68, 140.43, 139.15, 138.95, 138.61, 138.07, 137.79, 132.05, 131.73, 131.66, 131.42, 130.45, 129.97, 127.46, 127.14, 127.06, 126.83, 126.14, 125.68, 74.36 (O-CH₂-), 69.69 (O-CH₂-), 38.46, 32.22, 31.97, 31.93, 31.72, 31.36, 30.45, 30.02, 29.98, 29.67, 27.13, 23.02, 14.51.

MALDI-TOF MS: *m/z* (%): 3587.9 (100) [*M*⁺] (calcd for C₂₅₈H₃₉₀O₆: 3588.0).

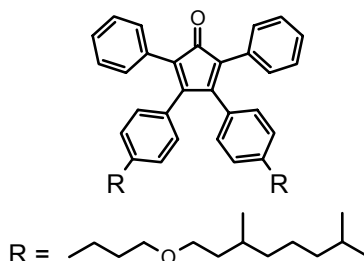
4,4'-Bis[3-(3,7-dimethyloctyloxy)propyl]benzil (87b)

To 16.2 g (81.67 mmol) of 3-(3,7-dimethyloctyloxy)propene (**82b**) in a dry 500 mL two-necked round bottom flask was slowly added 179.0 mL of a 0.5 M THF solution of 9-borabicyclo[3.3.1]nonane (9-BBN) under an argon atmosphere, and the resulting mixture stirred overnight at room temperature. 40.8 mL of 3 M aqueous NaOH solution was added via syringe, and after 15 min, 7.5 g (20.38 mmol) of 4,4'-dibromobenzil and 0.83 g (1.02 mmol) of [PdCl₂(dppf)]·CH₂Cl₂ were added, respectively. The reaction mixture was stirred at room temperature for another 5 hours. The product was extracted with dichloromethane, the organic phase washed with water three times and dried over magnesium sulfate. After evaporating the solvent, the residue was purified by column chromatography (silica gel, dichloromethane) to afford 7.4 g **87b** (60% yield) as a colorless oil.

¹H NMR (250 MHz, THF-d₈): δ = 7.92 (d, ³J(H,H) = 8.2 Hz, 4H, Ar-H), 7.26 (d, ³J(H,H) = 8.2 Hz, 4H, Ar-H), 3.45-3.30 (m, 8H, O-CH₂-), 2.74 (t, ³J(H,H) = 7.7 Hz, 4H, α-CH₂), 1.90-1.80 (m, 4H, β-CH₂), 1.65-1.05 (m, 20H, CH, CH₂), 0.92-0.82 (m, 18H, CH₃).

¹³C NMR (125 MHz, THF-d₈): δ = 197.57 (C=O), 148.25, 130.58, 129.59, 129.11, 70.35 (O-CH₂-), 69.78 (O-CH₂-), 40.28, 38.35, 37.86, 33.24, 32.19, 30.92, 28.92, 25.64, 23.06, 22.96, 20.09.

MS (FD, 8 kV): *m/z* (%): 606.9 (100) [*M*⁺] (calcd for C₄₀H₆₂O₄: 606.9).

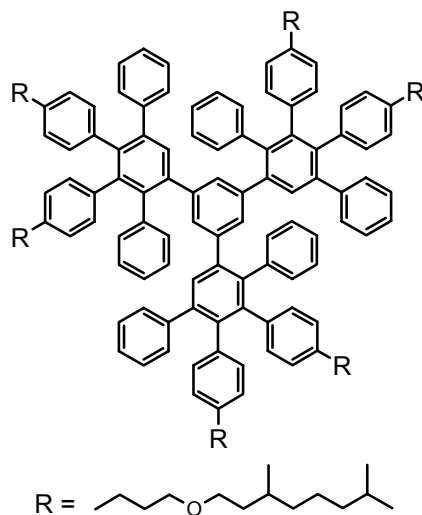
**3,4-Bis{4-[3-(3,7-dimethyloctyloxy)propyl]phenyl}-2,5-diphenyl
cyclopentadienone (88b)**

4.20 g (6.9 mmol) of 4,4'-bis[3-(3,7-dimethyloctyloxy)propyl]benzil (**87b**) and 1.46 g (6.9 mmol) of 1,3-diphenyl-2-propanone were dissolved in 20 mL of *tert*-butanol under argon, heated to 80 °C, and then 4.8 mL of a 0.8 M solution of tetrabutylammoniumhydroxide in methanol was quickly injected. After 50 minutes, the reaction was quenched by adding of water. The product was extracted with dichloromethane, the organic phase washed with water three times and dried over magnesium sulfate. After evaporating the solvent, the residue was purified by column chromatography (silica gel, petroleum ether/dichloromethane 3:7) to afford 3.8 g **88b** (71 % yield) as a purple oil.

¹H NMR (500 MHz, C₂D₂Cl₄): δ = 7.22-7.12 (m, 10H, Ar-H), 6.91 (d, ³J(H,H) = 7.9 Hz, 4H, Ar-H), 6.74 (d, ³J(H,H) = 7.6 Hz, 4H, Ar-H), 3.38-3.24 (m, 8H, O-CH₂-), 2.56 (t, ³J(H,H) = 7.6 Hz, 4H, α-CH₂), 1.80-1.72 (m, 4H, β-CH₂), 1.56-0.98 (m, 20H, CH, CH₂), 0.82-0.76 (m, 18H, CH₃).

¹³C NMR (125 MHz, C₂D₂Cl₄): δ = 201.17 (C=O), 155.20, 143.03, 131.30, 130.42, 129.69, 128.31, 128.21, 127.60, 125.09, 69.91 (O-CH₂-), 69.49 (O-CH₂-), 39.57, 37.67, 37.04, 32.40, 31.22, 30.22, 28.22, 24.96, 23.06, 22.96, 20.06.

MS (FD, 8 kV): *m/z* (%): 781.2 (100) [*M*⁺] (calcd for C₅₅H₇₂O₃: 781.2).

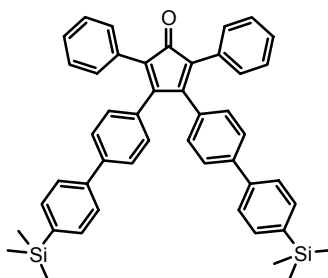
1,3,5-Tris{3',4'-di[4''-(3-(3,7-dimethyloctyloxy)propyl)phenyl]-2',5'-diphenylphenyl}benzene (89b)

70 mg (0.47 mmol) of 1,3,5-triethynylbenzene and 1.40 g (1.79 mmol) of 3,4-bis{4-[3-(3,7-dimethyloctyloxy)propyl]phenyl}-2,5-diphenylcyclopentadienone (**88b**) were dissolved in 15 mL of *o*-xylene and heated under an argon atmosphere for 22 h at 170 °C (oil bath temperature). After cooling to room temperature, the solvent was removed under reduced pressure and the residue purified by column chromatography (silica gel, petroleum ether/dichloromethane 7:3 to dichloromethane then THF) to afford 0.87 g (78% yield) **89b** as a colorless, highly viscous oil.

¹H NMR (500 MHz, C₂D₂Cl₄): δ = 7.13-6.95 (m, 15H, Ar-H), 6.80-6.45 (m, 45H, Ar-H), 3.32-2.98 (m, 24H, O-CH₂-), 2.45-2.25 (m, 12H, α-CH₂), 1.70-0.95 (m, 72H, CH, CH₂), 0.85-0.73 (m, 54H, CH₃).

¹³C NMR (125 MHz, C₂D₂Cl₄): δ = 142.16, 141.61, 140.66, 140.44, 139.16, 138.89, 138.55, 138.12, 137.82, 132.05, 131.74, 131.67, 131.39, 130.44, 129.98, 127.46, 127.11, 127.05, 126.80, 126.15, 125.67, 69.62 (O-CH₂-), 69.38 (O-CH₂-), 39.59, 37.70, 37.09, 31.95, 31.33, 30.24, 28.22, 24.96, 23.05, 22.96, 20.06.

MS (FD, 8 kV): *m/z* (%): 2408.9 (100) [*M*⁺] (calcd for C₁₇₄H₂₂₂O₆: 2409.7).

3,4-Bis[4'-(4''-trimethylsilylphenyl)phenyl]-2,5-diphenylcyclopentadienone (94)

1.2 g (2.2 mmol) of 3,4-bis(4-bromophenyl)-2,5-diphenylcyclopentadienone (**67**) and 2.1 g (10.8 mmol) of 4-(trimethylsilyl)phenylboronic acid were dissolved in 44 mL of toluene under argon atmosphere, then 22 mL of a 1 M aqueous potassium carbonate solution and 0.26 g (0.22 mmol) of tetrakis(triphenylphosphine)palladium(0) were added. The resultant mixture was heated under argon for 15 h at 95 °C. After cooling, the product was extracted with dichloromethane, the organic phase washed with water three times and dried over magnesium sulfate. After evaporating the solvent, the residue was purified by column chromatography (silica gel, petroleum ether/dichloromethane 2:1) to afford 1.4 g (93% yield) **94** as a purple solid.

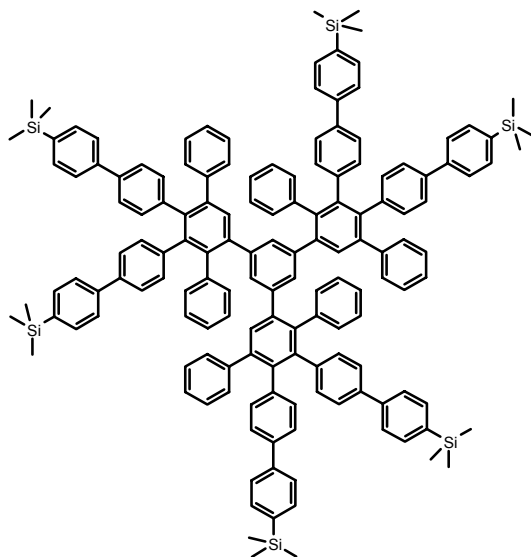
¹H NMR (500 MHz, CD₂Cl₂): δ = 7.64-7.58 (m, 8H, Ar-H), 7.49 (d, ³J(H,H) = 8.2 Hz, 4H, Ar-H), 7.36-7.26 (m, 10H, Ar-H), 7.09 (d, ³J(H,H) = 8.2 Hz, 4H, Ar-H), 0.31 (s, 18H, CH₃).

¹³C NMR (125 MHz, CD₂Cl₂): δ = 200.47 (C=O), 154.61, 141.40, 140.70, 140.35, 134.29, 132.58, 131.52, 130.62, 130.42, 128.45, 127.90, 126.78, 126.46, 126.13, -1.08 (Si-CH₃).

MS (FD, 8 kV): *m/z* (%): 680.9 (100) [*M*⁺] (calcd for C₄₇H₄₄OSi₂: 681.0).

m.p.: 218 °C

EA: calcd (%) for C₄₇H₄₄OSi₂: C 82.89, H 6.51; found: C 83.01, H 6.51.

1,3,5-Tris{3',4'-di[4''-(4'''-trimethylsilylphenyl)phenyl]-2',5'-diphenylphenyl}benzene (95)

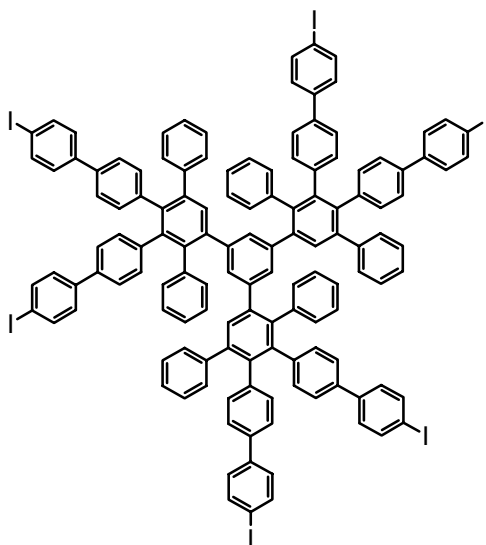
80 mg (0.53 mmol) of 1,3,5-triethynylbenzene and 1.2 g (1.76 mmol) of 3,4-bis[4'-(4''-trimethylsilylphenyl)phenyl]-2,5-diphenylcyclopentadienone (**94**) were dissolved in 8 mL of *o*-xylene under an argon atmosphere and the resultant mixture heated for 16 h at 170 °C. After cooling, the solvent was removed under reduced pressure and the residue purified by column chromatography (silica gel, petroleum ether/dichloromethane 3:1) to afford 0.98 g (87% yield) **95**, as a colorless solid.

¹H NMR (500 MHz, C₂D₂Cl₄): δ = 7.48-7.35 (m, 24H, Ar-H), 7.20-7.02 (m, 27H, Ar-H), 6.92-6.60 (m, 33H, Ar-H), 0.19 (s, 54H, CH₃).

¹³C NMR (125 MHz, C₂D₂Cl₄): δ = 141.84, 141.09, 140.89, 140.85, 140.76, 140.71, 140.64, 140.19, 140.06, 139.68, 139.32, 139.26, 138.58, 137.37, 137.04, 134.01, 132.40, 132.31, 132.04, 131.82, 130.42, 130.11, 127.70, 127.32, 126.46, 126.18, 125.98, 125.46, 125.15, -0.75 (Si-CH₃).

MS (FD, 8 kV): *m/z* (%): 2109.5 (100) [*M*⁺] (calcd for C₁₅₀H₁₃₈Si₄: 2109.3).

EA: calcd (%) for C₁₅₀H₁₃₈Si₆: C 85.42, H 6.59; found: C 85.36, H 7.35.

1,3,5-Tris{3',4'-di[4''-(4'''-iodophenyl)phenyl]-2',5'-diphenylphenyl}benzene (96)

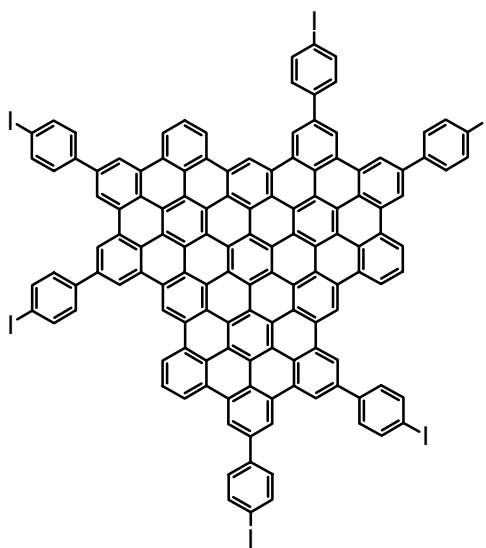
0.90 g (0.43 mmol) of 1,3,5-tris{3',4'-di[4''-(4'''-trimethylsilylphenyl)phenyl]-2',5'-diphenylphenyl}benzene (**95**) was dissolved in 200 mL of degassed chloroform, then 5.2 mL of a 1 M solution of iodine monochloride in dichloromethane was slowly added via syringe. The mixture was stirred for 2h under argon, then 100 mL of a 20% aqueous sodium disulphite solution was added to quench the reaction. The organic phase was washed with water three times, dried over magnesium sulfate and the solvent removed under reduced pressure. The residue was reprecipitated from chloroform and methanol, filtered and washed with methanol, and dried under vacuum to afford 0.95 g (92% yield) **96** as a colorless solid.

¹H NMR (500 MHz, C₂D₂Cl₄): δ = 7.62-7.50 (m, 12H, Ar-H), 7.18-6.92 (m, 40H, Ar-H), 6.86-6.58 (m, 32H, Ar-H).

¹³C NMR (125 MHz, C₂D₂Cl₄): δ = 141.71, 140.87, 140.80, 140.69, 140.58, 140.42, 140.38, 140.07, 139.97, 139.24, 138.42, 137.94, 137.91, 136.54, 136.26, 132.43, 132.35, 131.98, 131.90, 130.37, 130.05, 128.86, 127.72, 127.34, 126.50, 126.02, 125.41, 125.11, 93.00 (C-I), 92.92 (C-I).

MS (FD, 8 kV): *m/z* (%): 2431.5 (100) [*M*⁺] (calcd for C₁₃₂H₈₄I₆: 2431.6).

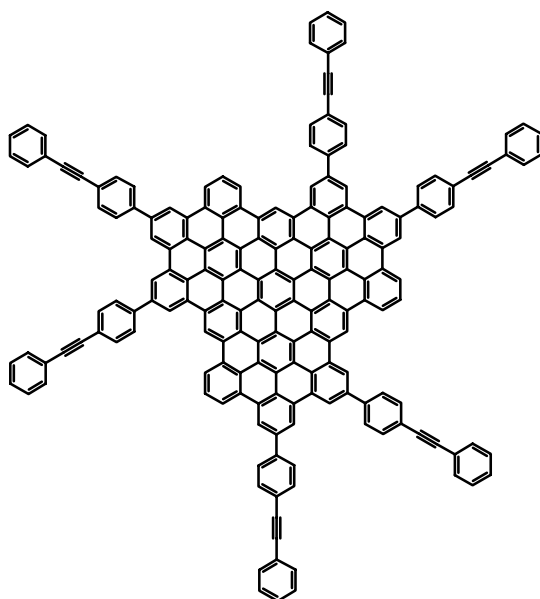
EA: calcd (%) for C₁₃₂H₈₄I₆: C 65.20, H 3.48; found: C 65.11, H 3.57.

Hexa(4-iodophenyl)-C96 (97)

0.25 g (0.10 mmol) of 1,3,5-tris[3',4'-di[4''-(4'''-iodophenyl)phenyl]-2',5'-diphenylphenyl}benzene (**96**) was dissolved in 200 mL of dichloromethane in a 500 mL two-necked round bottom flask. A constant stream of argon was bubbled into the solution through a glass capillary. A solution of 1.80 g (11.1 mmol) iron(III) chloride in 12 mL of nitromethane was then added dropwise via syringe. Throughout the duration of the reaction, a constant stream of argon was bubbled through the mixture to remove HCl formed *in situ*. Fresh dichloromethane was added intermittently to replace that which had evaporated. The reaction was stirred for 18 h and then quenched by addition of methanol. The precipitate was collected by filtration, washed with methanol, and dried under vacuum to afford 0.23 g (93% yield) **97** as a dark red-brown solid.

MALDI-TOF MS (TCNQ): m/z (%) = 2394.3 (72), 2395.3 (100), 2396.3 (74), 2397.3 (36), 2398.3 (18), 2399.3 (10); calcd for $C_{132}H_{48}I_6$: 2393.8 (68), 2394.8 (100), 2395.8 (73), 2396.8 (36), 2397.8 (13), 2398.8 (4).

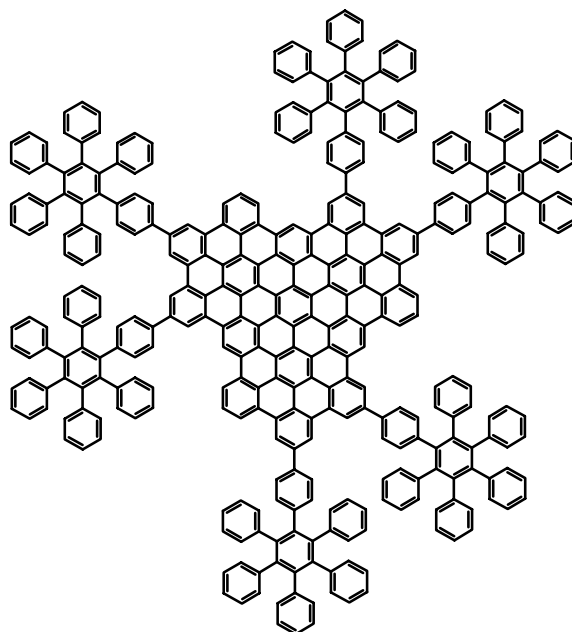
EA: calcd (%) for $C_{132}H_{48}I_6$: C 66.19, H 2.02; found: C 66.85, H 1.84.

Hexa[4-(ethynylphenyl)phenyl]-C96 (99)

A dry 25 mL Schlenk tube was charged with 200 mg (0.083 mmol) of hexa(4-iodophenyl)-C96 (**97**), 15 mg (0.013 mmol, 2.5 mol% per iodo) tetrakis(triphenylphosphine)palladium(0), 5 mg (0.026 mmol, 5 mol% per iodo) copper(I)iodide and 5 mL of piperidine. The mixture was degassed by two "freeze-pump-thaw" cycles and then 102 mg (1 mmol) phenylacetylene was added. The mixture was heated at 55 °C under argon for 24 h. After cooling, the mixture was poured into 150 mL methanol. The precipitate was collected by filtration, washed with methanol and dried under vacuum to afford 182 mg (97% yield) **99** as a dark red-brown powder.

MALDI-TOF MS (TCNQ): m/z (%) = 2239.0 (57), 2240.0 (100), 2241.0 (99), 2242.0 (71), 2243.0 (42), 2244.0 (23), 2245.0 (14); calcd for C₁₈₀H₇₈: 2238.6 (50), 2239.6 (99.9), 2240.6 (100), 2241.6 (66), 2242.6 (33), 2243.6 (13), 2244.6 (4).

EA: calcd (%) for C₁₈₀H₇₈: C 96.49, H 3.51; found: C 95.48, H 4.18.

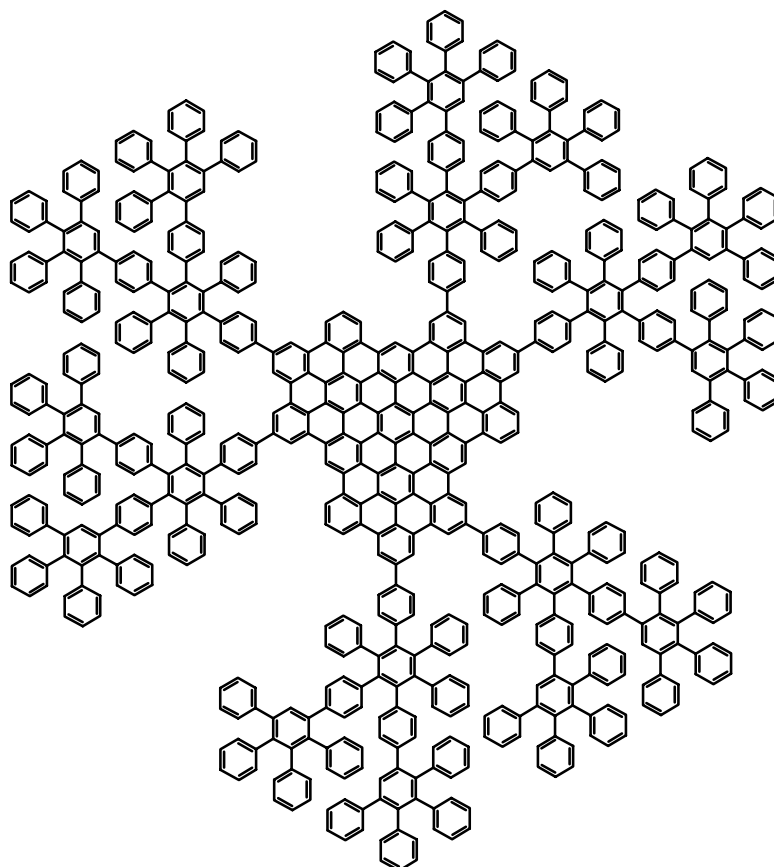
Dendronized superphenalene (91)

60 mg (0.027 mmol) of hexa[4-(ethynylphenyl)phenyl]-C96 (**99**) and 0.25 g (0.65 mmol) of tetraphenylcyclopentadienone were suspended in 2 mL of diphenyl ether under an argon atmosphere and the resulting mixture heated for 3 days at 250 °C using a thermostatically-controlled heating mantle. After cooling to room temperature, methanol was added to the reaction mixture, and the precipitate collected by filtration, washed with methanol and dried. The crude product was purified by column chromatography (silica gel, petroleum ether/dichloromethane 7:3 to 1:1, then THF) and dried under vacuum to afford 98 mg (84% yield) **91** as a dark red-brown solid.

MALDI-TOF MS (TCNQ): m/z (%) = 4379.6; calculated average mass for $C_{348}H_{198}$: 4379.4.

UV/Vis (THF, $C = 5.21 \cdot 10^{-6}$ M): λ_{max} (ϵ) = 488 nm (137240 $M^{-1}cm^{-1}$).

EA*: calcd (%) for $C_{348}H_{198}$: C 95.44, H 4.56; found: C 92.07, H 5.11.

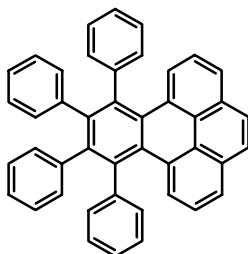
Dendronized superphenalene (92)

50 mg (0.022 mmol) of hexa[4-(ethynylphenyl)phenyl]-C96 (**99**) and 0.46 g (0.40 mmol) of **102** were suspended in 2 mL of diphenyl ether under an argon atmosphere and the resulting mixture heated for 5 days at 280 °C using a thermostatically-controlled heating mantle. After cooling to room temperature, methanol was added to the reaction mixture, and the precipitate collected by filtration, washed with methanol and dried. The crude product was purified by column chromatography (silica gel, petroleum ether/dichloromethane 7:3 to 1:1, then THF) and dried under vacuum to afford 135 mg (68 % yield) **92** as a dark red-brown solid.

MALDI-TOF MS (TCNQ): m/z (%) = 8946.2; calculated average mass for $C_{708}H_{438}$: 8945.2.

UV/Vis (THF, $C = 5.02 \cdot 10^{-6}$ M): λ_{max} (ϵ) = 486 nm (85800 $M^{-1}cm^{-1}$).

EA*: calcd (%) for $C_{708}H_{438}$: C 95.06, H 4.94; found: C 90.96, H 6.76.

9,10,11,12-Tetraphenylbenzo[e]pyrene (108).

0.406 g (1.0 mmol) of 1,3-diphenylcyclopenta[e]pyren-2-one (**106**) and 0.196 g (1.1 mmol) of diphenylacetylene were dissolved in 0.5 mL of diphenyl ether under an argon atmosphere and heated at 240 °C for 6 hours. After cooling, the crude product was purified by column chromatography (silica gel, petroleum ether/dichloromethane 5:1) to afford 0.194 g (35 % yield) **108** as a white solid.

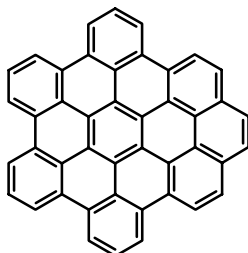
¹H NMR (250 MHz, CD₂Cl₂): δ = 7.97 (br, 2H), 7.95 (dd, ³J(H,H) = 7.6 Hz, ⁴J(H,H) = 1.0 Hz, 2H), 7.88 (dd, ³J(H,H) = 8.2 Hz, ⁴J(H,H) = 1.0 Hz, 2H), 7.39 (dd, ³J(H,H) = 8.1 Hz, 2H), 7.15-7.10 (m, 10H), 6.94-6.92 (m, 6H), 6.82-6.80 (m, 4H).

¹³C NMR (62.5 MHz, CD₂Cl₂): δ = 143.66, 141.25, 140.97, 138.44, 132.36, 131.90, 131.67, 131.13, 130.20, 128.35, 128.26, 127.29, 126.87, 126.52, 125.71, 125.58, 125.56, 124.78.

MS (FD, 8KV): m/z (%): 556.4 (100) [M⁺] (calcd for C₄₄H₂₈: 556.7).

UV/Vis (THF, C = 4.91 · 10⁻⁶ M): λ_{max} (ε) = 310 nm (49990 M⁻¹cm⁻¹).

EA: calcd (%) for C₄₄H₂₈: C 94.93, H 5.07; found: C 95.00, H 4.99.

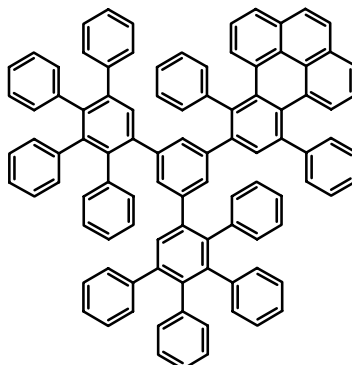
C₄₄H₁₈ PAH (103)

1.36 g (3.76 mmol) of copper(II) triflate was dried by heating under vacuum for 2h. After cooling, 0.50 g (3.76 mmol) of aluminium(III) chloride and 60 mL of carbon disulfide were added under an argon atmosphere. The mixture was suspended by intense stirring and 70 mg (0.13 mmol) of 9,10,11,12-tetraphenylbenzo[e]pyrene (**108**) dissolved in 5 mL carbon disulfide was added dropwise via syringe. The reaction was stirred for 20 h and then quenched by adding 150 mL methanol. The precipitate was collected by filtration, washed with methanol and dichloromethane, and dried under vacuum to afford 60 mg (87% yield) **103** as a dark brown solid.

MALDI-TOF MS (TCNQ): m/z (%) = 545.7 (100), 546.7 (69), 547.7 (29), 548.7 (8); calcd. for C₄₄H₁₈: m/z (%) = 546.0 (100), 547.1 (49), 548.1 (12), 549.1 (2).

UV/Vis (1,2,4-trichlorobenzene): λ_{\max} = 348, 363, 380, 414, 438.

EA: calcd (%) for C₄₄H₁₈: C 96.68, H 3.32; found: C 96.45, H 3.28.

1-(9',12'-Diphenylbenzo[e]pyren-11'-yl)-3,5-di(2',3',4',5'-tetraphenylphenyl)benzene (109)

300 mg (0.35 mmol) of 1,3-di(2',3',4',5'-tetraphenylphenyl)-5-ethynylbenzene (**72a**) and 185 mg (0.46 mmol) 1,3-diphenylcyclopenta[e]pyren-2-one (**106**) were dissolved in 3 mL of *o*-xylene under an argon atmosphere and the resultant mixture heated for 18 h at 170 °C. After cooling to room temperature, methanol was added to the reaction mixture. The precipitate was collected by filtration, washed with methanol and THF, and dried under vacuum to afford 320 mg (74 % yield) **109** as a colorless solid.

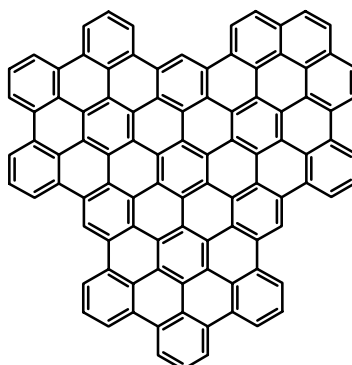
¹H NMR (500 MHz, C₂D₂Cl₄, 110 °C): δ = 8.20-7.65 (m, 9H), 7.45-6.60 (m, 55H).

¹³C NMR (125 MHz, C₂D₂Cl₄, 110 °C): δ = 145.34, 142.87, 142.19, 141.73, 140.87, 140.74, 140.53, 140.48, 140.42, 139.35, 139.26, 137.81, 137.73, 136.58, 133.19, 132.34, 132.01, 131.81, 131.76, 131.30, 131.05, 130.38, 130.21, 130.10, 129.98, 129.69, 128.99, 128.92, 128.68, 128.63, 128.37, 127.87, 127.43, 127.24, 127.18, 127.02, 126.84, 126.56, 126.44, 126.22, 126.01, 125.86, 125.51, 125.46, 125.40, 125.26, 124.66, 124.39, 123.96.

MS (FD, 8 kV): *m/z* (%) = 1241.8 (100) [M⁺] (calcd for C₉₈H₆₄: 1241.6).

UV/Vis (THF, C = 5.16 · 10⁻⁶ M): λ_{max} (ε) = 312 nm (52672 M⁻¹cm⁻¹).

EA: calcd (%) for C₉₈H₆₄: C 94.80, H 5.20; found: C 94.67, H 5.04.

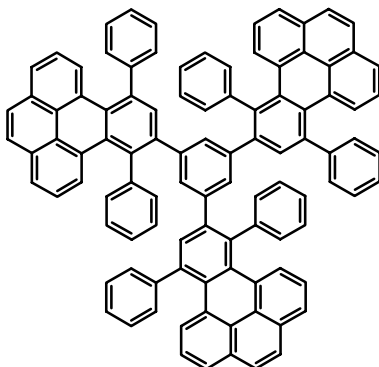
C₉₈H₃₀ PAH (104)

30 mg (0.024 mmol) of 1-(9',12'-diphenylbenzo[e]pyren-11'-yl)-3,5-di(2',3',4',5'-tetraphenylphenyl)benzene (**109**) was dissolved in 120 mL of dichloromethane in a 250 mL three-necked round bottom flask. A constant stream of argon was bubbled into the solution through a glass capillary. A solution of 693 mg (4.27 mmol) iron(III) chloride in 7 mL of nitromethane was then added dropwise via syringe. Fresh dichloromethane was added intermittently to replace that which had evaporated. After 9 h, a condenser was attached to the flask and the argon bubbling rate reduced. The reaction mixture was stirred for a further 15 h and then quenched by addition of methanol. The precipitate was collected by filtration, washed with methanol and dried under vacuum to afford 27 mg (92% yield) **104** as a black solid.

MALDI-TOF MS (TCNQ): m/z (%) = 1206.3 (89), 1207.3 (100), 1208.3 (54), 1209.2 (23), 1210.2 (14); calcd for C₉₈H₃₀: m/z (%) = 1206.2 (91), 1207.2 (100), 1208.2 (54), 1209.2 (19), 1210.2 (5).

UV/Vis (solid state): λ_{max} = 508 nm.

EA*: calcd (%) for C₉₈H₃₀: C 97.50, H 2.50; found: C 91.47, H 3.17.

1,3,5-Tris(9',12'-diphenylbenzo[e]pyren-11'-yl)benzene (110)

40 mg (0.27 mmol) of 1,3,5-triethynylbenzene and 360 mg (0.88 mmol) of 1,3-diphenylcyclopenta[*e*]pyren-2-one (**106**) were dissolved in 3 mL of *o*-xylene under an argon atmosphere and the resulting mixture heated for 24 h at 170 °C. Another 120 mg (0.30 mmol) of **106** was added and the reaction mixture heated at 170 °C for a further 24 h. After cooling to room temperature, methanol was added to the reaction mixture. The precipitate was collected by filtration, washed with methanol and THF, then dried under vacuum to afford 240 mg (70 % yield) **110** as a colorless solid.

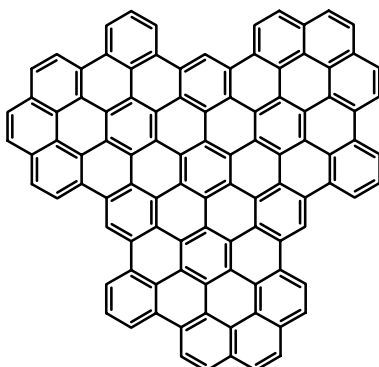
¹H NMR (500 MHz, C₂D₂Cl₄, 110 °C): δ = 8.22-7.68 (m, 24H), 7.54-6.98 (m, 33H), 6.74 (s, 3H).

¹³C NMR (125 MHz, C₂D₂Cl₄, 110 °C): δ = 145.40, 142.97, 140.84, 140.68, 139.33, 137.77, 136.60, 133.22, 132.42, 131.95, 131.04, 130.98, 130.32, 130.17, 130.10, 129.93, 129.88, 129.64, 129.03, 128.92, 128.69, 128.34, 127.85, 127.48, 127.23, 127.07, 126.94, 126.43, 126.01, 125.90, 125.50, 125.43, 124.65, 124.39, 123.96.

MS (FD, 8 kV): *m/z* (%) = 1286.4 (100) [M⁺] (calcd for C₁₀₂H₆₀: 1285.6).

UV/Vis (THF, C = 5.15 · 10⁻⁶ M): λ_{max} (ε) = 315 nm (106040 M⁻¹cm⁻¹).

EA: calcd (%) for C₁₀₂H₆₀: C 95.30, H 4.70; found: C 95.32, H 4.51.

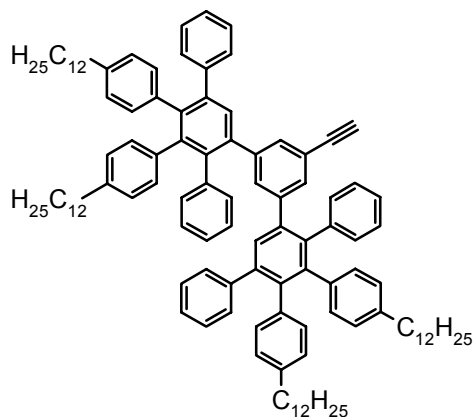
C₁₀₂H₃₀ PAH (105)

30 mg (0.023 mmol) of 1,3,5-tris(9',12'-diphenylbenzo[e]pyren-11'-yl)benzene (**110**) was dissolved in 120 mL of dichloromethane in a 250 mL three-necked round bottom flask. A constant stream of argon was bubbled into the solution through a glass capillary. A solution of 340 mg (2.10 mmol) iron(III) chloride in 4 mL of nitromethane was then added dropwise via syringe. Throughout the duration of the reaction, a constant stream of argon was bubbled through the mixture to remove HCl formed *in situ*. Fresh dichloromethane was added intermittently to replace that evaporated. The reaction was stirred for 10 h and quenched by addition of methanol. The precipitate was collected by filtration, washed with methanol and dried under vacuum to afford 24 mg (82% yield) **105** as a black solid.

MALDI-TOF MS (TCNQ): m/z (%) = 1254.5 (95), 1255.5 (100), 1256.5 (65), 1257.5 (26), 1258.5 (14), 1259.5 (8); calcd for C₁₀₂H₃₀: m/z (%) = 1254.2 (88), 1255.2 (100), 1256.2 (56), 1257.3 (21), 1258.3 (6), 1259.3 (2).

UV/Vis (solid state): λ_{max} = 535 nm.

EA*: calcd (%) for C₁₀₂H₃₀: C 97.59, H 2.41; found: C 87.36, H 3.64.

1,3-Di[3',4'-di(4''-dodecylphenyl)-2',5'-diphenylphenyl]-5-ethynylbenzene (72b)

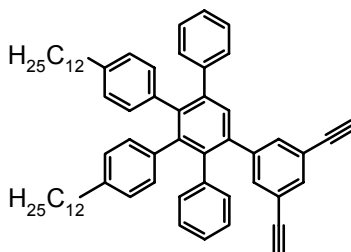
0.55 g (3.66 mmol) of 1,3,5-triethynylbenzene and 3.45 g (4.78 mmol) of 3,4-bis(4-dodecylphenyl)-2,5-diphenylcyclopentadienone (**55a**) were dissolved in 12 mL of *o*-xylene. The mixture was heated under an argon atmosphere from 100 °C to 140 °C, increasing the temperature in stepwise increments over 10 h. After cooling to room temperature, the solvent was removed under reduced pressure and the residue (mixture of **72b** and **71b**) purified by column chromatography (silica gel, petroleum ether/dichloromethane 9:1 to 4:1) to afford 1.69 g (30 % yield) **72b** as a colorless, highly viscous oil, which solidified upon standing.

¹H NMR (500 MHz, C₂D₂Cl₄): δ = 7.12-6.89 (m, 15H, Ar-H), 6.83-6.40 (m, 26H, Ar-H), 2.81(s, 1H, CH), 2.34-2.18 (m, 8H, α-CH₂), 1.40-0.90 (m, 80H, CH₂); 0.80 (t, ³J(H,H) = 6.9 Hz, 12H, CH₃).

¹³C NMR (125 MHz, C₂D₂Cl₄): δ = 142.08, 141.80, 140.64, 140.06, 139.87, 139.52, 139.29, 139.20, 137.66, 137.39, 133.01, 131.88, 131.59, 131.53, 131.22, 130.37, 127.65, 127.18, 127.11, 126.82, 126.25, 125.83, 120.39, 84.30, 76.69, 35.62, 35.56, 32.24, 31.46, 30.05, 29.99, 29.82, 29.70, 29.09, 28.98, 23.03, 14.55.

MS (FD, 8 kV): *m/z* (%): 1537.1 (100) [*M*⁺] (calcd for C₁₁₆H₁₄₂: 1536.4).

EA: calcd (%) for C₁₁₆H₁₄₂: C 90.68, H 9.32; found: C 90.48, H 9.29.

1-[3',4'-Di(4'' dodecylphenyl)-2',5'-diphenylphenyl]-3,5-diethynylbenzene (71b)

Compound **71b** was prepared as described above for compound **72b** (in the same reaction as a co-product). Purification by column chromatography (silica gel, petroleum ether/dichloromethane 9:1 to 4:1) afforded 1.55 g (50% yield) **71b** as a colorless solid.

¹H NMR (500 MHz, C₂D₂Cl₄): δ = 7.38 (s, 1H, Ar-H), 7.32 (s, 1H, Ar-H), 7.21 (s, 2H, Ar-H), 7.12-7.00 (br, 5H, Ar-H), 6.92-6.82 (br, 3H, Ar-H), 6.80-6.72 (br, 2H, Ar-H), 6.67-6.50 (m, 8H, Ar-H), 2.95 (s, 2H, CH), 2.36-2.20 (m, 4H, α-CH₂), 1.40-0.95 (m, 40H, CH₂); 0.81 (t, ³J(H,H) = 6.1 Hz, 6H, CH₃).

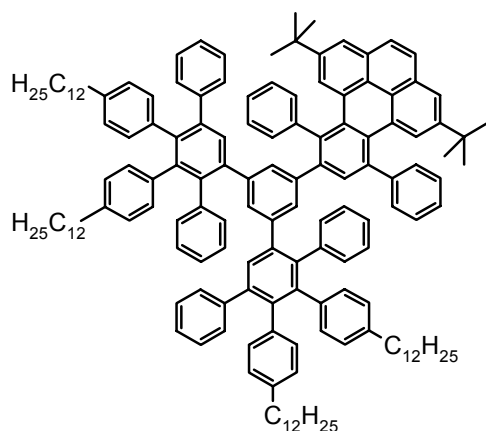
¹³C NMR (125 MHz, C₂D₂Cl₄): δ = 142.83, 142.43, 141.98, 140.90, 140.46, 140.05, 139.70, 139.41, 138.42, 137.48, 137.23, 134.33, 133.55, 131.74, 131.55, 131.49, 130.98, 130.25, 127.83, 127.28, 127.20, 126.92, 126.40, 126.01, 121.81, 83.03, 78.06, 35.63, 35.57, 32.23, 31.45, 30.04, 29.99, 29.82, 29.68, 29.10, 28.99, 23.03, 14.53.

MS (FD, 8 kV): *m/z* (%): 843.6 (100) [*M*⁺] (calcd for C₆₄H₇₄: 843.3).

m.p.: 96 °C

EA: calcd (%) for C₆₄H₇₄: C 91.16, H 8.84; found: C 90.62, H 8.74.

1-(2',7'-Di-*tert*-butyl-9',12'-diphenylbenzo[*e*]pyren-11'-yl)-3,5-di[3',4'-di(4''-dodecylphenyl)-2',5'-diphenylphenyl]benzene (112)



300 mg (0.20 mmol) of 1,3-di[3',4'-di(4''-dodecylphenyl)-2',5'-diphenylphenyl]-5-ethynylbenzene (**72b**) and 132 mg (0.25 mmol) of 2,7-di-*tert*-butyl-9,11-diphenylcyclopenta[*e*]pyren-10-one (**111**) were dissolved in 4 mL of *o*-xylene and heated under an argon atmosphere for 18 h at 170 °C oil bath temperature. After cooling to room temperature, the solvent was removed under reduced pressure and the residue purified by column chromatography (silica gel, petroleum ether/dichloromethane 6:1) to afford 365 mg (92 % yield) **112** as a colorless solid.

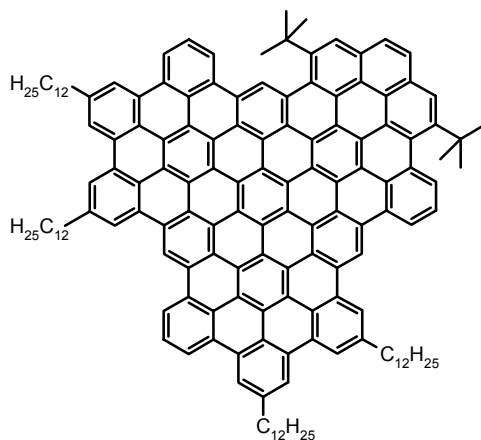
¹H NMR (250 MHz, C₂D₂Cl₄): δ = 8.10 (s, 1H, Ar-H), 7.96 (s, 1H, Ar-H), 7.86-7.78 (m, 4H, Ar-H), 7.42-7.28 (m, 5H, Ar-H), 7.14-6.45 (m, 47H, Ar-H), 2.35-2.16 (m, 8H, α-CH₂), 1.42-0.93 (m, 98H, CH₂, C(CH₃)₃), 0.80 (t, ³J(H,H) = 6.2 Hz, 12H, CH₃).

¹³C NMR (125 MHz, C₂D₂Cl₄, 110 °C): δ = 147.28, 147.08, 145.49, 143.03, 142.19, 141.85, 140.80, 140.66, 140.57, 140.36, 140.30, 139.74, 139.40, 139.31, 139.19, 138.97, 137.84, 137.56, 137.31, 133.31, 132.29, 132.11, 131.98, 131.65, 131.56, 131.46, 130.48, 130.38, 130.11, 129.73, 129.47, 129.29, 129.01, 128.79, 127.48, 127.11, 127.05, 126.73, 126.53, 126.15, 125.73, 123.67, 123.32, 122.10, 35.61, 35.55, 32.23, 31.63, 31.56, 31.44, 30.02, 29.98, 29.81, 29.68, 29.09, 28.99, 23.02, 14.52.

MS (FD, 8 kV): *m/z* (%) = 2026.1 (100) [M⁺] (calcd for C₁₅₄H₁₇₆: 2027.1).

UV/Vis (THF, C = 5.30 · 10⁻⁶ M): λ_{max} (ε) = 313 nm (51095 M⁻¹cm⁻¹).

EA: calcd (%) for C₁₅₄H₁₇₆: C 91.25, H 8.75; found: C 91.10, H 8.66.

Di(*tert*-butyl)-tetradodecyl substituted C98 PAH (113**)**

100 mg (0.049 mmol) of 1-(2',7'-di-*tert*-butyl-9',12'-diphenylbenzo[*e*]pyren-11'-yl)-3,5-di[3',4'-di(4''-dodecylphenyl)-2',5'-diphenylphenyl]benzene (**112**) was dissolved in 100 mL of dichloromethane in a 250 mL three-necked round bottom flask. A constant stream of argon was bubbled into the solution through a glass capillary. A solution of 680 mg (4.19 mmol) iron(III) chloride in 5 mL of nitromethane was then added dropwise via syringe. Throughout the duration of the reaction, a constant stream of argon was bubbled through the mixture to remove HCl formed *in situ*. Fresh dichloromethane was added intermittently to replace that which had evaporated. After 18 h, the reaction was quenched with methanol, and the precipitate was collected by filtration and washed with methanol. The residue was then redissolved in toluene and filtered through a short pad of silica gel to afford 70 mg (71 % yield) **113** as a chestnut red-brown waxy solid.

MALDI-TOF MS (TCNQ): m/z (%) = 1991.9 (67), 1992.8 (100), 1993.8 (92), 1994.9 (59), 1995.8 (32), 1996.8 (16); calcd for $C_{154}H_{142}$: m/z (%) = 1991.1 (58), 1992.1 (100), 1993.1 (86), 1994.1 (49), 1995.1 (21) 1996.1 (7).

UV/Vis (THF, $C = 5.95 \cdot 10^{-6}$ M): λ_{\max} (ϵ) = 474 nm (61940 $M^{-1}cm^{-1}$).

EA: calcd (%) for $C_{154}H_{142}$: C 92.82, H 7.18; found: C 92.87, H 7.07.



List of publications

(resulting from work in the group of Prof. Müllen)

1. Ž. Tomović, M. D. Watson, K. Müllen, "Superphenalene-Based Columnar Liquid Crystals", *Angew. Chem. Int. Ed.* **2004**, *43*, 755-758.
2. M. G. Debije, J. Piris, M. P. de Haas, J. M. Warman, Ž. Tomović, C. D. Simpson, M. D. Watson, K. Müllen, "The Optical and Charge Transport Properties of Discotic Materials with Large Aromatic Hydrocarbon Cores", *J. Am. Chem. Soc.* **2004**, *126*, 4641-4645.
3. Z. Wang, Ž. Tomović, M. Kastler, R. Pretsch, F. Negri, V. Enkelmann, K. Müllen, "Graphitic Molecules with Partial "Zig-Zag" Periphery", *J. Am. Chem. Soc.* **2004**, *126*, 7794-7795.
4. J. Wu, Ž. Tomović, V. Enkelmann, K. Müllen, "From Branched Hydrocarbon Propellers to C₃-Symmetric Graphite Disks", *J. Org. Chem.* **2004**, *69*, 5179-5186.
5. D. S. Su, R. E. Jentoft, J.-O. Müller, E. Jacob, C. D. Simpson, Ž. Tomović, K. Müllen, A. Messerer, U. Pöschl, R. Niessner, R. Schlögl, "Microstructure and oxidation behaviour of Euro IV diesel engine soot: a comparative study with synthetic model soot substances", *Catalysis Today*, **2004**, *90*, 127-132.
6. I. Gutman, Ž. Tomović, K. Müllen, J. P. Rabe, "On the distribution of π -electrons in large polycyclic aromatic hydrocarbons", *Chem. Phys. Lett.* **2004**, *397*, 412-416.

-
7. V. Palermo, M. Palma, Ž. Tomović, M. D. Watson, K. Müllen, P. Samorì, "Self-assembly of π -conjugated discs on heterogeneous surfaces: effect of the micro- and nano-scale dewetting", *Synth. Met.* **2004**, *147*, 117-121.
 8. W. Pisula, Ž. Tomović, B. Hamaoui, M. D. Watson, T. Pakula, K. Müllen, "Control of the homeotropic order of discotic hexa-*peri*-hexabenzocoronenes", *Adv. Func. Mater.* **2004**, *in press*.
 9. W. Pisula, Ž. Tomović, M. Stepputat, U. Kolb, T. Pakula, K. Müllen, "Uniaxial alignment of liquid crystalline discotics by solution processing", *Chem. Mater.* **2004**, *to be submitted*.
 10. V. Palermo, M. Palma, Ž. Tomović, M. D. Watson, K. Müllen, P. Samorì, "Unravelling the work function of self-assembled nanographene architectures by Kelvin-Probe Force Microscopy", *Adv. Mater.* **2004**, *to be submitted*.
 11. W. Pisula, Ž. Tomović, C. Simpson, M. Kastler, K. Müllen, T. Pakula, "Relation between core size, side chain length and the supramolecular organization of polycyclic aromatic hydrocarbons", *Chem. Mater.* **2004**, *to be submitted*.
 12. Ž. Tomović, K. Müllen, "Synthesis and properties of dendronized superphenalene graphite discs", *manuscript in preparation*.
 13. Z. Wang, Ž. Tomović, M. Kastler, W. Pisula, K. Müllen, "Synthesis and self-assembly properties of polycyclic aromatic hydrocarbons with partial "zig-zag" periphery", *manuscript in preparation*.

Curriculum Vitae

Personal details:

Name: Željko Tomović
Date of birth: 20 November 1976
Place of birth: Kragujevac, Serbia
Nationality: Serbian
Marital status: Married

Education:

1983–1995 Primary and secondary schooling in Kragujevac, Serbia.
1995–1999 Study of chemistry at the Faculty of Science, University of Kragujevac, Serbia.
07/1999 B.Sc. degree in chemistry. Thesis title: "Calculation and investigation of one topological index based on the product of the distances between vertices of the molecular graph". Work supervised by Prof. Dr. Ivan Gutman.
1999–2000 Postgraduate studies at the Faculty of Science, University of Kragujevac, Serbia.
12/2000 M.Sc. degree in chemistry. Thesis title: "Investigation of the possibility of application of iterated line graphs for predicting physico-chemical properties of alkanes". Work supervised by Prof. Dr. Ivan Gutman.
since 07/2001 Ph.D. studies at the Max-Planck-Institute for Polymer Research, Mainz, Germany, in the group of Prof. Dr. Klaus Müllen. Topic: New discotic liquid crystals based on large polycyclic aromatic hydrocarbons as materials for molecular electronics.